

THESIS
3
1999



LIBRARY
Michigan State
University

This is to certify that the

thesis entitled

Interactions of Dinuclear Transition
Metal Complexes With Amino Acids,
Nucleotides and DNA
presented by

Jennifer Simone Hess

has been accepted towards fulfillment
of the requirements for

M.S. degree in chemistry

Major professor

Date 12/17/98

PLACE IN RETURN BOX to remove this checkout from your record.
TO AVOID FINES return on or before date due.
MAY BE RECALLED with earlier due date if requested.

DATE DUE	DATE DUE	DATE DUE
_____	_____	_____
_____	_____	_____
_____	_____	_____
_____	_____	_____
_____	_____	_____

**INTERACTIONS OF DINUCLEAR TRANSITION METAL COMPLEXES WITH
AMINO ACIDS, NUCLEOTIDES, AND DNA**

By

Jennifer Simone Hess

A THESIS

**Submitted to
Michigan State University
In partial fulfillment of the requirements
For the degree of**

MASTER OF SCIENCE

Department of chemistry

1998

ABSTRACT

INTERACTIONS OF DINUCLEAR TRANSITION METAL COMPLEXES WITH AMINO ACIDS, NUCLEOTIDES, AND DNA

By

Jennifer Simone Hess

In the 1960's the discovery that *cis*-platin was a potent antitumor agent paved the way for the use of metal-based drugs in modern chemotherapeutic applications. The severe side effects exhibited by this drug have led to the investigation of new types of metal-based compounds as potential antitumor agents. Dinuclear transition metal compounds are among these compounds. These have been found to exhibit carcinostatic activity, and like *cis*-platin, are inhibitors of DNA replication. In order to understand potential mechanisms which could lead to the development of more effective treatments, the interactions of these antitumor agents with cellular molecules must be studied. Reactions of dinuclear compounds with thiol-dependent enzymes and/or DNA bases leading to distortions, may be responsible for their activity. In order to develop an understanding of the *in vivo* interactions these dinuclear compounds may undergo, reactions with cellular components were studied. Presented here are the results from the studies of dinuclear transition metal compounds with the amino acids methionine, cysteine, and glutathione along with the nucleotides adenosine, guanosine, and DNA.

TABLE OF CONTENTS

LIST OF TABLES.....	v
LIST OF FIGURES.....	vi
LIST OF ABBREVIATIONS.....	xii
CHAPTER I. INTRODUCTION	
INTRODUCTION	2
Mechanism of Action of <i>Cis</i> -platin	2
Dinuclear Antitumor Agents.....	10
CHAPTER II. REACTIONS OF DINUCLEAR TRANSITION METAL COMPOUNDS WITH AMINO ACIDS.....	
1. Introduction.....	18
2. Experimental.....	27
A. Synthesis	
Preparation of $\text{Rh}_2(\text{O}_2\text{CCH}_3)_4(\text{MET})_2$ (1).....	27
Preparation of $\text{Rh}_2(\text{CYS})_2(\text{H}_2\text{O})_4$ (2).....	28
Preparation of $\text{Rh}_2(\text{O}_2\text{CCH}_3)_2(\text{GSH})_2(\text{H}_2\text{O})_2$ (3).....	28
$[\text{Rh}_2(\text{O}_2\text{CCH}_3)_2(\text{CH}_3\text{CN})_6][\text{BF}_4]_2$ + Methionine (4).....	29
$[\text{Rh}_2(\text{O}_2\text{CCH}_3)_2(\text{CH}_3\text{CN})_6][\text{BF}_4]_2$ + Cysteine (5).....	29
$[\text{Rh}_2(\text{O}_2\text{CCH}_3)_2(\text{CH}_3\text{CN})_6][\text{BF}_4]_2$ + Glutathione (6).....	30
$\text{Rh}_2(\text{O}_2\text{CCH}_3)_4(\text{H}_2\text{O})_2$ + O-Methyl cysteine (7).....	30
$\text{Rh}_2(\text{O}_2\text{CCH}_3)_4(\text{H}_2\text{O})_2$ + 2-Aminothiophenol (8).....	30
$[\text{Rh}_2(\text{DTolF})_2(\text{CH}_3\text{CN})_6][\text{BF}_4]_2$ +Methionine (9).....	31
$[\text{Rh}_2(\text{O}_2\text{CCH}_3)_2(\text{CH}_3\text{CN})_6][\text{BF}_4]_2$ + Cysteine (10).....	31
$[\text{Rh}_2(\text{O}_2\text{CCH}_3)_2(\text{CH}_3\text{CN})_6][\text{BF}_4]_2$ + Glutathione (11).....	31
$\text{Re}_2(\text{O}_2\text{CCH}_2\text{CH}_3)_4\text{Cl}_2$ + Methionine (12).....	32
$\text{Re}_2(\text{O}_2\text{CCH}_2\text{CH}_3)_4\text{Cl}_2$ + Cysteine (13).....	32
$\text{Re}_2(\text{O}_2\text{CCH}_2\text{CH}_3)_4\text{Cl}_2$ + Glutathione (14).....	32
B. X-ray Structure Determination.....	33
3. Results and Discussion.....	35
A. Dirhodium Carboxylates.....	35
B. $[\text{Rh}_2(\text{O}_2\text{CCH}_3)_2(\text{CH}_3\text{CN})_6]^{2+}$ Reactions.....	48
C. Cysteine Mimic Reactions.....	52
D. $[\text{Rh}_2(\text{DTolF})_2(\text{CH}_3\text{CN})_6][\text{BF}_4]_2$ Reactions.....	57
E. $\text{Re}_2(\text{O}_2\text{CCH}_2\text{CH}_3)_4\text{Cl}_2$ Reactions.....	59
4. Conclusions.....	61

CHAPTER III. REACTIONS OF DIRHODIUM CARBOXYLATES WITH NUCLEOBASES.....	63
1. Introduction.....	64
2. Experimental.....	70
$\text{Rh}_2(\text{O}_2\text{CCH}_3)_4(\text{CH}_3\text{OH})_2 + \text{ATP}$ (15).....	70
$\text{Rh}_2(\text{O}_2\text{CCH}_3)_4(\text{CH}_3\text{OH})_2 + \text{GTP}$ (16).....	70
$\text{Rh}_2(\text{O}_2\text{CCH}_3)_4(\text{CH}_3\text{OH})_2 + 3', 5'\text{-TDP}$ (17).....	71
$\text{Rh}_2(\text{O}_2\text{CCH}_3)_4(\text{CH}_3\text{OH})_2 + \text{AMP}$ (18).....	71
$\text{Rh}_2(\text{O}_2\text{CCH}_3)_4(\text{CH}_3\text{OH})_2 + \text{GMP}$ (19).....	72
$[\text{Rh}_2(\text{O}_2\text{CCH}_3)_2(\text{CH}_3\text{CN})_6][\text{BF}_4]_2 + \text{GMP}$ (20).....	72
$[\text{Rh}_2(\text{O}_2\text{CCH}_3)_2(\text{CH}_3\text{CN})_6][\text{BF}_4]_2 + \text{AMP}$ (21).....	72
3. Results and Discussion.....	73
A. Adenosine Reactions.....	73
B. Guanosine Reactions.....	74
C. Thymidine.....	75
4. Conclusions.....	76
 CHAPTER IV. ^1H NMR REACTIONS OF AMINO ACIDS AND DNA PURINES WITH DIRHODIUM CARBOXYLATES.....	 78
1. Introduction.....	79
A. Competition Reactions.....	79
B. Reactions of Dirhodium Acetate Compounds.....	81
2. Experimental.....	83
A. Competition Reactions.....	83
B. Dirhodium Tetraacetate Reactions.....	86
3. Results and Discussion.....	90
A. Competition Reactions.....	90
B. Dirhodium Tetraacetate Reactions.....	99
4. Conclusions.....	116
A. Competition Reactions.....	116
B. Dirhodium Tetraacetate Reactions.....	117
 CHAPTER V. REACTIONS OF DIRHODIUM BIS-ACETATE WITH DNA	119
1. Introduction.....	120
2. Experimental.....	130
3. Results and Discussion.....	141
4. Conclusions.....	148
 APPENDIX.....	 149
 REFERENCES.....	 176

LIST OF TABLES

Table 1. IR stretches used in the determination of amino acid binding sites.....	38
Table 2. Proton resonances monitored during the course of the methionine/AMP competition experiment.....	92
Table 3. Proton resonances monitored throughout the course of the glutathione/AMP competition experiment.....	96
Table 4. Proton resonances monitored over time for the cysteine/AMP competition reaction.....	99
Table 5. Integration of bound:free acetate for the cysteine/dirhodium tetraacetate reaction.....	100
Table 6. Integration of bound: free acetate for glutathione/dirhodium tetraacetate reaction.....	102
Table 7. Integration of bound:free acetate for the $\text{Rh}_2(\text{OAc})_4(\text{ATP})_2 +$ cysteine reaction.....	106
Table 8. Integration of bound:free acetate for the $\text{Rh}_2(\text{OAc})_2(\text{GTP})_2 +$ cysteine reaction	108
Table 9. Integration of bound:free acetate for the reaction of dirhodium tetraacetate with O-Methyl cysteine.....	111
Table 10. DNA strands designed for crystallization studies.....	142

LIST OF FIGURES

Figure 1. The antitumor agent <i>cis</i> -platin.....	2
Figure 2. Second generation platinum drugs (a) oxaliplatin, (b) CHIP (iproplatin), (c) JM216, (d) diammine (1, 1-cyclobutanedicarboxylato)platinum(II) (carboplatin), (e) quinoline complex, and (f) DACCP.....	3
Figure 3. Side and top views of the three standard forms of DNA. B-DNA is the most common form. Major and minor grooves are denoted by arrows.....	5
Figure 4. DNA base pairing model showing Watson-Crick base pairs..	6
Figure 5. Binding modes of <i>cis</i> -platin (a) intrastrand cross-link, (b) interstrand cross-link, and (c) DNA-protein cross-link.....	8
Figure 6. Similarities between <i>cis</i> -platin and dinuclear antitumor agents.....	11
Figure 7. Dinuclear platinum antitumor agents, (a) [<i>trans</i> -PtCl(NH ₃) ₂] ₂ H ₂ N(CH ₂) _n NH ₂] ₂ ⁺ , and (b) [<i>cis</i> -PtCl(NH ₃) ₂] ₂ H ₂ N(CH ₂) _n NH ₂] ₂ ⁺	12
Figure 8. Dinuclear rhodium compounds that exhibit anticancer activity (a) dirhodium (II) carboxylates (R = CH ₃ , CH ₂ CH ₃ , or CH ₂ CH ₂ CH ₃), and (b) dirhodium (II) formamidinates. (L = solvent molecule).....	13
Figure 9. Dirhenium antitumor complexes (a) rhenium (III) carboxylates (R = CH ₃ , CH ₂ CH ₃ , or CH ₂ CH ₂ CH ₃), and (b) dirhenium bis-carboxylates (X = halogen, L = solvent molecule).....	15
Figure 10. Sulfur containing amino acids.....	19
Figure 11. Common binding modes of L-Methionine to a metal center (a) monodentate through sulfur; and (b) bidentate through sulfur and nitrogen forming a six membered ring.....	20
Figure 12. Novel cyclic trinuclear methionine compound.....	21
Figure 13. Tridentate binding of methionine to a Ru center.....	21

Figure 14. Postulated binding modes of Glutathine to a Pt(II) center...	22
Figure 15. Potential binding modes of L-Cysteine to a Pt(II) center.....	23
Figure 16. Rhodium tetraacetate products of Methionine (a) and Cysteine (b).....	24
Figure 17. pK_a values for the common binding sites on (a) methionine, (b) cysteine, and (c) glutathione.....	39
Figure 18. Structure of the 2:1 adduct formed in the reaction of methionine with dirhodium tetraacetate.....	40
Figure 19. ORTEP of $Rh_2(O_2CCH_3)_4(Met)_2$	42
Figure 20. Possible binding modes of glutathione to dirhodium Tetraacetate.....	43
Figure 21. Possible binding modes of cysteine	45
Figure 22. UV spectral study (a) dirhodium tetraacetate, (b) 1:1 ratio, (c) 1:2 ratio, (d) 1:3 ratio, and (e) 1:4 ratio.....	47
Figure 23. Possible binding modes of methionine to dirhodium bis-acetate.....	49
Figure 24. Proposed structures for the products of the reaction between cysteine and dirhodium bis-acetate.....	51
Figure 25. Possible binding modes of the cysteine mimics, O-Methyl cysteine and 2-aminothiophenol, to dirhodium tetraacetate.	53
Figure 26. (a) Proposed mechanism for the insertion reaction that takes place with the cysteine mimics in the presence of acetone, (b) structure of the products formed via this mechanism.....	54
Figure 27. ORTEP of the O-Methyl cysteine product of dirhodium tetraacetate.....	55
Figure 28. PLUTO of 2-aminothiophenol derivative of dirhodium tetraacetate.....	56
Figure 29. Possible binding modes of methionine to the partially solvated dirhodium ditolylformamidinate (DTolF) complex. (R = tolyl).....	58

Figure 30. Possible binding modes of cysteine to the partially solvated dirhodium ditolyformamidinate complex. (R = tolyl).....	59
Figure 31. Proposed structure of the product from the reaction of glutathione with dirhenium tetrapropionate.....	61
Figure 32. Binding modes of cis-platin to the DNA purines (a) adenosine and (b) guanosine. (Where R = sugar).....	64
Figure 33. Dinuclear carboxylate compounds of (a) ruthenium, (b) rhenium, and (c) rhodium that display antitumor activity.....	65
Figure 34. Interactions of (a) adenosine and (b) guanosine with dirhodium tetraacetate.....	66
Figure 35. ORTEP representation of $\text{cis-}[\text{Rh}_2(\text{DTolF})_2(9\text{-EtAH})_2(\text{CH}_3\text{CN})]^{2+}$ showing equatorially coordinated 9-ethylguanine ligands.	67
Figure 36. ORTEP representations of Head-to-head (a) and Head-to-tail (b) isomers of 9-Ethylguanine derivatives of dirhodium acetate.....	68
Figure 37. Binding modes of adenine and adenosine to dirhodium formamidinate compounds (a) axial through N3 and (b) through N1 and NH ₂ . (R = tolyl and R' = sugar).....	69
Figure 38. Equatorial bridging of AMP (a) 'head-to-head' and (b) 'head-to-tail' isomers.....	74
Figure 39. Possible isomers obtained in reactions of dirhodium tetraacetate with guanosine (a) 'head-to-head' and (b) 'head-to-tail'.....	75
Figure 40. Possible product from the reaction of 3' 5'-TDP with dirhodium tetraacetate (a) thymidine 3', 5'-diphosphate (b) proposed product.....	76
Figure 41. Intrastrand (a) , interstrand (b) and DNA-protein cross-links (c) formed by <i>cis</i> -platin interactions with DNA.....	79
Figure 42. Numbering scheme for the amino acids (a) methionine, (b) cysteine, and (c) glutathione.....	83

Figure 43. Proposed product from the competition reaction of $\text{Rh}_2(\text{O}_2\text{CCH}_3)_4$ with methionine and AMP.....	92
Figure 44. Proposed products formed in the competition reaction with glutathione and AMP.....	95
Figure 45. . Proposed products formed in the competition reaction with cysteine and AMP.....	98
Figure 46. Proposed products from the reaction of four equivalents of cysteine with dirhodium tetraacetate.....	101
Figure 47. Proposed products from the reaction of glutathione with dirhodium tetraacetate.....	103
Figure 48. Proposed product from the reaction of methionine with dirhodium tetraacetate.....	104
Figure 49. Proposed products from the reaction of cysteine with a dirhodium tetraacetate/ATP derivative.....	107
Figure 50. Proposed products from the reaction of cysteine with a dirhodium tetraacetate/GTP derivative.....	109
Figure 51. Proposed products from the reaction of cysteine with dirhodium bis-acetate.....	112
Figure 52. Proposed products from the reaction of O-methyl cysteine with dirhodium tetraacetate.....	113
Figure 53. Proposed products from the reaction of dirhodium tetraacetate with 2-aminothiophenol.....	115
Figure 54. Labeling scheme for 2-aminothiophenol.....	114
Figure 55. Potential hydrogen-bond interactions with base edges in A·T and G·C base pairs. Donors and acceptors are indicated by direction of the arrowheads.....	121
Figure 56. The minor groove binding drug Netropsin.....	122
Figure 57. Crystal structure of (a) anthramycin-d(CCAACGTTGG) ₂ and (b) netropsin-d(CGCGAATTCGCG) ₂	123
Figure 58. The minor groove binding drug Anthramycin.....	122

Figure 59. Structure of <i>cis</i> -platin-d(CCTCTGGTCTCC)- (GGAGACCAGAGG).....	125
Figure 60. Crystal structure of <i>cis</i> -platin bound to d(CGCGAATTCGCG). Arrows indicate the three <i>cis</i> -platin molecules bound to the DNA strand.....	128
Figure 61. ORTEP representation of <i>cis</i> -[Pt(NH ₃) ₂ {d(pGpG)}].....	129
Figure 62. ORTEP stereoview of the intrastrand <i>cis</i> -platin d(CpGpG) adduct.....	129
Figure 63. Hanging Drop Method of crystal growth.....	141
Figure 64. HPLC chromatograms of (a) 10-mer sc heated to 70°C for 52 h and (b) 11-mer sc heated at 37°C for 64 h.....	146
Figure 65. MS of TCT CTA ATC TC 11 mer.....	147
A1. Methionine/AMP NMR reaction (a) methionine/AMP standard, (b) ¹ H NMR at time = 0, (c) ¹ H NMR at time = 15 min, (d) ¹ H NMR at time = 2 h, (e) ¹ H NMR at time = 4 h, (f) ¹ H NMR at time = 24 h...	150
A2. Glutathione/AMP NMR reaction (a) glutathione/AMP standard, (b) ¹ H NMR at time = 0, (c) ¹ H NMR at time = 15 min, (d) ¹ H NMR at time = 2 h, (e) ¹ H NMR at time = 4 h, (f) ¹ H NMR at time = 24 h.....	153
A3. Cysteine/AMP NMR reaction (a) cysteine/AMP standard, (b) ¹ H NMR at time = 0, (c) ¹ H NMR at time = 15 min, (d) ¹ H NMR at time = 2 h, (e) ¹ H NMR at time = 4 h, (f) ¹ H NMR at time = 24 h.....	156
A4. ¹ H NMR reaction of Rh ₂ (O ₂ CCH ₃) ₄ with cysteine (a) 1:1 ratio, (b) 1:2 ratio, (c) 1:3 ratio, and (d) 1:4 ratio.....	159
A5. ¹ H NMR reaction of Rh ₂ (O ₂ CCH ₃) ₄ with glutathione (a) 1:1 ratio, (b) 1:2 ratio, (c) 1:3 ratio, and (d) 1:4 ratio.....	161
A6. ¹ H NMR reaction of Rh ₂ (O ₂ CCH ₃) ₄ with methionine (a) 1:1 ratio, (b) 1:2 ratio, (c) 1:3 ratio, and (d) 1:4 ratio.....	163
A7. ¹ H NMR reaction of Rh ₂ (O ₂ CCH ₃) ₄ (ATP) ₂ with cysteine (a) Rh ₂ (O ₂ CCH ₃) ₄ (ATP) ₂ standard, (b) 1:1 ratio, (c) 1:2 ratio, (d) 1:3 ratio, and (e) 1:4 ratio.....	165

A8. ^1H NMR reaction of $\text{Rh}_2(\text{O}_2\text{CCH}_3)_2(\text{GTP})_2$ with cysteine (a) $\text{Rh}_2(\text{O}_2\text{CCH}_3)_2(\text{GTP})_2$ standard, (b) 1:1 ratio, (c) 1:2 ratio, (d) 1:3 ratio, and (e) 1:4 ratio.....	168
A9. ^1H NMR reaction of $[\text{Rh}_2(\text{O}_2\text{CCH}_3)_2(\text{MeCN})_6][\text{BF}_4]_2$ with cysteine (a) 1:1 ratio, (b) 1:2 ratio, (c) 1:3 ratio, and (d) 1:4 ratio.....	171
A10. ^1H NMR reaction of $\text{Rh}_2(\text{O}_2\text{CCH}_3)_4$ with O-methyl cysteine (a) 1:1 ratio, (b) 1:2 ratio, (c) 1:3 ratio, and (d) 1:4 ratio..... (b)	173
A11. ^1H NMR reaction of $\text{Rh}_2(\text{O}_2\text{CCH}_3)_4$ with 2-Aminothiophenol (a) 1:1 ratio, (b) 1:2 ratio, (c) 1:3 ratio, and (d) 1:4 ratio.....	175

LIST OF ABBREVIATIONS

Å	Angstrom
br	broad
β	Bohr magneton
cm ⁻¹	wavenumber
°C	degree Celcius
d	doublet (NMR), deuterated
δ	parts per million (ppm)
ε	molar extinction coefficient
λ	wavelength
g	gram
mol	mole
h	hour
IR	infrared
k	Boltzmann constant
MHz	MegaHertz
M	molarity (moles per liter)

m	medium, multiplet
mL	milliliter
μ	bridging ligand, micro
nm	nanometer
NMR	nuclear magnetic resonance
v	frequency
s	singlet, strong
UV	ultraviolet
VIS	visible
w	weak
X	halide
DNA	deoxyribonucleic acid
RNA	ribonucleic acid
A	adenosine
G	guanosine
ATP	adenosine triphosphate
GTP	guanosine triphosphate
T	thymidine
C	cytidine
GSH	glutathione
CYS	cysteine
MET	methionine
9-EtGH	9-ethylguanine

9-EtAH	9-ethyladenine
DtOF	N, N'-p-tolylformamide
S	donor solvent
L	ligand

Chapter I
Introduction

Mechanism of Action of *Cis*-platin

In the early 1960's the study of the effect of electrical fields on *Escherichia Coli* bacteria led to the discovery that *cis*-diamminedichloroplatinum, or *cis*-platin, is a potent antitumor agent (Figure 1)¹. Although the compound is effective in the treatment of lung, bladder, head and neck, cervical, testicular and ovarian cancers, it causes severe side effects due to its extreme toxicity; these include nephrotoxicity, myelosuppression, ototoxicity, severe nausea and vomiting, peripheral neuropathies, and occasional cardiac abnormalities. In spite of this, FDA approval was granted in 1979 and many cancer patients have been receiving the drug as part of a standard chemotherapeutic regimen^{2,3}.

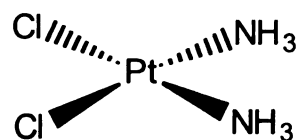
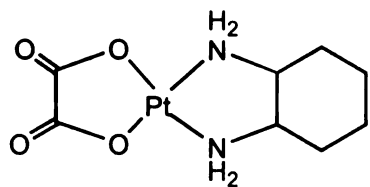
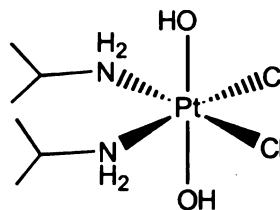


Figure 1. The antitumor agent *cis*-platin.

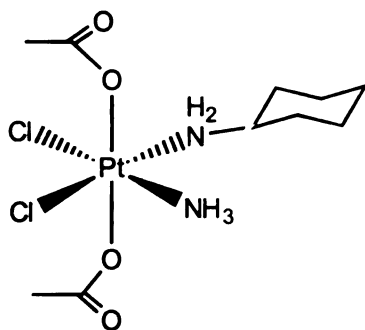
Second generation drugs (Figure 2) are being developed with the ultimate goal of increased activity and reduced toxicity. Many of these potential drugs are in clinical trials, and one of them, carboplatin, was recently approved in the United States for the treatment of ovarian and small lung cancers².



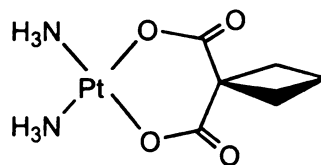
(a) Oxaliplatin



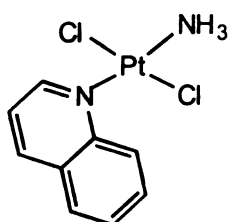
(b) CHIP (Iproplatin)



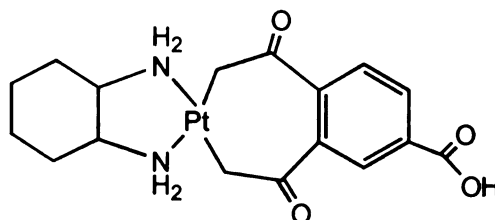
(c) JM 216



(d) Carboplatin



(e) quinoline complex



(f) DACCP

Figure 2. Second generation platinum drugs (a) oxaliplatin, (b) CHIP (iproplatin), (c) JM216, (d) diammine(1,1-cyclobutanedicarboxylato)platinum(II) (carboplatin), (e) quinoline complex , (f) DACCP.

The mechanism of action of these platinum anticancer agents is important to understand, as it may lead to the development of more successful antitumor drugs. The specific chemical reaction(s) responsible for the activity of *cis*-platin is thought to involve bifunctional attachment of the molecule to biomolecules, which abound with possible binding sites. The most widely studied platinum antitumor agent, *cis*-platin, impairs cell division without inhibiting cell growth, as does UV irradiation and hydroxyurea, thus the mechanism of replication inhibition is thought to follow a similar pathway. A culmination of experiments performed over the last 20 years has lead researchers to conclude that DNA synthesis is selectively inhibited, and thus somehow responsible for the anticancer activity³.

In spite of the large body of work on this subject, there is no direct evidence that the actual binding of DNA by *cis*-platin is the cause of its anticancer activity. Indeed some studies suggest that protein binding of *cis*-platin damaged DNA may be partly responsible for its activity. Regardless of the exact mode of action, it is irrefutable that *cis*-platin binds and distorts DNA. In order to understand the mechanism of this binding reaction, the intricacies of DNA structure must be explored.

Deoxyribonucleic acid (DNA) consists of two strands, namely a template strand and a compliment strand. Together these strands form a double helix that is coiled about an axis producing both major and minor grooves (Figure 3). Repeating deoxyribose phosphodiester units comprise the backbone of each DNA strand and serve to link together the four types of bases (Figure 4). The DNA backbone has a polarity, the 5' position of one pentose ring is connected to

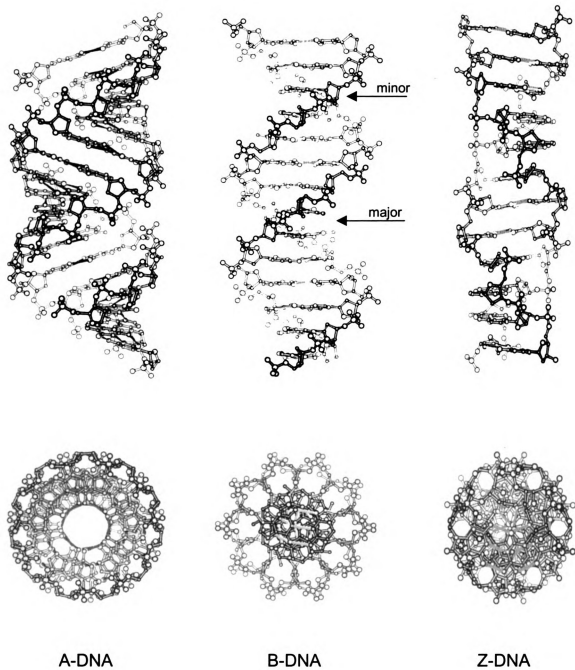


Figure 3. Side and top views of the three standard forms of DNA. B-DNA is the most common form. Major and minor grooves are denoted by arrows.

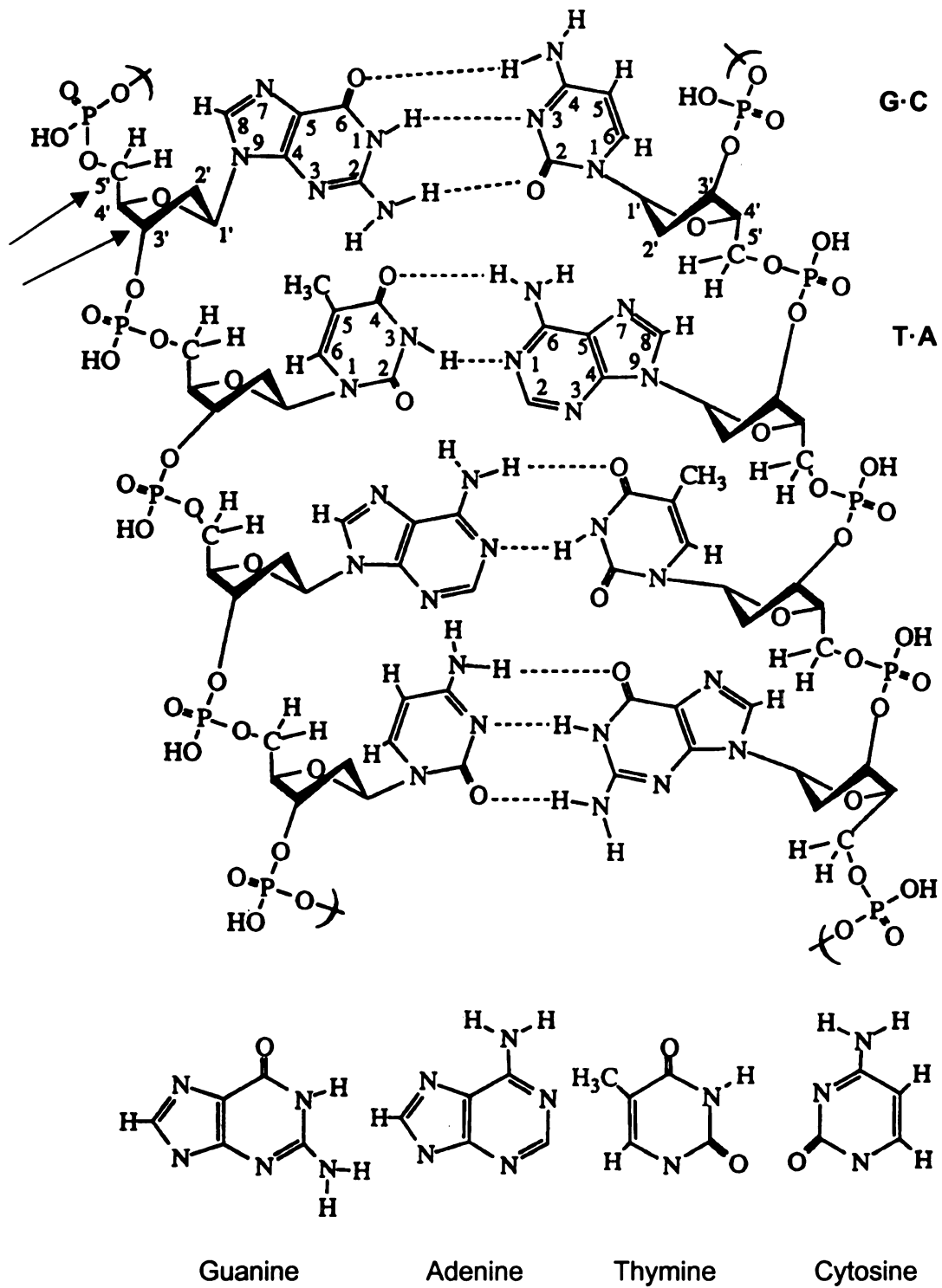


Figure 4. DNA base pairing model showing Watson-Crick base pairs.

the 3' position of the next pentose ring via 5'-3' phosphodiester linkages. The terminal nucleotide at one end possesses a free 5' group, and the terminal nucleotide on the other end possesses a free 3' group, thus creating a type of polarity. By convention, nucleic acid sequences are written as 5'-3'. The double helix is stabilized by hydrogen bonds between the Watson-Crick base pairs, adenine/thymine, and guanine/cytosine (Figure 4). Stacking interactions between base pairs also add to the stability of the helix. DNA occurs in three structural forms referred to as, A, B, and Z DNA. The B form is the most stable under physiological conditions and is the most common. A-DNA is favored in solutions absent of water and is shorter and has a larger diameter than B-DNA. It is not known whether this form is actually present in cells. Z-DNA is unusual in that it takes the form of a left handed helix unlike A- and B- DNA which are right handed helices. Alternating C and G base pairs can readily assume the Z-DNA structure which may play a role in the expression of certain genes ⁴.

There are a variety of DNA binding sites for anticancer agents. The negatively charged phosphate oxygen atoms, the phosphorous atoms, as well as the nitrogen and oxygen atoms of the bases are all potential sites for covalent and noncovalent binding. An alternate method of binding is intercalation whereby a planar molecule such as ethidium bromide, is inserted between base pairs. Most antitumor agents bind to DNA through noncovalent interactions or intercalation. *Cis-platin* is one of the few molecules to have been studied that forms a covalent bond with DNA ⁵.

The DNA binding of *cis*-platin occurs through two guanosine or adenosine molecules. There are three potential binding modes, namely interstrand, intrastrand, and DNA-protein cross-links (Figure 5). The most common binding mode is the intrastrand type. NMR and X-ray crystallography have shown that the most common intrastrand *cis*-platin cross-link is the GpG sequence. These intrastrand cross-links alter the normal conformation of DNA by disrupting Watson-Crick base pairing thereby causing a slight alteration in the double helix and destacking of base pairs. Interstrand cross-links and protein-DNA cross-links of *cis*-platin are rare and therefore will not be discussed ³.

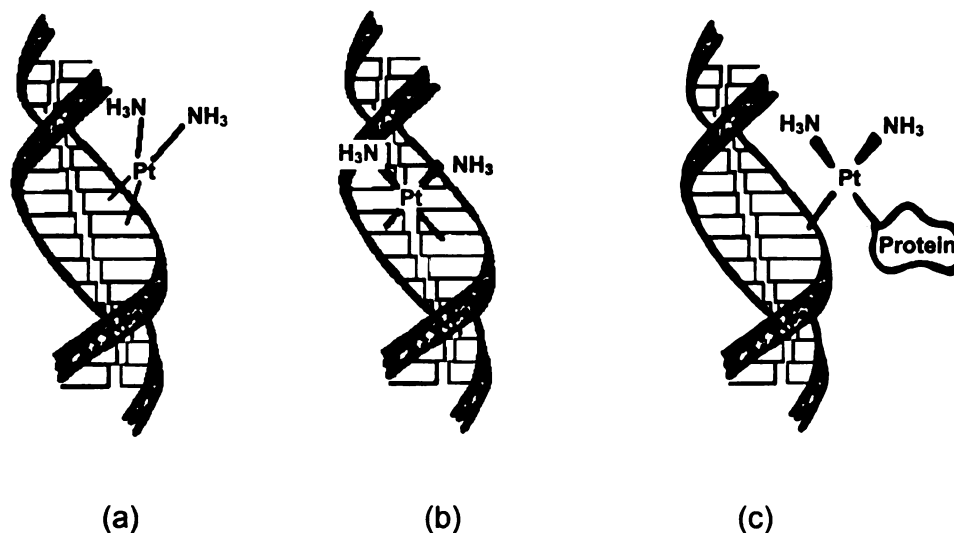


Figure 5. Binding modes of *cis*-platin (a) intrastrand cross-link, (b) interstrand cross-link, and (c) DNA-protein cross-link.

The importance of the issue of DNA binding is that even small and certainly large distortions to the DNA can alter protein recognition sequences.

75
76
77
78
79
80
81
82
83
84
85
86
87
88
89
90
91
92
93
94
95
96
97
98
99
100

This, in turn, may cause replication proteins to be incapable of recognizing their normal binding sites. Another possibility is that structural perturbations lead to the preferential binding of other proteins such as HMG domain proteins (High Mobility Group proteins which may function to control gene expression and higher-order structure, some of which are transcription factors) and histone H1. The recognition of *cis*-platin DNA adducts by HMG proteins may play a role in the cytotoxicity of the platinum compound, indeed it has been found that HMG proteins preferentially bind 1,2-d(GpG) *cis*-platin intrastrand cross-links. Binding of this protein spans a 14 nucleotide region with *cis*-platin located in the center^{6,7}.

DNA binding and unwinding are essential for the initiation of transcription and replication, both of which require proteins. HMG proteins can induce specific bending in the DNA and interact with distorted DNA. The protein SRY, an HMG transcriptional regulator, binds DNA by intercalation of its hydrophobic residues between base pairs. This serves to unstack base pairs which leads to an unwinding and a bending toward the major groove. These structural distortions also serve to widen the minor groove and are similar to those caused by the binding of *cis*-platin. Platinum coordination also unwinds and bends DNA, thereby opening and flattening the minor groove. Platination of DNA has been shown to block replication and transcription which is explained on the basis of protein binding to the *cis*-platin binding site⁶.

Other proteins besides SRY are also known to be diverted from normal functions by *cis*-platin bound DNA. Many proteins in the HMG box protein family, HMG 1 and 2, SSRP1 (human structure-specific recognition protein), Ixr 1 (yeast

intrastrand cross-link recognition protein) and human UBF (rRNA transcription factor), bind to distorted DNA, the consequence of which is bending and unwinding. TBP, the TATA binding protein, is another type of protein that is sequestered by *cis*-platin bound DNA from binding at its normal site. TBP is a protein that binds the promoter region for transcription (the TATA box); without TBP binding, transcription and hence replication cannot occur. The histone H1 protein binds *cis*-platin damaged DNA more strongly than HMG; these two proteins actually compete for binding of the *cis*-platin damaged DNA. Protein-drug-DNA complexes also prevent repair of the damaged strand, for example, HMG can inhibit nucleotide excision repair of *cis*-platin 1,2 intrastrand crosslinks. It seems likely that the majority of *cis*-platin's antitumor activity stems from protein binding to the *cis*-platin damaged DNA ^{7,8}.

Dinuclear Antitumor Agents

In the search for alternatives to *cis*-platin, dinuclear transition metal complexes that may exhibit similar DNA binding modes are being explored. These complexes are composed of two square planar metal units that are joined by a metal-metal bond (Figure 6). Among the complexes of this structural type found to exhibit anticancer activity are dinuclear ruthenium, rhodium, and rhenium complexes.

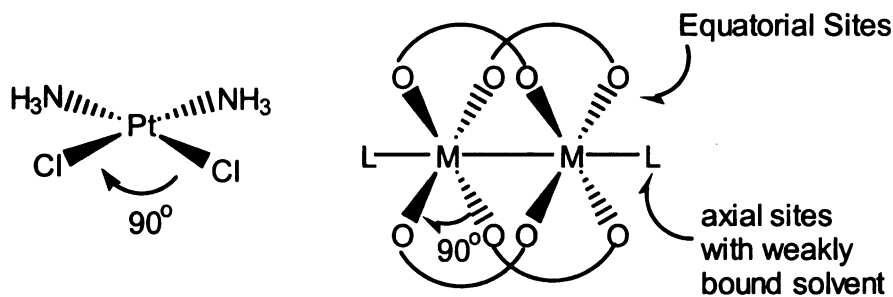


Figure 6. Similarities between *cis*-platin and dinuclear antitumor agents.

Dinuclear Platinum Compounds

The serious side effects of *cis*-platin led to the exploration of dinuclear platinum complexes (Figure 7). These compounds, while sharing a similar square planar motif, are active in cells that show resistance to *cis*-platin. These dinuclear platinum compounds have been found to cause more damage than the parent compound in lung cancer and other experimental cancer cells. Both inter- and intra-strand complexes are formed with the dinuclear platinum but severe DNA bending does not occur. The complexes bind at the GpG sites, and can also span across bases without difficulty to bind GCGC sites. Unlike the *cis*-platin isomers, both the *cis*- and *trans*- forms are active^{9,10}.

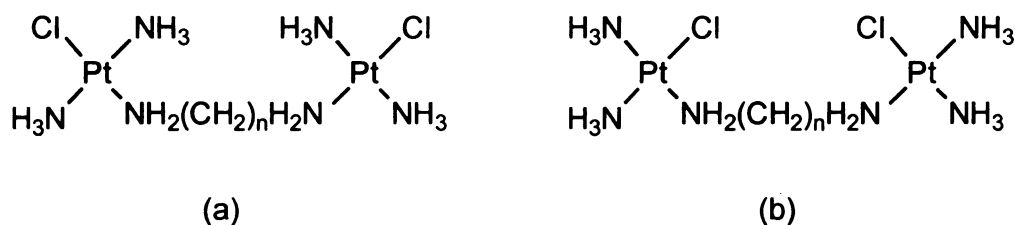


Figure 7. Dinuclear platinum antitumor agents, (a) $[\{trans\text{-PtCl(NH}_3)_2\}_2\text{H}_2\text{N(CH}_2)_n\text{NH}_2\}_2]^+$, and (b) $[\{cis\text{-PtCl(NH}_3)_2\}_2\text{H}_2\text{N(CH}_2)_n\text{NH}_2\}_2]^+$.

Platinum dinuclear compounds unwind DNA in a manner analogous to *cis*-platin, but do not bend DNA as *cis*-platin does. The bending of DNA by the parent compound is a likely signal for HMG family protein binding. HMG proteins recognize the DNA damage caused by the dinuclear compounds, but the recognition is not as effective. Thus it is unlikely that HMG proteins are responsible for the altered activity of the platinum dinuclear compounds. These new anticancer agents are being subjected to further research to determine what is responsible for their increased activity in *cis*-platin resistant cells.

Dinuclear Rhodium Compounds

In the 1970's dirhodium (II) carboxylate compounds (depicted in Figure 8a) were found to exhibit considerable antitumor activity in mice against Erlich ascites tumors and L1210 tumors¹¹. These compounds exhibit equivalent activity and lower toxicity than that of *cis*-platin. The anticancer activity of $\text{Rh}_2(\text{O}_2\text{CCR})_4\text{L}_2$ (where R = CH₃, CH₂CH₃, or CH₂CH₂CH₃) was studied, and the butyrate derivative was found to be the most potent inhibitor of replication,

followed by dirhodium propionate and finally dirhodium acetate. DNA binding experiments indicated that dirhodium tetracarboxylate compounds bind to double and single stranded DNA, polyA, polyG and ribonuclease AA. It has been speculated that the anticancer activity of these compounds arises from DNA binding^{13,14}.

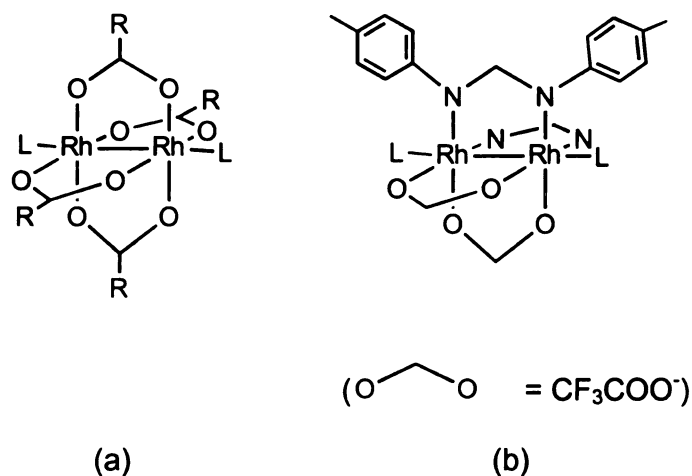


Figure 8. Dinuclear rhodium compounds that exhibit anticancer activity (a) dirhodium (II) carboxylates (R = CH₃, CH₂CH₃, or CH₂CH₂CH₃), and (b) dirhodium (II) formamidinates. (L = Solvent molecule).

It is known that dirhodium (II) carboxylate compounds inhibit DNA synthesis *in vivo*. A suggested mechanism of action is via enzyme binding through the -SH groups at or near the active sites. Protein binding has been found to deactivate the protein's function and could be related to the observed antitumor activity. Another possibility is the binding of an adenine residue through axial interactions to a dirhodium tetracarboxylate molecule¹².

A variation on the dirhodium (II) carboxylate compounds mentioned above is the dirhodium (II) formamidinate family of compounds. $\text{Rh}_2(\text{form})_2(\text{O}_2\text{CCF}_3)_2\text{H}_2\text{O}$ (form = N, N'-di-p-tolylformamidinate, DTolF) exhibits the same 'lantern' structure as the carboxylate derivatives (Figure 8b), and readily provides binding sites for biomolecules, since both the axial H_2O and equatorial trifluoroacetate ligands are easily labilized. The dirhodium (II) formamidinate compounds have been tested for antitumor activity against Yoshida ascites sarcoma, and T8 sarcoma. It was found that these compounds exhibit higher antitumor activity and reduced toxicity as compared to dirhodium (II) tetracarboxylate compounds ^{14,15}.

Dinuclear Rhenium Compounds

Rhenium is notable in that it is the least toxic metallic element. There have been no documented cases of rhenium poisoning thus making rhenium compounds the preferred choice for metal-based drugs such as antitumor compounds. Dirhenium carboxylate complexes, which exhibit the same lantern structure as the dirhodium carboxylates (Figure 9a), exhibit a bacteriostatic effect on *Escherichia Coli* strain W3350 (*thy*). These cells become elongated as in the case of *cis*-platin treated cells. The dirhenium compounds seem to selectively inhibit bacterial DNA synthesis with little or no effect on RNA synthesis ¹⁶.

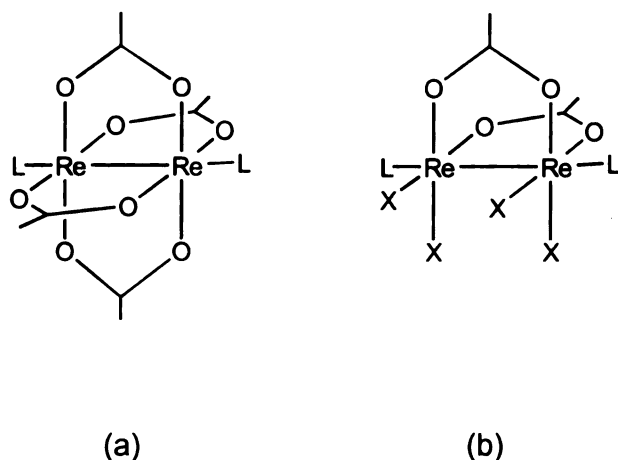


Figure 9. Dirhenium antitumor complexes (a) rhenium (III) carboxylates (R = CH₃, CH₂CH₃, or CH₂CH₂CH₃), and (b) dirhenium bis-carboxylates (X = halogen L = solvent molecule).

Antitumor studies were performed with the dirhenium tetracarboxylate compounds. It was found that dirhenium propionate is the most effective against replication, dirhenium tetraacetate is not as active and dirhenium tetrabutyrate shows higher toxicity without the benefit of much greater activity. These compounds are active against sarcoma S-180, leukemia P-388, and melanoma B-16. Unfortunately, the compounds are susceptible to decomposition in aqueous solutions, which requires the use of high doses to be effective. The decomposition products are thought to be inert insoluble rhenium oxides, which are deposited subcutaneously as a brownish material in the mice used in the studies.

The instability of the dirhenium tetracarboxylate compounds prompted the investigation of derivatives that would be much more stable in water. Dirhenium

bis-carboxylates (Figure 9b) were found to be interesting alternatives, as for example, bis (μ -propionato) diaquotetrabromodirhenium (III) which shows the highest activity and lowest toxicity. High doses were still needed to effect carcinostatic activity, however, and further studies have been hampered by this realization.

Chapter II
**Reactions of Dinuclear Transition Metal
Compounds with Amino Acids**

1. Introduction

The effectiveness of metal-based chemotherapeutics in the treatment of cancer cannot be understood without further investigation of chemical reactions between metal complexes and biomolecules. In the past, studies have focused on the interactions of *cis*-platin with DNA. Since DNA is thought to be the main target of *cis*-platin, much time has been devoted to studying the interactions between this compound and nucleotides. Molecules, such as proteins, also play a central role in modulating the activity of antitumor agents. Evidence has indicated that reactions with thiol-dependent enzymes are linked to *cis*-platin's anticancer activity as well ¹⁷. Sulfur-bound Pt(II) is still chemically reactive and may be able to go on to react with DNA.

Sulfur containing amino acids and proteins are thought to serve as possible binding sites for molecules such as *cis*-platin. Platinum is a soft acid, and sulfur is a soft base, thus a natural affinity exists. Oxygen and nitrogen are hard bases, so sulfur poses the largest 'threat' to decomposition of platinum compounds. To understand the nature of sulfur binding, reactions of antitumor compounds with amino acids such as cysteine and methionine, along with the tripeptide glutathione, have been extensively studied. (Figure 10) ^{3,4}.

This chemistry is important, as methionine and glutathione-platinum adducts have been found in the urine of patients undergoing treatment with *cis*-platin ¹⁸. An interesting consequence of protein binding is that dose limiting nephrotoxicity is due to the binding of Pt(II) to sulfhydryl groups in enzymes.

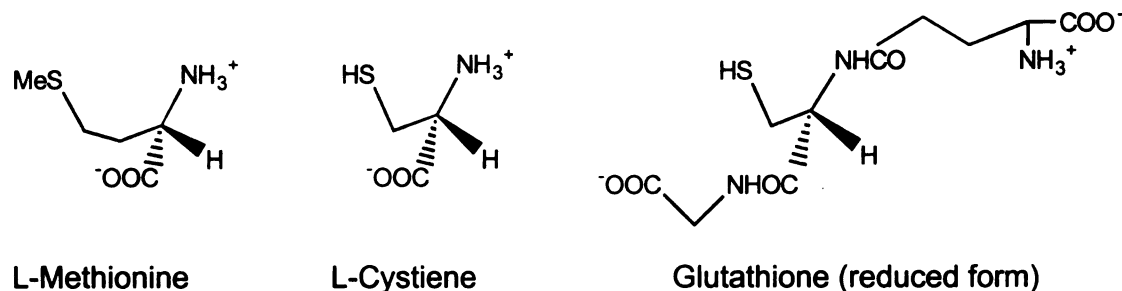


Figure 10. Sulfur containing amino acids.

Since sulfur containing amino acids and proteins play a vital role in the antitumor activity of agents such as *cis*-platin, it is important to discuss the biological importance of these molecules. The main point is that their functions can be disrupted if their concentrations are depleted by the binding of an antitumor agent, such as *cis*-platin or dirhodium tetraacetate. Both methionine and cysteine are used as precursors to the citric acid cycle, which is important in the production of ATP. Methionine is also an important factor in the synthesis of several biomolecules such as cysteine, creatine, proteins and polyamines. Cysteine is a key building block in the synthesis of glutathione. Glutathione acts as a peroxide scavenger which detoxifies the cell, and also protects red cells from oxidative damage and helps maintain their structure. Furthermore, glutathione acts as a redox buffer which maintains the heme in its ferrous state. A decrease in glutathione concentration can lead to hemolysis, or hemolytic anemia in which the cells are depleted of oxygen ⁴. The disruption of normal cell function and the inhibition of DNA synthesis are an important part of the antitumor activity of transition metal complexes.

Metabolites of *cis*-platin include platinum complexed to both methionine and glutathione. As mentioned earlier, platinum-methionine adducts were found in the urine of patients undergoing treatment with *cis*-platin¹⁸. L-Methionine contains three potential binding sites, namely a carboxylate, an amine, and a thioether group. The usual modes of binding are monodentate through the sulfur (Figure 11a), bidentate through the sulfur and the nitrogen (Figure 11b), and at low pH's (≤ 0.5) bidentate through the sulfur and oxygen^{19,20}.

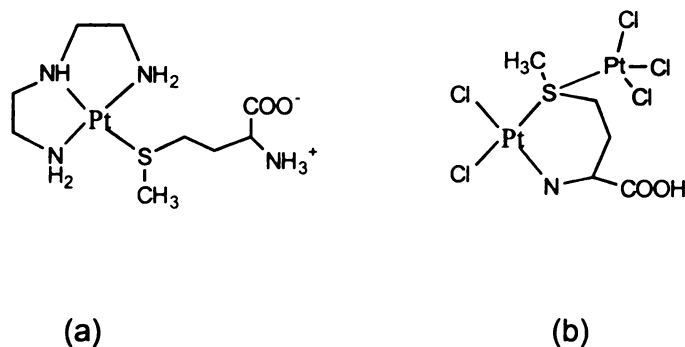


Figure 11. Common binding modes of L-Methionine to a metal center. (a) monodentate through sulfur; and (b) bidentate through sulfur and nitrogen forming a six membered ring.

The crystal structure of a novel cyclic trinuclear structure, [Pt₃(L-Met)₃].H₂O, was recently obtained by Davidson, *et al.* (Figure 12)¹⁸. Crystal structures of [Pt(L-Met)Cl₂], [Pt(Gly-L-Met)Cl], [Pt(L-H₃MetO)Cl₂], and [Pt(L-MetO)₂] have also been obtained. (L-MetO = L-Methionine S-oxide). An example of tridentate binding of L-Methionine to a metal center has been observed in the

complex $[(\eta^5\text{-Cp}^*)\text{Ru}(\text{L-Met})]$, a ruthenocene radiopharmaceutical compound that coordinates methionine through the nitrogen, sulfur and oxygen²² (Figure 13).

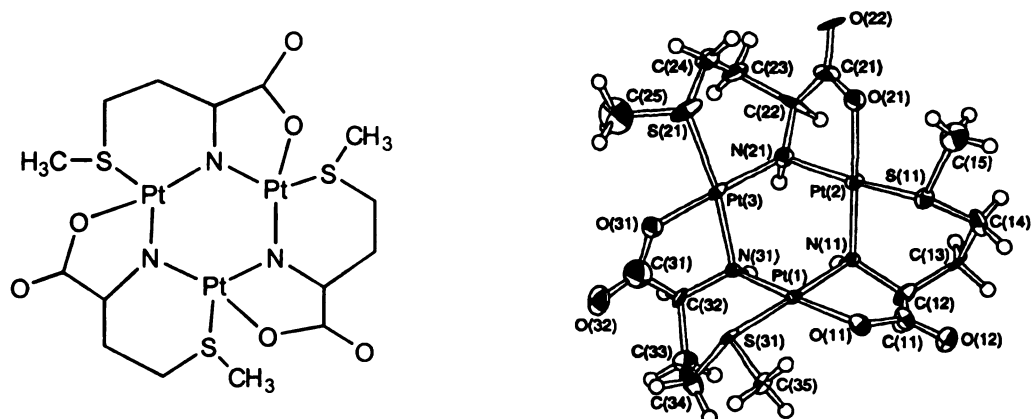


Figure 12. Novel cyclic trinuclear methionine compound.

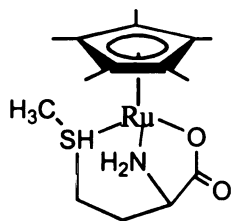


Figure 13. Tridentate binding of Methionine to a Ru center.

Glutathione plays a complex role in the metabolism of metal-based drugs. This tripeptide is the single most important source of intracellular non-protein sulfhydryls, with concentrations ranging from 1-10 mM depending on the cell type²⁰. Levels of glutathione present in the cell have important effects on the metabolism of *cis*-platin. Depletion of glutathione levels results in the increased

toxicity of kidney cells by the platinum drug. Pre-treatment of patients undergoing *cis*-platin therapy with glutathione results in reduced renal toxicity without depleting antitumor activity. It was found that *cis*-platin resistant tumor cells have increased levels of glutathione, and that depletion of the tripeptide levels can reverse this resistance. Intracellular glutathione appears to be involved in attenuating *cis*-platin induced nephrotoxicity, and pre-treatment with glutathione may be useful in protecting the kidneys from *cis*-platin toxicity. With six potential metal binding sites (sulfur, nitrogen from the glutamate amino, two carboxyl oxygens, and two peptide nitrogens) a number of adducts are possible, including bridging structures through the sulfur atom^{20,23-25} (Figure 14).

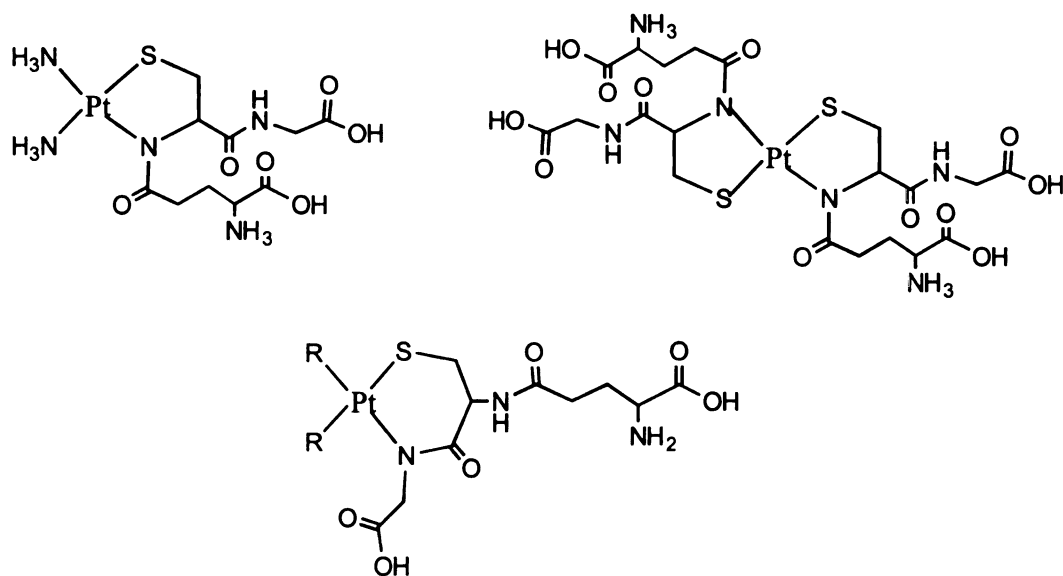


Figure 14. Postulated binding modes of Glutathione to a Pt(II) center.

In attempts to model protein binding of the sulfhydryl group to platinum(II), studies were carried out with the amino acid cysteine. Platination of proteins can occur through cysteine residues. It is thought to bind through the amino nitrogen and the sulfhydryl group to form a N, S- metallacycle. This type of complex has been found to be more thermodynamically stable than a dimetallic bis(μ -thiolato) complex. Possible chelating structures are depicted in Figure 15²⁶⁻²⁸.

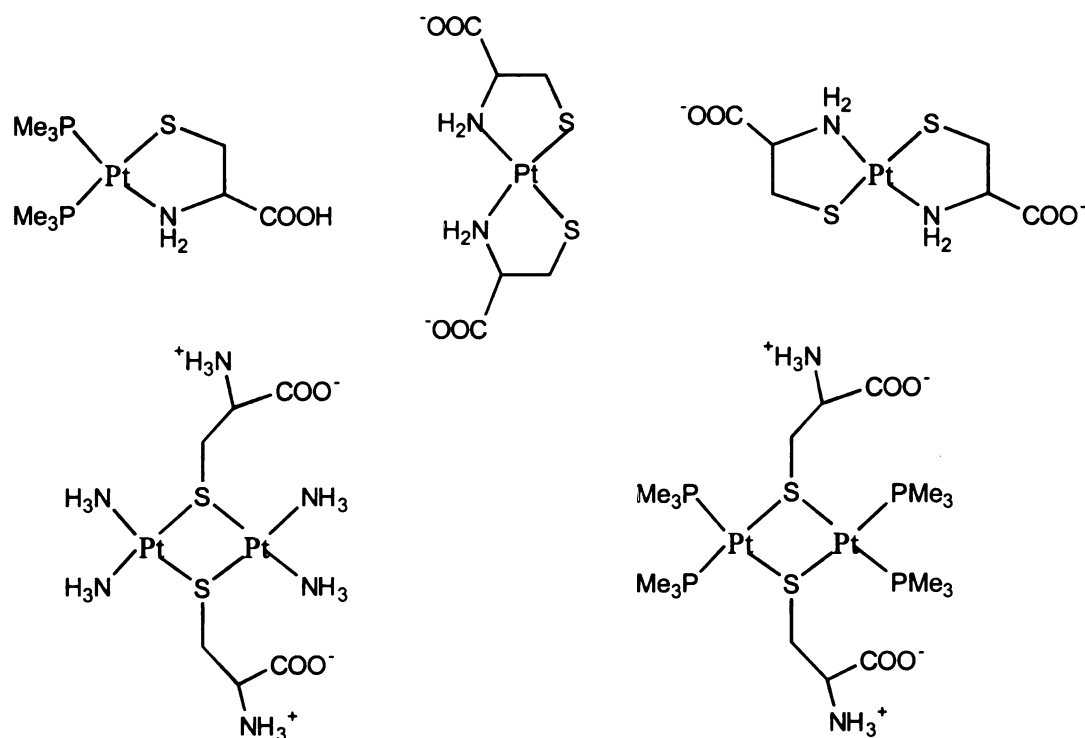


Figure 15. Potential binding modes of L-Cysteine to a Pt(II) center.

Elucidation of the mechanism by which activity occurs is fundamental in the study of any potential antitumor drug. Reactivity studies of the antitumor active compound, dirhodium tetraacetate, $\text{Rh}_2(\text{O}_2\text{CCH}_3)_4 \cdot 2\text{H}_2\text{O}$, with amino acids

have not been studied in detail, and the results that have been reported are not particularly compelling. In early studies with methionine and cysteine, it was thought that methionine reacted by replacing the axial water molecules (Figure 16a). Cysteine, on the other hand, was postulated to result in cleavage of the dirhodium carboxylate core to yield a paramagnetic bis-cysteine complex²⁹⁻³¹ (Figure 16b).

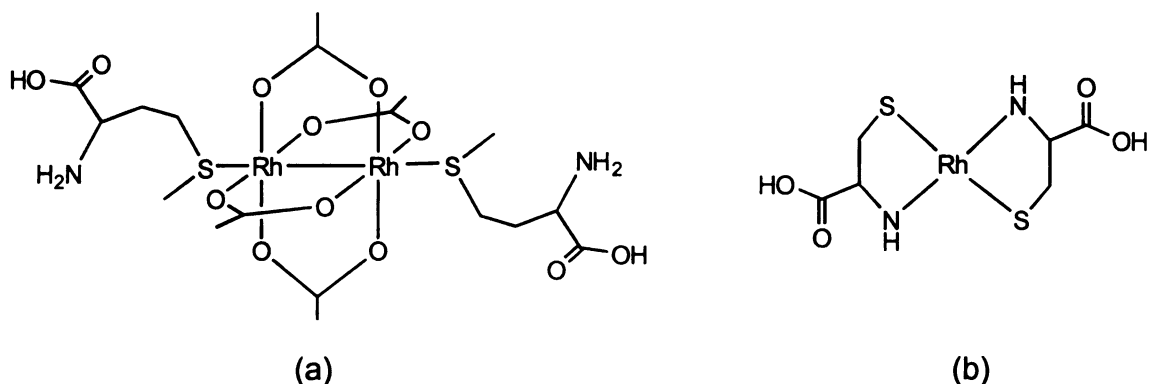


Figure 16. Rhodium tetraacetate products of Methionine (a) and Cysteine (b).

The destruction of the rhodium-rhodium bond was postulated based on the results from experiments aimed at understanding the metabolism of the antitumor compound. In a study involving mice implanted with Erlich ascites tumors, breakdown of the carboxylate cage was determined by the amount of ¹⁴CO₂ exhaled by the mice. Data obtained from injecting mice with ¹⁴C labeled dirhodium tetraacetate indicated that rhodium and ¹⁴C rapidly disappear during the first hour after dose administration and continue to decline for 6 h. It was reported that levels of dirhodium(II) acetate as measured by rhodium content were higher than levels obtained from ¹⁴C content. The conclusions drawn from

these results was that the dirhodium carboxylate cage was breaking down, since the ^{14}C label was being removed more quickly than the rhodium. It was reasoned that decomposition of dirhodium tetraacetate was generating acetate ions, which would be measured by the amount of $^{14}\text{CO}_2$ exhaled. The rhodium would form a nonabsorbable metabolite, thus escaping detection. Based on this study dirhodium(II) tetraacetate was claimed to react *in vivo* with cysteine to form an unstable rhodium complex which breaks down yielding acetate ions, H^+ , and an insoluble precipitate consisting of rhodium(III) and cysteine³³. The reaction of dirhodium tetraacetate with proteins containing an -SH moiety are thought to follow the same general pathway. It is important to point out, however, that the researchers failed to recognize that if the dirhodium tetraacetate led to production of a bis-acetate analog, $\text{Rh}_2(\text{O}_2\text{CCH}_3)_2$, and $2 \text{O}_2\text{CCH}_3^-$, the same results would be obtained from their experiment. We maintain that the evidence cited from this experiment does not irrefutably prove the breakdown of the cage structure.

Reaction of dirhodium tetraacetate with enzymes containing -SH groups lead to inactivation of the enzyme if the -SH group is at or near an active site. The reaction of cysteine with the compound is dramatically different than any other amino acid. This difference stems from the lack of reversible binding which is observed for the other amino acids. The conclusion that cysteine disrupts the carboxylate cage was demonstrated by ^1H NMR spectroscopy at pH 7.5. Addition of cysteine to dirhodium(II) acetate causes a shift in the acetate peak from bound acetate to free acetate. Integration indicates that the reaction is complete at a 1:4 ratio of dirhodium(II) acetate to cysteine. The hypothesis

posed by the researchers is that enzyme inhibition is due to initial interactions between one or more –SH groups and dirhodium(II) carboxylate, followed by cage breakdown and tight binding of rhodium(II) to the active site of the enzyme¹². The tentative conclusion was that the antitumor activity of dirhodium(II) carboxylates is due to the binding of enzymes or proteins containing -SH groups.

The –SH containing tripeptide, glutathione, was used for detoxification in P388 ascites tumors. An increased dose of glutathione was injected after administration of a toxic dose of dirhodium(II) tetrapropionate. This experiment resulted in detoxification of the metal drug along with an enhancement of antitumor activity. It was suggested that decomposition products could be the reason for this increased activity¹³. It is necessary to point out, however, that other possibilities exist, such as the formation of a bis-acetate adduct, or, as observed in the case of the platinum drugs, an amino acid-metal-DNA cross-link.

Due to the lack of solid evidence for the identity of products in dirhodium(II) tetraacetate reactions with amino acids and glutathione, it was deemed necessary to undertake detailed investigations of this chemistry to aid in elucidation of the antitumor action of the dirhodium carcinostatic compounds. The promising anticancer activity of other dimetal carboxylate compounds, such as the dirhodium formamidinate and dirhenium carboxylates prompted the investigation of these compounds as well. Each reaction was performed in bulk as well as in the NMR tube, which were monitored by ¹H NMR spectroscopy

(Chapter 4). The products were characterized by UV-VIS, IR, and NMR spectroscopies, mass spectrometry and elemental analysis when possible.

2. Experimental

A. Synthesis

All reactions were carried out under inert conditions via standard Schlenk line techniques. The dirhodium complexes, $\text{Rh}_2(\text{O}_2\text{CCH}_3)_2\cdot\text{L}_2$ and $[\text{Rh}_2(\text{O}_2\text{CCH}_3)_2(\text{CH}_3\text{CN})_6][\text{BF}_4]_2$ were prepared by literature procedures. The amino acids methionine, glutathione, and cysteine as well as the cysteine mimics, O-Methyl Cysteine and 2-Aminithiophenol, were purchased from Sigma and Aldrich and used without further purification.

Preparation of $\text{Rh}_2(\text{O}_2\text{CCH}_3)_4(\text{MET})_2$ (1)

To a solution of $\text{Rh}_2(\text{O}_2\text{CCH}_3)_4\cdot 2\text{MeOH}$ (0.100 g, 0.2 mmol) in 50 mL DD H_2O , methionine (0.0596 g, 0.4 mmol) was added, which led to a color change from blue-green to dark violet. The reaction was stirred for 24 h at room temperature after which time the volume was reduced to ~ 10 mL on a rotoevaporator and excess acetone was added to precipitate the violet compound. IR (KBr) ν cm^{-1} : 1588 (NH_3^+), 1433, 1600 (COO^-). ^1H NMR (D_2O) δ ppm: 1.71 (s, bound acetate), 1.83 (CH_3), 2.36 (γCH_2), 2.94 (NH_2), 3.79 (αCH). UV-vis spectroscopy (H_2O): λ_{max} = 562 nm (ϵ = 245 $\text{Lmol}^{-1}\text{cm}^{-1}$). Elemental analysis calc'd for $\text{Rh}_2\text{C}_{18}\text{O}_{12}\text{N}_2\text{S}_2\text{H}_{34}$: C, 26.99; H, 4.25; N, 3.93. Found: C, 26.88; H, 4.29; N, 3.67. Electrospray MS: m/z^+ 740 [2 Met + 2 Rh + 4 acetate] $^+$,

681 [2 Met + 2Rh + 3 acetate]⁺, 621 [2 Met + 2Rh + 2 acetate]⁺, 592 [1 Met + 2Rh + 4 acetate]⁺.

Preparation of Rh₂(CYS)₄(H₂O)₄ (2)

To a solution of Rh₂(O₂CCH₃)₄·2MeOH (0.100 g, 0.2 mmol) in 10 mL of DDH₂O, was added 0.8 mmol cysteine, which led to the immediate formation of a rust-brown solution. The solution was stirred for 2 h at room temperature and the volume was reduced to 5 mL on a rotoevaporator. The rust colored product was precipitated by the addition of excess acetone. IR (KBr) ν cm⁻¹: 1615, 1196 (NH₂), 1624, 1390 (COO⁻). ¹H NMR (D₂O) δ ppm: 3.24 (m, β CH₂), 3.95 (α CH). UV-vis spectroscopy (H₂O): λ_{\max} = 586 nm (ϵ = 70 Lmol⁻¹cm⁻¹). Elemental Analysis calc'd for Rh₂C₁₂O₁₀N₂S₂H₁₄: C, 18.91; H, 4.20; N, 7.30. Found: C, 18.95; H, 3.80; N, 7.36. Electrospray MS: m/z⁺ 718 [2Rh + 4 cys + 2 H₂O – 8H], 599 [2Rh + 3 cys + 2 H₂O – 6H], 480 [2Rh + 2 cys + 2 H₂O – 4H], 342.93 [2Rh + 1 cys + 2 H₂O – 2H], 241 [Rh + cys + H₂O – H].

Preparation of Rh₂(O₂CCH₃)₂(GSH)₂(H₂O)₂ (3)

Glutathione (0.246 g, 0.8 mmol) was added to a solution of Rh₂(O₂CCH₃)₄·2MeOH (0.100 g, 0.2 mmol) in 10-15 mL of DD H₂O. After 5 minutes the solution became dark green, and 20 minutes later it became brown with the appearance of a red crystalline precipitate. The solution was stirred overnight at room temperature with no further color change. The precipitate was removed by filtration, and a yellow-orange solid was obtained from the filtrate by the addition of excess acetone. IR (KBr) ν cm⁻¹: 3067, 1610, 1234 (NH₂), 1540 (NH₃⁺), 1648, 1412 (COO⁻). ¹H NMR (D₂O) δ ppm: 1.74 (bound acetate), 2.00

(CH₂) 2.37, 3.15 (CH₂), 3.63 (CH), 3.77 (CH₂), 4.58 (αCH). UV-vis spectroscopy: $\lambda_{\max} = 562 \text{ nm}$ ($\epsilon = 62 \text{ Lmol}^{-1}\text{cm}^{-1}$). Elemental Analysis calc'd for Rh₂C₂₄O₁₈N₆S₂H₂₄: C, 29.56; H, 4.50; N, 8.60. Found: C, 29.48; H, 4.51; N, 8.86. Electrospray MS: m/z⁺ 1054 [2 gsh + 2 Rh + 2 acetate + 5 H₂O -4H], 884 [2 gsh + 2 Rh + acetate], 825 [2 gsh + 2 Rh - 4H].

[Rh₂(O₂CCH₃)₂(CH₃CN)₆][BF₄]₂ + Methionine (4)

Methionine (0.226 g, 0.10 mmol) was added to a solution of dirhodium bis-acetate (0.050 g, 0.050 mmol) in 10 mL of DD H₂O at 25 °C. Upon addition, the color changed to a reddish-orange. The reaction stirred overnight after which the volume was reduced to 5 mL and acetone was added to precipitate the red product. IR (KBr) $\nu \text{ cm}^{-1}$: 3053, 1452 (NH₃⁺), 1620, 1410 (COO⁻). UV-vis spectroscopy: $\lambda_{\max} = 529 \text{ nm}$ ($\epsilon = 154 \text{ Lmol}^{-1}\text{cm}^{-1}$). ¹H NMR $\delta \text{ ppm}$: 2.06 (acetate), 2.10 (βCH₂), 2.47 (CH₃), 2.49 (γCH₂), 3.70 (t, αCH). Elemental Analysis calc'd for Rh₂C₁₄O₁₀N₂S₂H₃₁: C, 22.8; H, 4.1; N, 4.7. Found: C, 21.7; H, 4.4; N, 4.73.

[Rh₂(O₂CCH₃)₂(CH₃CN)₆][BF₄]₂ + Cysteine (5)

Cysteine (0.0398 g, 0.20 mmol) was added to a solution of dirhodium bis-acetate (0.050 g, 0.050 mmol) in 10 mL of DD H₂O at 25 °C. The color immediately changed to dark red and then brown within a few minutes. The reaction was stirred for 2 h, reduced to ~5 mL and treated with acetone to precipitate a dark yellow solid. IR (KBr) $\nu \text{ cm}^{-1}$: 3075, 1539 (NH₃⁺), 1649, 1410 (COO⁻). UV-vis spectroscopy: $\lambda_{\max} = 517 \text{ nm}$ ($\epsilon = 130 \text{ Lmol}^{-1}\text{cm}^{-1}$). ¹H NMR $\delta \text{ ppm}$: 2.05 (s, acetate), 3.15-2.76 (βCH₂), 3.63 (αCH) 3.77, (s, unk). Elemental

Analysis calcd for $\text{Rh}_2\text{C}_{16}\text{O}_{12}\text{N}_4\text{S}_4\text{H}_{26}$: C, 24.8; H, 3.4; N, 7.2. Found: C, 24.0; H, 4.1; N, 6.9.

$[\text{Rh}_2(\text{O}_2\text{CCH}_3)_2(\text{CH}_3\text{CN})_6][\text{BF}_4]_2$ + Glutathione (6)

Glutathione (0.0967 g, 0.20 mmol) was added to a solution of rhodium bis-acetate (0.050 g, 0.050 mmol) in 10 mL of DD H_2O at 25 °C. Upon mixing, the color changed immediately to a dark red-orange. The reaction was stirred overnight, the volume was reduced, and acetone was used to precipitate a brown solid. IR (KBr) ν cm^{-1} : 3100, 1586 (NH_3^+), 1623, 1490 (COO^-). UV-vis spectroscopy (H_2O): $\lambda_{\text{max}} = 515$ nm ($\epsilon = 467$ $\text{Lmol}^{-1}\text{cm}^{-1}$). ^1H NMR (500 MHz, D_2O) δ ppm: 2.02 (acetate), 2.14 (CH_2), 2.51 (CH_2), 2.90-3.22 (βCH_2), 3.88 (CH), 3.94 (CH_2).

$\text{Rh}_2(\text{O}_2\text{CCH}_3)_4$ + O-MeCYS (7)

O-Methyl cysteine (0.1357 g, 0.79 mmol) was added to a solution of $\text{Rh}_2(\text{O}_2\text{CCH}_3)_4$ (100 mg, 0.197 mmol) in 20 mL of DD H_2O under N_2 . Immediately upon addition of the O-methyl cysteine, the solution became yellow; the color gradually changed to orange, and finally became a dark reddish orange. The solution was stirred for 2 h at room temperature, reduced in volume and treated with an excess of acetone to precipitate the product. UV-Vis spectroscopy (H_2O): $\lambda_{\text{max}} = 525$ nm. ^1H NMR (D_2O) δ ppm: 1.82 (s, acetate), 2.15 (acetone adduct), 3.33 (αCH), 3.81 (CH_3), 4.50 (βCH_2).

$\text{Rh}_2(\text{O}_2\text{CCH}_3)_4$ + 2-Aminothiophenol (8)

A solution of $\text{Rh}_2(\text{O}_2\text{CCH}_3)_4 \cdot 2\text{H}_2\text{O}$ (100 mg, 0.197 mmol) in 15 mL CH_3OH , was treated with 0.08 mL of 2-aminothiophenol (0.79 mmol) under an N_2

atmosphere. Immediately upon addition, the solution became a reddish-orange. The reaction was stirred for 2 h at room temperature, the volume was reduced, and excess acetone was added to precipitate the product. Uv-vis spectroscopy: $\lambda_{\text{max}} = 537 \text{ nm}$. $^1\text{H NMR}$ (CD_3OD), δ ppm: 1.85 (s, acetate), 6.89 (t, phenyl), 7.09 (d, phenyl), 7.53 (d, phenyl), 7.65 (t, phenyl).

$[\text{Rh}_2(\text{DTolF})_2(\text{CH}_3\text{CN})_6][\text{BF}_4]_2$ + Methionine (9)

A solution of $[\text{Rh}_2(\text{DTolF})_2(\text{CH}_3\text{CN})_6][\text{BF}_4]_2$ (0.100 g, 0.10 mmol) in 15 mL of CH_3OH was added to a solution of methionine (0.0274 g, 0.2 mmol) in 5 mL of DD H_2O . The resulting solution gradually changed from green to dark grey. EPR spectroscopy shows a broad signal indicative of one unpaired electron $g = 1.87$.

$[\text{Rh}_2(\text{DTolF})_2(\text{CH}_3\text{CN})_6][\text{BF}_4]_2$ + Cysteine (10)

A solution of $[\text{Rh}_2(\text{DTolF})_2(\text{CH}_3\text{CN})_6][\text{BF}_4]_2$ (.100g, 0.1 mmol) in 15 mL of CH_3OH was added to a solution of cysteine (0.446 g, 0.2 mmol) in 15 mL of DD H_2O . The reaction was stirred overnight during which time, the solution became a yellow-orange color. The solution was filtered under N_2 and excess solvent reduced *in vacuo*. IR (KBr) $\nu \text{ cm}^{-1}$: 1580 (N-C-N), 3025, 1052 (NH_3^+), 1622, 1390 (COO^-). $^1\text{H NMR}$ (CD_3OD) δ ppm: 2.03 (CH_3CN), 2.45 (CH_3CN), 2.95 (βCH_2), 3.30 (CH_3), 3.63 (t, αCH), 7.27 (tolyl), 7.32 (tolyl).

$[\text{Rh}_2(\text{DTolF})_2(\text{CH}_3\text{CN})_6][\text{BF}_4]_2$ + Glutathione (11)

A solution of $[\text{Rh}_2(\text{DTolF})_2(\text{CH}_3\text{CN})_6][\text{BF}_4]_2$ (0.050 g, 0.05 mmol) in 15 mL of CH_3OH was added to a solution of glutathione (0.57 g, 0.2 mmol) in 15 mL of DD H_2O . Upon mixing, the solution became olive green and was allowed to stir

overnight. The brown precipitate that formed was collected and washed with CH₃OH. IR (KBr) ν cm⁻¹: 1583 (N-C-N), 3070, 1504 (NH₃⁺), 1616, 1405 (COO⁻).

Re₂(O₂CCH₂CH₃)₄Cl₂ + Methionine (12)

A solution of Re₂(O₂CCH₂CH₃)₄Cl₂ (0.025 g, 0.35 mmol) in 2.5 mL of CH₃OH was added to a solution of methionine (0.1012 g, 0.7 mmol) in 2 mL of DD H₂O. The two solutions were mixed and an additional 2 mL of DD H₂O was added to increase the solubility of methionine. The color changed from orange to bright green and then gradually darkened. The reaction was stirred overnight, after which time a brown solid was collected and washed with DD H₂O.

Re₂(O₂CCH₂CH₃)₄Cl₂ + Cysteine (13)

A solution of Re₂(O₂CCH₂CH₃)₄Cl₂ (0.025 g, 0.35 mmol) in 2.5 mL of CH₃OH was added to a solution of cysteine (0.1644 g, 1.4 mmol) in 2 mL of CH₃OH and 0.5 mL of DD H₂O. Upon mixing, the solution turned green, but within a few seconds the solution became orange, and finally dark brown. The reaction was stirred for 3 h, after which time a brown precipitate was removed by filtration and washed with H₂O.

Re₂(O₂CCH₂CH₃)₄Cl₂ + Glutathione (14)

A solution of Re₂(O₂CCH₂CH₃)₄Cl₂ (0.025 g, 0.35 mmol) in 2.5 mL of CH₃OH was added to a solution of glutathione (0.4174 g, 1.4 mmol) in 3.5 mL of CH₃OH and 0.5 mL of DD H₂O. The resulting mixture became a cloudy green color, then progressed to a light brown color which darkened and took on a reddish hue. After a few minutes, the solution turned dark purple and a precipitate was observed to form. The reaction was stirred for 4 h, after which

time a purple solid was collected. ^1H NMR (D_2O) δ ppm: 2.01 (CH_2), 2.38 (CH_2), 3.14-2.76 (β CH_2), 3.66 (α CH), 4.59 (CH_2). ^{13}C NMR (D_2O) δ ppm: 171.64, 170.46, 169.30 (carboxylate), 50.57 (α CH), 49.37 (CH), 38.50 (CH_2), 35.43 (CH_2), 28.05 (β CH_2), 22.24 (CH_2). Elemental Analysis calc'd for $\text{ReC}_{20}\text{O}_{12}\text{N}_2\text{S}_2\text{H}_{30}$: C, 33.8; N, 11.9; H, 4.7. Found: C, 33.4; N, 12.08; H, 5.50.

B. Xray Structure Determination

A hemisphere of data was collected for compounds (1) and ome, a sphere of data was collected for athph on a Siemens SMART diffractometer at $-100 \pm 2^\circ\text{C}$ with graphite monochromated Mo $\text{K}\alpha$ radiation ($\lambda_\alpha = 0.71073 \text{ \AA}$) and were corrected for Lorentz and polarization effects. The frames were integrated with the Siemens SAINT software package, and the data was corrected for absorption using the SADABS program. The structures were solved using the SHELXS program and refinements were carried out by full matrix least-squares calculations on F^2 using the SHELXL-97 program.

Crystals of $\text{Rh}_2(\text{O}_2\text{CCH}_3)_4(\text{MET})_2$ were obtained from the slow diffusion of a dirhodium tetraacetate solution in acetone into a solution of methionine in water. Several days later, a violet rectangular platelet of dimensions $0.57 \times 0.13 \times 0.16 \text{ mm}$ was obtained. A total of 1321 frames were collected at $-100 \pm 2^\circ\text{C}$ with a scan width of 0.3° in ω and an exposure time of 30 sec/frame from which 45 reflections were selected for indexing. The reflections were refined to give unit cell parameters for an orthorhombic cell. The data collected were integrated using an orthorhombic cell to yield a total of 3983 unique reflections. After data reduction, 2445 unique reflections remained. The R_{int} and R_{sigma} were 0.1198

and 0.1738 respectively. The positions of the rhodium atoms were located by direct methods. The remaining non-hydrogen atoms were located through successive cycles of least-squares refinements and difference Fourier maps. All non-hydrogen atoms were refined anisotropically. The final full matrix least squares reveal maximum and minimum peak heights of 4.86 and -3.06 , respectively with residuals of $R_1 = 0.1777$ and $wR_2 = 0.4222$ for 140 parameters and 1 restraints. The final goodness of fit was 2.609.

Crystals of the dirhodium tetraacetate O-methyl cysteine derivative (7) were obtained from the slow diffusion of a dirhodium tetraacetate solution in acetone into a solution of O-methyl cysteine in water. Several days later, a red rectangle of dimensions $0.18 \times 0.05 \times 0.08$ mm was obtained. A total of 1321 frames were collected at -100 ± 2 °C with a scan width of 0.3° in ω and an exposure time of 30 sec/frame from which 57 reflections were selected for indexing. The reflections were refined to give unit cell parameters for a tetragonal cell. The data collected were integrated using a tetragonal cell to yield a total of 5165 unique reflections. After data reduction, 2727 unique reflections remained. The R_{int} and R_{sigma} were 0.1087 and 0.3332 respectively. The positions of the rhodium atoms were located by direct methods. The remaining non-hydrogen atoms were located through successive cycles of least-squares refinements and difference Fourier maps. All non-hydrogen atoms were refined anisotropically. The final full matrix least squares reveal maximum and minimum peak heights of 0.72 and -0.84 , respectively with residuals of $R_1 = 0.0509$ and

$wR_2 = 0.1412$ for 127 parameters and 3 restraints. The final goodness of fit was 0.578.

Crystals of the dirhodium tetraacetate 2-aminothiophenol derivative (8) were obtained from the slow diffusion of a dirhodium tetraacetate solution in acetone into a solution of 2-aminothiophenol in methanol. Several days later, a red rectangle of dimensions 0.518 x 0.104 x 0.181 mm was obtained. A total of 6345 frames were collected at -100 ± 2 °C with a scan width of 0.3 ° in ω and an exposure time of 30 sec/frame from which 63 reflections were selected for indexing. The reflections were refined to give unit cell parameters for a triclinic cell. The data collected were integrated using a triclinic cell to yield a total of 16335 unique reflections. After data reduction, 7810 unique reflections remained. The R_{int} and R_{sigma} were 0.0657 and 0.1511 respectively. The positions of the rhodium atoms were located by direct methods. The remaining non-hydrogen atoms were located through successive cycles of least-squares refinements and difference Fourier maps. All non-hydrogen atoms were refined anisotropically. The final full matrix least squares reveal maximum and minimum peak heights of 5.72 and -4.21 , respectively with residuals of $R_1 = 0.3532$ and $wR_2 = 0.5761$ for 1137 parameters and 2 restraints.

3. Results and Discussion

A. Dirhodium Tetraacetate Reactions

The reactions of dirhodium carboxylate compounds with different types of axial donors lead to color changes that are useful for the identification of

derivative compounds. With oxygen donors such as water or methanol, the complex takes on a blue or green color. The axial binding of nitrogen or sulfur donors causes the compound to be red to orange in color, whereas with phosphorous donors, a red to yellow color ensues. There are two transitions that are important for these compounds, one at ~600 nm and one at ~450 nm. The 600 nm band is a transition assigned to Rh-Rh π^* - Rh-Rh σ^* . This band is most sensitive to changes in the axial ligands. It remains essentially constant for oxygen donors and becomes blue-shifted with nitrogen or sulfur donors. The band at 450 nm is due to more than one transition, one of which is the Rh-Rh π^* - O σ^* transition. Obviously, it is sensitive to changes in the equatorial ligands, but it shows little or no change with different axial donors³³. The color of the dirhodium carboxylate derivatives, which is due to the visible transition at ~600 nm is a convenient characterization aid when amino acids are used as ligands.

Infrared spectroscopy is also a useful tool for the characterization of dirhodium tetraacetato-amino acid complexes. The amino acids contain three groups that can be used as probes to determine the binding site(s) of the amino acid to the dirhodium compound (Table 1)³⁴. Uncoordinated amino groups exhibit peaks in the range of 1585-1683 cm^{-1} and 1492-1534 cm^{-1} , whereas coordinated amino groups are shifted to 1610-1620 cm^{-1} and 3090-3340 cm^{-1} . This indicates that the amino group is participating in bonding with the metal. The S-C stretch is present around 2500 cm^{-1} , which is dramatically shifted to higher frequencies upon metal binding to the sulfur. The carboxylate group shifts are also useful for determining whether or not the carboxylate group is

participating in binding. For the amino acid complexes with dirhodium tetraacetate, however, the carboxylate modes from the dirhodium compound (1589 and 1440 cm^{-1}) and the amino acid carboxylate peaks (ranging from 1597-1610 cm^{-1} and 1410-1415 cm^{-1}) overlap with each other, thus making it difficult to ascertain if carboxylate binding has occurred.

In order to fully characterize these compounds, numerous factors must be taken into account. The electronic spectral properties are important, but they do not always give the entire picture. Along with these tools, ^1H NMR spectroscopy is used to account for peak shifting near the proposed binding site. Elemental analyses and mass spectrometry were performed in some cases to help determine the nature of the product formed. When possible, X-ray analyses were used to determine the structures of the compounds.

$\text{Rh}_2(\text{O}_2\text{CCH}_3)_4$ + Methionine (1)

The compound formed in this reaction is thought to be a simple 1:2 axial adduct of $\text{Rh}_2(\text{O}_2\text{CCH}_3)_4$ ²⁹. An instantaneous reaction takes place upon addition of the amino acid to dirhodium tetraacetate, accompanied by a color change from blue-green to violet. This color change indicates that either a nitrogen or sulfur donor is bound in the axial position. The electronic spectral data are in accord with axial binding of a nitrogen or sulfur donor as the visible transition is blue-shifted from $\lambda_{\text{max}} = 585$ for dirhodium tetraacetate³³. Based on the pKa's for the possible binding sites of the amino acid (Figure 17), the most likely donor is the nitrogen, however, the sulfur atom has the highest affinity toward the rhodium atom.

Table 1. IR stretches used in the determination of amino acid binding sites.

<u>Functional Group</u>	<u>IR Stretch (cm⁻¹)</u>
NH₂	
Coordinated	3230-3340
	3090-3280
	1610-1620
	1023-1060
Uncoordinated	1585-1683
	1492-1534
	1110-1237
COO⁻	
Coordinated	1589-1643
	1347-1411
Uncoordinated	1597-1610
	1410-1415
Tetraacetate	1589
	1440

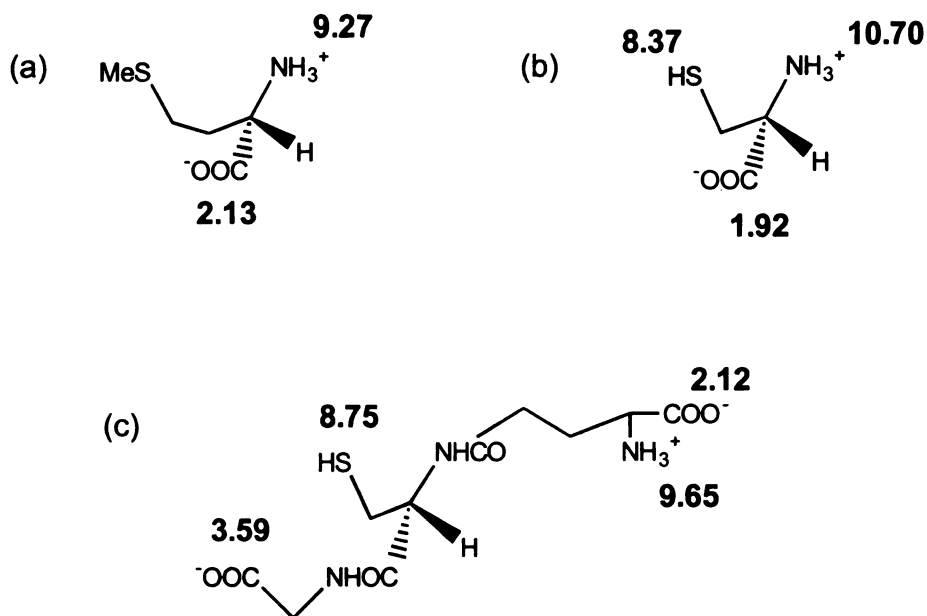


Figure 17. pK_a values for the common binding sites on (a) methionine, (b) cysteine, and (c) glutathione.

The infrared spectra of the compound shows that the amino acid is coordinated through only one functional group. A stretch at 1588 cm⁻¹ indicates the presence of an uncoordinated amino group. With this binding site ruled out, the sulfur and carboxylate groups are the best prospects for binding. The S-C stretch has shifted, an indication that the sulfur is involved in binding. Carboxylate peaks occur at 1433 and 1600 cm⁻¹, which are located at the positions for uncoordinated carboxylates. These data point to a simple axial adduct bound through the sulfur atom.

The characterization of dirhodium-amino acid derivatives by ¹H NMR spectroscopy is useful for predicting the binding site of the amino acid. The

amino acid groups nearest the dirhodium binding should exhibit the greatest shift in the spectrum. Methionine peaks indicate a change in the electronic environment near the sulfur atom. The protons next to the sulfur, γCH_2 and CH_3 , show the greatest downfield shift. These data indicates that the sulfur, rather than the amino or carboxylate groups, participates in binding to the metal.

Once the binding site is determined, the next step is to identify the exact structure of the compound formed in the reaction. Elemental analysis and electrospray mass spectrometry were used to confirm the formulation as a 2:1 axial adduct. The electrospray MS data show a peak at m/z^+ 740, which corresponds to two rhodium atoms, two methionine molecules, and four acetate ions. Further support is lent by the elemental data, which corresponds to the formula $\text{Rh}_2(\text{O}_2\text{CCH}_3)_4(\text{Met})_2$ (Figure 18).

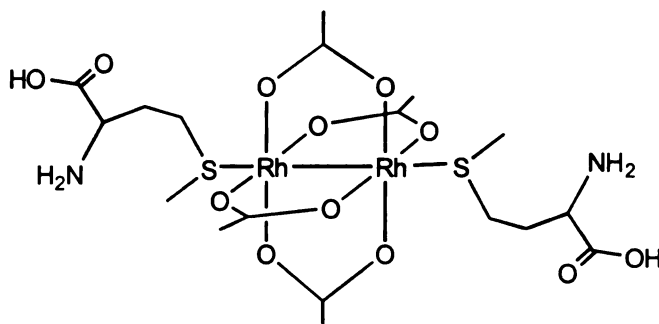


Figure 18. Structure of the 2:1 adduct formed in the reaction of methionine with dirhodium tetraacetate.

An ORTEP representation of $\text{Rh}_2(\text{O}_2\text{CCH}_3)_4(\text{Met})_2$ which crystallizes in the orthorhombic space group $\text{P2}_1\text{22}_1$ is depicted in Figure 19. The structure depicts

a dirhodium tetraacetate core with two axially bound methionine ligands. The rhodium-rhodium bond length is 2.44 Å which is longer than the corresponding dirhodium tetraacetate bis water adduct which has a rhodium-rhodium bond length of 2.386(1) Å. This structure was not completely solved due to a twinning problem. Looking at the systematic absences, it is apparent that the space group is $P2_122_1$, however, further refinement in a twinning program is needed to fully solve the structure. The final R was 17.7%.

$Rh_2(O_2CCH_3)_4 + \text{Glutathione (3)}$

If -SH containing biomolecules destroy the dinuclear unit of $Rh_2(O_2CCH_3)_4$ as has been suggested in the early literature, then glutathione should be capable of effecting this type of decomposition as well. Upon reaction of glutathione with dirhodium tetraacetate, a yellow-orange compound is formed. The yellow-orange color of this compound indicates a possible sulfur or nitrogen binding to the metal center. Ultraviolet-visible spectroscopy revealed the presence of a band at 582 nm and a shoulder at ~440 nm. This suggests that the nature of the equatorial ligand has changed while the axial ligand has remained the same.

Infrared analysis shows that the glutathione molecule is coordinating through more than one binding site. The spectra reveal the presence of both coordinated (3067 and 1610 cm^{-1}) and uncoordinated (1540 cm^{-1}) amino groups. The S-C stretch has shifted such that it overlaps with another peak, indicating that sulfur is involved in binding as well. Carboxylate peaks appear at 1648 and 1412 cm^{-1} , not clearly indicating the presence of carboxylate binding, or lack thereof. It appears that both amino groups and the sulfur are involved in binding

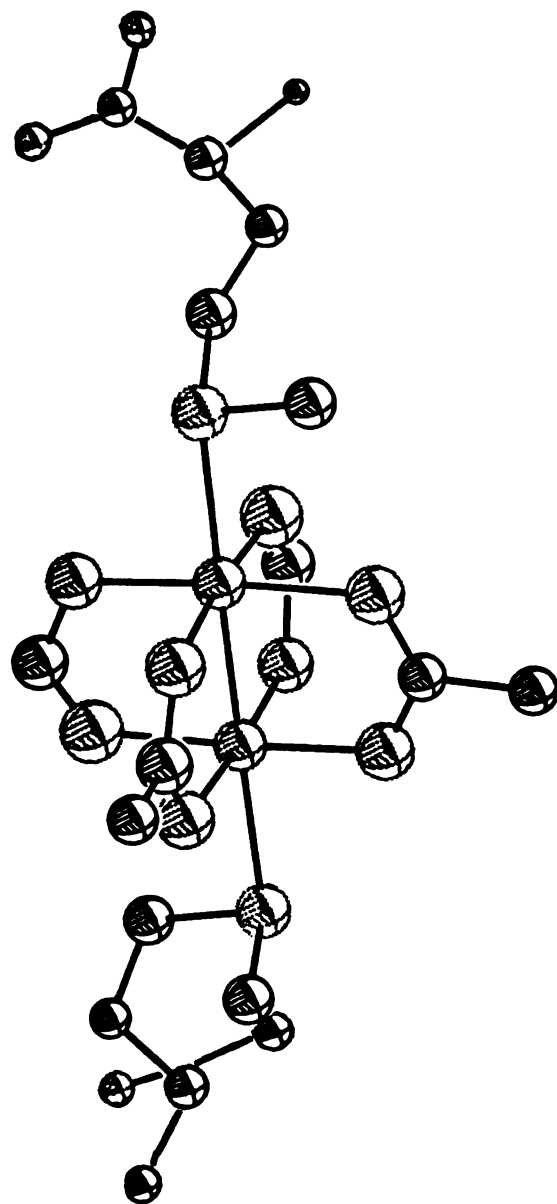


Figure 19. ORTEP representation of $\text{Rh}_2(\text{O}_2\text{CCH}_2)_4(\text{MET})_2$.

to the metal center. The most probable binding modes are indicated in Figure 20.

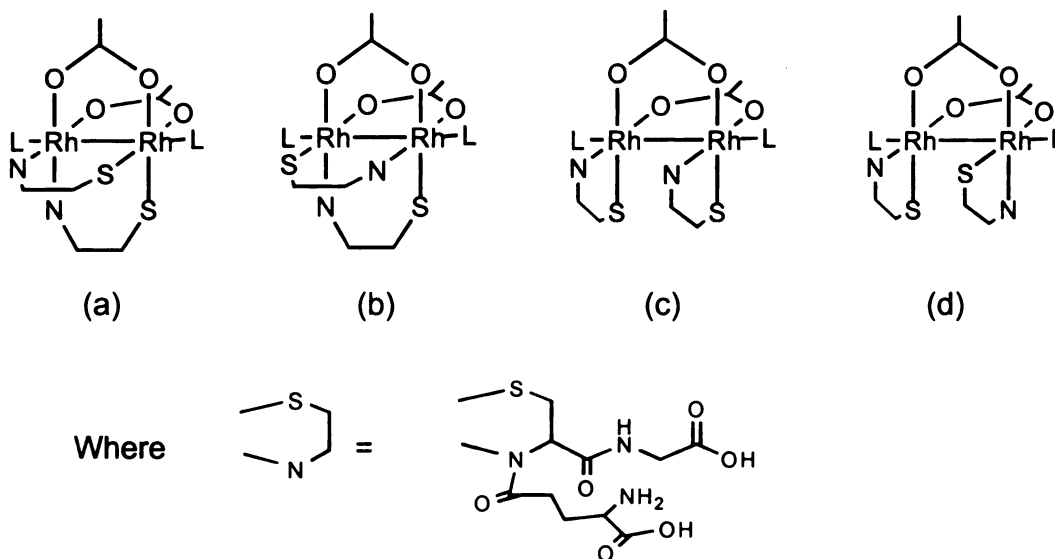


Figure 20. Possible binding modes of glutathione to dirhodium tetraacetate.

^1H NMR data indicate shifts in the proton resonances closest to the sulfhydryl group. The γCH_2 peak shifts by the greatest amount and splits into a quartet of doublets. This indicates a change in the environment of the protons nearest the sulfur atom. The data point to a type of bis-chelating/bidentate interaction between glutathione and dirhodium tetraacetate. The presence of an electronic transition at 582 nm suggests that the Rh-Rh bond is still intact, however further analysis is needed to fully understand the nature of binding that had occurred.

Elemental analysis and mass spectrometry were performed in order to aid in the identification of the new compound. Electrospray MS shows the presence of a peak at 1054 m/z^+ , which corresponds to two rhodium atoms, two

glutathione molecules, two acetate ions, five water molecules and four H⁺ ions. Elemental analysis further supports the MS data, and leads to a formulation of Rh₂(O₂CCH₃)₂(Gsh)₂(H₂O)₄. These findings are not in accordance with the accepted notion that all –SH containing biomolecules destroy the dirhodium unit. As can be ascertained from the above data, the rhodium-rhodium bond is indeed intact, with two acetates being substituted by two glutathione molecules.

Rh₂(O₂CCH₃)₄ + Cysteine (2)

In attempts to debunk early reports that cysteine, possessing the –SH moiety, leads to mononuclear compounds^{11,12,29,32}, the reaction with dirhodium tetraacetate was performed. This reaction is not as biologically relevant as the glutathione reaction, since both the amino and carboxylate groups are free instead of bound, as would be the case in a protein. The formation of a rust colored product does not fit into the color scheme for a simple axial donor of nitrogen or sulfur based on earlier electronic spectral reports, leaving open the possible equatorial binding mode of either a nitrogen or sulfur donor (Figure 21). Electronic spectral data revealed a transition at $\lambda_{\text{max}} = 586 \text{ nm}$, suggesting that the dirhodium bond is still intact and the axial donor is an oxygen atom.

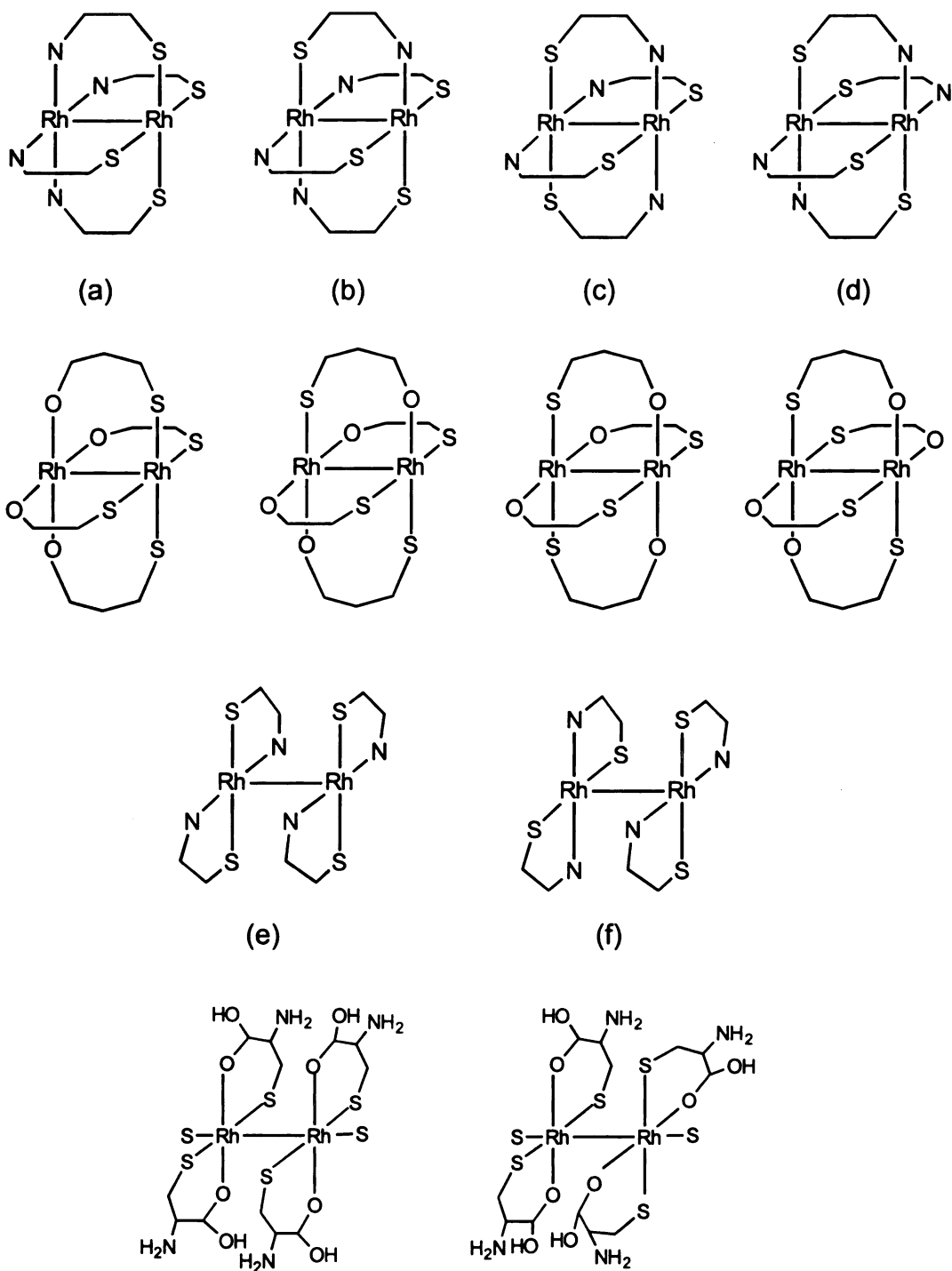


Figure 21. Possible binding modes of cysteine.

In an attempt to understand the nature of binding in the compound, an electronic spectral study was undertaken (Figure 22). Up to eight equivalents of cysteine were added to a solution of dirhodium tetraacetate. The presence of the band at ~580-600 was unaltered, leading one to conclude that the dinuclear core was still intact. With the addition of each successive equivalent, the ~450 nm transition became more blue shifted until it became a shoulder on another peak. These results suggest that the equatorial ligands are being replaced by cysteine.

Infrared data reveal the presence of two types of binding for cysteine. Amino peaks appear in the spectra at 1615 and 1196 cm^{-1} , which could indicate either coordinated or uncoordinated amino groups. The S-C stretch has shifted into a neighboring peak. As usual, the carboxylate modes do not clearly indicate the presence or absence of binding. Stretches at 1624 and 1390 cm^{-1} could indicate that the carboxylate group is coordinated, but, overlap of peaks in this region renders a definitive assignment difficult. What is clear, however, is that the sulfhydryl group is involved in some type of binding to the metal center.

Due to the difficulty in deciding the nature of this compound, elemental analysis and electrospray mass spectrometry were performed. Elemental data support the formulation $\text{Rh}_2(\text{Cys})_4(\text{H}_2\text{O})_2$. Electrspray MS results show a peak at m/z^+ 718 that can be assigned to two rhodium atoms, four cysteine molecules, two water molecules and eight H^+ ions. These data indicate that cysteine does not destroy the dinuclear unit, but that it replaces all four acetate ligands.

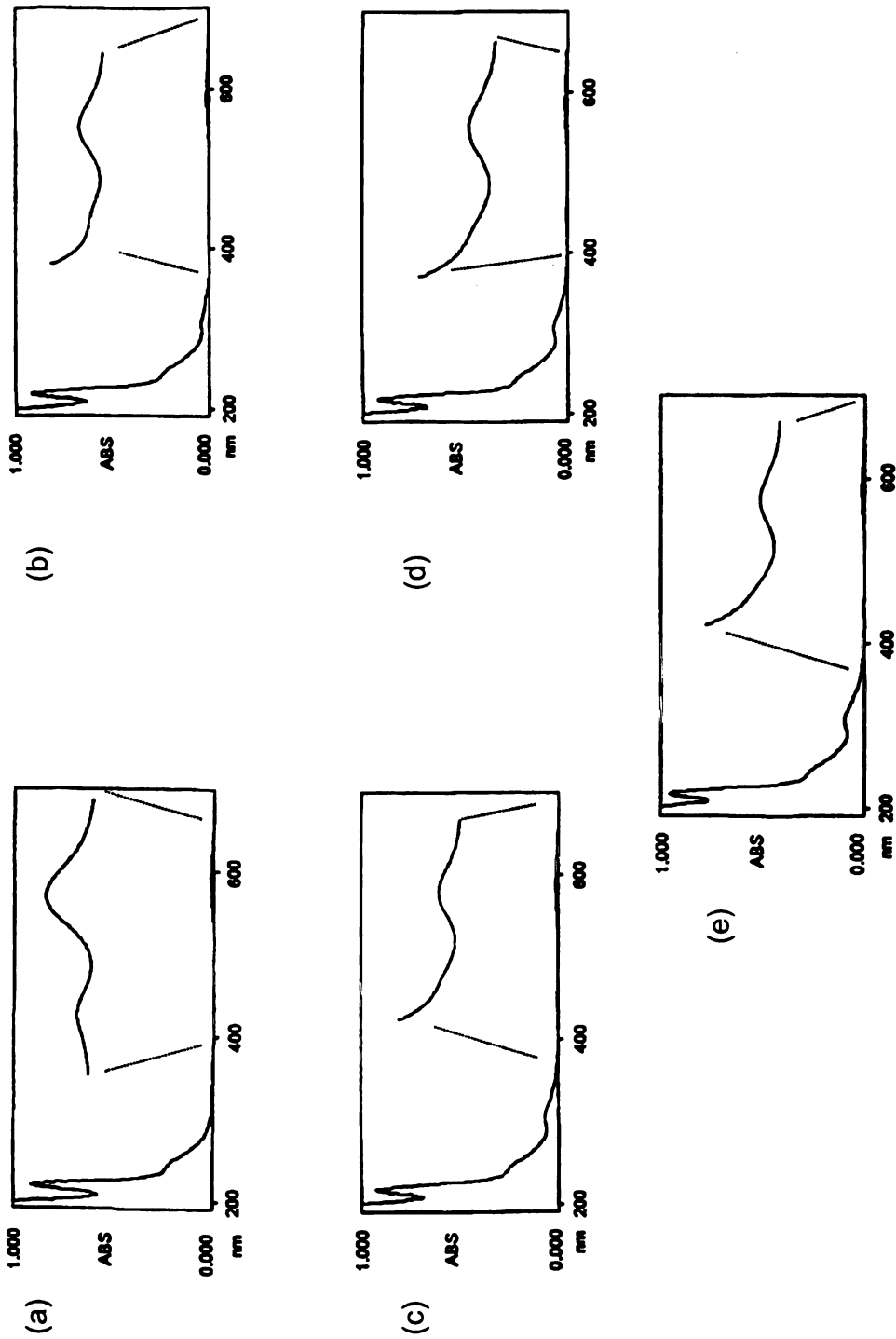


Figure 22. UV spectral study (a) dirrhodium tetraacetate, (b) 1:1 ratio, (c) 1:2 ratio, (d) 1:3 ratio, and (e) 1:4 ratio.

B. $[\text{Rh}_2(\text{O}_2\text{CCH}_3)_2(\text{CH}_3\text{CN})_6]^{2+}$ Reactions

Since the dirhodium compounds previously studied in our labs reveal that DNA purines are capable of replacing two bridging carboxylate ligands³⁶, the dirhodium bis-acetate reactions were explored with amino acids. The replacement of two acetate groups signifies that the active form of the compound may be the bis-acetate adduct. If the –SH containing amino acids are going to destroy the carboxylate cage, the breakdown should occur more quickly with two of the four acetates already released.

$[\text{Rh}_2(\text{O}_2\text{CCH}_3)_2(\text{CH}_3\text{CN})_6]^{2+}$ + Methionine (4)

Methionine was added to a solution of dirhodium bis-acetate in a 2:1 ratio, as in the case for the tetraacetate reaction. We anticipated that the product would not be a simple axial adduct, since solvated equatorial binding sites are available in addition to the axial positions. The product resulting from this reaction is red in color. The electronic absorption data show a band at 529 nm, which represents a shift of ~38 nm from the parent bis-acetate compound.

Infrared data reveal more about the nature of the product. The presence of uncoordinated amino groups at 1452 cm^{-1} lead to the conclusion that the amino group does not participate in binding. Carboxylate peaks at 1620 and 1410 cm^{-1} are not particularly helpful about lending insight into binding modes, but they are in the range for coordinated carboxylate groups. The parent compound, dirhodium bis-acetate, shows an intense stretch due to the $[\text{BF}_4]^-$ anion, which is absent in the methionine complex. This would suggest the

formation of a neutral compound, since the counterions are no longer present. The net charge on the methionine ligands would then be 1⁻.

¹H NMR spectroscopy measured on the dirhodium bis-acetate products do not aid in the determination of the binding site(s) of the methionine ligand. Each of the proton resonances exhibits a shift as compared to the free amino acid. It would be expected that the CH₃ and γCH₂ would shift the most, however, since the amino acid is presumably binding through two functional groups this would result in shifting of the αCH and βCH₂ resonances as well.

Due to the lack of hard evidence for the exact nature of this product, elemental analysis was obtained to determine the number of methionine ligands bound to the bis-acetate core. The results are in accord with the formula, Rh₂(O₂CCH₃)₂(Met)₂(H₂O)₂. Based on the pK_a values (Figure 17) for the free amino acid, the most likely binding sites are through the nitrogen and sulfur atoms, but IR data does not support this conclusion. It appears that the carboxylate oxygen and sulfur atoms participate in binding instead (Figure 23).

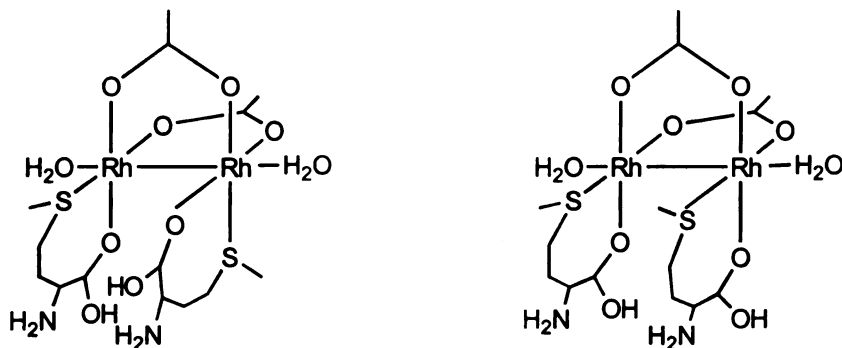


Figure 23. Possible binding modes of methionine to dirhodium bis-acetate.

[Rh₂(O₂CCH₃)₂(CH₃CN)₆]²⁺ + Cysteine (5)

If cysteine destroys the dirhodium unit, it should break down the bis-acetate cage as well. The product from this reaction is dark yellow, a slightly different color than the dirhodium tetraacetate product. The visible spectrum shows a band at 517 nm, shifted from the 567 nm band of the parent compound.

IR data show the usual shifting of the S-C stretch, indicating that sulfur is binding to the metal center. Amino stretches appear at 3975 and 1539 cm⁻¹ indicating possible coordination to the metal. Carboxylate peaks are at 1649 and 1410 cm⁻¹, indicating that this functional group is a possible binding site as well. As was the case for the methionine derivative, the [BF₄]⁻ anions are absent in the cysteine product, leading to the conclusion that the cysteine groups have a net charge of 1⁻.

¹H NMR spectroscopy was performed in order to determine the binding modes of the amino acid. Both the αCH and βCH₂ resonances shift upon coordination to the bis-acetate compound. As was the case for the dirhodium tetraacetate cysteine derivative, the βCH₂ protons are present in a quartet of doublets which appears to be a common occurrence in NMR spectra of dirhodium complexes bound to both glutathione and cysteine.

Elemental analysis was performed to determine the number of cysteine molecules bound to the dirhodium core. The data indicate that the likely formula for the product of this reaction is Rh₂(O₂CCH₃)₂(Cys)₂ (Figure 24). It appears that the reaction of cysteine with dirhodium bis-acetate does not break the dinuclear core as was reported for the corresponding tetraacetate reaction.

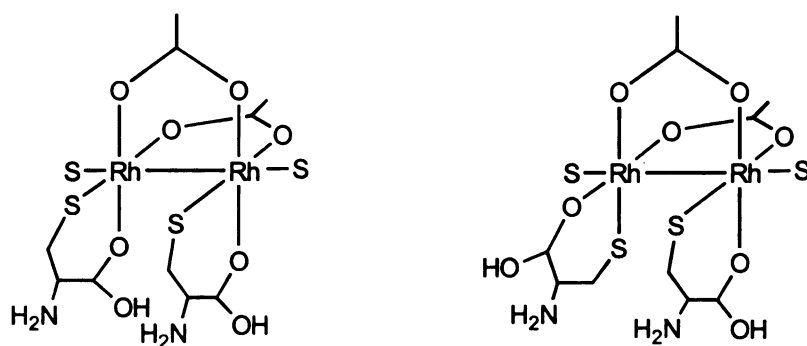


Figure 24. Proposed structures for the products of the reaction between cysteine and dirhodium bis-acetate (S = solvent).

$[\text{Rh}_2(\text{O}_2\text{CCH}_3)_2(\text{CH}_3\text{CN})_6]^{2+} + \text{Glutathione (6)}$

Glutathione was added to rhodium tetraacetate in a 4:1 ratio, and the resulting solid was brownish-red, unlike the product obtained from dirhodium tetraacetate. Since glutathione does not destroy the metal-metal bond in dirhodium tetraacetate reactions, it seemed unlikely that it would cause the bis-acetate to break down. A transition at 515 nm is observed in the visible spectrum, which is shifted from 567 nm of the bis-acetate precursor complex.

Infrared analysis show sulfur binding has occurred according to the shift of the S-C stretch. Amino stretches appear at 3100 and 1586 cm^{-1} , indicating the possibility of coordination. Once again, the stretches of the carboxylate groups at 1623 and 1490 cm^{-1} , do not provide definitive evidence for or against coordination. Unlike the methionine and cysteine cases, the B-F stretch in the

[BF₄]⁻ anion is present at 1085 cm⁻¹. This indicates that the glutathione molecules do not neutralize the charge on the rhodium atoms.

The binding sites appear to be through the sulfur and the amino group, which would give a five membered ring. By ¹H NMR spectral analysis, the peak shifts correspond to the proposed product (Figure 20). The proton resonances shift most for the gsh1 and gsh2 peaks. The quartet of doublets appears as expected and is assigned to gsh3.

C. Cysteine Mimic Reactions

As a result of the controversy surrounding the stability of the dirhodium tetraacetate core in the presence of -SH containing molecules, cysteine mimics were explored. These molecules, O-methylcysteine and 2-aminothiophenol, were chosen because they contain the SH-C-C-NH₂ moiety. Since the mimics contain the same reactive sites as cysteine, the reactions should proceed in a similar manner. These molecules are soluble in a variety of organic solvents, therefore the chemistry is not limited to reactions in water.

The reactions appeared to follow that of cysteine, with the solutions becoming dark upon addition of the ligand. The compounds are nearly the same color as the cysteine derivatives, but the similarities end there. Electronic spectral analyses of the compounds reveal transitions at 525 nm for the O-MeCys product and 537 nm for the 2-AThPh compound. ¹H NMR data show the presence of bound acetate as well as aromatic peaks for the phenol ring of 2-AThPh. The O-MeCys product exhibits an acetate peak and the O-MeCys peaks. The presence of bound acetate in the NMR spectra suggest that these

mimics do not behave in the same manner as cysteine with dirhodium tetraacetate. This could be due to a chelation through the O and S functional groups, rather than the N and S functional groups as previously thought for cysteine (Figure 25).

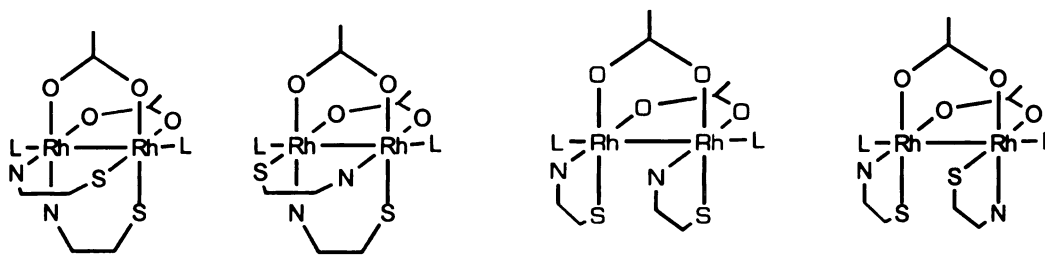
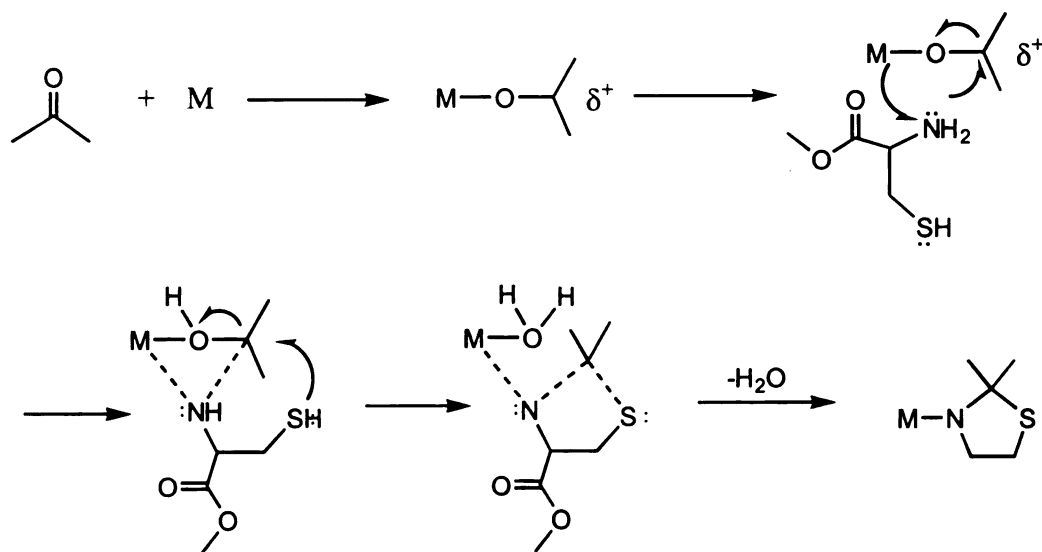


Figure 25. Possible binding modes of the cysteine mimics, O-Methyl cysteine and 2-aminothiophenol, to dirhodium tetraacetate. N-C-C-S = cysteine mimic.

Compound (7) crystallizes in the tetragonal space group $P4(3)$ with the asymmetric unit consisting of a dirhodium tetraacetate unit and one O-methyl cysteine ligand (Figure 27). The rhodium-rhodium bond length is 2.41(3) Å which is longer than the corresponding parent compound bond length, this could be due to stronger interactions of the axial sulfur and nitrogen donors which are coordinated at Rh-N distance of 2.40(2) Å and a Rh-S distance of 2.53(5) Å.

A PLUTO representation of compound (8) which crystallizes in the triclinic space group $P-1$ is presented in Figure 28. The structure consists of two dirhodium tetraacetate units linked together by a 2-aminothiophenol ligand through the sulfur and the nitrogen atoms. From the unit cell, it is apparent that

(a)



(b)

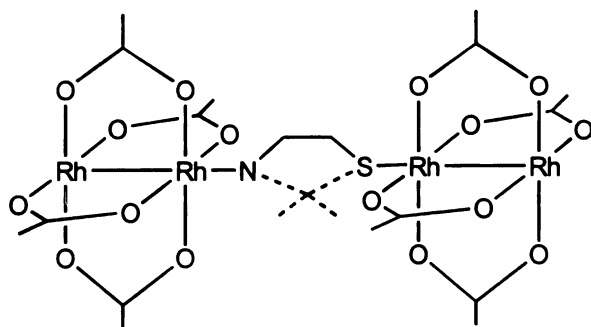


Figure 26. (a) Proposed mechanism for the insertion reaction that takes place with the cysteine mimics in the presence of acetone, (b) structure of the products formed via this mechanism.

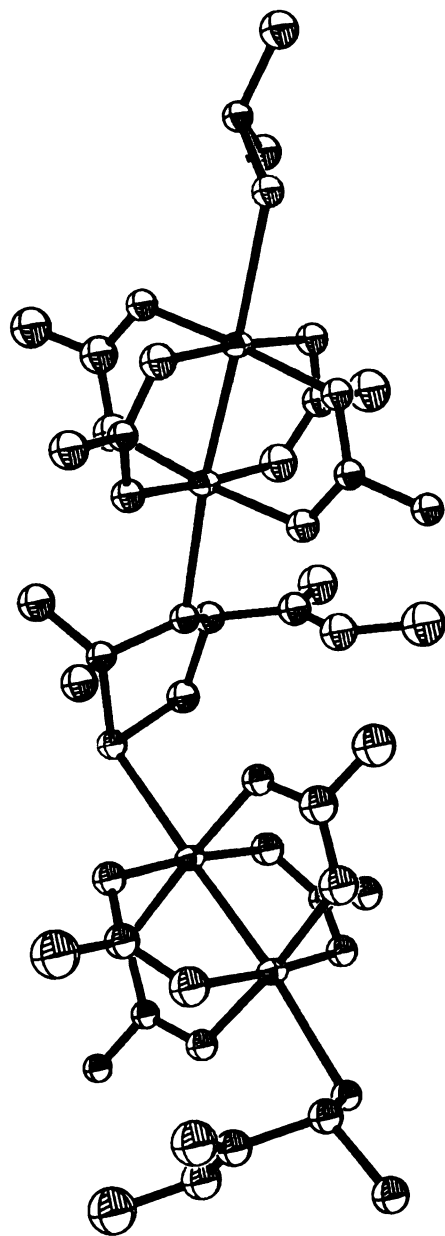


Figure 27. ORTEP of the O-methyl cysteine product of dirhodium tetraacetate.

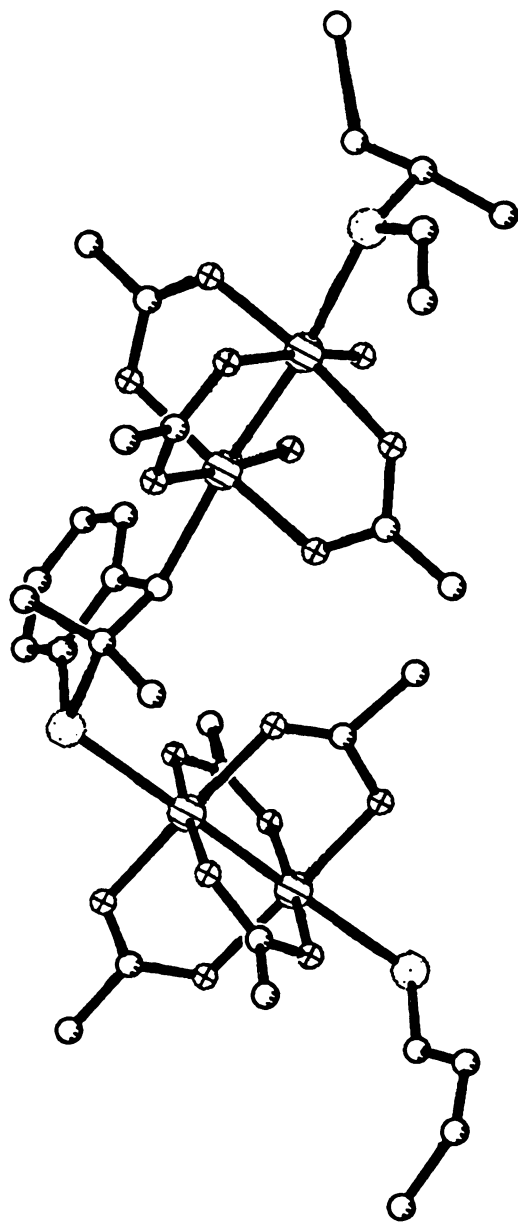


Figure 28. PLUTO of 2-aminothiophenol derivative of dirhodium tetraacetate.

the structure is a twin therefore, additional twinning parameters will need to be used in order to fully solve this structure.

D. $[\text{Rh}_2(\text{DTolF})_2(\text{CH}_3\text{CN})_6][\text{BF}_4]_2$ Reactions

The partially solvated complex, $[\text{Rh}_2(\text{DTolF})_2(\text{CH}_3\text{CN})_6][\text{BF}_4]_2$ was used in place of its parent complex, $\text{Rh}_2(\text{DTolF})_2(\text{O}_2\text{CCF}_3)_2$. Since the ditolylylformamidinate trifluoroacetate compound has been found to lose two trifluoroacetate groups, it seemed logical to begin with the solvated compound that would be present *in vivo*. Naturally, this connotes that the CH_3CN ligands will be replaced by H_2O in aqueous media.

$[\text{Rh}_2(\text{DTolF})_2(\text{CH}_3\text{CN})_6][\text{BF}_4]_2$ + Methionine (9)

Two equivalents of methionine were added to the partially solvated dirhodium bis-formamidinate compound. The solution changed from green to dark grey. This grey color for dirhodium complexes is typically an indication of a paramagnetic species. EPR spectroscopy was performed, and indeed a broad signal at $g = 1.87$ was found. Elemental analysis was performed on the product and the results point to the formula $\text{Rh}_2(\text{DTolF})_2(\text{Met})_2(\text{H}_2\text{O})_2$ (Figure 29).

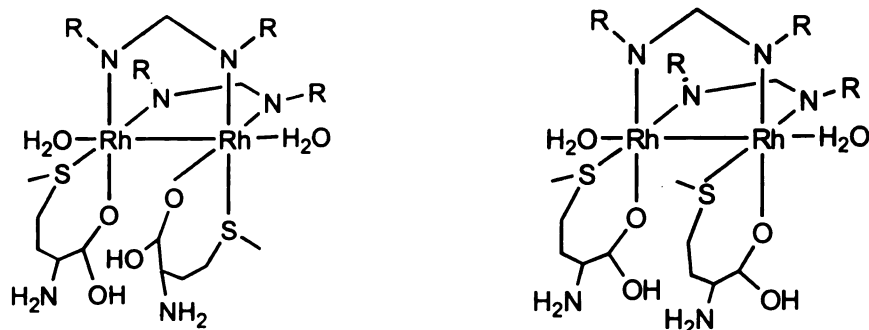


Figure 29. Possible binding modes of methionine to the partially solvated dirhodium ditolylformamidinate (DTolF) complex. (R = tolyl)

[Rh₂(DTolF)₂(CH₃CN)₆][BF₄]₂ + Cysteine (10)

Four equivalents of cysteine were added to the partially solvated dirhodium formamidinate compound. The color of the compound is yellow-orange, which is similar to the colors of the other cysteine products. Infrared spectroscopy shows the absence of an S-C stretch, as is expected for sulfur binding. The N-C-N bend is observed at 1580 cm⁻¹, which indicates that the bridging ligands are still in place. Uncoordinated amino peaks appear at 1052 cm⁻¹. Carboxylate peaks appear at 1622 and 1390 cm⁻¹, indicating that the carboxylate groups are coordinated. ¹H NMR spectroscopy shows shifts in both the αCH and βCH₂ proton resonances, as is expected upon cysteine coordination to a dirhodium center. Proposed products are depicted in Figure 30.

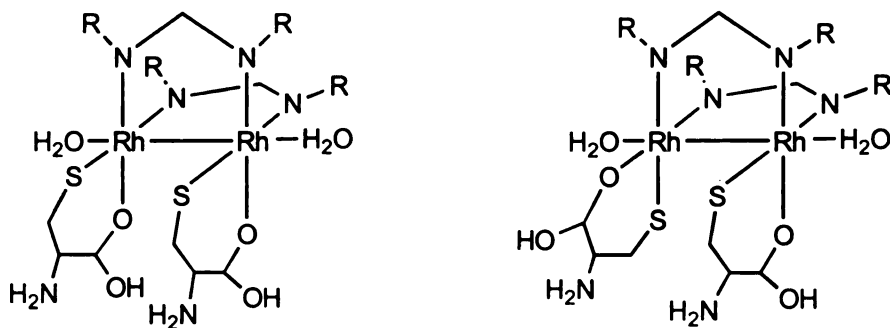


Figure 30. Possible binding modes of cysteine to the partially solvated dirhodium ditolylformamidinate complex. (R = tolyl)

[Rh₂(DTolF)₂(CH₃CN)₆][BF₄]₂ + Glutathione (11)

Four equivalents of glutathione were added to the partially solvated dirhodium bis-formamidinate compound. The brown compound precipitated from solution as an insoluble product. Infrared data show that the sulfur is participating in binding to the metal center. The presence of a bend at 1583 cm⁻¹ due to N-C-N illustrates the rhodium-rhodium bond is still intact. Amino peaks at 1504 cm⁻¹ correspond to uncoordinated amino stretches. Carboxylate peaks at 1616 and 1405 cm⁻¹ may correspond to a coordinated carboxylate group. These derivatives appear to resemble the proposed products of [Rh₂(DTolF)₂(CH₃CN)₆][BF₄]₂ with cysteine in Figure 30.

E. Re₂(O₂CCH₂CH₃)₄Cl₂ Reactions

Due to the anticancer activity and low toxicity of the dirhenium tetracarboxylate compounds¹⁶, reactions of amino acids with

$\text{Re}_2(\text{O}_2\text{CCH}_2\text{CH}_3)_4\text{Cl}_2$ were explored. Since this compound is known to eventually decompose in aqueous solutions, the reactions were performed in methanol with only 5% water to aid the solubility of the amino acids.

$\text{Re}_2(\text{O}_2\text{CCH}_2\text{CH}_3)_4\text{Cl}_2$ + Methionine (12) and $\text{Re}_2(\text{O}_2\text{CCH}_2\text{CH}_3)_4\text{Cl}_2$ + Cysteine (13)

These reactions undergo many color changes until they reach a final brown color with the deposition of brown precipitates. The precipitates are unidentifiable by IR spectroscopy and elemental analyses, but are most likely some form of rhenium oxide decomposition products, as was suggested in the mouse studies.

$\text{Re}_2(\text{O}_2\text{CCH}_2\text{CH}_3)_4\text{Cl}_2$ + Glutathione (14)

Four equivalents of glutathione were added to a solution of dirhenium tetrapropionate. The color changes are essentially the same as for the methionine and cysteine complexes, except that the color progresses from brown to a purplish brown color with a purple solid being obtained. This solid which is highly water soluble is thought to be $\text{Re}(\text{Gsh})_2$ by elemental analysis. Both ^1H and ^{13}C NMR spectroscopy were used to discern the nature of ligand binding. Shifts occur for the βCH_2 and the αCH peaks along with a CH_2 peak indicating that glutathione is coordinated through the sulfur and an amino group (Figure 31).

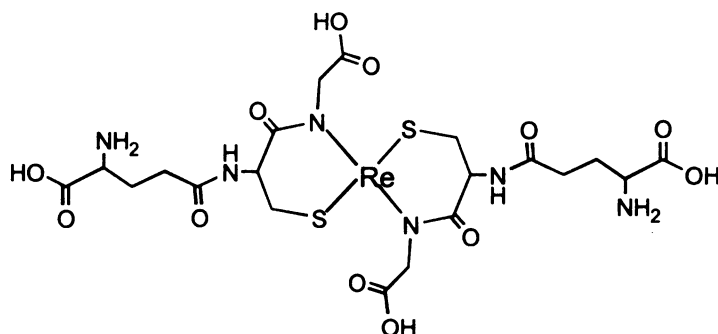


Figure 31. Proposed structure of the product from the reaction of glutathione with dirhenium tetrapropionate.

4. Conclusions

The reactions of sulfur containing amino acids with dirhodium tetraacetate produced interesting results. The methionine reaction proceeded according to the earlier literature proposal of axial binding to the dirhodium core. The –SH containing reactions, however, do not proceed with breakdown of the dinuclear unit as was postulated in the early literature. The reaction of dirhodium tetraacetate with glutathione leads to the displacement of two acetate ligands by two glutathione molecules. Obviously the dinuclear cage is still intact. It would appear from these results that not all –SH containing biomolecules serve to destroy the dinuclear unit. The cysteine reaction shows the displacement of all four acetates by four cysteine molecules, but according to the electronic spectral data, the rhodium-rhodium bond is still intact. Conclusions in the early literature about the stability of the dirhodium carboxylate core are false, as can be concluded from the evidence of the NMR studies presented in Chapter 4.

Dirhodium bis-acetate was used in reactions with the sulfur containing amino acids to determine if the amino acids would break down the core in the absence of two bridging ligands. Instead of a simple axial adduct, the reaction with methionine leads to a bis-chelating product. From IR spectral analysis, the binding sites appear to be the oxygen and sulfur atoms. The cysteine derivative also appears to contain two anionic chelating cysteines that bind through the oxygen and sulfur atoms as well. Glutathione, which chelates through the nitrogen and sulfur atoms, is neutral as verified by the presence of $[\text{BF}_4]^-$ stretches in the infrared.

Reactions of the antitumor active dirhodium formamidinate compound were explored with the sulfur containing amino acids. Methionine forms a paramagnetic compound with the partially solvated ditolylformamidinate compound, with evidence pointing towards one unpaired electron. Cysteine appears to form an oxygen-sulfur chelate with the formamidinate compound. Glutathione also forms a bis-chelating interaction, most likely through the oxygen and sulfur as well.

The reactions with dirhenium tetrapropionate result in different types of products. Cysteine and methionine derivatives both result in the formation of a brown precipitate that is most likely the decomposition product mentioned in the mice studies. The glutathione product, however, is a soluble purple compound that consists of two glutathione ligands chelated to one rhenium atom.

Chapter III

Reactions of Dirhodium Carboxylates with Nucleobases

1. Introduction

Studies involving the carcinostatic activity of transition metal antitumor agents point to the conclusion that this behavior is a consequence of the interactions of these compounds with DNA. The antitumor agent *cis*-platin is known to react with both guanine and adenine residues (Figure 32) on DNA by forming 1, 2-intrastrand cross-links. These conformations cause the DNA to bend and distort, possibly leading to the sequestering of proteins to this site. Ultimately this could be responsible for the inhibition of replication. It is not known whether the actual DNA binding event is the cause of antitumor activity, however, or if the activity stems from the binding of proteins to the damaged site^{34,36,37}.

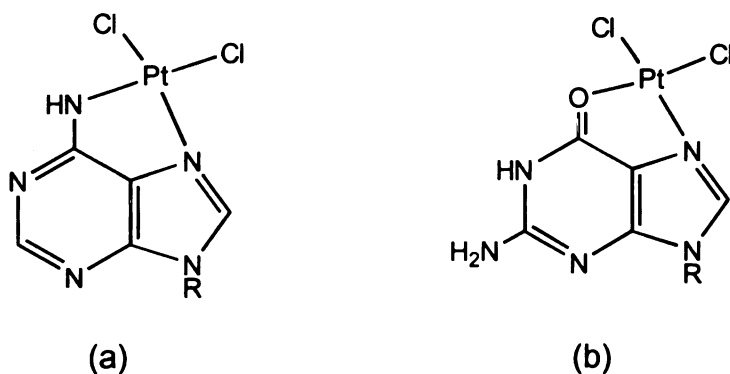


Figure 32. Binding modes of *cis*-platin to the DNA purines (a) adenosine and (b) guanosine. Where R = sugar.

The search for antitumor agents that are active against *cis*-platin resistant cancers has led to the investigation of dimetal carboxylate compounds as alternatives. Among these dimetal carboxylates are compounds containing the

transition metals ruthenium, rhenium, and rhodium (Figure 33). The cause for the carcinostatic activity displayed by the dinuclear compounds may be a result of enzyme deactivation, replication inhibition from nucleotide binding (thus depleting the substrate pool), binding to a single stranded DNA template, or a combination of these events ³⁸⁻⁴¹.

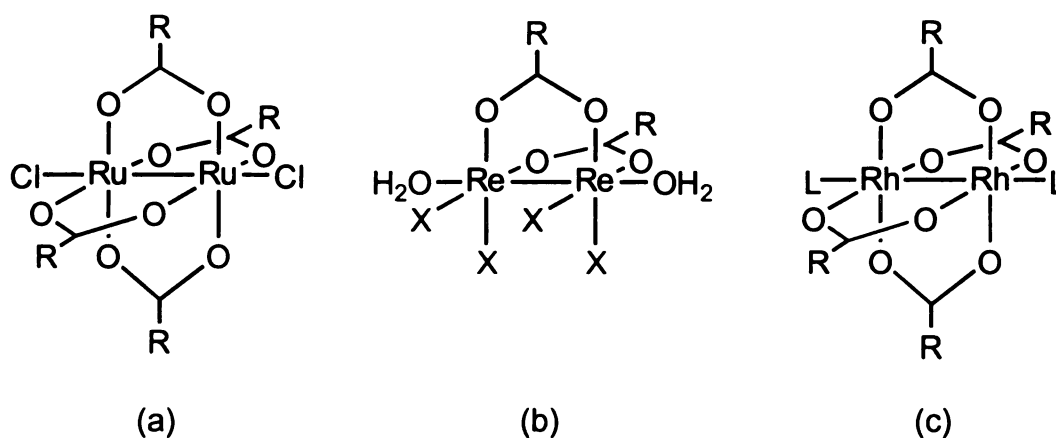


Figure 33. Dinuclear carboxylate compounds of (a) ruthenium, (b) rhenium, and (c) rhodium that display antitumor activity.

Antitumor agents such as the dirhodium carboxylate complexes exhibit anticancer activity that is thought to be a result of binding to the DNA template. Early studies involving the binding of dirhodium carboxylates to nucleosides and nucleotides indicated that the compounds are reactive with poly A sequences, but not poly G ³⁸. Reactions of dirhodium tetraacetate with DNA purines revealed that adenine binds axially through N7, with the exocyclic amino group participating in hydrogen binding with a carboxylate oxygen (Figure 34a). Steric repulsions between the guanine O6 and the carboxylate oxygen, however, would

be expected to prevent axial binding of this nucleotide (Figure 34b). It has also been noted that adenine is able to interact axially through π bonding interactions⁴²⁻⁴⁷.

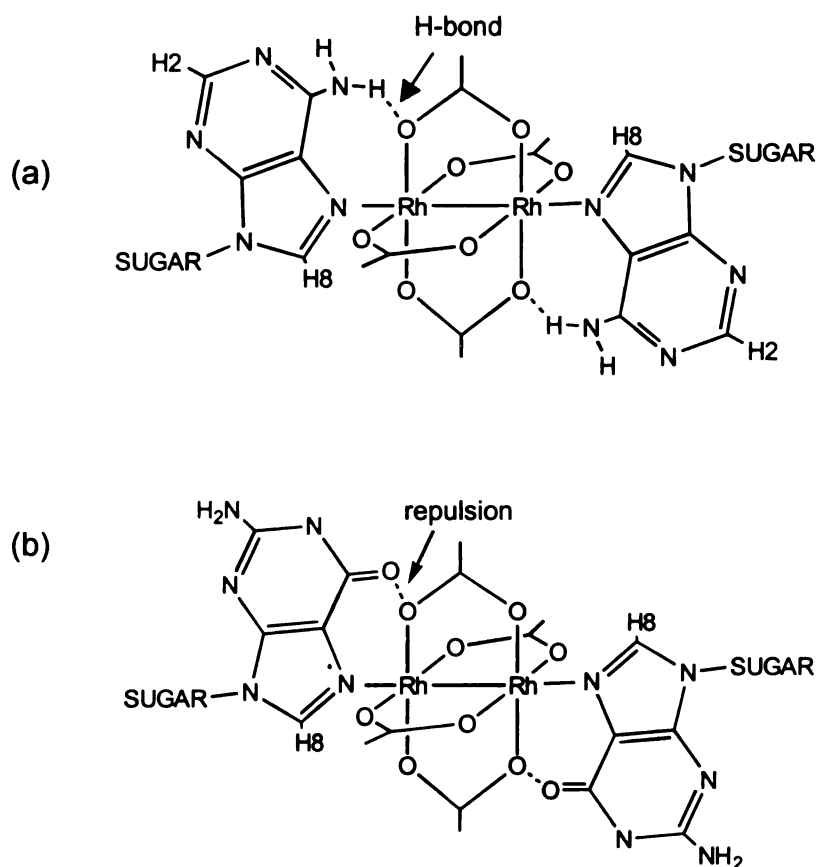


Figure 34. Interactions of (a) adenosine and (b) guanosine with dirhodium tetraacetate.

Contrary to earlier literature reports that suggested only axial binding was possible⁵¹⁻⁵³, studies in our laboratories show that dirhodium carboxylate and dirhodium formamidinate react with purines via substitution of two equatorial carboxylate ligands^{40,48-50}. 9-ethyladenine reacts with

$[\text{Rh}_2(\text{DTolF})_2(\text{MeCN})_6][\text{BF}_4]_2$ to form a bidentate bridge across the dimetal center through the N7 and exocyclic NH_2 sites (Figure 35)⁵⁰. The 9-ethylguanine molecule reacts with $[\text{Rh}_2(\text{DTolF})_2(\text{O}_2\text{CCF}_3)_2(\text{MeCN})_2][\text{BF}_4]_2$ by replacing the two trifluoroacetate ligands to form a bidentate bridge through the N7 and O6 atoms. The 9-ethylguanine ligand can bind in a 'head-to-head' or 'head-to-tail' fashion as indicated in Figure 36⁴⁰. This same type of isomer formation was observed in reactions of dirhodium compounds with 9-ethyladenine. Since DNA bases are arranged in a 'head-to-head' fashion, these are the best models for the mechanism of action on the template strand.

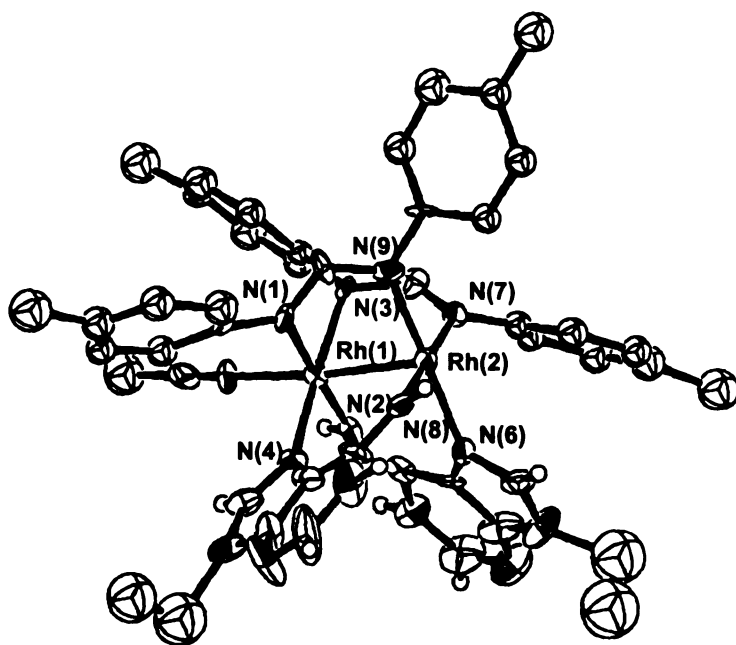


Figure 35. ORTEP representation of $\text{cis}-[\text{Rh}_2(\text{DTolF})_2(9\text{-EtAH})_2(\text{CH}_3\text{CN})]^{2+}$ showing equatorially coordinated 9-ethylguanine ligands.

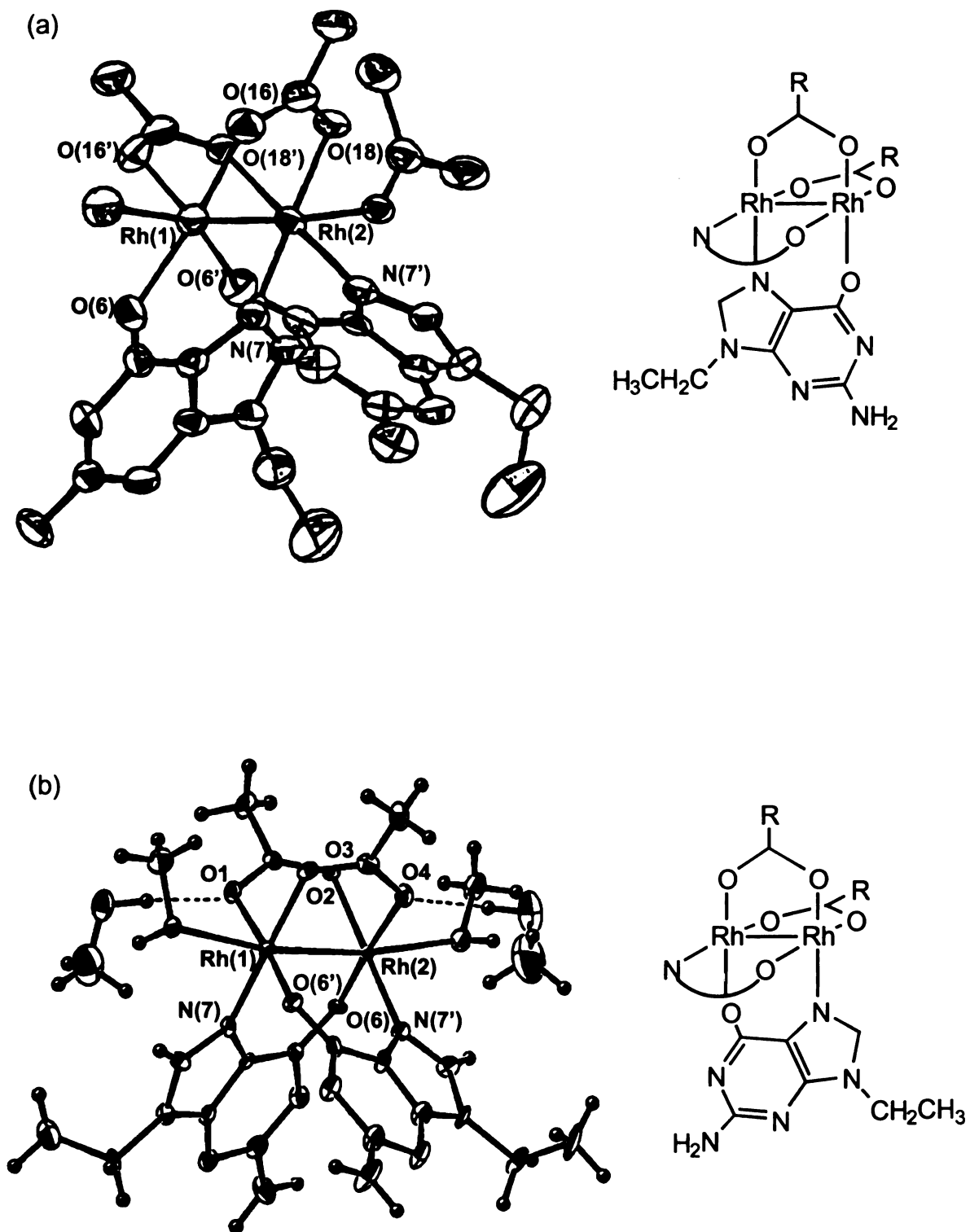


Figure 36. ORTEP representations of Head-to-head (a) and Head-to-tail (b) isomers of 9-Ethylguanine derivatives of dirhodium acetate.

The antitumor activity of the dimetal compound $[\text{Rh}_2(\text{DtolF})_2(\text{O}_2\text{CCF}_3)_2(\text{MeCN})_2][\text{BF}_4]_2$ is a result of the open axial positions, as well as the easily labilized trifluoroacetate ligands. The lability of these groups allows for mono and bidentate neutral ligands to bind, e.g. 9-ethylguanine and 9-ethyladenine. Studies performed with adenine and adenosine show that two different types of binding can occur. Adenine was found to coordinate axially through the N3 atom (Figure 37a), whereas adenosine was observed to coordinate equatorially through the N1 and exocyclic NH_2 groups (Figure 37b). Coordination of adenosine in this fashion leads to a mixed valence product. The blue color of the complex indicates the presence of Rh_2^{5+} , the result of a single electron oxidation. These findings suggest that the adenosine ligands are acting as bidentate mono-anionic ligands. In reactions of the $[\text{Rh}_2(\text{DtolF})_2(\text{O}_2\text{CCF}_3)_2(\text{MeCN})_2][\text{BF}_4]_2$ complex, the antitumor activity may be a result of axial coordination, equatorial coordination, or merely redox processes¹⁵.

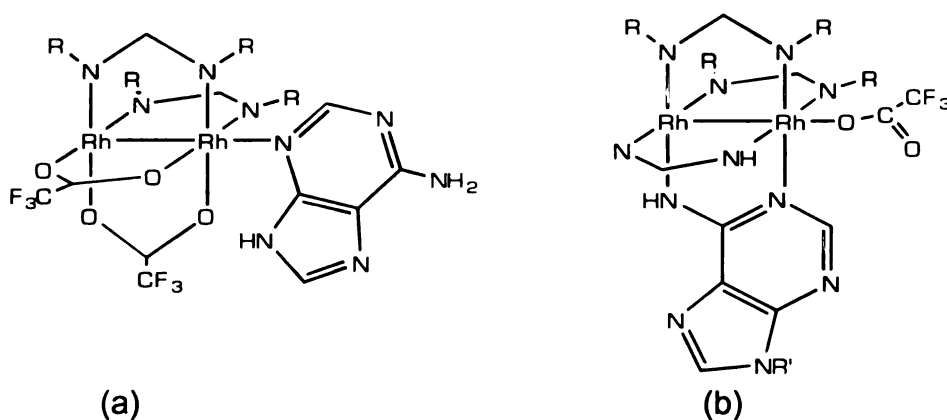


Figure 37. Binding modes of adenine and adenosine to dirhodium formamidinate compounds (a) axial through N3 and (b) equatorially through N1 and NH_2 . (R = tolyl and R' = sugar).

In light of these findings, the reactions of dirhodium tetraacetate and the dirhodium bis-acetate derivative with different nucleobases were explored. Adenosine and guanosine mono- and tri-phosphates were reacted with both dinuclear carboxylate compounds in order to confirm the early literature reports about the reactivity of these compounds with nucleobases. The reaction of 3',5'-thymidine diphosphate was also explored.

2. Experimental

$\text{Rh}_2(\text{O}_2\text{CCH}_3)_4 \cdot 2\text{CH}_3\text{OH} + \text{ATP}$ (15)

Adenosine triphosphate (0.108 g, 0.1 mmol) was added to a solution of $\text{Rh}_2(\text{O}_2\text{CCH}_3)_4 \cdot 2\text{CH}_3\text{OH}$ (0.050g, 0.1 mmol) in 20 mL of DDH₂O. The solution immediately changed from blue-green to purple. After stirring for 24 h, the solution was concentrated on a rotoevaporator, and a purple solid was obtained by the addition of excess ethanol. ¹H NMR (D₂O) δ ppm: 1.78 (acetate), 4-5 (sugar), 6.5 (H1'), 8.45 (H2), 8.75 (H8). ³¹P NMR (Na₃PO₄ reference) δ ppm: -10.8 (d), -11.3 (d), -23.0 (t).

$\text{Rh}_2(\text{O}_2\text{CCH}_3)_4 \cdot 2\text{CH}_3\text{OH} + \text{GTP}$ (16)

Guanosine triphosphate (0.051g, 0.1 mmol) was added to a solution of $\text{Rh}_2(\text{O}_2\text{CCH}_3)_4 \cdot 2\text{CH}_3\text{OH}$ (0.050g, 0.1 mmol) in 15 mL of DDH₂O. The solution was stirred for 2 days with no noticeable color change. The mixture was then heated to 65°C and stirred overnight which led to the production of an emerald green solution. The solution was concentrated on a rotoevaporator and excess ethanol was added to precipitate a green solid. ¹H NMR (D₂O) δ ppm: 1.8

(acetate), 3.5-5 (sugar), 5.7 (H1'), 8.6 (H8). ³¹P NMR (Na₃PO₄ reference) δ ppm: -9.1, -9.8, -10.3.

Rh₂(O₂CCH₃)₄·2CH₃OH + 3',5'-TDP (17)

Thymidine diphosphate (0.026 g, 0.05 mmol) was added to a solution of Rh₂(O₂CCH₃)₄·2CH₃OH in 10 mL of DDH₂O. The reaction mixture was stirred for several days without noticeable color change. The solution was then heated to 65°C and stirred for four days. After this time the solution had become green. The solution was concentrated on a rotoevaporator and excess ethanol was added to precipitate a yellow solid. ¹H NMR (D₂O) δ ppm: 1.79 (CH₃), 3.6-5 (sugar), 6.12 (NH), 7.65 (H4). ³¹P NMR (Na₃PO₄ reference) δ ppm: 0.510, 0.390.

Rh₂(O₂CCH₃)₄·2CH₃OH + AMP (18)

Adenosine monophosphate (0.144g, 0.395 mmol) was added to a solution of Rh₂(O₂CCH₃)₄·2CH₃OH (100 mg, 0.197 mmol) in 10 mL of NaH₂PO₄ buffer at a pH of 7.0. Immediately upon addition of the nucleotide the solution changed from blue green to purple. The solution was stirred at 37°C for 24 h and a purple solid was obtained from the addition of excess methanol. ¹H NMR (D₂O) δ ppm: 1.86 (acetate), 3.5-5 (sugar), 6.02 (H1'), 8.55 (H2), 8.69 (H8). Elemental Analysis calculated for Rh₂O₂₄C₂₆N₁₀P₂H₄₁. Calc: C, 25.4; N, 9.3; H, 4.9. Found: C, 24.6; N, 8.5; H, 4.0.

Rh₂(O₂CCH₃)₄·2CH₃OH + GMP (19)

Guanosine monophosphate (0.1604 g, 0.395 mmol) was added to a solution of Rh₂(O₂CCH₃)₄·2CH₃OH (100 mg, 0.197 mmol) in 10 mL of NaH₂PO₄ buffer at a pH of 7.0. The reaction was heated to 60°C for 24 h, after which time the

solution was green. A green solid was obtained by the addition of excess methanol. ^1H NMR (D_2O) δ ppm: 1.79 (acetate), 3.5-5 (sugar), 5.75 ($\text{H}1'$), 8.64 (H8).

$[\text{Rh}_2(\text{O}_2\text{CCH}_3)_2(\text{CH}_3\text{CN})_6][\text{BF}_4]_2 + \text{GMP}$ (20)

Guanosine monophosphate (0.1231g, 0.3 mmol) was added to a solution of $[\text{Rh}_2(\text{O}_2\text{CCH}_3)_2(\text{CH}_3\text{CN})_6][\text{BF}_4]_2$ (100 mg, 0.15 mmol) in 10 mL of DDH_2O . Immediately upon addition, the solution became a pinkish-red. The solution was evaporated to yield a purplish solid. ^1H NMR (D_2O) δ ppm: 1.933 (acetate), 3.8-4.2 (sugar), 5.78 ($\text{H}1'$), 8.041 (H8). ^{31}P NMR (Na_3PO_4 reference) δ ppm: -7.8. Elemental analysis calculated for $\text{Rh}_2\text{O}_{14}\text{C}_{24}\text{N}_{11}\text{B}_2\text{F}_8\text{PH}_{27}$. Calc: C, 21.6; N, 10.3; H, 3.7. Found: C, 22.6; N, 9.7; H, 3.9.

$[\text{Rh}_2(\text{O}_2\text{CCH}_3)_2(\text{CH}_3\text{CN})_6][\text{BF}_4]_2 + \text{AMP}$ (21)

Adenosine monophosphate (0.1096 g, 0.3 mmol) was added to a solution of $[\text{Rh}_2(\text{O}_2\text{CCH}_3)_2(\text{CH}_3\text{CN})_6][\text{BF}_4]_2$ (100 mg, 0.15 mmol) in 10 mL of DDH_2O . The solution changed from purple to pink upon addition of the nucleotide. ^1H NMR (D_2O) δ ppm: 1.963 (acetate), 3.5-4.5 (sugar), 6.042 ($\text{H}1'$), 8.245 (H2), 8.470 (H8). ^{31}P NMR (Na_3PO_4 reference) δ ppm: -15.2. Elemental analysis calculated for $\text{Rh}_2\text{O}_{22}\text{N}_{10}\text{C}_{22}\text{B}_2\text{F}_8\text{P}_2\text{H}_{28}$. Calc: C, 21.6; N, 11.4; H, 3.2. Found: C, 22.2; N, 11.1; H, 3.5.

3. Results and Discussion

A. Adenosine reactions

Reactions of dirhodium tetraacetate with AMP and ATP lead to products with two types of ligands. ^1H and ^{31}P NMR spectroscopy were used to

characterize the nature of the products. In the ^1H NMR spectra, certain peaks were observed to shift downfield from the free nucleotide resonances. The H8 proton in the product shifts by 0.5 ppm, the H2 shifts by 0.3 ppm, and the H1' shifts by 0.36 ppm. ^{31}P NMR data show only slight chemical shifts, with two of the phosphorus peaks having shifted by ~ 0.27 ppm, and the third having changed position by 0.5 ppm. Preliminary studies indicate that two adenosine ligands are bound axially to the dirhodium tetraacetate core (Figure 34a) as was suggested in the early literature.

Reactions of the partially solvated complex $[\text{Rh}_2(\text{O}_2\text{CCH}_3)_2(\text{CH}_3\text{CN})_6][\text{BF}_4]_2$ led to different results. Upon addition of two equivalents of AMP, the solution becomes red, instead of the purple color obtained with the dirhodium tetraacetate. The ^1H NMR spectrum shows the same general pattern as the dirhodium tetraacetate derivative, *i.e.* the H8 and H2 protons shift by 0.27 and 0.15 ppm respectively. ^{31}P NMR spectroscopy shows a negligible shift in the phosphorous resonance. These data taken together with elemental analysis results lead to the conclusion that the adenine ligands are equatorially bound to the dirhodium core (Figure 38).

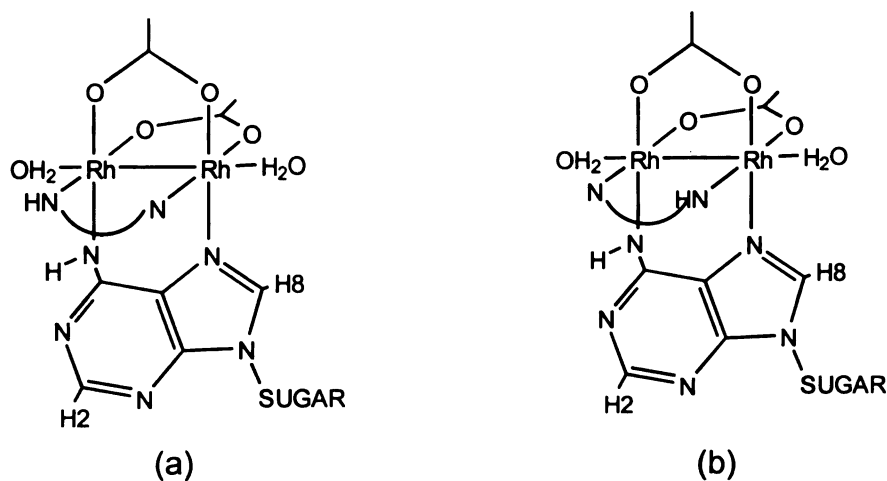


Figure 38. Equatorial bridging of AMP (a) 'head-to-head' and (b) 'head-to-tail' isomers.

B. Guanosine Reactions

Despite early literature reports, we have found that dirhodium tetraacetate does indeed react with guanine bases. Upon heating the reactions to 60°C, the solution becomes green, indicating that a reaction has taken place. ^1H NMR spectroscopy shows that two guanosine ligands have substituted for two bridging acetate ligands. The H8 proton shifts by 0.75 ppm indicating that binding at the N7 site has occurred. ^{31}P NMR spectroscopy shows minimal shifts for each of the three phosphate resonances. The same type of reaction occurs with the dirhodium bis-acetate to give what we formulate as $[\text{Rh}_2(\text{O}_2\text{CCH}_3)_2(\text{GMP})_2(\text{H}_2\text{O})_2][\text{BF}_4]_2$ (Figure 39).

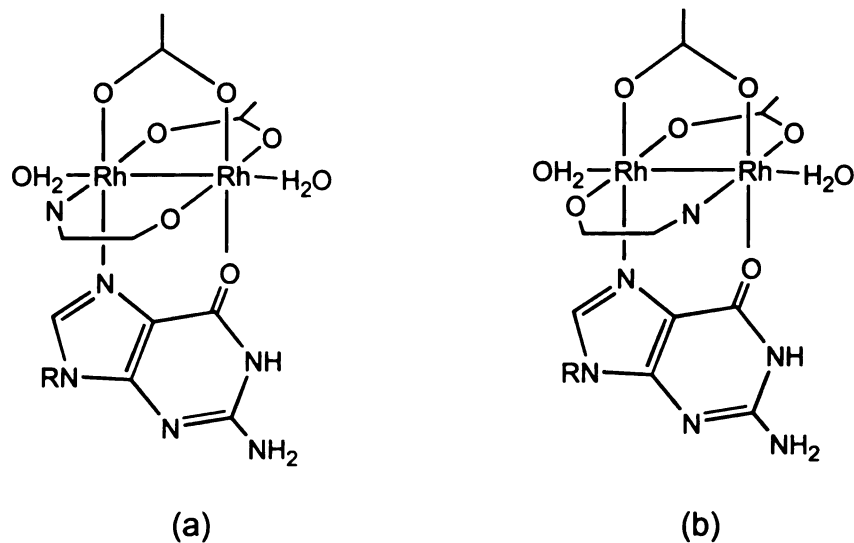


Figure 39. Possible isomers obtained in reactions of dirhodium tetra- and bis-acetate with guanosine (a) 'head-to-head' and (b) 'head-to-tail'.

C. Thymidine Reaction

The reaction of thymidine with dirhodium tetraacetate was not expected to occur, since the pyrimidine nucleobases are not as basic as purines. Upon heating the reaction for 2 weeks at 60°C, however, a change in color ensues. A yellow solid was obtained from the green solution by precipitation with acetone. The ^1H NMR spectrum shows minimal shifts for the proton resonances, but there is a shift of a sugar resonance. Only a slight shift of 0.05 ppm occurs for the remaining sugar protons. According to integration, there are two TDP ligands and two acetate ligands on the dirhodium tetraacetate core. The nature of this binding is uncertain, as this particular reaction has not been performed with dirhodium tetraacetate or any of the other carcinostatic transition metal complexes under investigation. ^{31}P NMR spectroscopy shows a shift for the phosphorous

resonances of 0.39 and 1.24 ppm. From the data it appears that TDP has replaced two equatorial acetate ligands and is binding through the phosphorous atoms (Figure 40).

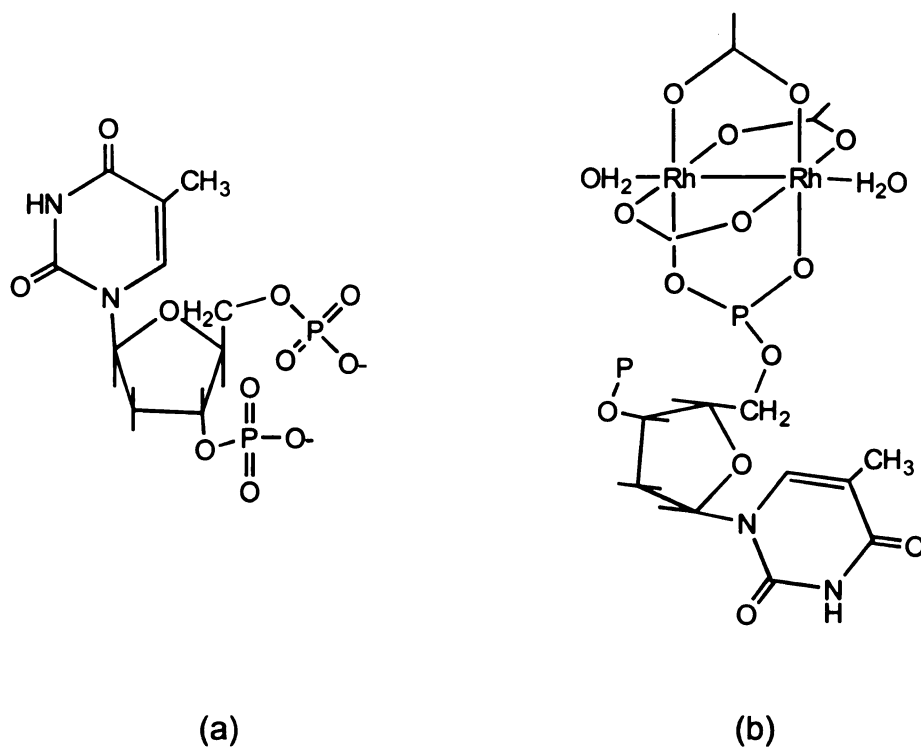


Figure 40. Possible product from the reaction of 3', 5' TDP with dirhodium tetraacetate (a) thymidine 3',5'-diphosphate (b) proposed product.

4. Conclusions

Despite early literature reports on the reactivity of the purine nucleobases with dirhodium carboxylates that indicated only axial adenine binding was possible, we have found unprecedented binding modes for these ligands in our laboratories. Adenine and its derivatives were found to axially bind the dirhodium tetraacetate core as was suspected, but it is also capable of forming a bidentate bridge across the rhodium-rhodium bond via N7/NH₂ interactions with

$[\text{Rh}_2(\text{DTolF})_2(\text{CH}_3\text{CN})_6][\text{BF}_4]_2$ and $[\text{Rh}_2(\text{O}_2\text{CCH}_3)_2(\text{CH}_3\text{CN})_6][\text{BF}_4]_2$. The guanine and guanosine bases were reported to be unreactive with respect to the dirhodium carboxylate compounds due to a lack of observed color change during the reaction. Our studies have shown that guanine does, in fact, bind to the dirhodium core in a unique bridging mode involving the N7 and O6 atoms. ^1H NMR studies indicate that the purines form 1:2 adducts with dirhodium tetraacetate and dirhodium bis-acetate. These results may shed light on the possible interactions of dirhodium carboxylate compounds with both double-stranded and single-stranded DNA

DNA pyrimidines do not possess the favorable Lewis base properties necessary to react with dirhodium carboxylates. Thymidine, 3', 5'-diphosphate, however, was found to react with dirhodium tetraacetate under forcing conditions. The reaction required high temperatures and a long period of time to ensue. Forcing the reaction to occur resulted in the binding of the dirhodium complex to the phosphate groups rather than to the base itself. Due to the extreme conditions of this reaction, it is not likely to be representative of cellular conditions.

Chapter IV

¹H NMR Studies of amino acids and DNA purines with Dirhodium Tetraacetate Derivatives

1. INTRODUCTION

A. Competition Reactions

Cis-platin's antitumor activity is thought to be a result of the formation of inter- and intra-strand cross-links with DNA (Figure 41a, b) or DNA-protein cross-links (Figure 41c). Although the biological role is not clear, it has been postulated that platinum mediated DNA-protein cross-links may be involved in the mechanism of action of *cis*-platin⁴. Direct platination of replication enzymes is another possible mechanism for the antineoplastic activity displayed by *cis*-platin. Platination of DNA polymerase is known to inhibit replication via binding of the cysteine residues of the zinc finger domains. This causes the release of zinc thereby inhibiting the enzyme's ability to function in replication²⁶.

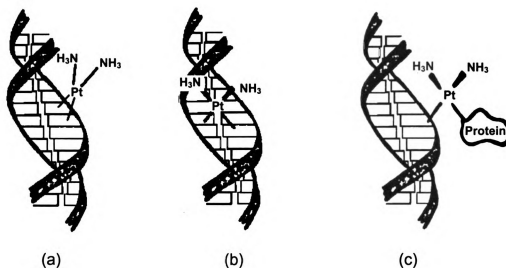


Figure 41. Intrastrand (a), interstrand (b) and DNA-protein cross-links (c) formed by *cis*-platin interactions with DNA.

Metal ions are reactive towards both peptides and proteins. Furthermore, the close association of DNA and proteins, especially in nucleosome cores (DNA wound around an octamer of proteins to form a more compact structure) would help facilitate these cross-linking interactions. It has been suggested that formation of stable platinum mediated DNA-protein crosslinks *in vivo* may involve sulfur containing amino acids ⁴. Model studies were performed with *cis*-platin using amino acids with a high affinity to platinum. These amino acids were constrained to bind the metal atom through their side chains, since this is most likely to occur with a protein residue. The platinum-amino acid complexes were then reacted with nucleotides. In competitive binding studies, the platinum complexes were found to bind the amino acid first, and subsequently to the nucleotide ⁵⁴.

In a related study of platinum-methionine adducts found in the urine of patients undergoing treatment with *cis*-platin, it was found that GMP selectively displaces the sulfur bound methionine. The bis-chelate, [Pt(MET-H-S,N)₂], a byproduct of *cis*-platin metabolism, is unreactive towards nucleobases at neutral pH. By monitoring the reactions by ¹H NMR spectroscopy, it was found that intermolecular displacement of the sulfur bound methionine occurs by N7 bound 5'-GMP ^{55,56}.

Platinum has a higher affinity for sulfur ligands than it does for nitrogen ligands, thus sulfur biomolecules diminish the antitumor activity of platinum complexes. Sulfur nucleophiles have even been used as rescue agents to remove excess platinum from the body during *cis*-platin therapy ²⁵. Displacement

reactions will most likely be facilitated if the methionine adduct is formed by an accessible met residue on a DNA binding protein ⁵⁷.

Competitive binding studies of dirhodium(II) acetate with the sulfur containing amino acids, cysteine and methionine, as well as with glutathione were performed with the nucleotide AMP. These experiments were modeled after the ¹H NMR spectral studies mentioned above ^{56,58,59}.

B. Reactions of Dirhodium Acetate Compounds

According to reports by Bear, *et al.*, the interaction of dirhodium(II) carboxylates with –SH containing biomolecules results in deactivation of the carboxylate compound. These studies focused primarily on reactions of dirhodium(II) tetraacetate with the amino acid cysteine, and led to claims that interactions of these compounds results in the breakdown of the dirhodium carboxylate cage. This purportedly yields an insoluble rhodium(III) cysteine species, acetate ions, and H⁺ ^{12,13}.

Additional experiments were performed in an attempt to support the conclusion that breakdown of the carboxylate cage occurs upon introduction of dirhodium tetraacetate into tumor cells. Studies involving mice implanted with Erlich ascites tumors and injected with dirhodium(II) acetate were performed, and metabolism of the compound was followed. It was found that dirhodium tetraacetate breaks down into its components within 2 h of injection. This claim is based on analyses using ¹⁴C labeled acetate coupled with the tracking of rhodium being achieved by atomic absorption spectroscopy. Results indicated

that the ^{14}C label was being removed more rapidly than the rhodium, which was attributed to the decomposition of dirhodium tetraacetate into easily mobile OAc^- and insoluble rhodium residues. If the dirhodium tetraacetate compound lost only two acetate ions (and not four), however, the results from tracking studies would still be consistent with the fact that acetate ions are removed at a faster rate than rhodium. The researchers suggest complete decomposition as an explanation for the results, without weighing any alternatives³². The loss of two bridging ligands is common for the paddlewheel structures that exhibit antitumor activity; a good example of this behavior is exhibited by the mixed ligand complex, $\text{Rh}_2(\text{O}_2\text{CCF}_3)_2(\text{DTolF})_2(\text{H}_2\text{O})_2$, which loses the two trifluoroacetate ligands upon reaction with DNA¹¹. The researchers had no definitive proof for their claims, they only pose the decomposition hypothesis as a possible explanation for their data.

In order to determine the validity of the results obtained from the aforementioned experiments, ^1H NMR studies were repeated under the same conditions as previously reported¹¹. Reactions were monitored with cysteine, glutathione (which contains a cysteine moiety), methionine, as well as the cysteine mimics, O-Methyl cysteine and 2-Aminothiophenol. All the above mentioned molecules contain the $-\text{SH}$ moiety in question, except for methionine, which contains $-\text{S}-\text{CH}_3$, which is expected to bind axially, with no perturbation to the cage structure. This reaction was performed to determine what effect axial binding has on the acetate shifts in the NMR. Reactions of the $-\text{SH}$ containing

amino acids were performed in an effort to test the notion that all –SH containing amino acids cause the breakdown of the dirhodium carboxylate cage.

Another type of experiment being pursued involves the reaction of dirhodium tetraacetate derivatives with cysteine. For these reactions, dirhodium tetraacetate is reacted first with ATP or GTP, then cysteine is added; the reaction is monitored over time by ^1H NMR spectroscopy. The reactions were carried out in order to determine whether or not cysteine would react with the nucleotide bound rhodium and lead to breakdown of the dirhodium carboxylate unit.

2. EXPERIMENTAL

A. Competition Reactions

The reactions were carried out in a 50 mM NaH_2PO_4 buffer solution at pH 7 in D_2O . ^1H NMR spectral measurements were performed on a Varian 300 MHz instrument at time = 0, 15 minutes, 2, 4, and 24 hours. Standard ^1H NMR spectra of the amino acid/nucleotide mixtures were measured, and the reaction progress was monitored.

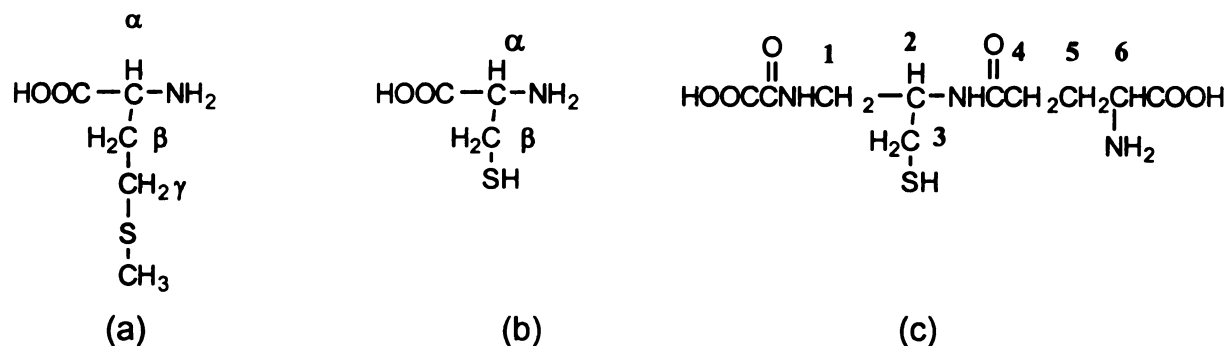


Figure 42. Numbering scheme for the amino acids. (a) methionine, (b) cysteine, and (c) glutathione.

Methionine/AMP NMR tube reaction (1)

A ^1H NMR spectrum of a 1:1 methionine:AMP mixture was recorded for use as a reference. ^1H NMR (D_2O) δ : 1.96 (met CH_3), 2.00 (m, met βCH_2), 2.47 (t, met γCH_2), 3.69 (met αCH), 3.88, 4.20, 4.33 (AMP sugar), 5.97 (d, ade $\text{H}1'$), 8.07 (ade $\text{H}2$), 8.39 (ade $\text{H}8$). A 4 mM solution of dirhodium tetraacetate in deuterated buffer, ^1H NMR (D_2O) δ : 1.74 (s, CH_3), was added to an 8 mM solution of 1:1 methionine:AMP. At time = 0 minutes ^1H NMR (D_2O) δ : 1.76 (s, CH_3), 2.01 (m, met βCH_2), 2.52 (t, met γCH_2), 3.71 (met αCH), 6.01 (ade $\text{H}1'$), 8.18 (ade $\text{H}2$), 8.46 (ade $\text{H}8$). At time = 15 min ^1H NMR (D_2O) δ : 1.76 (s, CH_3), 2.00 (s, acetate, met βCH_2), 2.52 (t, met γCH_2), 3.71 (met αCH), 6.01 (ade $\text{H}1'$), 8.18 (ade $\text{H}2$), 8.45 (ade $\text{H}8$). At time = 2 h ^1H NMR (D_2O) δ : 1.76 (s, CH_3), 2.01 (acetate, met βCH_2), 2.52 (t, met γCH_2), 3.71 (met αCH), 6.02 (ade $\text{H}1'$), 8.20 (ade $\text{H}2$), 8.45 (ade $\text{H}8$). At time = 4h ^1H NMR (D_2O) δ : 1.76 (s, CH_3), 2.02 (acetate, met βCH_2), 2.54 (t, met γCH_2), 3.71 (met αCH), 6.03 (ade $\text{H}1'$), 8.21 (ade $\text{H}2$), 8.47 (ade $\text{H}8$). At time = 24 h ^1H NMR (D_2O) δ : 1.76 (s, CH_3), 2.02 (acetate, met βCH_2), 2.54 (t, met γCH_2), 3.71 (met αCH), 6.02, 6.03 (ade $\text{H}1'$), 8.21 (ade $\text{H}2$), 8.47 (ade $\text{H}8$).

Glutathione/AMP NMR tube reaction (2)

A ^1H NMR spectrum of a 1:1 glutathione:AMP mixture was recorded for use as a reference. ^1H NMR (D_2O) δ : 2.01 (gsh4), 2.39 (gsh5), 2.78 (gsh3), 3.61 (gsh6), 3.61 (gsh1), 4.40 (gsh2), 5.95, 5.97 (d, ade $\text{H}1'$), 8.07 (ade $\text{H}2$), 8.37 (ade $\text{H}8$). A 4 mM solution of dirhodium tetraacetate in deuterated buffer, ^1H

NMR (D_2O) δ : 1.74 (s, CH_3), was added to an 8 mM solution of 1:1 glutathione:AMP. At time = 0 1H NMR (D_2O) δ : 1.75, 1.76 (CH_3), 2.00 (gsh4), 2.39 (gsh5), 2.79 (gsh3), 3.61 (gsh6), 3.61 (gsh1), 4.40 (gsh2), 6.02 (d, ade H1'), 8.18 (ade H2), 8.45 (ade H8). At time = 15 min 1H NMR (D_2O) δ : 1.74, 1.77 (CH_3), 2.00 (gsh4), 2.39 (gsh5), 3.61 (gsh6), 3.61 (gsh1), 5.98, 6.00 (d, ade H1'), 8.14 (ade H2), 8.42 (ade H8). At time = 2 h 1H NMR (D_2O) δ : 1.74, 1.77 (CH_3), 2.00 (gsh4), 2.37 (gsh5), 3.61 (gsh6), 3.61 (gsh1), 5.98, 6.00 (d, ade H1'), 8.12 (ade H2), 8.42 (ade H8). At time = 4 h 1H NMR (D_2O) δ : 1.74, 1.77 (CH_3), 2.00 (gsh4), 2.36 (gsh5), 3.61 (gsh6), 3.61 (gsh1), 5.98, 6.00 (d, ade H1'), 8.14 (ade H2), 8.42 (ade H8). At time = 24 h 1H NMR (D_2O) δ : 1.75, 1.77 (CH_3), 2.00 (gsh4), 2.37 (gsh5), 3.61 (gsh6), 3.61 (gsh1), 5.98, 6.00 (d, ade H1'), 8.13 (ade H2), 8.42 (ade H8).

Cysteine/AMP NMR tube reaction (3)

A 1H NMR spectrum of a 1:1 cysteine:AMP mixture was recorded for use as a reference. 1H NMR (D_2O) δ : 2.88 (cys βCH_2), 3.82 (cys αCH), 5.95, 5.97 (d, ade H1'), 8.07 (ade H2), 8.38 (ade H8). A 4 mM solution of dirhodium tetraacetate in deuterated buffer, 1H NMR (D_2O) δ : 1.74 (s, CH_3), was added to an 8 mM solution of 1:1 cysteine:AMP. At time = 0 1H NMR (D_2O) δ : 1.75 (s, CH_3), 2.93 (cys βCH_2), 3.82 (cys αCH), 5.96, 5.98 (d, ade H1'), 8.10 (ade H2), 8.40 (ade H8). At time = 15 min 1H NMR (D_2O) δ : 1.74 (s, CH_3), 2.92 (cys βCH_2), 3.82 (cys αCH), 5.96, 5.98 (d, ade H1'), 8.08 (ade H2), 8.39 (ade H8). At time = 2 h 1H NMR (D_2O) δ : 1.74 (s, CH_3), 2.86 (cys βCH_2), 3.82 (cys αCH), 5.96, 5.98 (d, ade H1'), 8.08 (ade H2), 8.39 (ade H8). At time = 4 h 1H NMR (D_2O) δ : 1.74 (s, CH_3),

2.88 (cys β CH₂), 5.96, 5.98 (d, ade H1'), 8.08 (ade H2), 8.39 (ade H8). At time = 24 h ¹H NMR (D₂O) δ : 1.74 (s, CH₃), 2.98 (cys β CH₂), 3.95 (cys α CH), 5.96, 5.98 (d, ade H1'), 8.08 (ade H2), 8.39 (ade H8).

B. Dirhodium Tetraacetate Reactions

Each reaction was carried out in a 50 mM NaH₂PO₄ buffer solution at a pH of 7.5 in D₂O. ¹H NMR spectra were performed on a Varian 300 MHz instrument for each of the experiments, except for the 2-aminothiophenol reaction which was measured with a Varian 500 MHz instrument. Standard NMR spectra of the starting materials, Rh₂(O₂CCH₃)₄(CH₃OH)₂, Rh₂(O₂CCH₃)₄(ATP)₂, Rh₂(O₂CCH₃)₂(GTP)₂(H₂O)₂, and [Rh₂(O₂CCH₃)₂(CH₃CN)₆][BF₄]₂ were obtained, and reaction progress was monitored according to these spectra.

Rh₂(O₂CCH₃)₄(CH₃OH)₂ + cysteine (4)

A 0.4 M solution of Rh₂(O₂CCH₃)₄(CH₃OH)₂ was placed in an NMR tube and titrated with a 0.4 M solution of cysteine in increments of one equivalent up to four equivalents. ¹H NMR spectra were recorded at a 1:1 ratio, 1:2 ratio, 1:3 ratio, and 1:4 ratio of dirhodium tetraacetate to cysteine. Reaction progress was monitored by shifts in the acetate peak. ¹H NMR (D₂O), 1:1 ratio, δ ppm: 1.62 (s, bound acetate) 1.79 (s, free acetate). ¹H NMR (D₂O), 1:2 ratio, δ ppm: 1.62 (s, bound acetate), 1.79 (s, free acetate). ¹H NMR (D₂O), 1:3 ratio, δ ppm: 1.62 (s, bound acetate), 1.79 (s, free acetate). ¹H NMR (D₂O), 1:4 ratio, δ ppm: 1.62 (s, bound acetate), 1.79 (s, free acetate).

Rh₂(O₂CCH₃)₄(CH₃OH)₂ + glutathione (5)

A 0.4 M solution of Rh₂(O₂CCH₃)₄(CH₃OH)₂ was placed in an NMR tube and titrated with a 0.4 M solution of glutathione in increments of one equivalent up to four equivalents. ¹H NMR spectra were recorded at a 1:1 ratio, 1:2 ratio, 1:3 ratio, and 1:4 ratio of dirhodium tetraacetate to glutathione. Reaction progress was monitored by shifts in the acetate peak. ¹H NMR (D₂O), 1:1 ratio, δ ppm: 1.67 (s, bound acetate) 1.84 (s, free acetate). ¹H NMR (D₂O), 1:2 ratio, δ ppm: 1.67 (s, bound acetate) 1.84 (s, free acetate). ¹H NMR (D₂O), 1:3 ratio, δ ppm: 1.67 (s, bound acetate) 1.84 (s, free acetate). ¹H NMR (D₂O), 1:4 ratio, δ ppm: 1.67 (s, bound acetate) 1.84 (s, free acetate).

Rh₂(O₂CCH₃)₄(CH₃OH)₂ + methionine (6)

A 0.4 M solution of Rh₂(O₂CCH₃)₄(CH₃OH)₂ was placed in an NMR tube and titrated with a 0.4 M solution of methionine in increments of one equivalent up to four equivalents. ¹H NMR spectra were recorded at a 1:1 ratio, 1:2 ratio, 1:3 ratio, and 1:4 ratio of dirhodium tetraacetate to methionine. Reaction progress was monitored by shifts in the acetate peak. ¹H NMR (D₂O), 1:1 ratio, δ ppm: 1.65 (s, bound acetate), 2.02 (s, new acetate). ¹H NMR (D₂O), 1:2 ratio, δ ppm: 1.65 (s, bound acetate), 2.00 (s, new acetate). ¹H NMR (D₂O), 1:3 ratio, δ ppm: 1.65 (s, bound acetate), 1.97 (s, new acetate). ¹H NMR (D₂O), 1:4 ratio, δ ppm: 1.65 (s, bound acetate), 1.95 (bs, new acetate).

Rh₂(O₂CCH₃)₄(ATP)₂ + cysteine (7)

A 0.4 M solution of Rh₂(O₂CCH₃)₄(ATP)₂ was placed in an NMR tube and titrated with a 0.4 M solution of cysteine in increments of one equivalent up to

four equivalents. ^1H NMR spectra were recorded at a 1:1 ratio, 1:2 ratio, 1:3 ratio, and 1:4 ratio of $\text{Rh}_2(\text{O}_2\text{CCH}_3)_4(\text{ATP})_2$ to cysteine. Reaction progress was monitored by shifts in the acetate resonance. ^1H NMR (D_2O), standard, δ ppm: 1.73 (s, bound acetate), 8.28 (s, ade H2), 8.49 (s, ade H8). ^1H NMR (D_2O), 1:1 ratio, δ ppm: 1.73 (s, bound acetate), 1.88 (s, free acetate), 6.03 (ade H1'), 8.27 (s, ade H2), 8.47 (s, ade H8). ^1H NMR (D_2O), 1:2 ratio, δ ppm: 1.73 (s, bound acetate), 1.88 (s, free acetate), 6.03 (d, ade H1'), 8.27 (s, ade H2), 8.47 (s, ade H8). ^1H NMR (D_2O), 1:3 ratio, δ ppm: 1.73 (s, bound acetate), 1.88 (s, free acetate), 6.02 (d, ade H1'), 8.27 (s, ade H2), 8.46 (s, ade H8). ^1H NMR (D_2O), 1:4 ratio, δ ppm: 1.73 (s, bound acetate), 1.88 (s, free acetate), 6.03 (d, ade H1'), 8.26 (s, ade H2), 8.46 (s, ade H8).

$\text{Rh}_2(\text{O}_2\text{CCH}_3)_2(\text{GTP})_2(\text{H}_2\text{O})_2$ + cysteine (8)

A 0.4 M solution of $\text{Rh}_2(\text{O}_2\text{CCH}_3)_2(\text{GTP})_2(\text{H}_2\text{O})_2$ was placed in an NMR tube and titrated with a 0.4 M solution of cysteine in increments of one equivalent up to four equivalents. ^1H NMR spectra were taken at a 1:1 ratio, 1:2 ratio, 1:3 ratio, and 1:4 ratio of $\text{Rh}_2(\text{O}_2\text{CCH}_3)_2(\text{GTP})_2(\text{H}_2\text{O})_2$ to cysteine. Reaction progress was monitored by shifts in the acetate peak. ^1H NMR (D_2O), standard, δ ppm: 1.98 (s, bound acetate), 8.63 (s, gua H8). ^1H NMR (D_2O), 1:1 ratio, δ ppm: 1.81 (s, free acetate), 1.98 (s, bound acetate), 5.73 (d, gua H1'), 8.60 (s, gua H8). ^1H NMR (D_2O), 1:2 ratio, δ ppm: 1.81 (s, free acetate), 1.98 (s, bound acetate), 5.71 (d, gua H1'), 7.90 (s, gua H2), 8.63 (s, gua H8). ^1H NMR (D_2O), 1:3 ratio, δ ppm: 1.81 (s, free acetate), 1.98 (s, bound acetate), 5.69, 5.71 (d, gua H1'), 7.90 (s, gua H2), 8.62 (s, gua H8). ^1H NMR (D_2O), 1:4 ratio, δ ppm: 1.81 (s, free acetate),

1.98 (s, bound acetate), 5.69, 5.71 (d, gua H1'), 7.90 (s, gua H2), 8.61 (s, gua H8).

[Rh₂(O₂CCH₃)₂(CH₃CN)₆][BF₄]₂ + cysteine (9)

A 0.4 M solution of [Rh₂(O₂CCH₃)₂(CH₃CN)₆][BF₄]₂ was placed in an NMR tube and titrated with a 0.4 M solution of cysteine in increments of one equivalent up to four equivalents. ¹H NMR spectra were taken at a 1:1 ratio, 1:2 ratio, 1:3 ratio, and 1:4 ratio of rhodium bisacetate to cysteine. Reaction progress was monitored by shifts in the acetate peak. ¹H NMR (D₂O), standard, δ ppm: 1.79 (s, bound acetate). ¹H NMR (D₂O), 1:1 ratio, δ ppm: 1.79 (s, bound acetate). ¹H NMR (D₂O), 1:1 ratio, δ ppm: 1.79 (s, bound acetate). ¹H NMR (D₂O), 1:2 ratio, δ ppm: 1.79 (s, bound acetate). ¹H NMR (D₂O), 1:3 ratio, δ ppm: 1.79 (s, bound acetate). ¹H NMR (D₂O), 1:4 ratio, δ ppm: 1.79 (s, bound acetate).

Rh₂(O₂CCH₃)₄(CH₃OH)₂ + O-Methyl cysteine (10)

A 0.4 M solution of Rh₂(O₂CCH₃)₄(CH₃OH)₂ was placed in an NMR tube and titrated with a 0.4 M solution of O-Methyl cysteine in increments of one equivalent up to four equivalents. ¹H NMR spectra were recorded at a 1:1 ratio, 1:2 ratio, 1:3 ratio, and 1:4 ratio of rhodium tetraacetate to O-Methyl cysteine. Reaction progress was monitored by shifts in the acetate peak. ¹H NMR (D₂O), 1:1 ratio, δ ppm: 1.74 (s, bound acetate), 1.92 (s, acetate). ¹H NMR (D₂O), 1:2 ratio, δ ppm: 1.74 (s, bound acetate), 1.92 (s, acetate). ¹H NMR (D₂O), 1:3 ratio, δ ppm: 1.74 (s, bound acetate), 1.92 (s, acetate). ¹H NMR (D₂O), 1:4 ratio, δ ppm: 1.74 (s, bound acetate), 1.92 (s, acetate).

Rh₂(O₂CCH₃)₄(CH₃OH)₂ + 2-aminothiophenol (11)

A 0.4 M solution of Rh₂(O₂CCH₃)₄(CH₃OH)₂ was placed in an NMR tube and titrated with a 0.4 M solution of 2-aminothiophenol in increments of one equivalent up to four equivalents. ¹H NMR spectra were recorded at a 1:1 ratio, 1:2 ratio, 1:3 ratio, and 1:4 ratio of rhodium tetraacetate to 2-aminothiophenol. Reaction progress was monitored by shifts in the acetate peak. ¹H NMR (CD₃OD), 1:1 ratio, δ ppm: 1.82 (s, bound acetate). ¹H NMR (CD₃OD), 1:2 ratio, δ ppm: 1.87 (s, bound acetate), 1.87 (s, acetate). ¹H NMR (CD₃OD), 1:3 ratio, δ ppm: 1.86 (s, bound acetate), 1.88 (s, acetate). ¹H NMR (CD₃OD), 1:4 ratio, δ ppm: 1.90 (s, bound acetate), 1.93 (s, acetate).

3. Results and Discussion

A. Competition Reactions

Methionine/AMP NMR tube reaction (1)

This reaction was performed to determine whether one type of cellular biomolecule is preferred over the other. Both methionine and AMP are capable of behaving as axial ligands, so a preference for one should be possible to observe. Since sulfur is a stronger donor than nitrogen, it would seem likely that the methionine would be preferred over the AMP. In order to ascertain whether this is the case, there are three sets of resonances that are important to monitor in the NMR spectra. These are the acetate, methionine and adenine ¹H NMR peaks which shift upon their coordination with dirhodium tetraacetate. By

monitoring these shifts, the course of the reaction can be determined (Table 2, Figure A1).

Upon addition of dirhodium tetraacetate to the methionine/AMP solution, the acetate peak shifts from 1.74 to 2.01 ppm for a change of 0.27 ppm. This downfield shift is in accordance with the spectrum of the bulk product and signifies axial binding of the amino acid. Throughout the rest of the experiment, a gradual shift downfield occurs until after 24 h the final acetate peak position is at 2.02 ppm.

Methionine peaks shift as expected for an axially bound sulfur donor ligand. The $-SCH_3$ shifts upfield from 1.96 ppm in the standard to 1.76 ppm after 24 h. The α CH resonance begins to shift at time zero, moving 0.02 ppm, and remaining constant for the duration of the experiment. The γ CH₂ peak shifts until it reaches 2.04 ppm for a total shift of 0.08 ppm. The β CH₂ shift coincides with the acetate peak. Changes in the resonances of these protons are expected, with the γ CH₂ closest to the sulfur binding site, showing the greatest shift upon binding, followed by the β CH₂ then the α CH resonances.

The adenine region reveals binding of the nucleotide as well. The H8 proton shifts throughout the entire experiment by a total of 0.09 ppm, H2 shifts 0.14 ppm, and H1' shifts 0.06 ppm. This indicates adenine coordination to the metal as well. In the bulk product, significant shifts are observed in the H8/H2 region of the spectrum as well.

From the aforementioned data, it is apparent that dirhodium tetraacetate reacts with both methionine and AMP (Figure 43) and that when both reagents

are present, neither inhibits binding of the other. This is an encouraging result, as it shows that the amino acid does not sequester the dirhodium tetraacetate and keep it from reacting with the nucleotide. It is therefore possible that, in the cell, proteins that contain methionine residues bind to the dirhodium molecule which then goes on to form an adduct with DNA and inhibit replication.

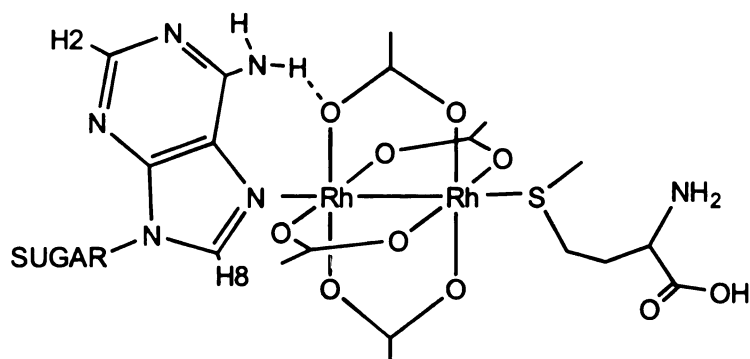


Figure 43. Proposed product from the competition reaction of $\text{Rh}_2(\text{O}_2\text{CCH}_3)_4$ with methionine and AMP.

Table 2. Proton resonances monitored during the course of the methionine/AMP competition experiment.

	Standard	t=0 min	t=15 min	t=2 h	t=4 h	t=24 h
Ade H8	δ 8.34	δ 8.46	δ 8.45	δ 8.45	δ 8.47	δ 8.47
Ade H2	δ 8.07	δ 8.18	δ 8.18	δ 8.20	δ 8.21	δ 8.21
Ade H1'	δ 5.97 δ 5.95	δ 6.01	δ 6.01	δ 6.02	δ 6.03	δ 6.03 δ 6.02
Met CH_3	δ 1.96	δ 1.76				
Met βCH_2	δ 2.00	δ 2.01	δ 2.00	δ 2.01	δ 2.02	δ 2.02
Met γCH_2	δ 2.47	δ 2.52	δ 2.52	δ 2.52	δ 2.54	δ 2.54
Met αCH	δ 3.69	δ 3.71				
Acetate	δ 1.74	δ 2.01	δ 2.00	δ 2.01	δ 2.02	δ 2.02

Glutathione/AMP NMR tube reaction (2)

Since glutathione resembles a protein with a cysteine moiety, this is an important reaction to monitor by NMR spectroscopy. Previous results of reactions of $\text{Rh}_2(\text{O}_2\text{CCH}_3)_4$ with glutathione support the conclusion that the molecule binds equatorially in a 2:1 fashion by replacing two of the acetates on the tetraacetate core. The question remains, however, whether this dirhodium-glutathione adduct is able to react further with DNA, or whether the dirhodium complex has been deactivated with respect to further substitution, as is the case with *cis*-platin. The answer is obtained by monitoring changes in the acetate, glutathione (gsh2 and gsh3 protons, Figure A2c), as well as adenine regions of the spectrum (Table 3, Figure A2).

Upon addition of dirhodium tetraacetate to the glutathione/AMP mixture, the bound acetate shifts to 1.76 ppm, and a free acetate peak appears at 1.75 ppm. As time progresses, further shifts in the acetate peak are negligible with the final values being 1.75 ppm for free and 1.77 ppm for bound acetate. The overall shift in these peaks is 0.03 ppm for bound acetate and 0.00 ppm for the free acetate. These results support the previous conclusion that two acetates are released in the glutathione reaction with rhodium tetraacetate.

The binding of glutathione to the dirhodium tetraacetate core can be observed by the loss of the free gsh3 peak as well as the gsh2 peak. After 15 minutes, the gsh3 peak has diminished in intensity, and less intense features downfield begin to appear. These new resonances are identical to the ones that comprise the quartet of doublets in the bulk $\text{Rh}_2(\text{OAc})_2(\text{GSH})_2(\text{H}_2\text{O})_4$ product.

The gsh2 peak has shifted into the HDO peak and is no longer visible. Reduction of the gsh3 peak continues through 2 hours into the reaction after which time it is no longer visible. All other GSH peaks exhibit negligible shifts.

The peaks used to monitor AMP reactions are the H8, H2 and the H1' groups. Each of these peaks shifts at the time of mixing. The overall shifts for H8, H2, and the H1' protons are 0.05, 0.06, and 0.03 ppm, respectively. These data indicate that the AMP is binding as well, most likely in the axial positions based on the bulk reaction (Figure 44).

The results of this experiment support the conclusion that when faced with both glutathione (an -SH containing amino acid) and a nucleotide, dirhodium tetraacetate reacts with both simultaneously. In the presence of the -SH containing tripeptide, glutathione, dirhodium tetraacetate is able to bind the nucleotide adenine. These results refute the earlier conclusion that all -SH containing biomolecules deactivate the tetraacetate by breaking down the core. From the spectra it is clear that both biomolecules are binding. On a more general level, the data suggest that the binding of a cysteine moiety on a protein will not disable the ability of dirhodium acetate to bind DNA.

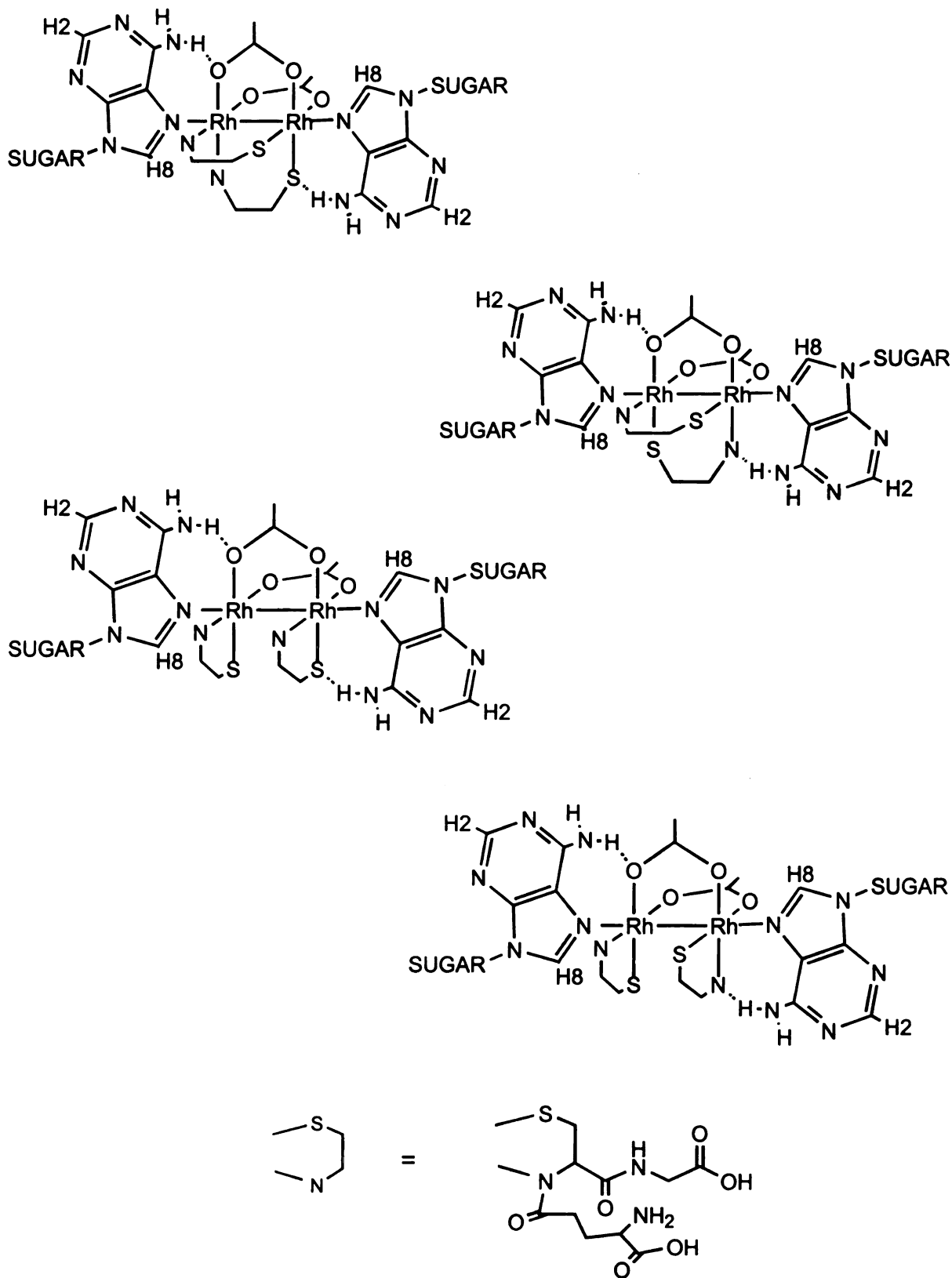


Figure 44. Proposed products formed in the competition reaction with glutathione and AMP.

W
P
a
in
is
pre
ab.

Table 3. Proton resonances monitored throughout the course of the glutathione/AMP competition experiment.

	Standard	t=0 min	t=15 min	t=2 h	t=4 h	t=24 h
Ade H8	δ 8.37	δ 8.45	δ 8.42	δ 8.42	δ 8.42	δ 8.42
Ade H2	δ 8.07	δ 8.18	δ 8.14	δ 8.12	δ 8.14	δ 8.13
Ade H1'	δ 5.97 δ 5.95	δ 6.02	δ 6.00 δ 5.98	δ 6.00 δ 5.98	δ 6.00 δ 5.98	δ 6.00 δ 5.98
Gsh 4	δ 2.01	δ 2.00				
Gsh 5	δ 2.30	δ 2.39	δ 2.39	δ 2.37	δ 2.36	δ 2.37
Gsh 3	δ 2.78	δ 2.79	δ sm	δ sm	δ 2.83	δ 2.84
Gsh 6	δ 3.61					
Gsh 1	δ 3.61					
Gsh 2	δ 4.40	δ 4.40				
Acetate	δ 1.74	δ 1.76 δ 1.75	δ 1.77 δ 1.74	δ 1.77 δ 1.74	δ 1.77 δ 1.74	δ 1.77 δ 1.75

Cysteine/AMP NMR tube reaction (3)

Since cysteine concentrations in the cell are much lower than the concentrations of methionine and glutathione, this reaction is not as indicative of what may happen in a cell treated with dirhodium tetraacetate. The reaction was performed because previous researchers had reported some surprising results about this reaction that we found difficult to accept. Furthermore cysteine is an important moiety in a large number of proteins, although the glutathione reaction is a better model for reactions of proteins with antitumor agents.

Reactions of $\text{Rh}_2(\text{O}_2\text{CCH}_3)_4$ with cysteine proceed differently than the previous two reactions (Table 4, Figure A3) in that the acetate is immediately labilized within the time of mixing (time zero) as indicated by the appearance of

free acetate resonances. Based on other NMR experiments and on the bulk reaction, this is not an unexpected result. Displacement of all the acetate ligands appears to be the trend for cysteine reactions with dirhodium tetraacetate.

Cysteine peak shifts occur for both the α CH and β CH₂ groups. At time zero, the β CH₂ experiences the greatest shift (0.05 ppm) whereas the α CH does not appear to have shifted. After 15 minutes, the β CH₂ remains essentially unchanged, but it decreases in intensity and the familiar quartet of doublets begins to appear in the expected position. The α CH peak decreases in intensity and begins to appear downfield of a sugar peak. This trend continues until the original peak has disappeared and the new peak remains unchanged after 24 h.

An unusual shifting of the adenine resonances occurs throughout the course of the reaction. At the time of mixing, H8 has shifted by 0.02 ppm, H2 by 0.03 ppm and H1' by 0.01 ppm, a clear indication that the nucleotide is reacting. After 5 minutes has elapsed, the peaks begin to shift upfield again. H8 moves by 0.01, H2 by 0.02, and H1' by 0.01 for shifts of 0.01 for H8, 0.01 for H2, and 0.00 for H1'. These values remain essentially constant throughout the rest of the experiment. It appears as though the AMP reacts initially, but then is released after about fifteen minutes. One possible explanation for this is that axial binding of AMP to the core would no longer be stabilized by H-bonding of the exocyclic amine group in the absence of acetate oxygen atoms (Figure 45). The lack of stabilization via hydrogen bonding is the reason that guanine was originally thought to be unreactive towards dirhodium tetraacetate. Indeed guanine purines

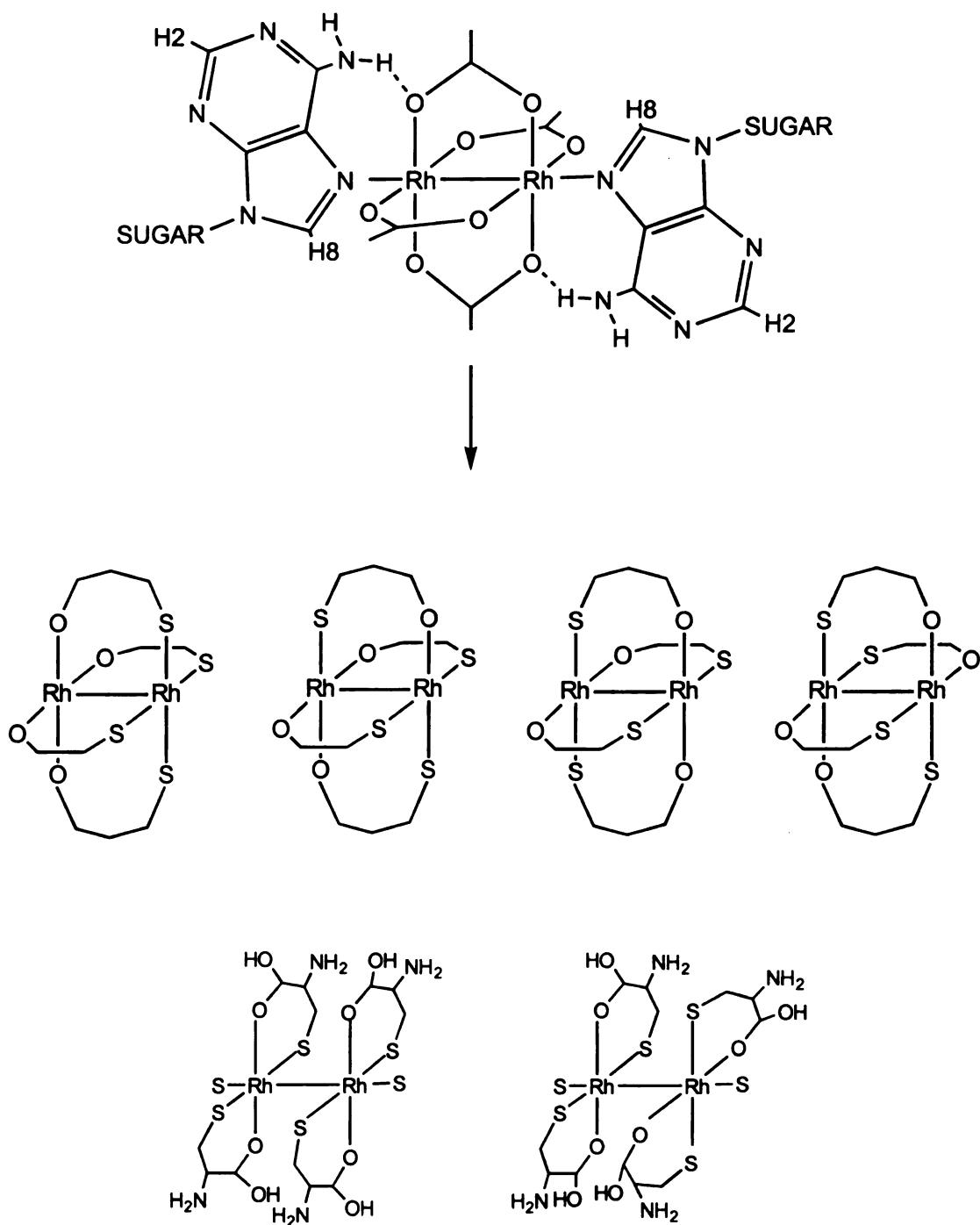


Figure 45. Proposed products formed in the competition reaction with cysteine and AMP.

A
t
s
d
st
los

are found to bind equatorially instead of axially, most likely due to repulsive interactions between the O6 ketone and acetates. If cysteine is a better equatorial ligand than AMP, it may not allow AMP to compete for the equatorial sites.

Table 4. Proton resonances monitored over time for the cysteine/AMP competition reaction.

	Standard	t=0 min	t=15 min	t=2 h	t=4 h	t=24 h
Ade H8	δ 8.38	δ 8.40	δ 8.39	δ 8.39	δ 8.39	δ 8.39
Ade H2	δ 8.07	δ 8.10	δ 8.08	δ 8.08	δ 8.08	δ 8.08
Ade H1'	δ 5.97 δ 5.95	δ 5.98 δ 5.96				
Cys βCH ₂	δ 2.88	δ 2.93	δ 2.92s	δ 2.86s	δ 2.88	δ 2.98
Cys αCH	δ 3.82	δ 3.82	δ 3.82	δ 3.82	δ sh	δ 3.95
Acetate	δ 1.74	δ 1.75	δ 1.74	δ 1.74	δ 1.74	δ 1.74

B. Dirhodium Tetraacetate Reactions

Rh₂(O₂CCH₃)₄(CH₃OH)₂ + cysteine (4)

This reaction was performed in order to verify the results of previous experiments that claimed cysteine disrupts the cage of the dirhodium tetraacetate molecule. One equivalent of cysteine was titrated into a solution of dirhodium tetraacetate for a total of four equivalents. As can be clearly seen in the ¹H NMR spectra after addition of each equivalent (Figure A4), the original acetate peak decreases and a new peak appears. Integration of these two peaks (Table 5) shows that after the addition of one equivalent of cysteine, one acetate has been lost from the dirhodium tetraacetate core. The addition of a second equivalent of

cysteine gives a 1:1 ratio of bound acetate to new acetate, resulting from the displacement of two acetates. Three equivalents of cysteine result in the displacement of yet another acetate, leaving one bound acetate. The addition of the fourth and final equivalent of cysteine, results in the replacement of all original acetate ligands. To determine which type of acetate the peak at 1.79 ppm corresponded to (free or bound), a solution of NaO_2CCH_3 was added to the reaction. This resulted in the increase of the new acetate resonance, leading to the conclusion that cysteine causes the displacement of all bound acetate ligands from the dirhodium core (Figure 46).

Table 5. Integration of bound:free acetate for the cysteine/dirhodium tetraacetate reaction.

Ratio	Bound	Free	Integration
Tetraacetate	1.62		
1:1	1.62	1.79	1.0:0.32
1:2	1.62	1.79	1.0:0.65
1:3	1.62	1.79	1.0:0.33
1:4	1.62	1.79	1.0:0.13

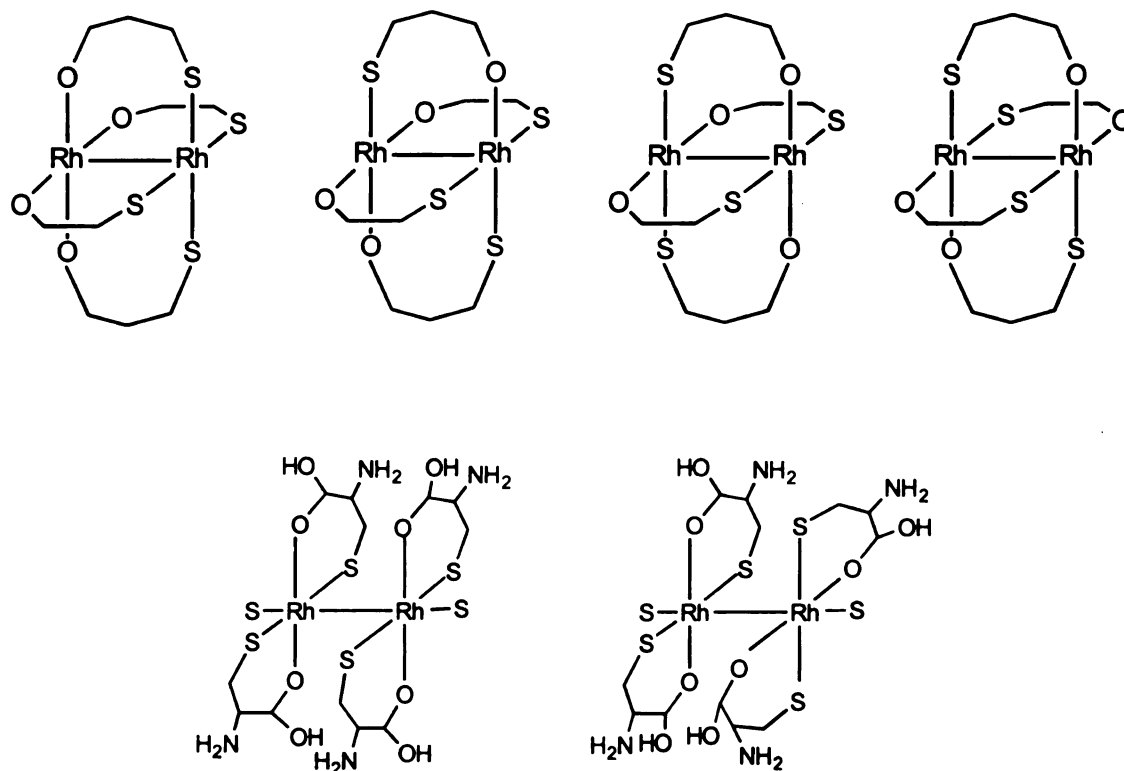


Figure 46. Proposed products from the reaction of four equivalents of cysteine with dirhodium tetraacetate.

$\text{Rh}_2(\text{O}_2\text{CCH}_3)_4(\text{CH}_3\text{OH})_2$ + glutathione (5)

This experiment was carried out in the same manner as the cysteine experiment. Since free $-\text{SH}$ containing biomolecules are claimed to be capable of destroying the tetraacetate cage, it is reasonable to assume that glutathione should cause the same type of reaction as cysteine. As can be observed from the NMR data (Figure A5, Table 6), this is not the case. The addition of one equivalent of glutathione causes free acetate to appear in the NMR spectrum (close to a 1:3 ratio of free:bound). Following the addition of a second

equivalent, the free acetate peak increases in intensity, and the ratio is close to a 1:1 ratio of bound:free acetate. The addition of the third and fourth equivalent causes little additional change in the spectrum. It appears from these data that glutathione does not react with dirhodium tetraacetate in a manner akin to cysteine. Instead of replacing all of the acetate groups, two remain attached to the dirhodium core (Figure 47). This is further supported by elemental analyses carried out on the bulk product which support the formulation of the product as $\text{Rh}_2(\text{O}_2\text{CCH}_3)_4(\text{GS})_2(\text{H}_2\text{O})_4$.

Table 6. Integration of bound:free acetate for the glutathione/dirhodium tetraacetate reaction.

Ratio	Bound	Free	Integration
Tetraacetate	1.62		
1:1	1.67	1.84	1.0:0.20
1:2	1.67	1.84	1.0:0.44
1:3	1.67	1.84	1.0:0.72
1:4	1.67	1.84	1.0:1.0

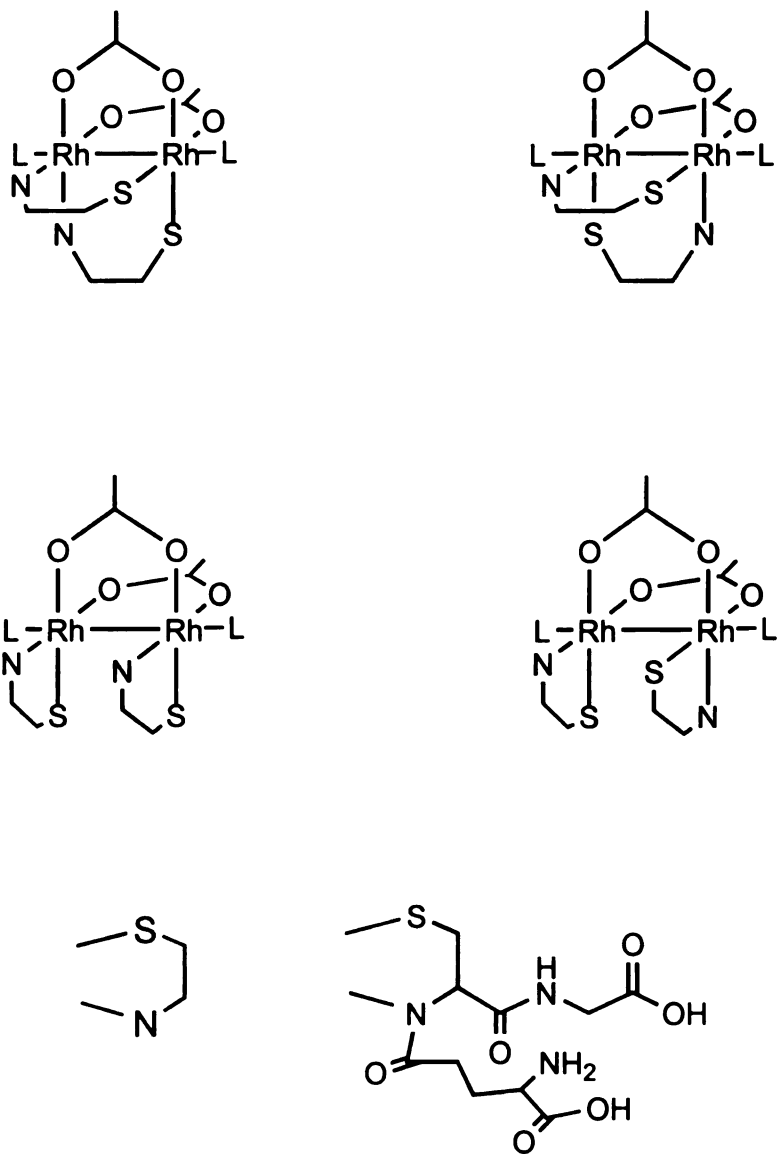


Figure 47. Proposed products from the reaction of glutathione with dirhodium tetraacetate

$\text{Rh}_2(\text{O}_2\text{CCH}_3)_4(\text{CH}_3\text{OH})_2$ + methionine (6)

Following the same procedures as above, the methionine reaction was performed in an effort to document the type of reaction that takes place with an $-\text{SCH}_3$ containing molecule. If methionine reacts with dirhodium tetraacetate to form an axial bond through the sulfur atom, the acetate peak should shift accordingly. The addition of one equivalent of methionine leads to the appearance of a broad resonance at 2.02 ppm (Figure A6). This is thought to be an acetate peak associated with an axially bound methionine. Integration is inconclusive due to the presence of an overlapping βCH peak. The addition of a second equivalent of methionine causes the peak to increase in intensity. This trend continues with the addition of the third and fourth equivalents as well. This type of behavior is different than that observed for reactions of the $-\text{SH}$ containing biomolecules. This is obviously due to differences in the lability of acetate ligands in the presence of axial methionine versus the equatorial glutathione and cysteine molecules (Figure 48).

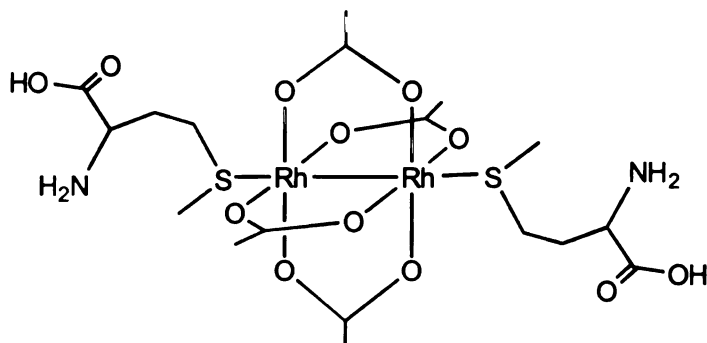


Figure 48. Proposed product from the reaction of methionine with dirhodium tetraacetate.

Rh₂(O₂CCH₃)₄(ATP)₂ + cysteine (7)

This reaction was performed under the same conditions as the dirhodium tetraacetate reactions. The purpose of this experiment is to ascertain the influence of a nucleotide co-ligand on the reaction with cysteine. The reaction was followed by NMR spectroscopy through the addition of four equivalents of cysteine (Figure A7, Table 7). The standard (A7a) shows an acetate peak at 1.73 ppm. The addition of one equivalent of cysteine (A7b) leads to the appearance of a peak at 1.88 in a one to three ratio with the bound acetate resonance. Also of note is the shift of the H8 resonance from 8.49 to 8.47 ppm. The addition of a second equivalent (A7c) leads to an increase in intensity of the free acetate peak, which now integrates at a 1:1 ratio with the bound acetate. The H8 peak continues to shift upfield and is now at 8.47 ppm. Three equivalents lead to a further increase in the intensity of the free acetate peak, but the integration is still at a 1:1 ratio. The H8 resonance shifts to 8.46 ppm. The final addition of cysteine (A7e) does not seem to affect the spectrum. The ratio of bound to free acetate remains at 1:1 and the position of the H8 proton remains constant.

Table 7. Integration of bound:free acetate for the $\text{Rh}_2(\text{O}_2\text{CCH}_3)_4(\text{ATP})_2$ + cysteine reaction.

Ratio	Bound	Free	Integration
Standard	1.73		
1:1	1.73	1.88	1.0:0.24
1:2	1.73	1.88	1.0:0.43
1:3	1.73	1.88	1.0:0.81
1:4	1.73	1.88	1.0:0.95

Shifts are observed in the H8 proton since it is closest to the site of metallation and would be most sensitive to any changes in the electronic environment around the dirhodium core. From this experiment it is apparent that the nucleotide, in this case ATP, bound to the dirhodium core prevents the displacement of all bound acetates as opposed to the dirhodium tetraacetate experiment with cysteine. Extrapolated to a cellular setting, one may speculate that DNA bound dirhodium acetate would not be readily destroyed by an amino acid such as cysteine. The amino acid could complex itself with the rhodium-DNA adduct, but would not lead to loss of DNA interactions (Figure 49).

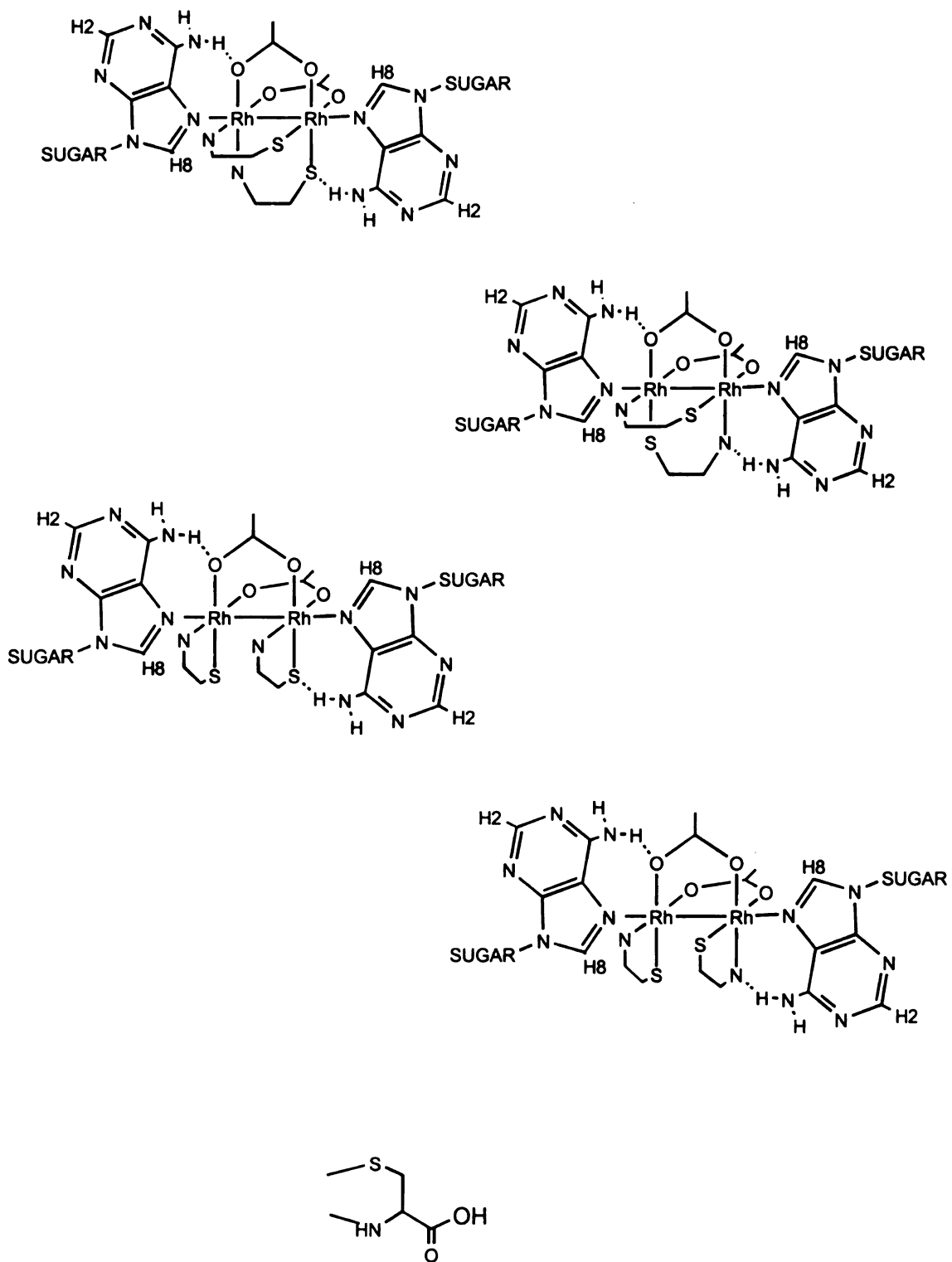


Figure 49. Proposed products from the reaction of cysteine with a dirhodium tetraacetate/ATP derivative.

Rh₂(O₂CCH₃)₂(GTP)₂ + cysteine (8)

If the trend as in the same as the ATP reaction, one may expect that reaction of the GTP-rhodium adduct with cysteine will lead to an incomplete substitution of acetate ligands. The bound acetate peak appears at 1.98 ppm in the standard (Figure A8, Table 8). The addition of one equivalent of cysteine lead to the appearance of a small peak at 1.81 ppm. Two equivalents of cysteine cause an increase in intensity of this new peak, and a slight shift in the H8 proton resonance. The addition of three equivalents does not lead to an increase in the intensity of the new acetate peak. The fourth equivalent shows no change in the acetate region, but the H8 peak shifts by ~0.02 ppm upfield from its original position. This experiment reveals that at most only one of the acetate ligands is replaced by cysteine, but that the parent molecule is still intact (Figure 50).

Table 8. Integration of bound:free acetate for the Rh₂(O₂CCH₃)₂(GTP)₂ + cysteine reaction.

<u>Ratio</u>	<u>Bound</u>	<u>Free</u>	<u>Integration</u>
Standard	1.98		
1:1	1.98	1.81	1.0:0.10
1:2	1.98	1.81	1.0:0.44
1:3	1.98	1.81	1.0:0.43
1:4	1.98	1.81	1.0:0.49

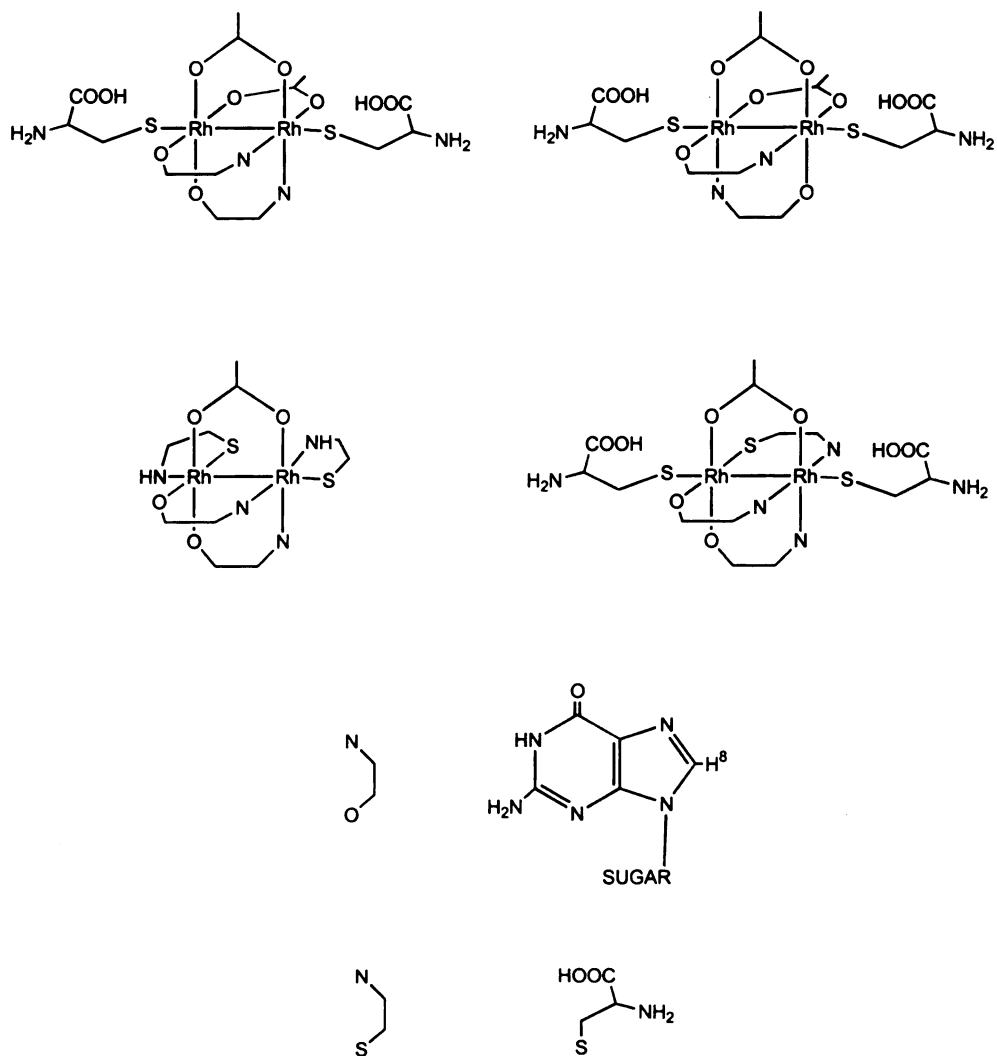


Figure 50. Proposed products from the reaction of cysteine with a dirhodium tetraacetate/GTP derivative

[Rh₂(O₂CCH₃)₂(CH₃CN)₆][BF₄]₂ + cysteine (9)

This reaction was performed to determine whether or not cysteine has the same effect on the bis-acetate as it does on the tetraacetate compound. Following the titration by ¹H NMR spectroscopy (Figure A9), it is observed that the reaction that takes place is different than what was anticipated, namely that the two acetate ligands would be replaced by two cysteine molecules. With the addition of each equivalent of cysteine, only one acetate peak is present. Since the appearance of another acetate peak, namely the free acetate peak, does not occur, any shifts in the peak resonance would be due to bound acetate influenced by the changes introduced by the presence of a new ligand (Figure 51). The acetate peak is at 1.79 ppm for the standard spectrum, and shifts to 1.80 ppm during the course of the reaction.

Rh₂(O₂CCH₃)₄(CH₃OH)₂ + O-Methyl cysteine (10)

Since the O-Methyl cysteine molecule possesses the same active binding site as cysteine, namely the HS-C-C-NH₂ moiety, it was expected that the NMR reaction would show the displacement of all the acetate ligands (Figure A10, Table 9). With the addition of one equivalent of O-Mecys, the appearance of a new acetate peak at 1.92 ppm is apparent. Integration against the initial acetate peak shows less than a 1:3 ratio. The addition of a second equivalent shows an increase in the intensity of the new peak which now integrates as one acetate to three acetate ligands. The addition of three and four equivalents of O-Methyl cysteine lead to an integration of 1:1 for initial:new acetate. This reaction was expected to result in the displacement of all four acetates, but instead, only two

were substituted (Figure 52). This reaction seems to follow the trend of the glutathione rather than the cysteine chemistry.

Table 9. Integration of bound:free acetate for the reaction of O-methyl cysteine with dirhodium tetraacetate.

Ratio	Bound	Free	Integration
Standard	1.67		
1:1	1.67	1.72	1.0:0.21
1:2	1.67	1.72	1.0:0.35
1:3	1.67	1.72	1.0:0.47
1:4	1.67	1.72	1.0:0.49

$\text{Rh}_2(\text{O}_2\text{CCH}_3)_4(\text{CH}_3\text{OH})_2$ + 2-aminothiophenol (11)

The ^1H NMR tube reaction of 2-aminothiophenol proved to be more difficult than the previous reactions as CD_3OD was required to solubilize the 2-aminothiophenol. The tetraacetate was dissolved in the D_2O buffer used for all the other experiments. With the addition of one equivalent of 2-aminothiophenol, a shoulder appears on the downfield side of the acetate peak (Figure A11). Integration is not possible due to the close proximity of these peaks. Two equivalents lead to an increase in the shoulder, and a slight shifting of the phenol protons. Addition of a third and fourth equivalent serve to increase the intensity

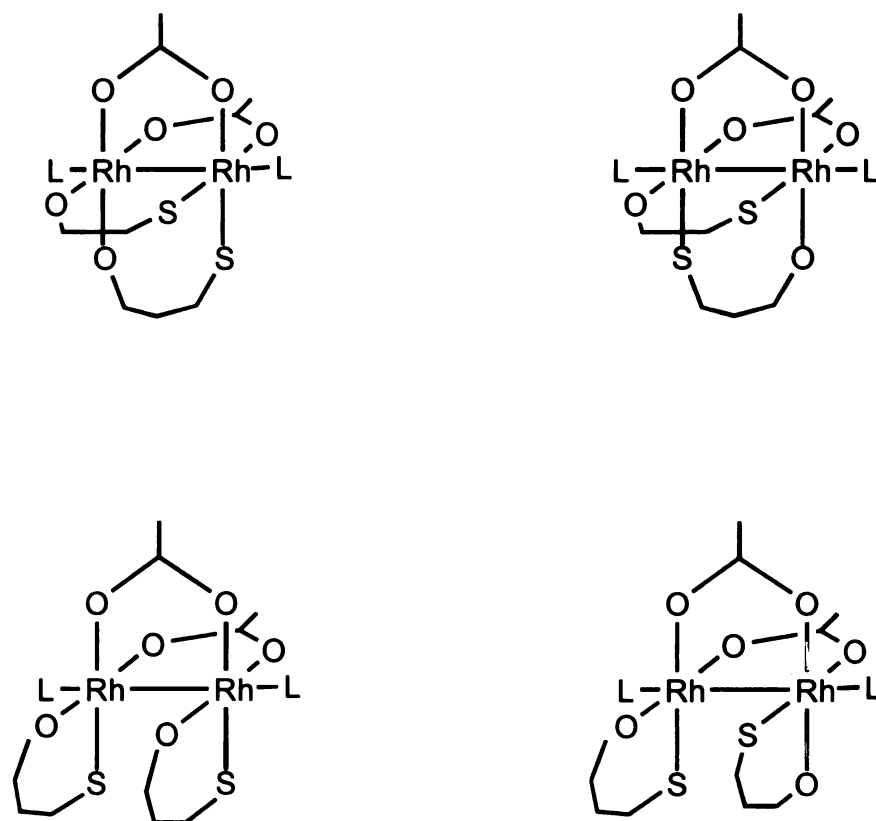


Figure 51. Proposed products from the reaction of cysteine with dirhodium bis-acetate.

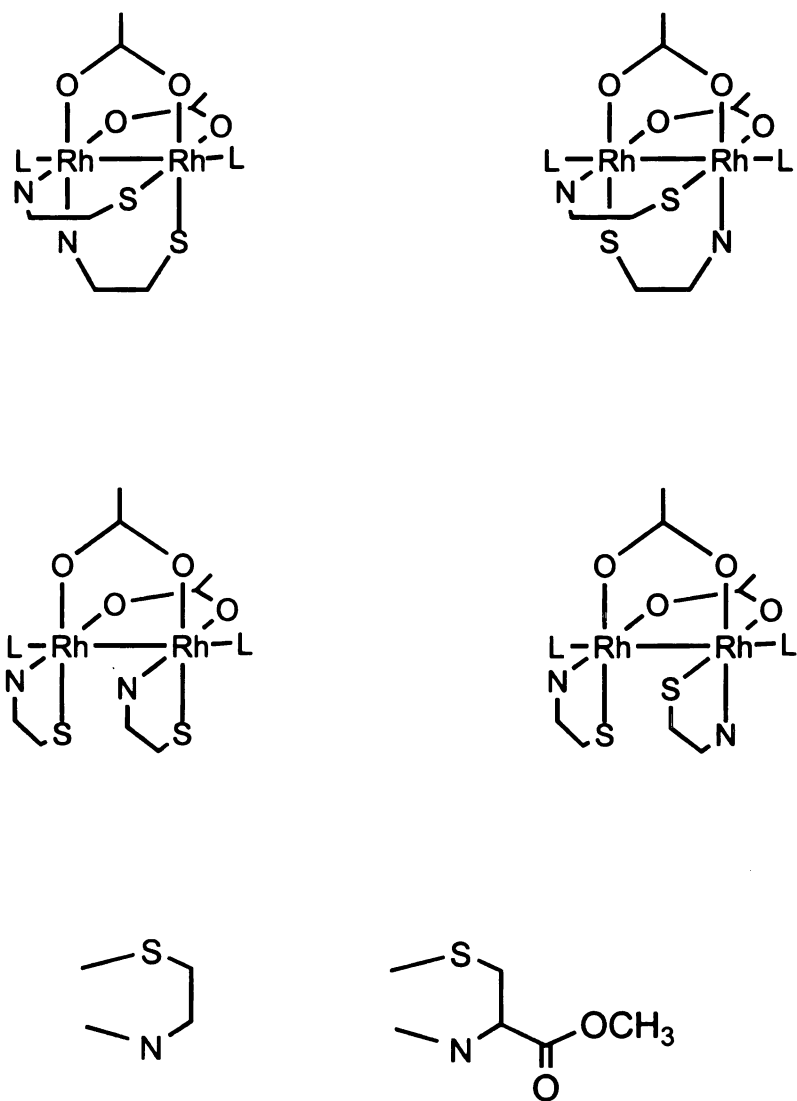


Figure 52. Proposed products from the reaction of O-methyl cysteine with dirhodium tetraacetate.

of the shoulder and to further increase the shifting of the phenol protons (Figure 54), for total shifts of 0.06 (b), 0.10 (a), 0.05 (d), and 0.04 (c) ppm. These data support the conclusion that this ligand exhibits a binding behavior different from that of cysteine (Figure 53) in that it does not replace the acetate ligands.

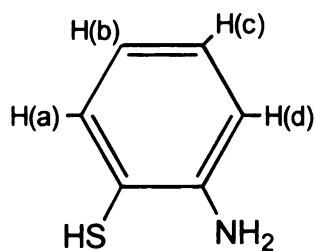


Figure 54. Labeling scheme for 2-aminothiophenol.

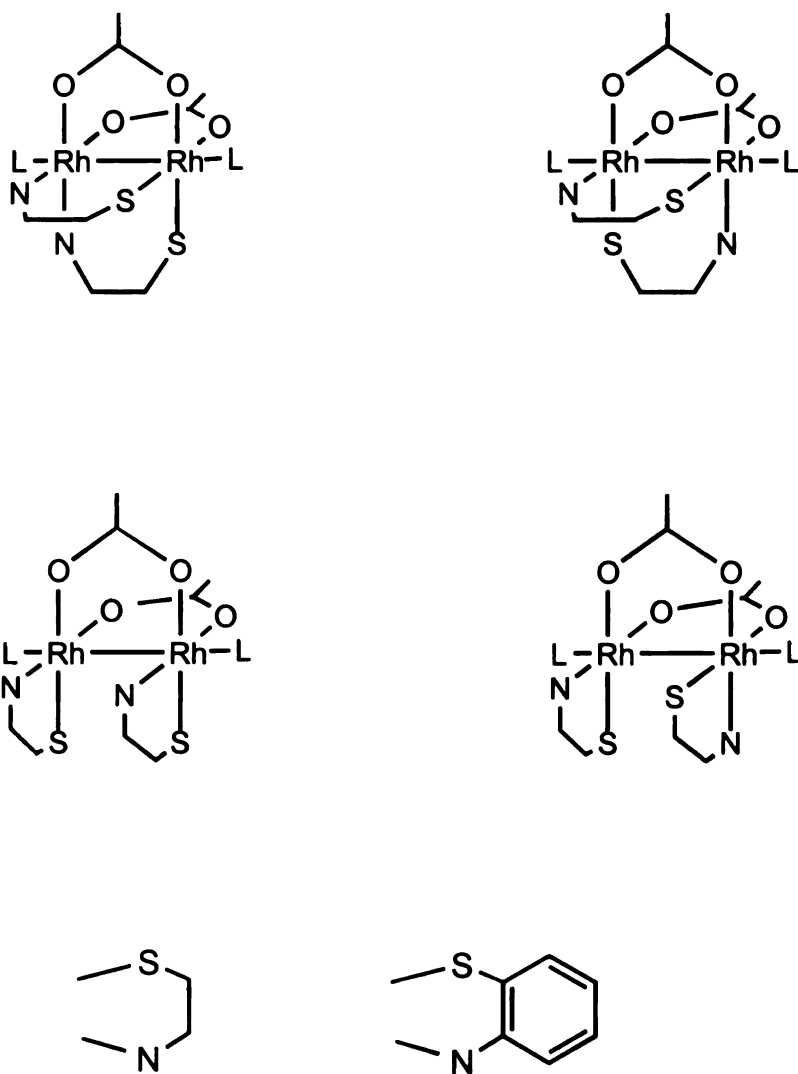


Figure 53. Proposed products from the reaction of dirhodium tetraacetate with 2-aminothiophenol.

4. Conclusions

A. Competition reactions

Reactions of dirhodium tetraacetate in which both amino acids and nucleotides are present have led to interesting conclusions about the reactivity of antitumor agents such as *cis*-platin and dirhodium tetraacetate. This type of reaction allows one to determine which biomolecule is preferred, if a preference indeed exists. The possibility of protein-metal-DNA crosslinking can be envisioned due to the outcome of these reactions. The competition reactions with methionine and glutathione reveal that, although binding of an amino acid occurs, this does not prevent binding of the nucleotide and vice versa. The reactions show that when faced with both an amino acid and a nucleotide, the dirhodium compounds react with both types of molecules. One of the more important outcomes of this work is the realization that binding of an –SH containing peptide, glutathione, does not result in a deactivation of the dirhodium acetate compound as previously postulated. The cysteine reaction is different in that both the amino acid and the nucleotide react at the start of the reaction, but with time, the AMP seems to be selectively removed from the dirhodium compound. This could be the result of steric interactions between the amino group on the adenine and the bridging cysteine. The stabilizing influence of hydrogen bonds is no longer possible without the acetate ligands, and the adenine may not be a good axial ligand in the absence of these interactions. In the final analysis, the most important reactions are those with glutathione and

methionine, as these indicate that, even in the presence of sulfur containing amino acids, dirhodium tetraacetate is still capable of reacting with DNA purines.

B. Dirhodium Tetraacetate Reactions

Titration of the sulfur containing amino acids cysteine, methionine, and glutathione into solutions of dirhodium tetraacetate and its derivatives has led to some interesting findings. In the case of methionine, a simple axial addition is observed, whereas with glutathione, displacement of two acetates is preferred. Finally, cysteine displaces all four acetate ligands to give a single, diamagnetic product. This latter result is in accordance with the earlier experiments that suggest cysteine breaks the carboxylate cage. The claims of a Rh(II) mononuclear product have been refuted, however, as we have incontrovertible evidence that the Rh-Rh bond has not been broken. Earlier literature had claimed that reactions of dirhodium tetraacetate with -SH containing biomolecules causes this breakdown to occur. Results from the glutathione experiment have proven this claim to be unfounded. In the case of cysteine, mass spectrometry and elemental analyses on the bulk product (Chapter 2) point to the conclusion that the acetates are replaced by cysteine ligands, but that the dinuclear rhodium core is still intact.

Cysteine mimics, such as O-Methyl cysteine and 2-Aminothiophenol, were studied to determine if molecules with the same HS-C-C-NH₂ moiety as cysteine would lead to substitution of the acetate ligands. The reaction of O-Methyl cysteine with dirhodium tetraacetate did not follow the expected pattern for a

nitrogen-sulfur bridging molecule. Instead of substituting all four of the acetate ligands, it appears that only two of the acetates are replaced during the course of the reaction. 2-Aminothiophenol gave similar results. Although integration is hindered by the close proximity of the two acetate peaks, it appears that incomplete substitution of the bound acetate is occurring. Due to these findings, the question is posed about the potential binding sites of the amino acid cysteine. The mimics were chosen for their H₂N-C-C-SH moiety, which was considered to be the reactive group on the cysteine molecule. Since these molecules do not behave in the same manner as cysteine, it seems logical to conclude that the carboxylate group is playing a role in the metal reactivity of the complex.

Experiments wherein dirhodium tetraacetate that had been previously reacted with a nucleotide was followed by treatment with cysteine supports the conclusion that the reaction with cysteine is not destructive to the dinuclear structure. Both the ATP and GTP reactions indicate displacement of acetate ligands is occurring, but, complete substitution does not occur. After the fourth equivalent of cysteine has been added, the core structure is still intact. It is possible to predict from these model studies that dirhodium tetraacetate/DNA adducts would not be disrupted due to the presence of a strong amino acid, such as cysteine.

Chapter V
Reactions of Dirhodium Bis-acetate with DNA

1. Introduction

Inhibition of DNA replication can be achieved by the interaction of DNA with an agent that binds either by covalent or non-covalent interactions. Noncovalent antitumor compounds include intercalators and minor groove binding molecules. Intercalators exhibit a high degree of sequence specificity and are composed of functional groups attached to a planar aromatic chromophore. Anthracyclines, which demonstrate anticancer activity, consist of a sugar group that can position itself in the minor groove by hydrogen bonding to base pair edges (Figure 55). Likely targets include CpG and TpG, as a result of the favorable binding site on the exocyclic N2 of guanosine. Intercalation of these types of compounds causes the minor groove to widen, resulting in an overall distortion of the helix ⁵.

The minor groove of DNA is an optimal target for antitumor compounds. A molecule that binds to the minor groove is able to evade the major groove repair enzymes. A majority of these agents inhibit transcription and/or replication and have been shown to interfere with DNA topoisomerase II (introduces negative supercoils in DNA, and is necessary for DNA synthesis to occur). Although minimal structural distortion occurs, more subtle alterations to recognition signals for regulatory proteins may occur, causing a lack of sequence recognition by the protein, thereby inhibiting DNA replication and/or repair. Two examples of the drugs that cause this activity to occur are netropsin and anthramycin ^{60,61}. Netropsin (Figure 56) is a naturally occurring antibiotic that exhibits both

anticancer and antiviral activity. This activity stems from its ability to bind the minor groove of

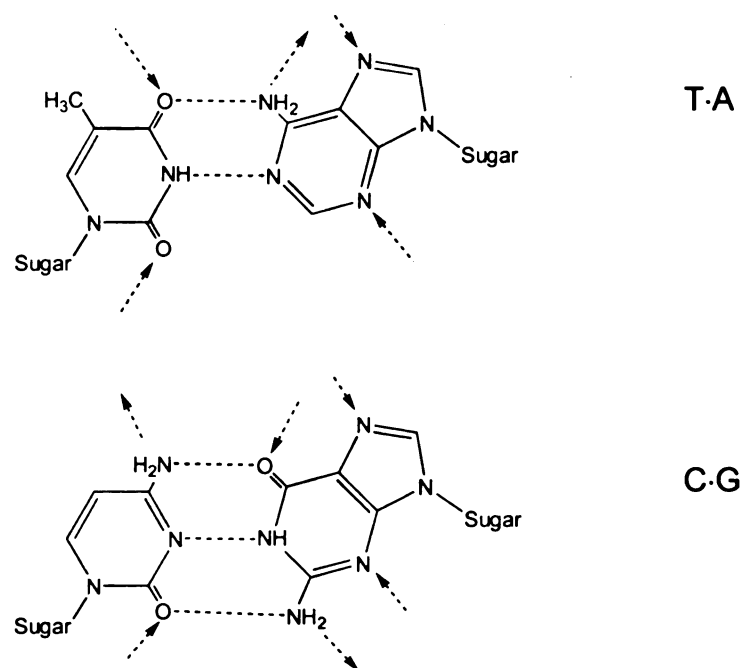


Figure 55. Potential hydrogen-bond interactions with base edges in A·T and G·C base pairs. Donors and acceptors are indicated by direction of the arrowheads.

DNA, specifically AT rich regions. A crystal structure of a netropsin adduct has been obtained with the decamer d(CGCAATTGCG) (Figure 57b). Netropsin has also been crystallized with several other strands of DNA, e. g. d(CGCGAATTCGCG)₂ and d(CGCAAATTTGCG)₂. Information obtained from crystal structures of these drugs is important in the design and synthesis of analogues with altered sequence specificity, for example preferential GC base pair binding⁶⁰.

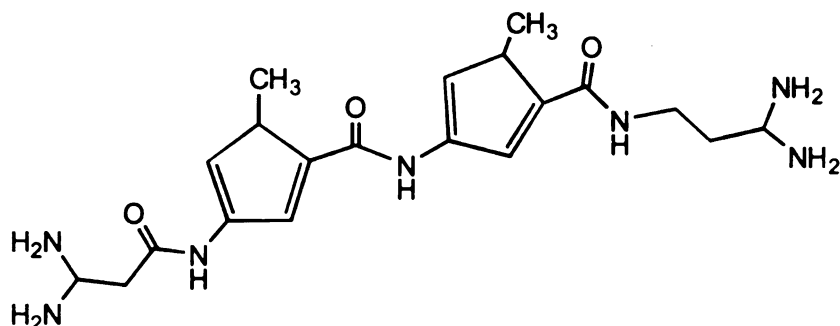


Figure 56. The minor groove binding drug Netropsin.

Anthramycin (Figure 58) is a naturally occurring anti-tumor antibiotic that has been crystallized with the decamer d(CCAACGTTGG) (Figure 57a). The drug was found to covalently bind in a 2:1 ratio with DNA and to target the 5'-GGT sequences at each end of the duplex. Binding causes an overall decrease in the width of the minor groove. Like netropsin, amide tails participate in hydrogen bonding to base pair edges. From these structures, and others like them, it is possible to identify two important factors in the binding of minor groove drugs, these are groove width alterations and hydrogen bonding to base edges⁶¹.

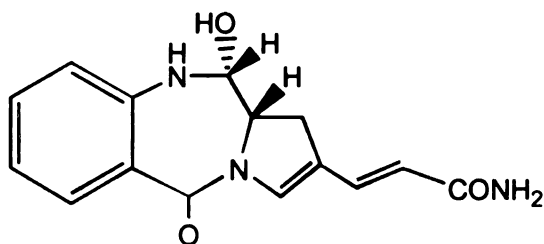
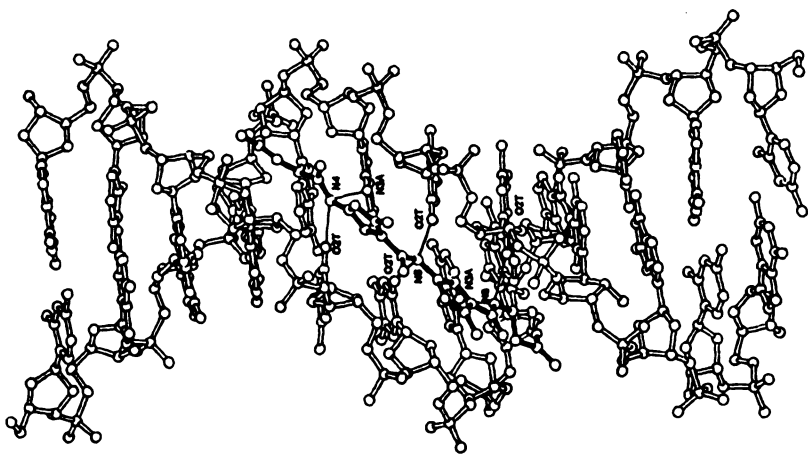
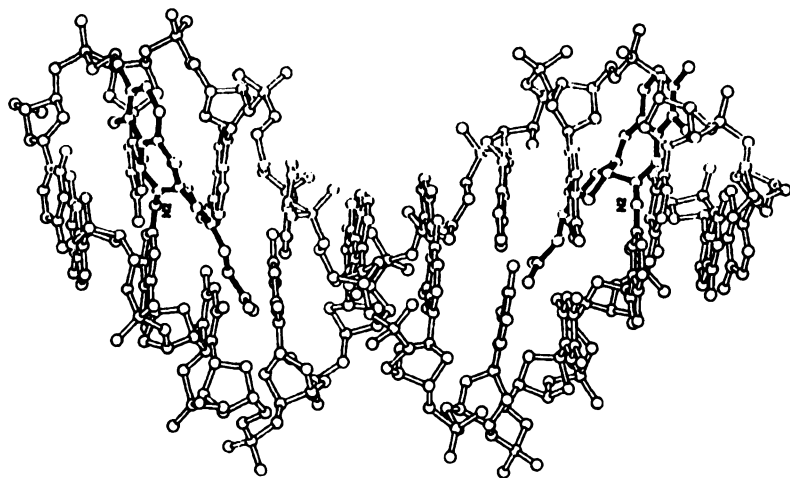


Figure 58. The minor groove binding drug Anthramycin.



(a)



(b)

Figure 57. Crystal structure of a) anthramycin-d(CCAACGTTGG)₂ and b) netropsin-d(CGCGAATTCGG)₂.

Macroscopic DNA properties, such as bending of the helix upon drug binding, remain to be assessed and understood at the molecular level. This is important for minor groove binding drugs since these interactions may be connected to the drugs' ability to interfere with gene regulatory proteins. In some cases, these interactions induce large structural changes in DNA.

Unlike the non-covalent binding compounds, very few covalent complexes have been crystallized with DNA. Covalent complexes that bind DNA include *cis*-platin, mitomycin nitrogen mustards, and anthramycin. In this work, we hope to add dirhodium bis-acetate to this relatively short list. One reason for the paucity of these structures is that crystallization of covalent complexes has proven to be exceedingly difficult. To date, there are only two known structures involving a covalently bound transition metal complex with DNA ⁵. The most recognized structure consists of the antitumor active *cis*-platin bound to the DNA dodecamer d(CCTCTGGTCTCC)·(GGAGACCAGAGG) (Figure 59). Upon binding to this double stranded oligonucleotide, *cis*-platin forms 1, 2 intrastrand cross-links between two neighboring guanine bases on the same strand. The formation of this cross-link causes the DNA to become severely distorted, resulting in a ~40° bend in the DNA. This structure is the first example of a covalently bound transition metal compound with double stranded DNA ⁶³.

The ability to crystallize this type of complex is important for future Pt drug design, and for a general understanding of the mechanism by which these compounds kill tumor cells. Metallation of the DNA strand causes the duplex to bend towards the major groove and leads to the formation of a type of A/B

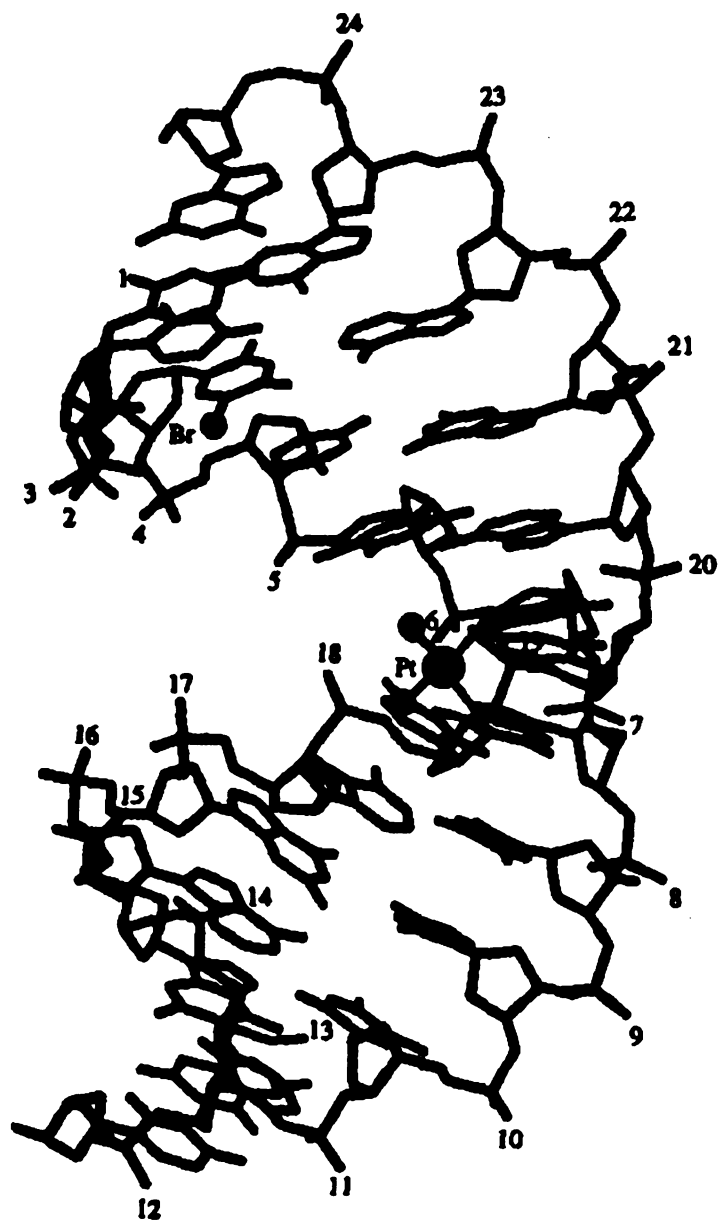


Figure 59. Structure of *cis*-platin-d(CCTCTGGTCTCC)-(GGAGACCAGAGG).

hybrid. This type of hybrid may serve as a cellular recognition signal for certain proteins. This phenomena is thought to occur in the case of other A/B hybrid DNA strands that contain recognition sequences for certain proteins.

Part of *cis*-platin's potent activity is linked to its ability to distort DNA which causes proteins, such as HMG1, to bind these sites thereby diverting the protein from normal activities. In addition, these proteins serve to shield the *cis*-platin adducts from excision repair. The binding of *cis*-platin to DNA causes the helix to bend, thereby exposing the minor groove. This exposure allows proteins, such as HMG/SRY, to bind via their hydrophobic residues which further disrupts base pair stacking. HMG binding to the distorted DNA causes the bend angle to increase by 30-50° which alleviates some of the strain placed on the *cis*-platin molecule ⁶.

Although the modes of binding are different, the covalent and non-covalent drugs seem to share the same general properties. Coordination of *cis*-platin to the GG nucleotides results in hydrogen bonding between one of the platinum ammine ligands and the terminal oxygen of a guanosine terminal phosphate. Metallation of the DNA also results in destacking of the bases and a distortion of the platinum coordination geometry. Another consequence of *cis*-platin binding is major groove compression and minor groove widening to resemble A DNA. It is clear that both classes of antitumor compounds possess the ability to hydrogen bond and cause groove width distortion ^{5,63}.

Another type of *cis*-platin binding to DNA was observed when the drug was diffused into pregrown crystals of d(CGCGAATTCGCG)₂. Crystals were

grown of the sequence, and *cis*-platin was added to the crystals which led to its incorporation into the structure. The X-ray data that were obtained (Figure 60) indicate that DNA did not become distorted, but there was a clear indication of *cis*-platin's affinity for guanine⁶⁴.

To understand the nature of *cis*-platin binding on a smaller scale, smaller di- and tri-nucleotides were used. Crystal structures were obtained with the dinucleotide d(pGpG) (Figure 61) and the trinucleotide d(CpGpG) (Figure 62). Lippard's d(pGpG) structure shows the formation of two Pt-N bonds to the N(7) atoms of the two adjacent guanine nucleotides⁶⁵. Base stacking is disrupted by the binding of *cis*-platin as indicated by the dodecamer crystal structure and NMR modeling studies⁶⁶. Since *cis*-platin was known to preferentially bind guanine, Reedijk and coworkers opted to study the effect of platinum binding on the stacking interactions of neighboring bases. Tripeptides were designed that contain the GpG moiety and in the case of d(CpGpG), the oligonucleotide was crystallized with bound *cis*-platin. It was found that hydrogen bonding between the amino groups and O6 occurs. The cytosine forms hydrogen bonds with a cytosine on a neighboring molecule⁶⁷. These studies revealed that even simple oligonucleotides exhibit the disruption of base pair stacking and hydrogen bonding that occur with the larger pieces of DNA.

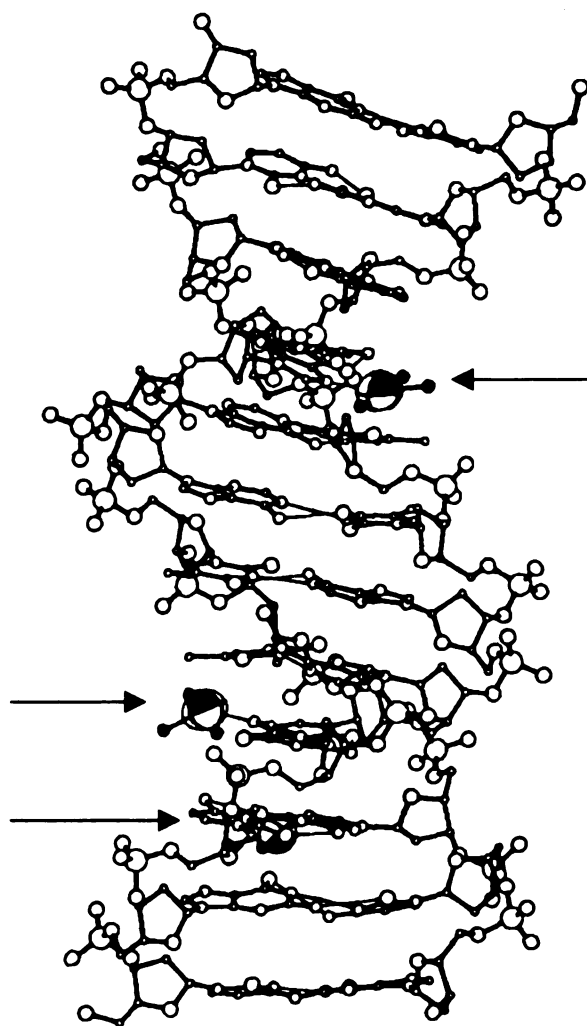


Figure 60. Crystal structure of *cis*-platin bound to d(CGCGAATTCGCG). Arrows indicate the three *cis*-platin molecules bound to the DNA strand.

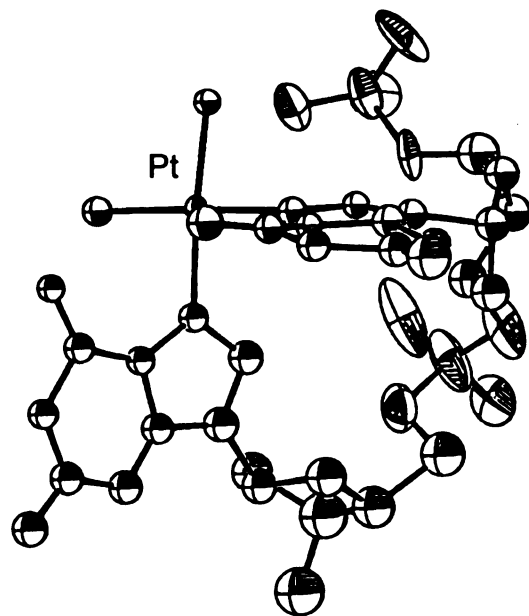


Figure 61. ORTEP representation of *cis*-[Pt(NH₃)₂{d(pGpG)}].

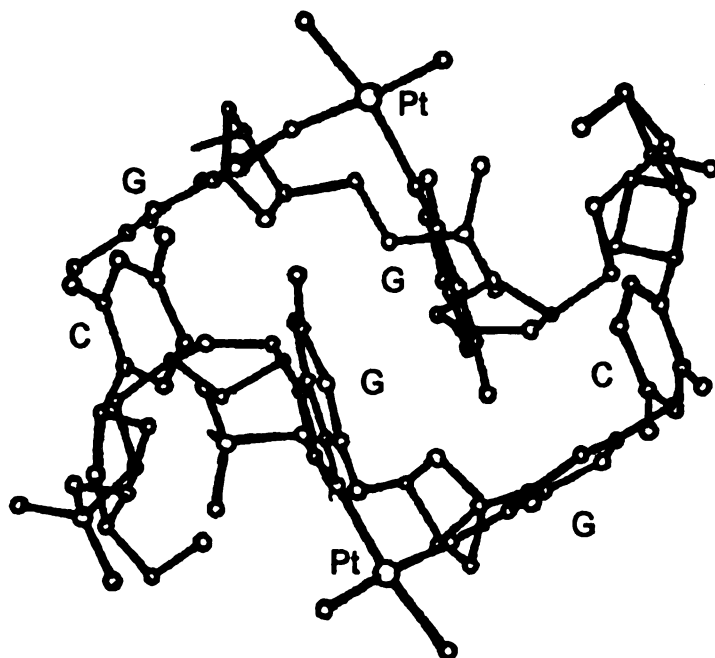


Figure 62. ORTEP stereoview of the intrastrand *cis*-platin d(CpGpG) adduct.

2. Experimental

Each DNA strand was obtained from Yale and purified by anion exchange HPLC on a Perkin Elmer Diode array HPLC equipped with a Source Q15 Anion exchange column. After purification, the DNA was concentrated on a DEAE (Diethylaminoethyl) Cellulose column, then desalted via either G-25 Size Exclusion Sephadex column or by using Centricon SR-3. The resulting strands were then annealed to their complements and set up in boxes for crystallization.

A. Reactions

[Rh₂(O₂CCH₃)₂(CH₃CN)₆][BF₄]₂ + TGC GTT AAC GC (1)

A solution of [Rh₂(O₂CCH₃)₂(CH₃CN)₆][BF₄]₂ (1.9 mg, 3 μmol) in 50 μL of DD H₂O was added to a solution of 11-mer (3 μmol) in 150 μL DD H₂O. The resulting solution immediately turned bright orange upon addition of the dirhodium bis-acetate precursor. The mixture was heated to 70°C for 52 h. At the end of the reaction time, the solution was greenish-brown color.

[Rh₂(O₂CCH₃)₂(CH₃CN)₆][BF₄]₂ + CGC AAT TGC G (2)

A solution of [Rh₂(O₂CCH₃)₂(CH₃CN)₆][BF₄]₂ (1.9 mg, 3 μmol) in 50 μL of DD H₂O was added to a solution of 10-mer (3 μmol) in 150 μL DD H₂O. The resulting solution immediately turned a bright reddish-orange color upon addition of the dirhodium bis-acetate. The mixture was heated to 70°C for 52 h during which time the color turned greenish-brown.

[Rh₂(O₂CCH₃)₂(CH₃CN)₆][BF₄]₂ + CCT CTG GTC TCC (3)

A solution of [Rh₂(O₂CCH₃)₂(CH₃CN)₆][BF₄]₂ (3.8 mg, 6 μmol) in 50 μL of DD H₂O was added to a solution of the GG 12-mer (3 μmol) in 200 μL DD H₂O.

The resulting solution immediately turned a bright orange upon addition of the dirhodium bis-acetate. The volume was increased to 400 μL , and the resulting solution was heated to 70°C for 72 h. At the end of the reaction time, the solution was a greenish-brown color.

$[\text{Rh}_2(\text{O}_2\text{CCH}_3)_2(\text{CH}_3\text{CN})_6][\text{BF}_4]_2$ + CCT CTA ATC TCC (4)

A solution of $[\text{Rh}_2(\text{O}_2\text{CCH}_3)_2(\text{CH}_3\text{CN})_6][\text{BF}_4]_2$ (3.8 mg, 3 μmol) in 50 μL of DD H₂O was added to a solution of the AA 12-mer (3 μmol) in 150 μL DD H₂O. The resulting solution immediately turned a bright reddish-orange upon addition of the dirhodium bis-acetate. The volume was brought to 400 μL , and the resulting solution was heated to 70°C for 72 h. At the end of the reaction time, the solution was a greenish-brown color.

$[\text{Rh}_2(\text{O}_2\text{CCH}_3)_2(\text{CH}_3\text{CN})_6][\text{BF}_4]_2$ + TCT AAT CT (5)

A solution of $[\text{Rh}_2(\text{O}_2\text{CCH}_3)_2(\text{CH}_3\text{CN})_6][\text{BF}_4]_2$ (3.0 mg, 4 μmol) in 50 μL of DD H₂O was added to a solution of the 8-mer (2 μmol) in 150 μL DD H₂O. The resulting solution immediately turned bright orange upon addition of the dirhodium bisacetate. The volume was increased to 400 μL , and the resulting solution was heated to 37°C for 72 h. At the end of the reaction time, the solution was a reddish-purple color.

$[\text{Rh}_2(\text{O}_2\text{CCH}_3)_2(\text{CH}_3\text{CN})_6][\text{BF}_4]_2$ + CTC TAA TCT T (6)

A solution of $[\text{Rh}_2(\text{O}_2\text{CCH}_3)_2(\text{CH}_3\text{CN})_6][\text{BF}_4]_2$ (3.0 mg, 4 μmol) in 50 μL of DD H₂O was added to a solution of the 10-mer (2 μmol) in 150 μL DD H₂O. The resulting solution immediately turned bright orange upon addition of the dirhodium bisacetate. The volume was increased to 400 μL , and the resulting

solution was heated to 37°C for 72 h. At the end of the reaction time, the solution was a reddish-purple color.

[Rh₂(O₂CCH₃)₂(CH₃CN)₆][BF₄]₂ + GAG ATT AGA GA (7)

A 2 μmol quantity of the 11-mer was dissolved in 400 μL of degassed DD H₂O. To this was added 65 μL of a 0.04 M degassed [Rh₂(O₂CCH₃)₂(CH₃CN)₆][BF₄]₂ solution (1:1.3 ratio). The resulting pink solution was heated at 37°C for 72 h. At the end of the reaction time, the solution was a reddish-purple color.

[Rh₂(O₂CCH₃)₂(CH₃CN)₆][BF₄]₂ + CCT CTA ATC TCC (8)

A 4 μmol aliquot of the 12-mer was dissolved in 400 μL of degassed DD H₂O. To this was added 65 μL of a 0.04 M degassed [Rh₂(O₂CCH₃)₂(CH₃CN)₆][BF₄]₂ solution (1:1.3 ratio). The solution, which immediately turned orange, was heated at 37°C for 72 h. At the end of the reaction time, the solution was a reddish-purple color.

B. Anion Exchange HPLC Purification.

1. Unmetallated Strands

Each unmetallated strand was purified using a NaOH/NaCl eluant system. The DNA was dissolved in a 10 mM NaOH solution and purified one micromole at a time using a gradient. Eluent A: 10 mM NaOH, 0.2 M NaCl, eluant B: 10 mM NaOH, 1 M NaCl.

GGA GAC CAG AGG was purified by the following gradient: 5 minutes gradient 36% B, 60 minutes gradient 41% B, 5 minutes gradient 100% B, 5 minutes isocratic 100% B, 5 minutes gradient 0% B.

GGA GAT TAG AGG was purified by the following gradient: 5 minutes gradient 40% B, 60 minutes gradient 45% B, 5 minutes gradient 100% B, 5 minutes isocratic 100% B, 5 minutes gradient 0% B.

GAG ATT AGA A was purified by the following gradient: 5 minutes gradient 30% B, 60 minutes gradient 35% B, 5 minutes gradient 100% B, 5 minutes isocratic 100% B, 5 minutes gradient 0% B.

GAG TTA GA was purified by the following gradient: 5 minutes gradient 30% B, 60 minutes gradient 35% B, 5 minutes gradient 100% B, 5 minutes isocratic 100% B, 5 minutes gradient 0% B.

GAG ATT AGA GA was purified by the following gradient: 5 minutes gradient 35% B, 60 minutes gradient 40% B, 5 minutes gradient 100% B, 5 minutes isocratic 100% B, 5 minutes gradient 0% B.

TGG AGA TTA GAG G was purified by the following gradient: 5 minutes gradient 66% B, 60 minutes gradient 71% B, 5 minutes gradient 100% B, 5 minutes isocratic 100% B, 5 minutes gradient 0% B.

AGG AGA TTA GAG G was purified by the following gradient: 5 minutes gradient 66% B, 60 minutes gradient 71% B, 5 minutes gradient 100% B, 5 minutes isocratic 100% B, 5 minutes gradient 0% B.

2. Metallated Strands

Each reacted strand was purified using an acetate buffer system. The DNA was purified one micromole at a time using a gradient. Eluent A: 0.02 M NaO₂CCH₃, 20% CH₃CN, eluant B: 0.02 M NaO₂CCH₃, 1.2 M KCl, 20% CH₃CN.

TGC GTT AAC GC was purified by the following gradient: 5 minutes gradient 40% B, 60 minutes gradient 45% B, 5 minutes gradient 100% B, 5 minutes isocratic 100% B, 5 minutes gradient 0% B.

GCG TTA ACG C was purified by the following gradient: 5 minutes gradient 40% B, 60 minutes gradient 45% B, 5 minutes gradient 100% B, 5 minutes isocratic 100% B, 5 minutes gradient 0% B.

CCT CTG GTC TCC was purified by the following gradient: 5 minutes gradient 30% B, 30 minutes gradient 40% B, 5 minutes gradient 100% B, 5 minutes isocratic 100% B, 5 minutes gradient 0% B.

CCT CTA ATC TCC was purified by the following gradient: 5 minutes gradient 30% B, 30 minutes gradient 40% B, 5 minutes gradient 100% B, 5 minutes isocratic 100% B, 5 minutes gradient 0% B.

CTC TAA TCT T was purified by the following gradient: 5 minutes gradient 35% B, 30 minutes gradient 40% B, 5 minutes gradient 100% B, 5 minutes isocratic 100% B, 5 minutes gradient 0% B.

CTC AAT CT was purified by the following gradient: 5 minutes gradient 30% B, 30 minutes gradient 35% B, 5 minutes gradient 100% B, 5 minutes isocratic 100% B, 5 minutes gradient 0% B.

TCT CTA ATC TC was purified by the following gradient: 5 minutes gradient 28% B, 30 minutes gradient 33% B, 5 minutes gradient 100% B, 5 minutes isocratic 100% B, 5 minutes gradient 0% B.

CCT CTA ATC TCC was purified by the following gradient: 5 minutes gradient 30% B, 30 minutes gradient 37% B, 5 minutes gradient 100% B, 5 minutes isocratic 100% B, 5 minutes gradient 0% B.

C. DEAE column

The purpose of this column is to concentrate a large volume of sample into a few milliliters. Diethylaminoethyl cellulose (DEAE) resin is equilibrated with 10 mM TRIS buffer. The DNA sample is diluted up to four times its original concentration with 10 mM TRIS, and loaded onto a 10 cm x 1.5 cm column. The DNA is then eluted from the column by a 10 mM TRIS, 1 M NaCl solution and collected in 1 mL fractions that are screened by UV at 265 nm.

D. G-25 Sephadex column

The G-25 Sephadex column is used to desalt DNA fractions after the DEAE column has been run. Salty DNA is loaded onto the column, eluted with DD H₂O and collected in 1 mL fractions that are screened by UV absorbance at 265 nm. The samples are then dried in a centrivap to concentrate.

E. Centricon SR-3

Centricon SR-3 were used to simultaneously concentrate and desalt larger strands of DNA (12bp and larger). Samples were placed in the Centricons and centrifuged at 6500 RPM until minimal volume was achieved, usually after 2h. The samples were washed with two portions of 2 mL DD H₂O to desalt. The final volume was between 40-100 μ L.

F. Concentrations

The concentration of the samples was determined by Beer's law: $A=b\epsilon c$. Molar absorptivity coefficients for each DNA strand were obtained from the biopolymer calculator on the Yale web site. The molar absorptivity coefficient for dirhodium bis-acetate transitions were determined by UV analysis at 265 nm using a known concentration of the sample. The samples were dissolved in 200-400 μ L of DD H₂O for a final concentration of 10 mg/mL.

G. Annealing

Annealing the reacted strands to their complements was achieved by heating the samples to 100°C followed by a gradual cooling to room temperature.

H. Crystallization screens

The following crystallization screens were obtained from the Hampton Research Catalog:

Nucleic Acid Mini-Screen (NAM)

1. 10% MPD, pH 5.5, 20 mM Cobalt Hexamine, 20 mM MgCl₂
2. 10% MPD, pH 5.5, 20 mM Cobalt Hexamine, 80 mM NaCl, 20 mM MgCl₂
3. 10% MPD, pH 5.5, 20 mM Cobalt Hexamine, 12 mM NaCl, 20 mM MgCl₂
4. 10% MPD, pH 5.5, 20 mM Cobalt Hexamine, 40 mM LiCl, 20 mM MgCl₂
5. 10% MPD, pH 6.0, 12 mM Spermine tetra-HCl, 80 mM KCl, 20 mM MgCl₂
6. 10% MPD, pH 6.0, 12 mM Spermine tetra-HCl, 80 mM KCl
7. 10% MPD, pH 6.0, 12 mM Spermine tetra-HCl, 80 mM NaCl, 20 mM MgCl₂
8. 10% MPD, pH 6.0, 12 mM Spermine tetra-HCl, 80 mM NaCl

9. 10% MPD, pH 6.0, 12 mM Spermine tetra-HCl, 80 mM NaCl, 12 mM KCl,
20 mM MgCl₂
10. 10% MPD, pH 6.0, 12 mM Spermine tetra-HCl, 12 mM NaCl, 80 mM KCl
11. 10% MPD, pH 6.0, 12 mM Spermine tetra-HCl, 80 mM NaCl, 20 mM BaCl₂
12. 10% MPD, pH 6.0, 12 mM Spermine tetra-HCl, 80 mM KCl, 20 mM BaCl₂
13. 10% MPD, pH 6.0, 12 mM Spermine tetra-HCl, 80 mM SrCl₂
14. 10% MPD, pH 7.0, 12 mM Spermine tetra-HCl, 80 mM KCl, 20 mM MgCl₂
15. 10% MPD, pH 7.0, 12 mM Spermine tetra-HCl, 80 mM KCl
16. 10% MPD, pH 7.0, 12 mM Spermine tetra-HCl, 80 mM NaCl, 20 mM MgCl₂
17. 10% MPD, pH 7.0, 12 mM Spermine tetra-HCl, 80 mM NaCl
18. 10% MPD, pH 7.0, 12 mM Spermine tetra-HCl, 80 mM NaCl, 12 mM KCl,
20 mM MgCl₂
19. 10% MPD, pH 7.0, 12 mM Spermine tetra-HCl, 12 mM NaCl, 80 mM KCl
20. 10% MPD, pH 7.0, 12 mM Spermine tetra-HCl, 80 mM NaCl, 20 mM BaCl₂
21. 10% MPD, pH 7.0, 12 mM Spermine tetra-HCl, 80 mM KCl, 20 mM BaCl₂
22. 10% MPD, pH 7.0, 12 mM Spermine tetra-HCl, 40 mM LiCl, 80 mM SrCl₂,
20 mM MgCl₂
23. 10% MPD, pH 7.0, 12 mM Spermine tetra-HCl, 40 mM LiCl, 80 mM SrCl₂
24. 10% MPD, pH 7.0, 12 mM Spermine tetra-HCl, 80 mM SrCl₂, 20 mM MgCl₂

Where MPD= 2-methyl-2,4-pentane diol, the buffer consists of 40 mM sodium cacodylate, and the dehydrant is 35% v/v MPD.

Natrix Formulation (with slight modification)

1. 0.01 M Mg Chloride, 0.05 M Sodium Citrate pH 5.6, 2.0 M Lithium Sulfate
2. 0.01 M Mg Acetate, 0.05 M Sodium Citrate pH 5.6, 2.5 M Ammonium Sulfate
3. 0.1 M Mg Acetate, 0.05 M Sodium Citrate pH 5.6 20% MPD
4. 0.2 M KCl, 0.01 M Mg Sulfate, 0.05 M Sodium Citrate pH 5.6, 10% PEG 400
5. 0.2 M KCl, 0.01 M Mg Chloride, 0.05 M Sodium Citrate pH 5.6, 5% PEG 8000
6. 0.1 M Ammonium Sulfate, 0.01 M Mg Chloride. 0.05 M Sodium Citrate pH 5.6, 20% PEG 2000
7. 0.02 Mg Chloride, 0.05 M Sodium Cacodylate pH 6.0, 15% Isopropanol
8. 0.005 M Mg Sulfate, 0.1 M Ammonium Acetate, 0.05 M Sodium Cacodylate pH 6.0, 0.6 M NaCl
9. 0.1 M KCl, 0.01 M Mg Chloride, 0.05 M Sodium Cacodylate pH 6.0, 10% PEG 400
10. 0.005 M Mg Sulfate, 0.05 M Sodium Cacodylate pH 6.0, 5% PEG 4000
11. 0.01 M Mg Chloride, 0.05 M Sodium Cacodylate pH 6.0, 1.0 M Lithium Sulfate
12. 0.01 M Mg Sulfate, 0.05 M Sodium Cacodylate pH 6.0, 1.8 M Lithium Sulfate
13. 0.015 M Mg Acetate, 0.05 M Sodium Cacodylate pH 6.0, 1.7 M Ammonium Acetate
14. 0.1 M K Chloride, 0.025 M Mg Chloride, 0.05 M Sodium Cacodylate pH 6.0, 15% Isopropanol
15. 0.04 M Mg Chloride, 0.05 M Sodium Cacodylate pH 6.0, 5% MPD
16. 0.04 M Mg Acetate, 0.05 M Sodium Cacodylate pH 6.0, 30% MPD

- 17.0.2 M KCl, 0.01 M Ca Chloride, 0.05 M Sodium Cacodylate pH 6.0, 10% PEG 4000
- 18.0.01 M Mg Acetate, 0.05 M PIPES pH 6.5, 1.3 M Lithium Sulfate
- 19.0.01 M Mg Sulfate, 0.05 M PIPES pH 6.5, 2.0 M Ammonium Sulfate
- 20.0.1 M Ammonium Acetate, 0.015 M Mg Acetate, 0.05 M PIPES pH 6.5, 10% Isopropanol
- 21.0.2 M KCl, 0.005 M Mg Chloride, 0.05 M PIPES pH 6.5, 10% 1,6 hexanediol
- 22.0.08 M Mg Acetate, 0.05 M PIPES pH 6.5, 15% PEG 400
- 23.0.2 M KCl, 0.01 M Mg Chloride, 0.05 M PIPES pH 6.5, 10% PEG 4000
- 24.0.2 M Ammonium Acetate, 0.01 M Ca Chloride, 0.05 M PIPES pH 6.5, 10% PEG 4000
- 25.0.08 M Mg Acetate, 0.05 M PIPES pH 6.5, 30% PEG 4000
- 26.0.2 M KCl, 0.1 M Mg Acetate, 0.05 M PIPES pH 6.5, 10% PEG 8000
- 27.0.2 M Ammonium Acetate, 0.01 M Mg Acetate, 0.05 M PIPES pH 6.5, 30% PEG 8000
- 28.0.05 M Mg Sulfate, 0.05 M HEPES pH 7.0, 1.6 M Lithium Sulfate
- 29.0.01 M Mg Chloride, 0.05 M HEPES pH 7.0, 4.0 M Lithium Chloride
- 30.0.01 M Mg Chloride, 0.05 M HEPES pH 7.0, 1.6 M Ammonium Sulfate
- 31.0.005 M Mg Chloride, 0.05 M HEPES pH 7.0, 25% PEG 400
- 32.0.2 M KCl, 0.01 M Mg Chloride, 0.05 M HEPES pH 7.0, 20% 1,6 hexanediol
- 33.0.2 M Ammonium Chloride, 0.01 M Mg Chloride, 0.05 M HEPES pH 7.0, 30% 1,6 hexanediol
- 34.0.1 M KCl, 0.005 M Mg Sulfate, 0.05 M HEPES pH 7.0, 15% MPD

- 35.0.1 M KCl, 0.01 M Mg Chloride, 0.05 M HEPES pH 7.0, 5% PEG 400
- 36.0.1 M KCl, 0.01 M Ca Chloride, 0.05 M HEPES pH 7.0, 10% PEG 400
- 37.0.2 M KCl, 0.025 M Mg Sulfate, 0.05 M HEPES pH 7.0, 20% PEG 400
- 38.0.2 M Ammonium Acetate, 0.15 M Mg Acetate, 0.05 M HEPES pH 7.0, 5%
Peg 4000
- 39.0.1 M Ammonium Acetate, 0.02 M Mg Chloride, 0.05 M HEPES pH 7.0, 5%
PEG 8000
- 40.0.01 M Mg Chloride, 0.05 M TRIS HCl pH 7.5, 1.6 M Ammonium Sulfate
- 41.0.1 M KCl, 0.015 M Mg Chloride, 0.05 M TRIS HCl pH 7.5, 10% PEG 400
- 42.0.01 M Mg Chloride, 0.05 M TRIS HCl pH 7.5, 5% Isopropanol
- 43.0.01 M Mg Chloride, 0.05 M Ammonium Acetate, 0.05 M TRIS HCl pH 7.5,
10% MPD
- 44.0.2 M KCl, 0.05 M Mg Chloride, 0.05 M TRIS HCl pH 7.5, 10% PEG 4000
- 45.0.025 M Mg Sulfate, 0.05 M TRIS HCl pH 8.5, 1.8 M Ammonium Sulfate
- 46.0.005 M Mg Sulfate, 0.05 M TRIS HCl pH 8.5, 35% 1,6 hexanediol
- 47.0.1 M KCl, 0.01 M Mg Chloride, 0.05 M TRIS HCl pH 8.5, 30% PEG 400
- 48.0.01 M Ca Chloride, 0.2 M Ammonium Chloride, 0.05 M TRIS HCl pH 8.5,
30% PEG 4000

Biological Buffers used:

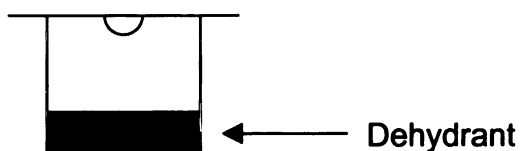
PIPES-1,4-Piperazinediethanesulfonic acid]

HEPES- N-[2-Hydroxyethyl]piperazine-N'-[2-ethanesulfonic acid]

TRIS-tris[Hydroxymethyl]aminomethane

These screens were used in the Hanging Drop method of crystal growth. 4x6 well-plates were used and 500 μL of buffer or dehydrant was placed each well. On a plastic microscope cover slip, 2 μL of a 10 mg/mL DNA solution and 2 μL buffer were placed in a drop. The cover slip was then suspended over the well (Figure 63). Slow diffusion then takes place which can eventually lead to crystal growth.

Figure 63. Hanging Drop Method of crystal growth



3. Results and Discussion

Each of the DNA strands was specifically designed to have a single binding site, namely AA or GG (Table 10). The 10 mersc and 11 mersc were created to be self complementary so that each strand in the duplex would have a potential binding site for the rhodium bis-acetate. Several of the DNA strands have overhangs of one base pair, which is useful as an anchor for packing interactions in crystal growth. The AA binding site is preferred due to higher product yields and shorter reaction times with $[\text{Rh}_2(\text{O}_2\text{CCH}_3)_2(\text{CH}_3\text{CN})_6]^{2+}$.

Table 10. DNA strands designed for crystallization studies.

Strand	Binding site	Name
TGC GTT AAC GC CG CAA TTG CGT	AA	11 mersc
GCG TTA ACG C CGC AAT TGC G	AA	10 mersc
CCT CTG GTC TCC GGA GAC CAG AGG	GG	GG 12mer
CCT CTA ATC TCC GGA GAT TAG AGG	AA	AA 12 mer
CTC TAA TCT T GAG ATT AGA A	AA	10 mer
CTC AAT CT GAG TTA GA	AA	8 mer
TCT CTA ATC TC GA GAT TAG AGA	AA	11 mer
CC TCT AAT CTC C TGG AGA TTA GAG G	AA	2A-13 mer
CC TCT AAT CTC C AGG AGA TTA GAG G	AA	3A-13 mer

At the outset of this research, it was believed that the DNA product could only be formed in good yields by heating the reaction to fairly high temperatures, *i.e.* 70°C for 72 hours. The product of the high temperature reaction eluted from the HPLC column only at the highest salt concentrations, and was obtained in very low yields (around 30%). The use of buffers and different reaction times did not improve the yields. It seemed unusual that the reaction would proceed only under the harshest of conditions; indeed this suspicion was confirmed by the results of a MALDI mass spectrometry experiment performed on the reacted 12 mer GG product. The results showed that the high temperature product is an adduct bound to several dirhodium units.

The antitumor active compound, $\text{Rh}_2(\text{OAc})_4(\text{H}_2\text{O})_2$, inhibits DNA replication under normal cellular conditions, *i.e.* 37°C. Rethinking the strategy resulted in a radical change in protocol. Obviously, the products that form at biological temperature should be the adducts that cause a halt in cancer cellular replication, thus the reaction was performed at 37°C with the 8- and 10-mers in hopes of obtaining the biologically relevant product. HPLC purification revealed a large metallated peak eluting at about 30-40 % B along with a small peak eluting at high salt concentrations (Figure 64). The new peak was collected and desalted according to the usual protocols then submitted for mass spectrometric analysis. The results showed that the rhodium bis-acetate is bound to the DNA in the expected 1:1 ratio (Figure 65). This is the first definitive proof that the dirhodium bis-acetate is intact and bound to a single site on the DNA strand, most likely the target site. Based on charge considerations, the phosphate backbone seems to

be a likely target as well, however, there are no structures in the NADB where a charged group is in close proximity with the DNA backbone. Due to the lack of binding of charged antitumor complexes to the phosphate groups on DNA, it seems likely that the dirhodium bis-acetate is bound to purine sites on the strand.

The MALDI mass spectroscopic data shows that the adduct $\text{Rh}_2(\text{O}_2\text{CCH}_3)_2\text{-d}(\text{TCTCTAATCTC})$ was formed in the milder reaction. Four assignable peaks appear in the spectrum. The peak at 3567 corresponds to the $[\text{DNA} + \text{Rh}_2(\text{O}_2\text{CCH}_3)_2 - 3\text{H}]^-$ peak. Another peak appears at 3506 which corresponds to $[\text{DNA} + \text{Rh}_2(\text{O}_2\text{CCH}_3) - 4\text{H}]^-$. $[\text{DNA} + \text{Rh}_2 - 5\text{H}]^-$ occurs at 3446, and $[\text{DNA} - \text{H}]^-$ occurs at 3245. These results are clear evidence that the reaction proceeds as expected at 37°C.

Attempts to crystallize these Rh-DNA complexes has proven to be difficult. Each DNA strand has been set up in boxes with the crystallization screens previously mentioned. Most of the DNA strands produce a precipitate upon slow diffusion with the dehydrant. The 70°C reactions produced unusual looking precipitates, which appeared to be brown in color. Small microcrystalline precipitates of the AA-12 mer appeared, but attempts to maximize their size were unsuccessful. The 10-mer formed multiple, thin platelets in the NAM as did the 11-mer. No single crystals have been observed to date. At 4°C, the 10-mer formed very tiny crystals with the NAM but produced nothing at room temperature. The 11-mer formed tiny crystals that were larger than the 10-mer, so the conditions were optimized in attempts of growing larger crystals. The

other DNA strands formed precipitates in some of the conditions, but no crystalline materials are visible at this time.

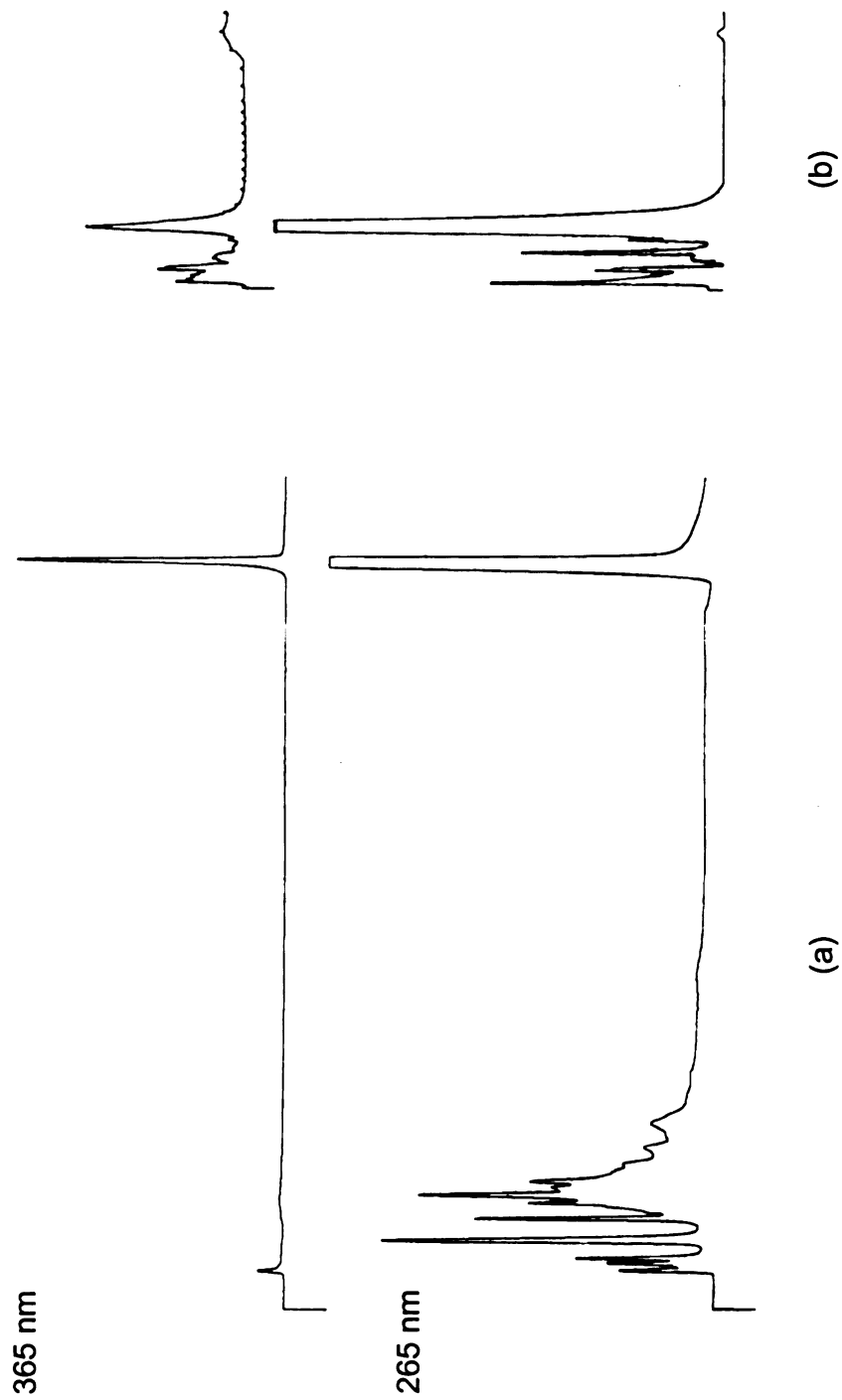


Figure 64. HPLC chromatograms of (a) 10-merisc heated to 70°C for 52 h and (b) 11-mer heated at 37°C for 64 h.

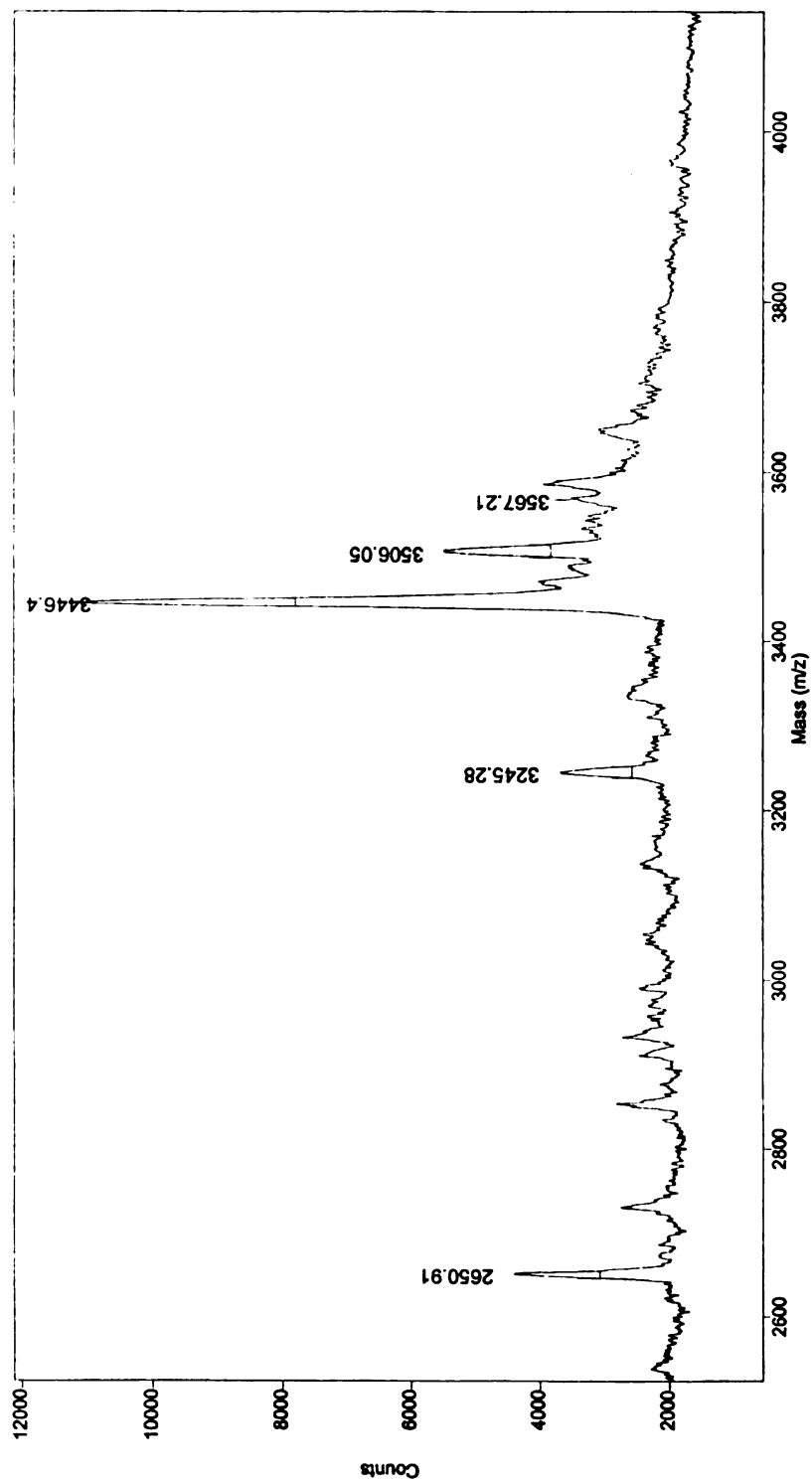


Figure 65. MS of TCT CTA ATC TC 11 mer . Peak at 3867.6 corresponds to $[\text{DNA} + \text{Rh}_2(\text{OAc})_2 - \text{H}]^+$, $3809.09 [\text{DNA} + \text{Rh}_2(\text{OAc})_2 - 2\text{H}]^+$, $3749.0 [\text{DNA} + \text{Rh}_2 - 3\text{H}]^+$.

4. Conclusions

It is now known that upon reaction with DNA, $[\text{Rh}_2(\text{O}_2\text{CCH}_3)_2(\text{CH}_3\text{CN})_6][\text{BF}_4]_2$ forms a 1:1 adduct as expected based upon model studies with nucleotides. The presence of two acetates and two rhodium atoms as confirmed by MALDI-MS revealed that the reaction does proceed at 37°C. The most likely site of binding is to the AA target site, however, without a crystal structure or definitive 2D-NMR data, it is not possible to draw a firm conclusion. Crystallization studies look promising, with the formation of tiny crystals of the AA 11 mer as a starting point. Regrettably, large single x-ray quality crystals have not been obtained to date with the DNA strands mentioned in this chapter.

APPENDIX

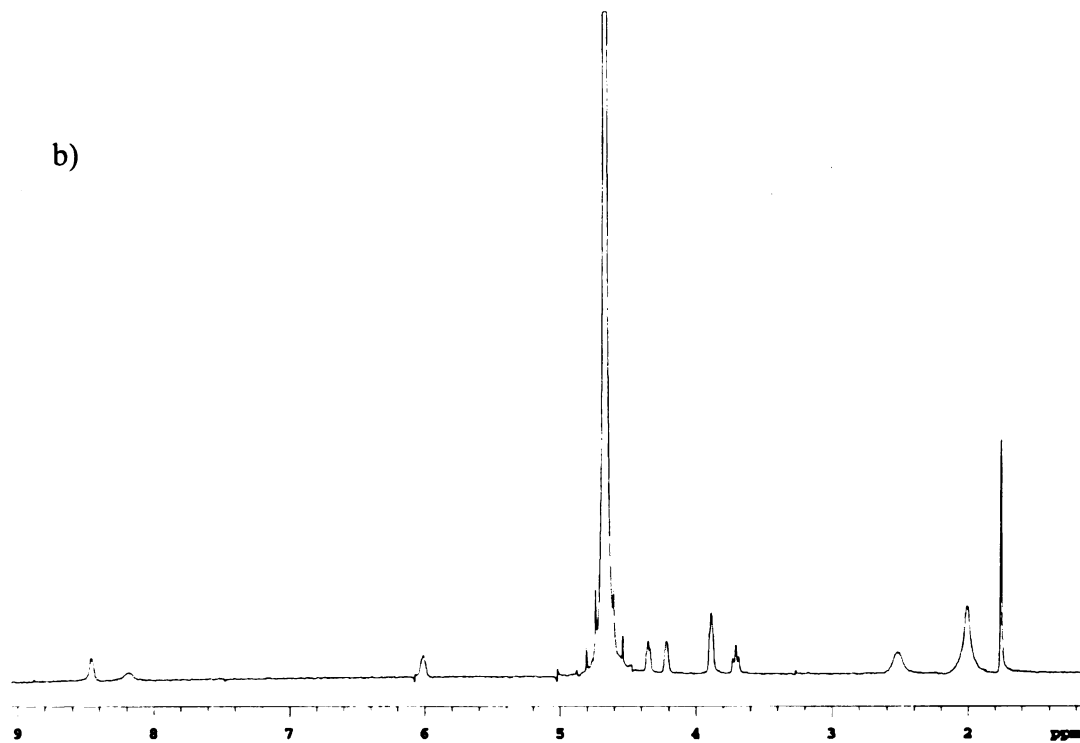
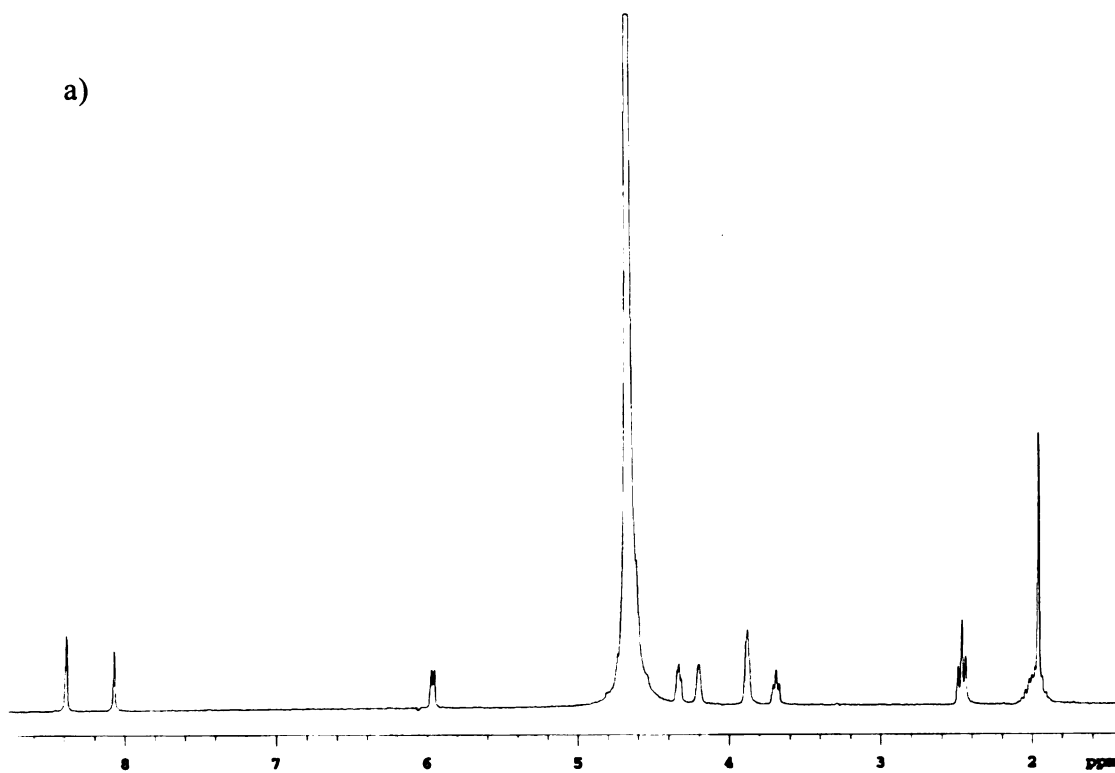
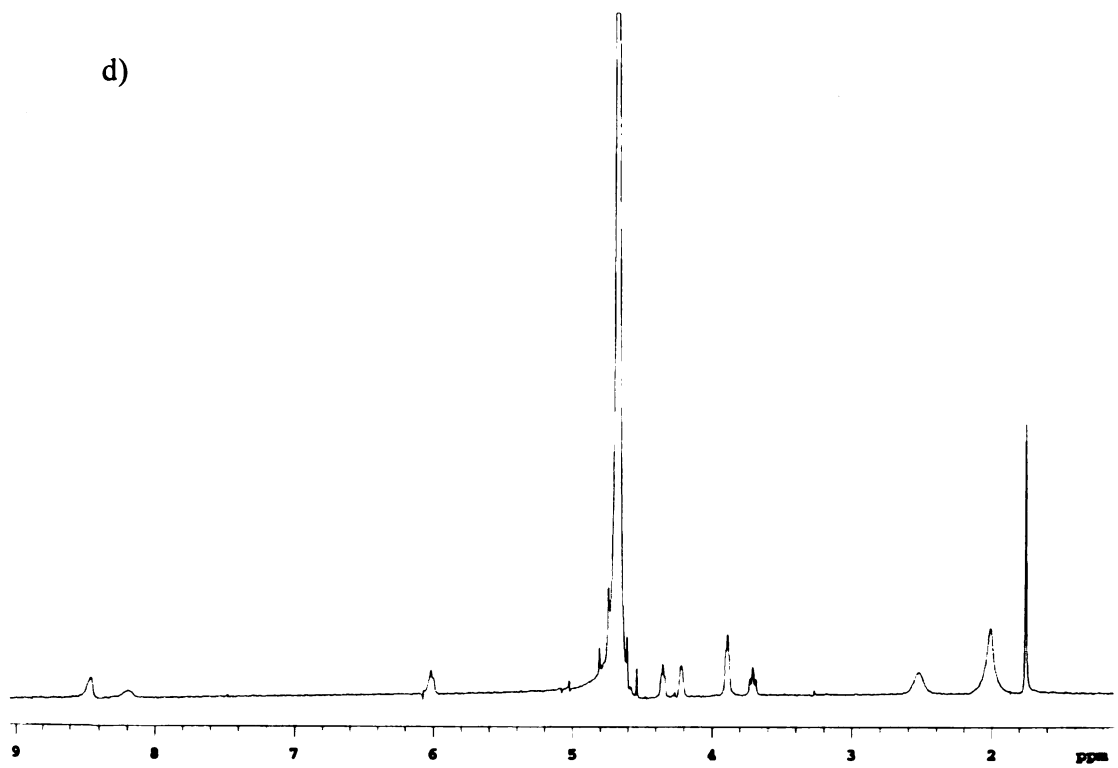
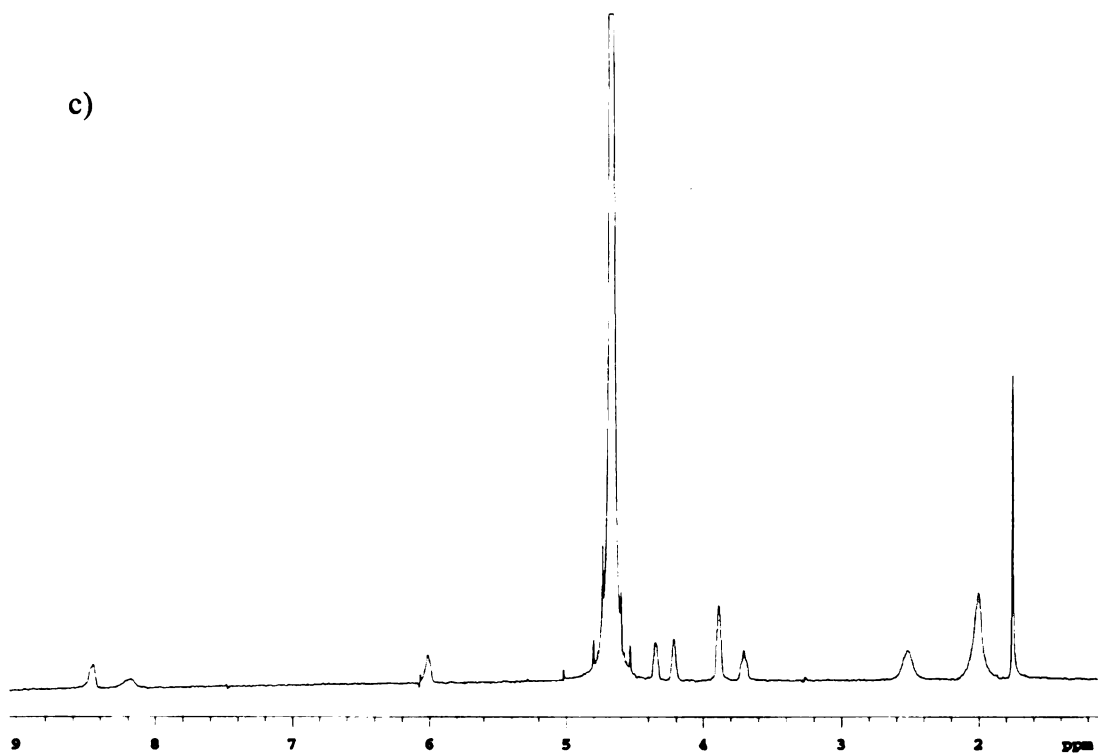
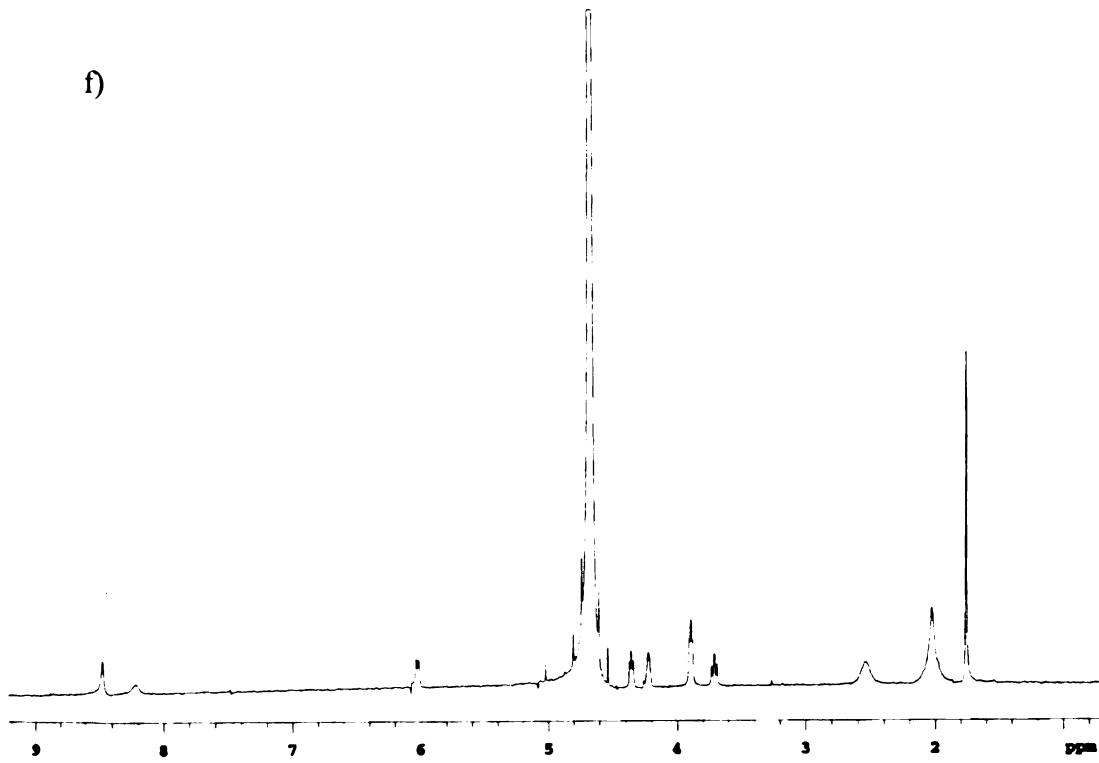
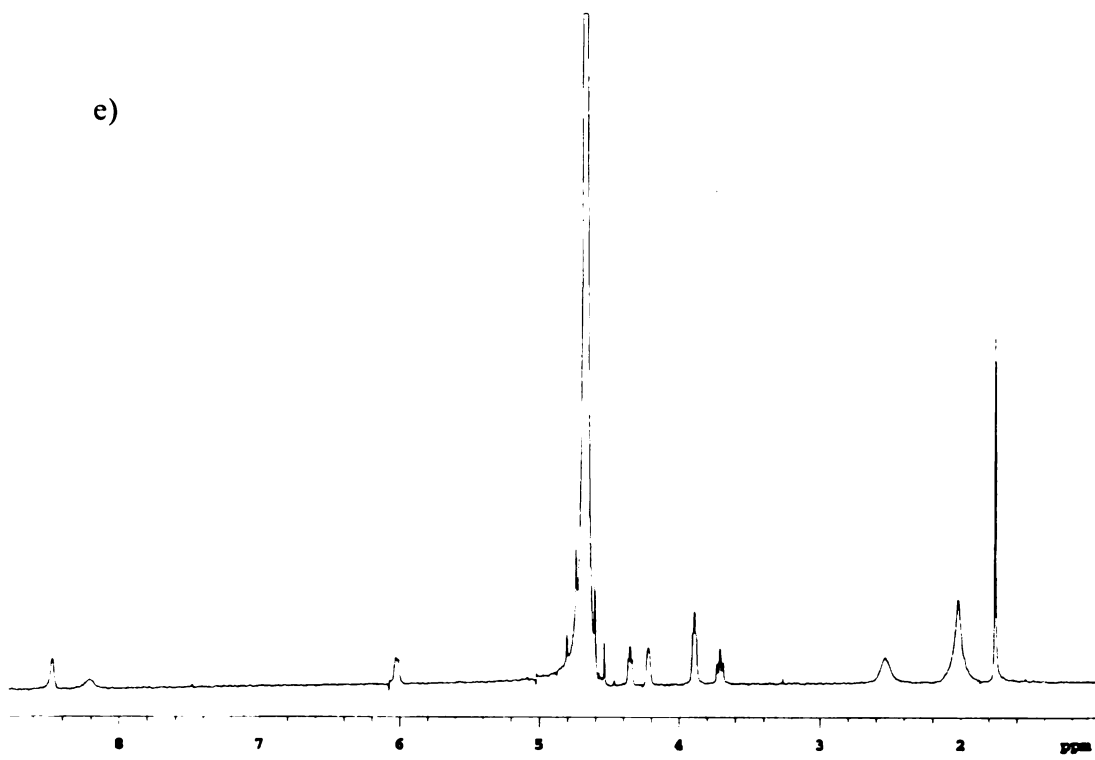


Figure A1. Methionine/AMP NMR reaction. a) methionine/AMP standard, b) ^1H NMR at time = 0, c) ^1H NMR at time = 15 min, d) ^1H NMR at time = 2 h, e) ^1H NMR at time = 4 h, f) ^1H NMR at time = 24 h.





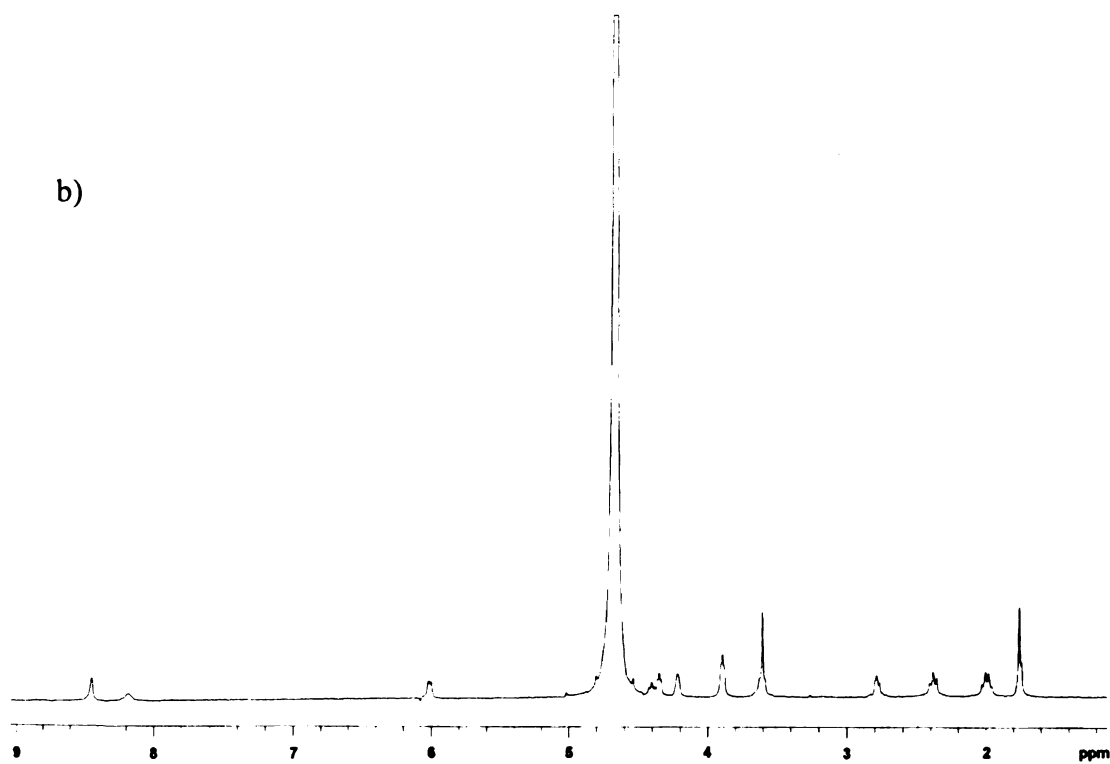
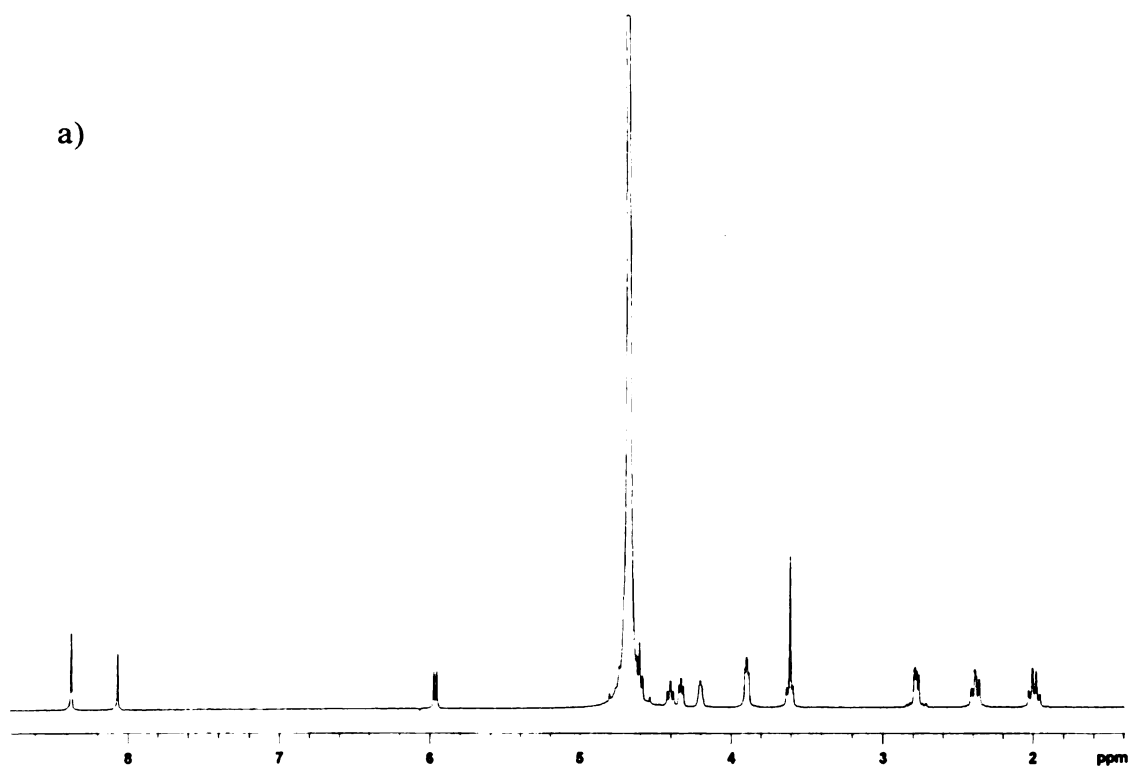
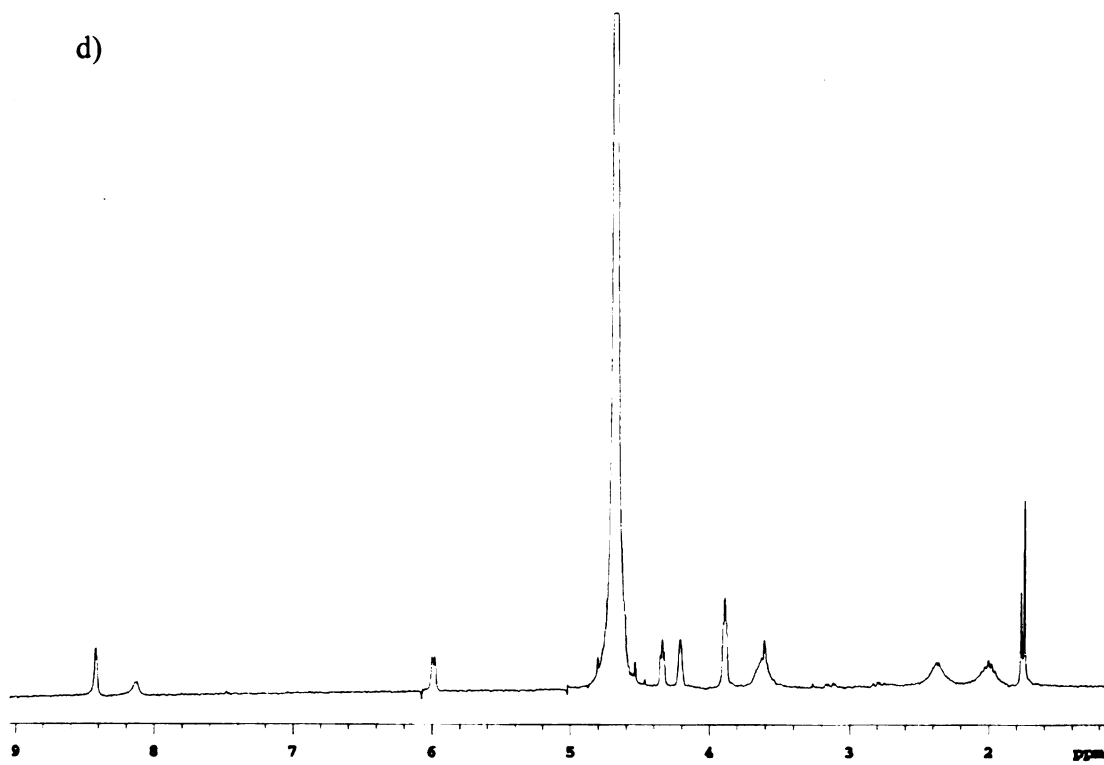
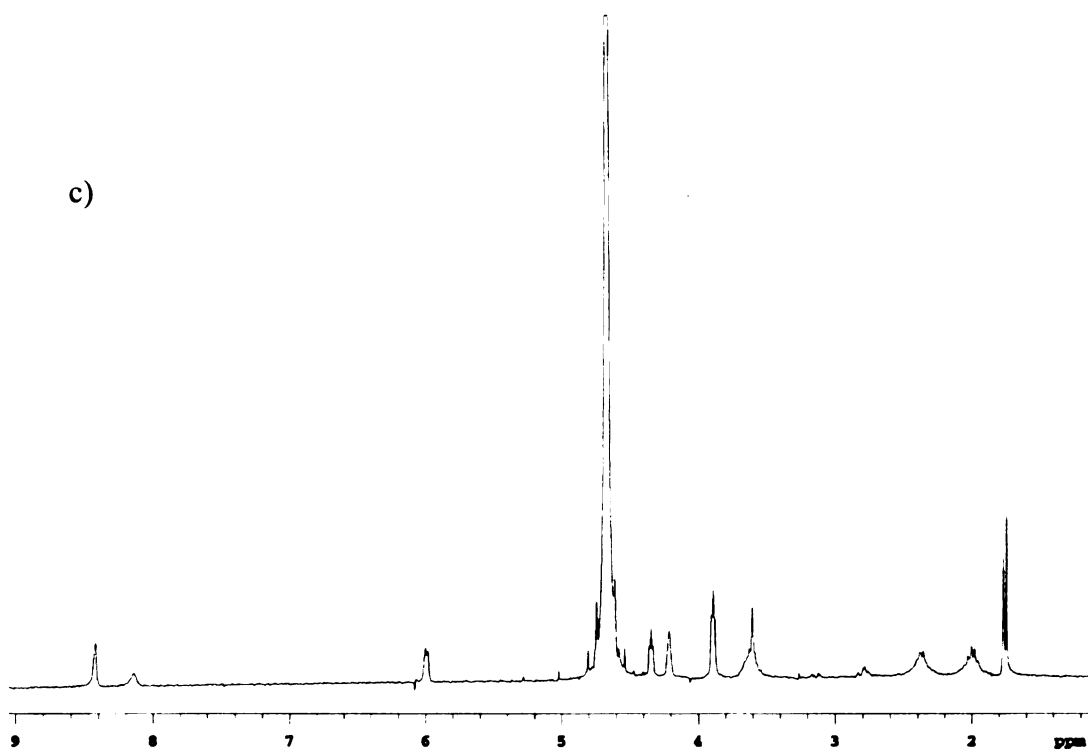
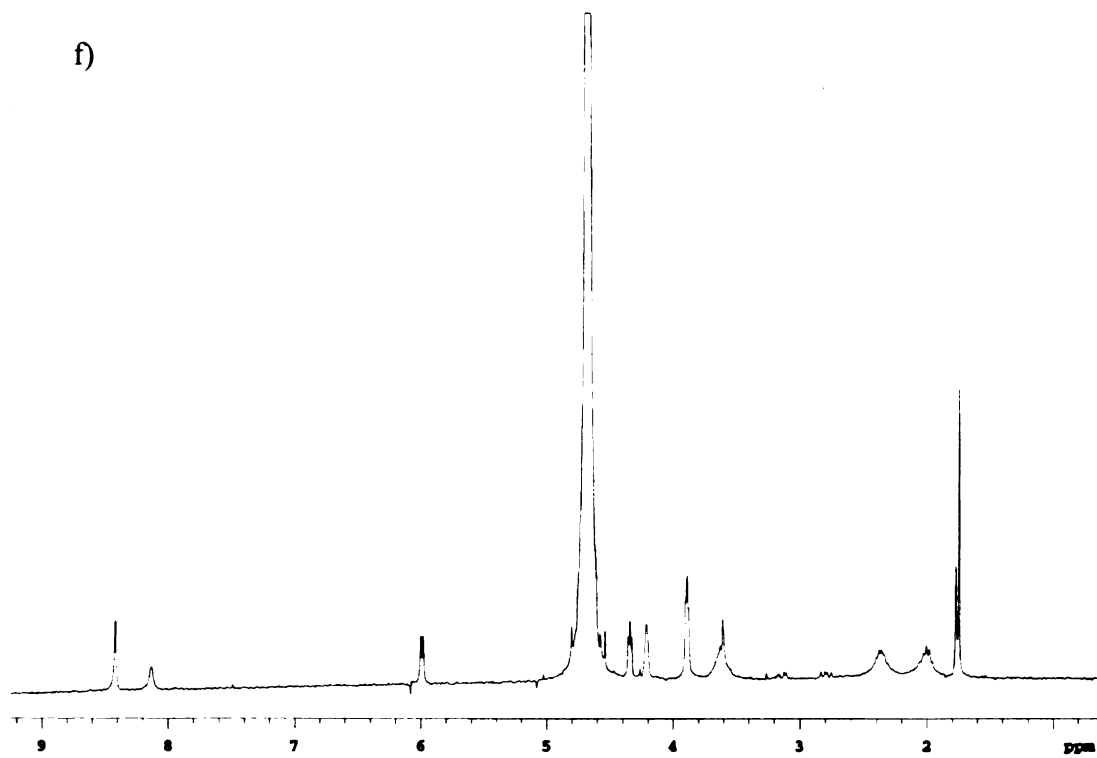
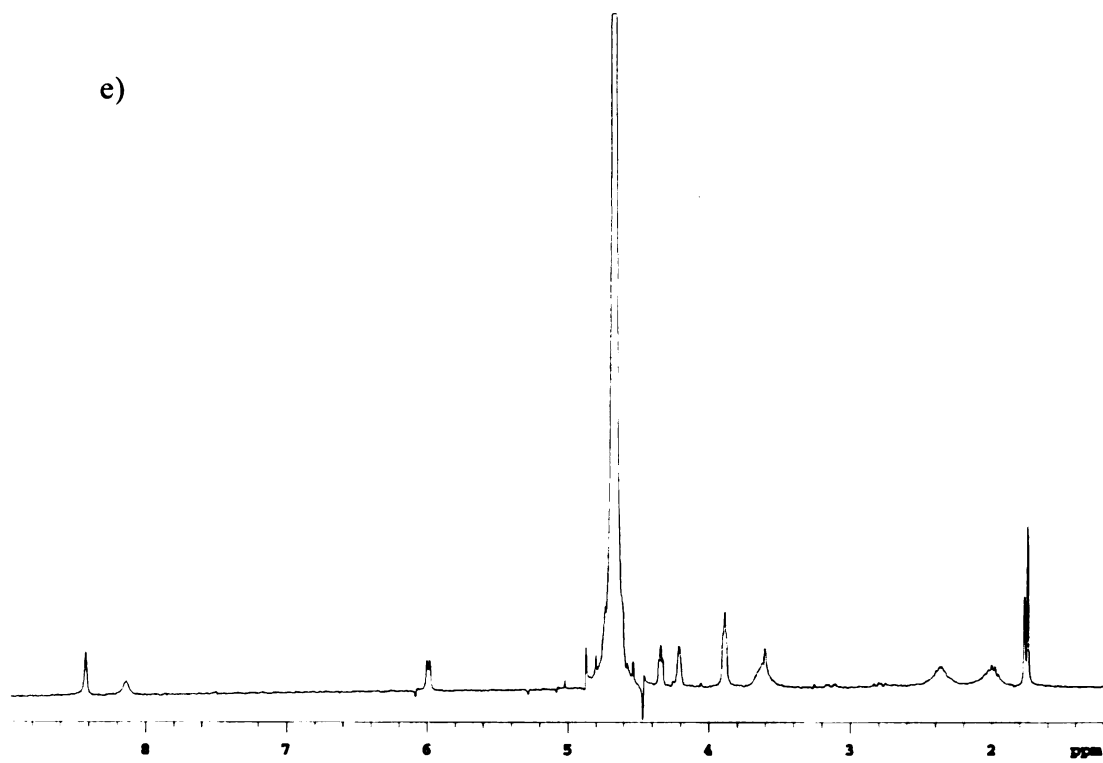


Figure A2. Glutathione/AMP NMR reaction. a) glutathione/AMP standard, b) ^1H NMR at time = 0, c) ^1H NMR at time = 15 min, d) ^1H NMR at time = 2 h, e) ^1H NMR at time = 4 h, f) ^1H NMR at time = 24 h.





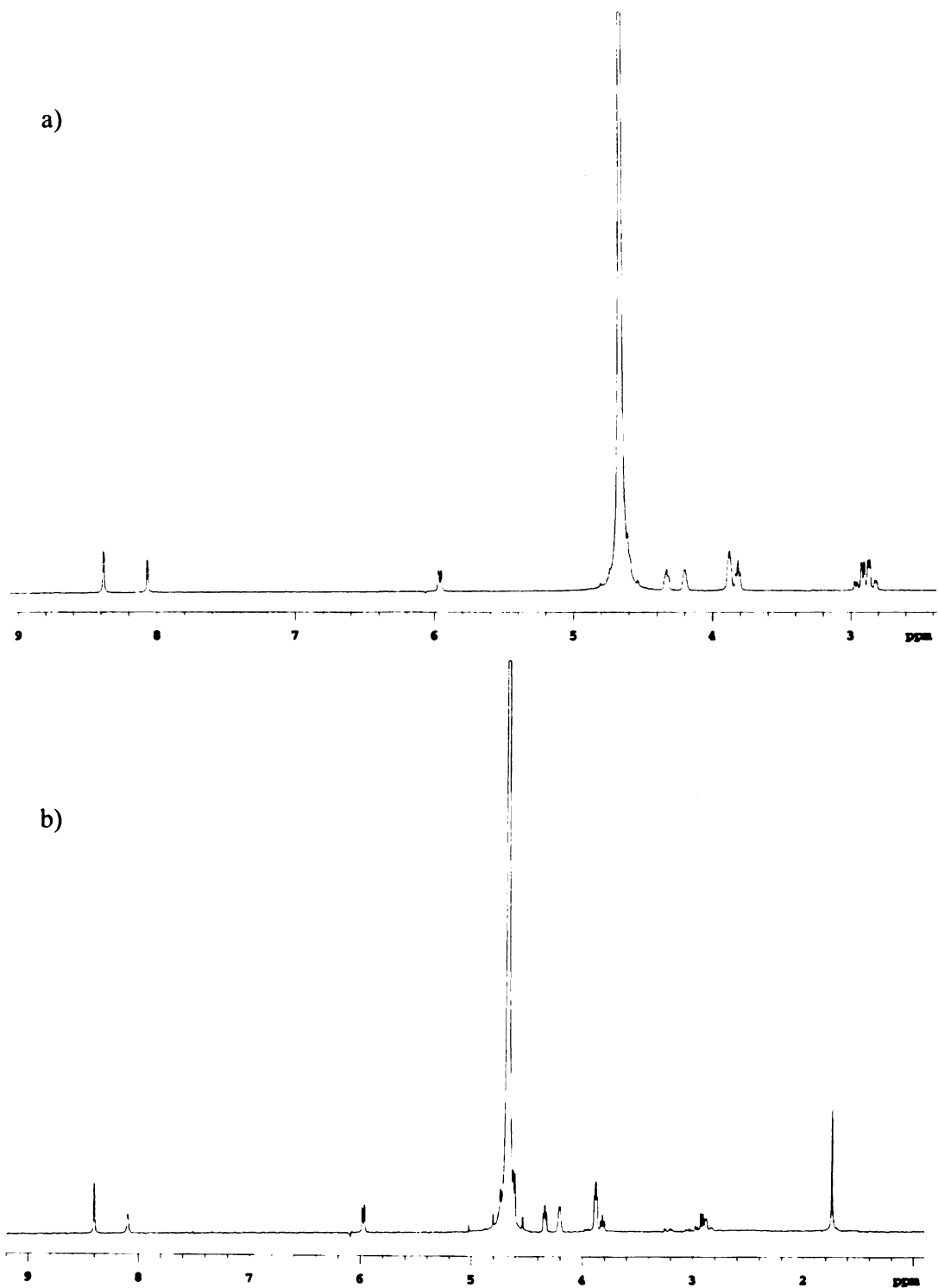
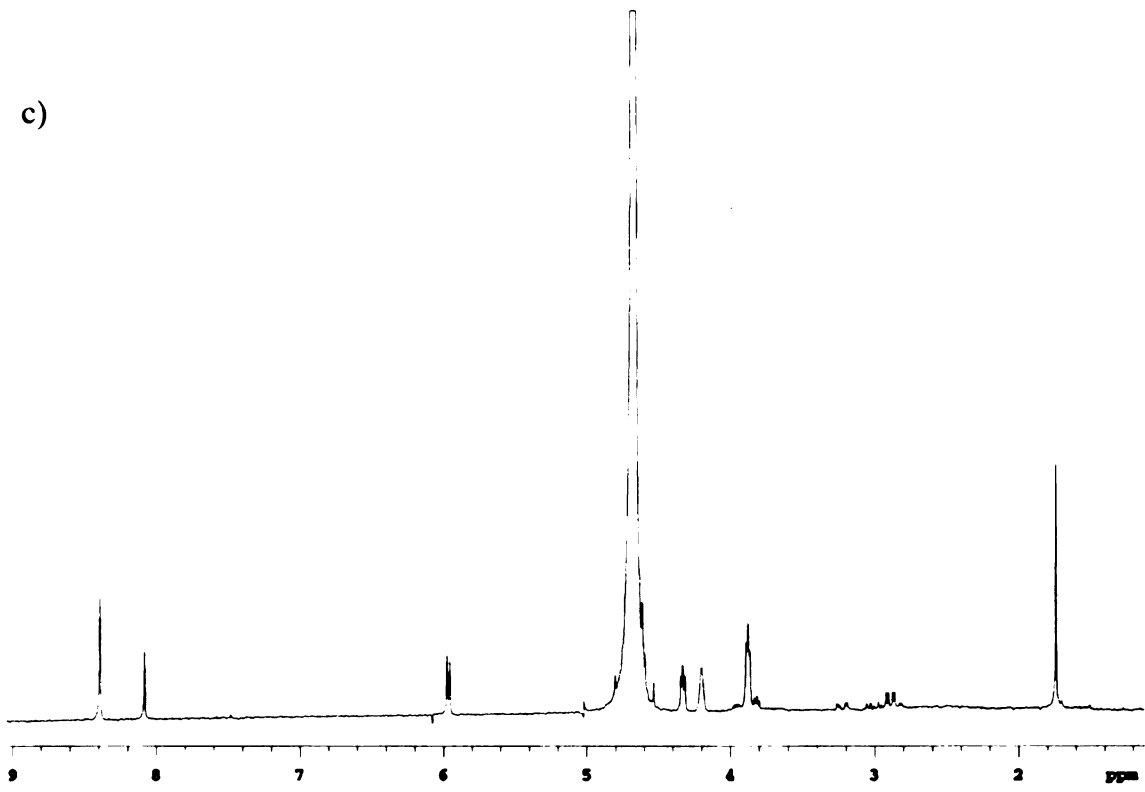
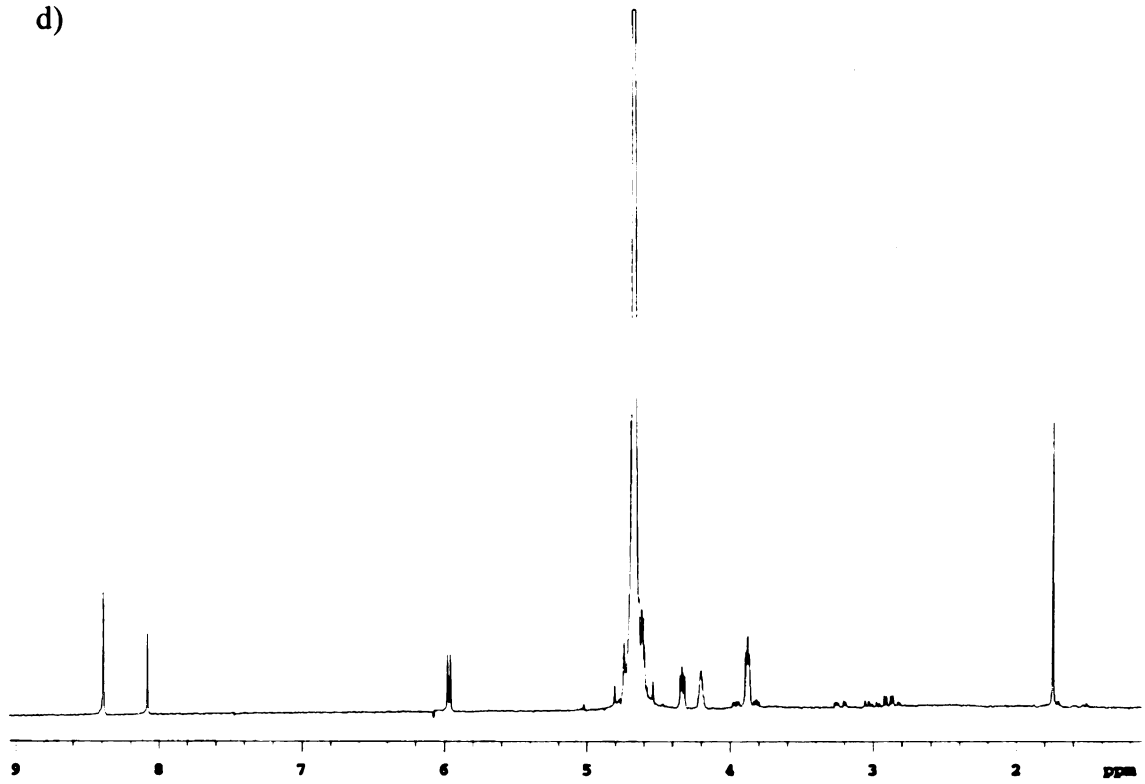


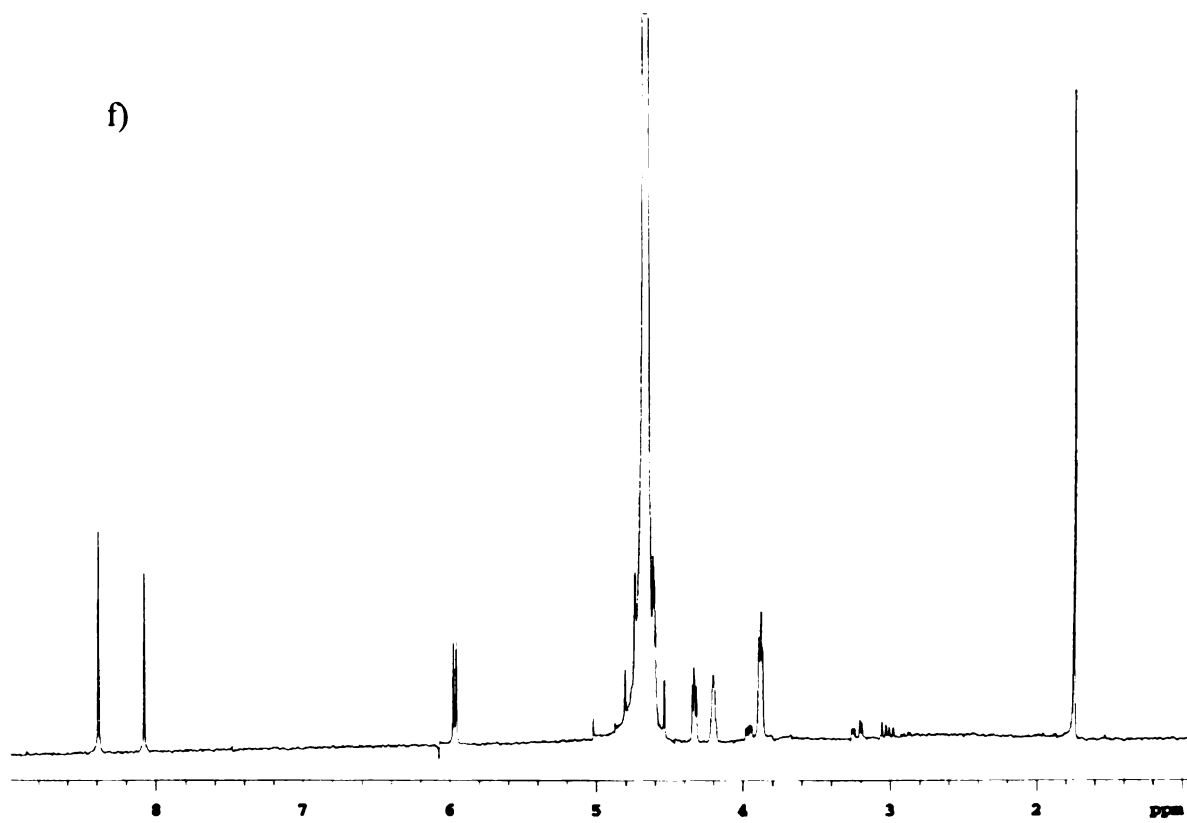
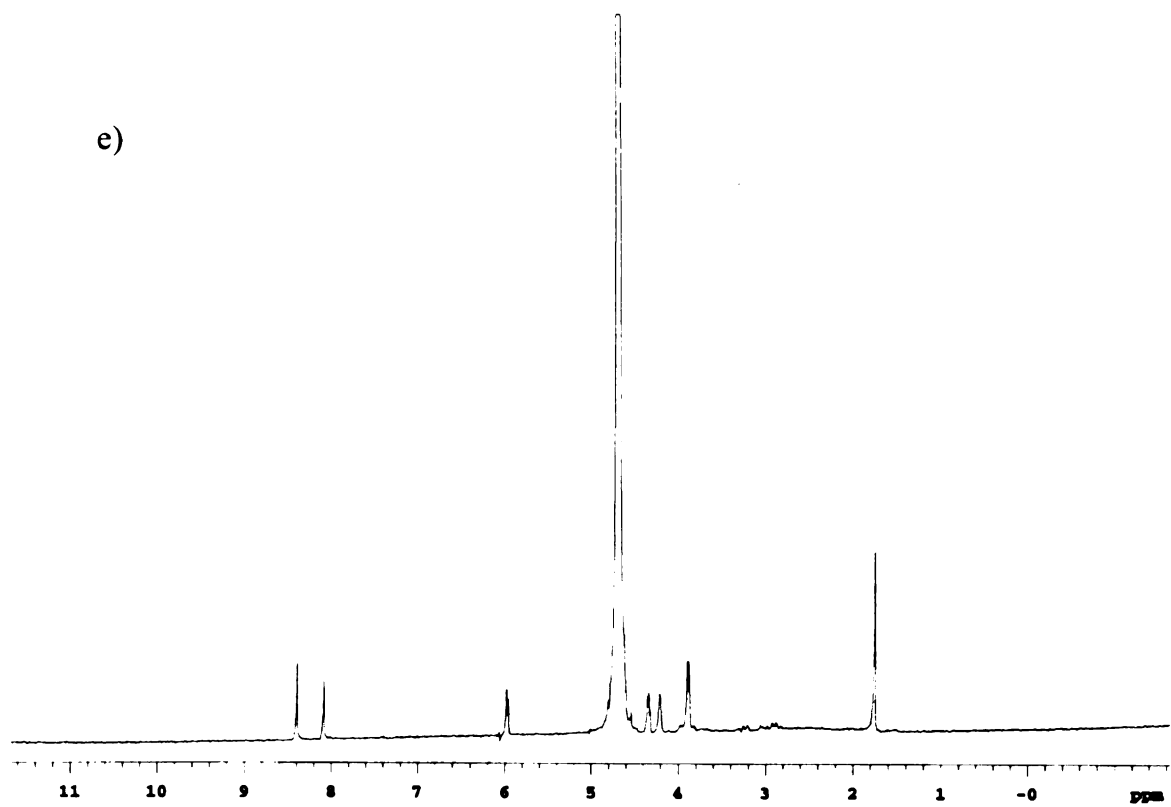
Figure A3. Cysteine/AMP NMR reaction. a) cysteine/AMP standard, b) ¹H NMR at time = 0 c) ¹H NMR at time = 15 min, d) ¹H NMR at time = 2 h, e) ¹H NMR at time = 4h, f) ¹H NMR at time = 24 h.

c)



d)





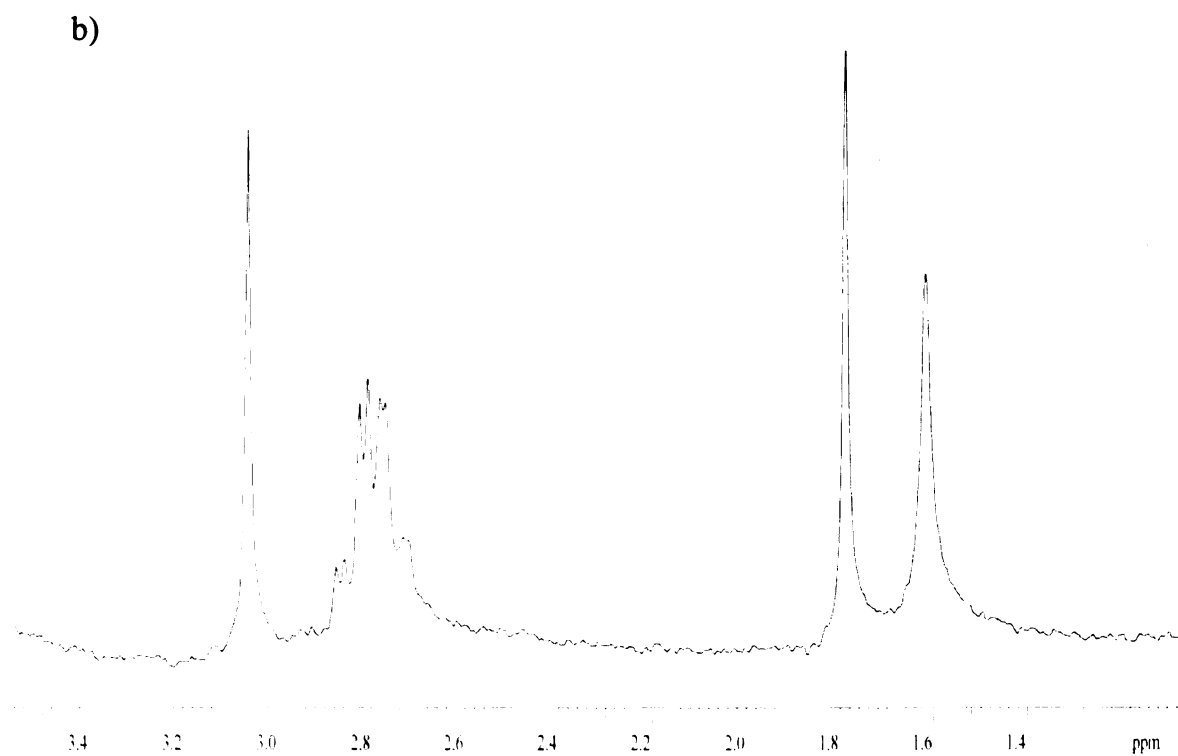
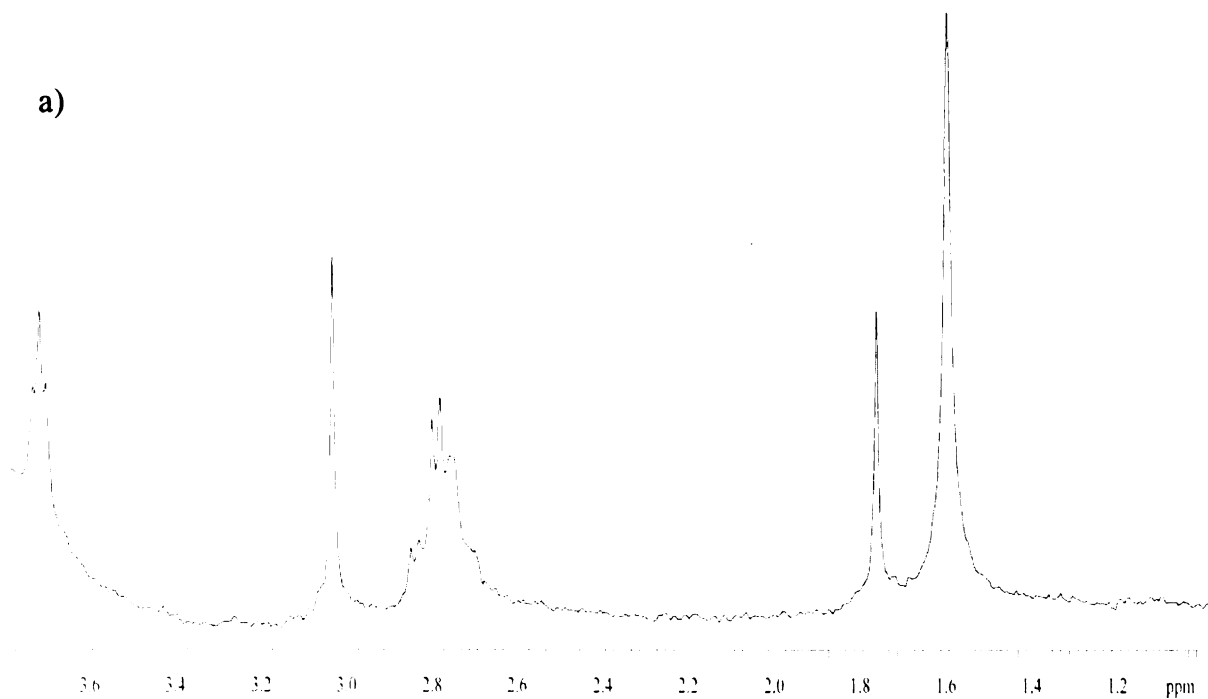
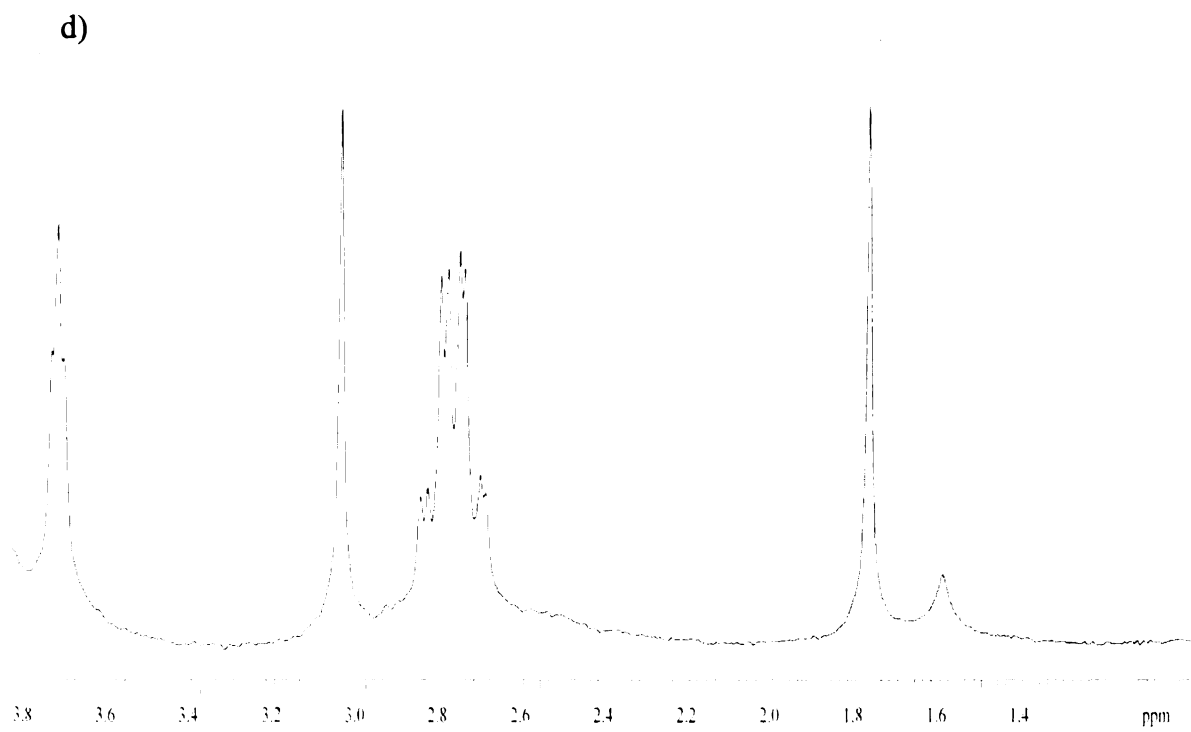
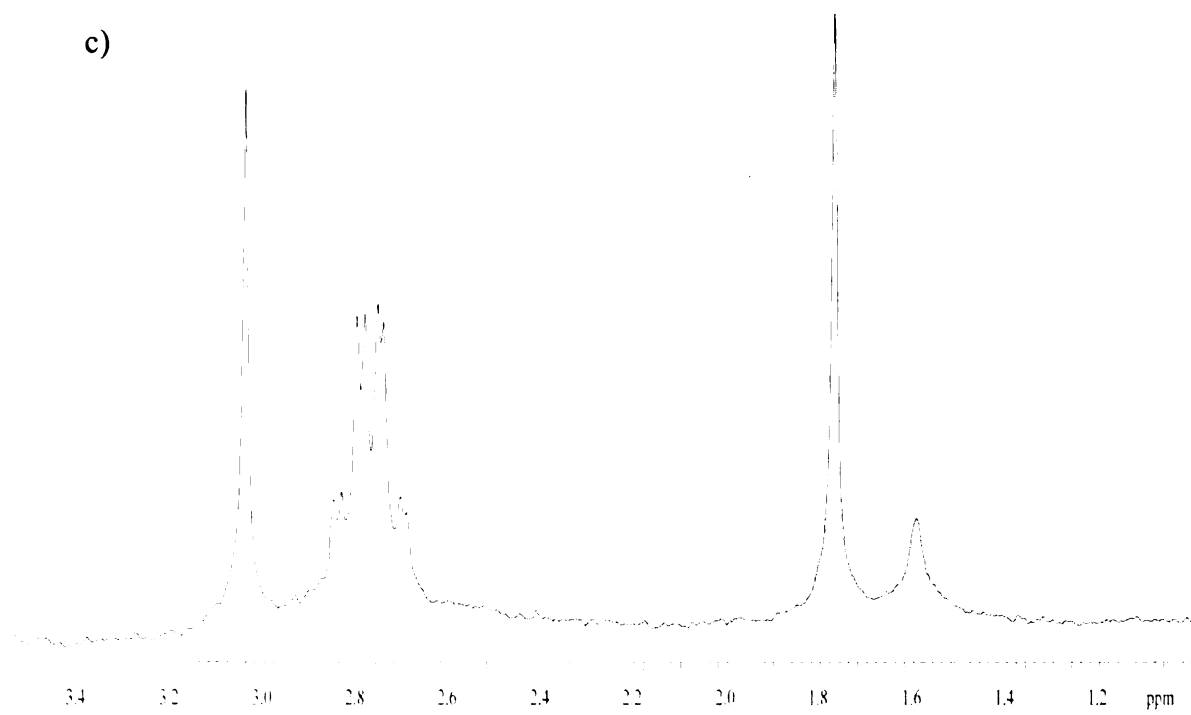


Figure A4. ^1H NMR reaction of $\text{Rh}_2(\text{O}_2\text{CCH}_3)_4$ with cysteine. a) 1:1 ratio, b) 1:2 ratio, c) 1:3 ratio, and d) 1:4 ratio.



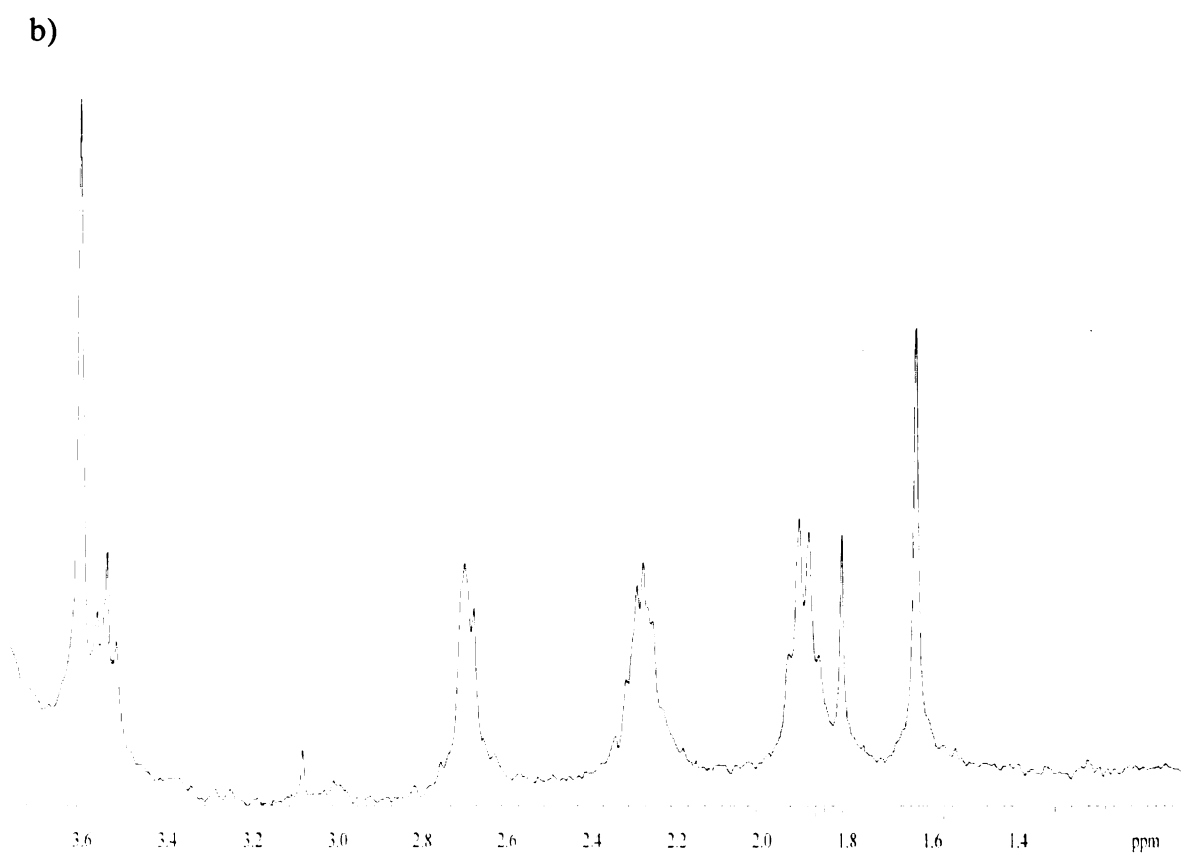
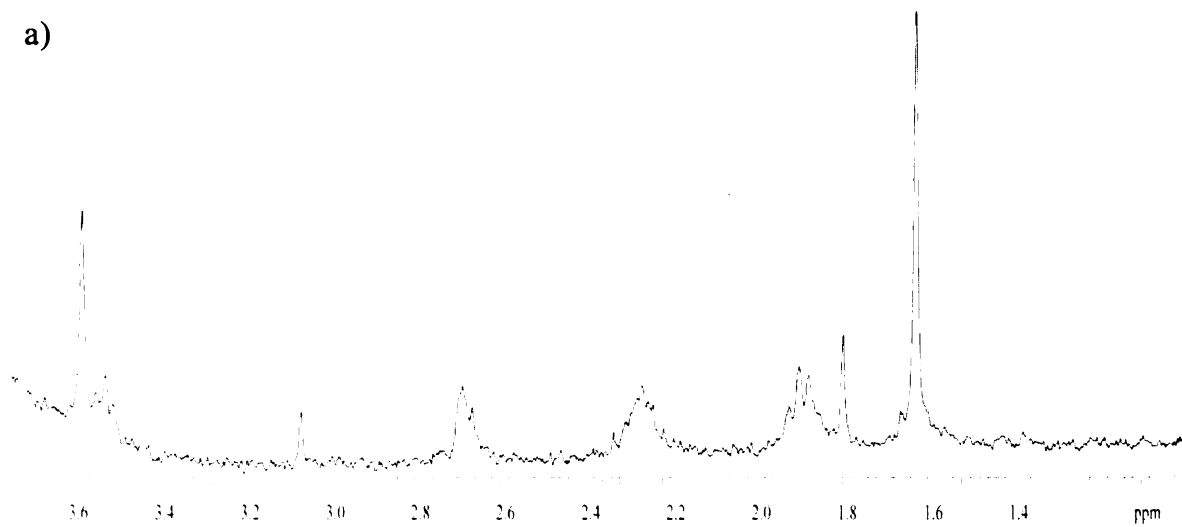
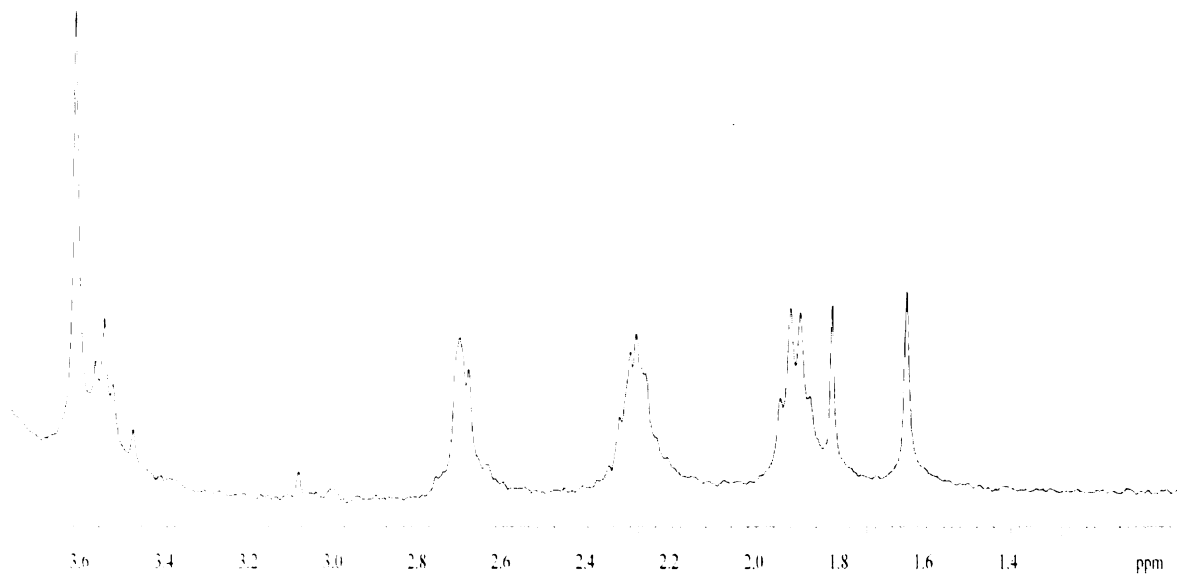
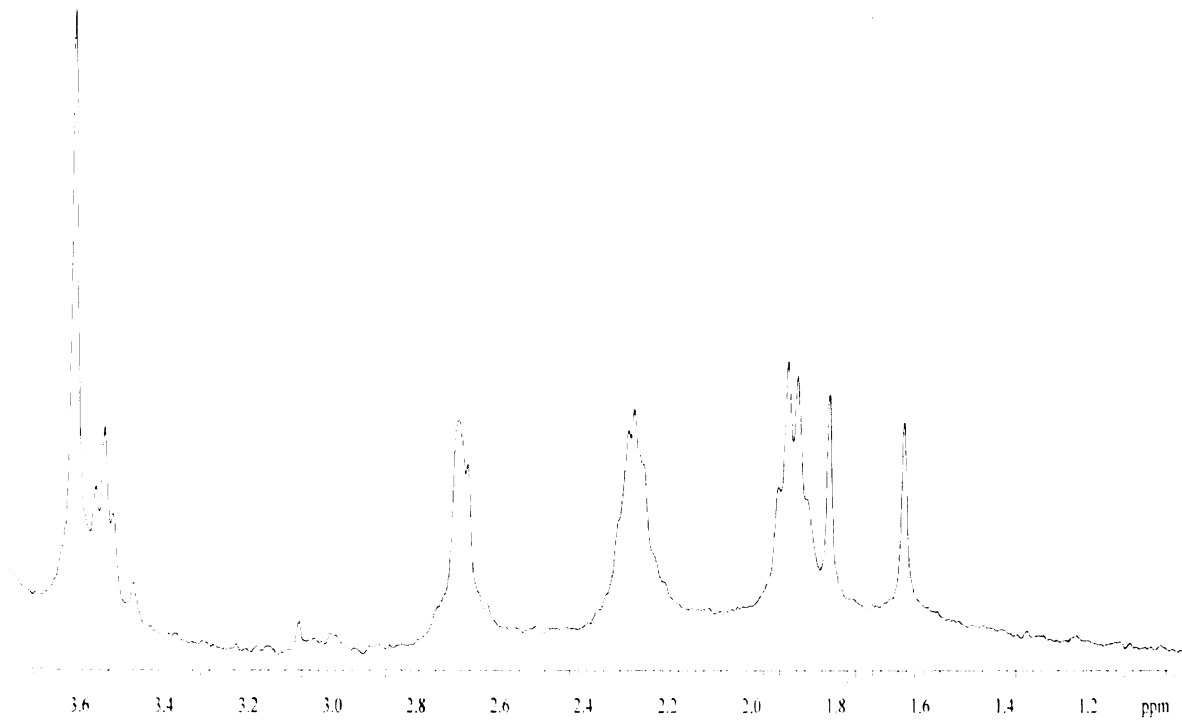


Figure A5. ^1H NMR reaction of $\text{Rh}_2(\text{O}_2\text{CCH}_3)_4$ with glutathione. a) 1:1 ratio, b) 1:2 ratio, c) 1:3 ratio, and d) 1:4 ratio.

c)



d)



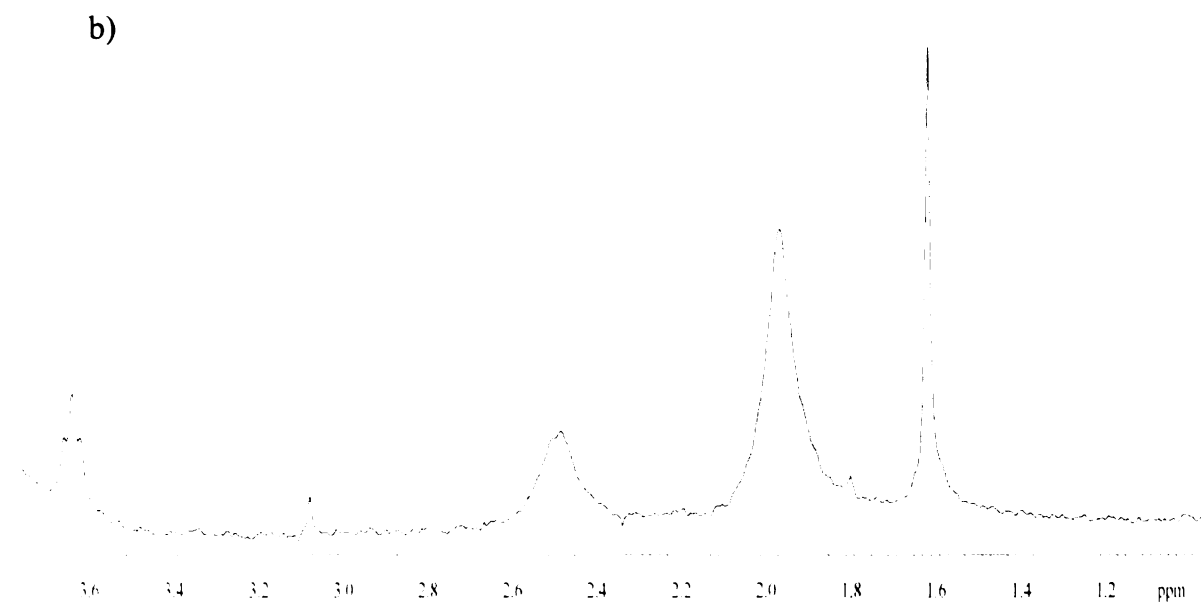
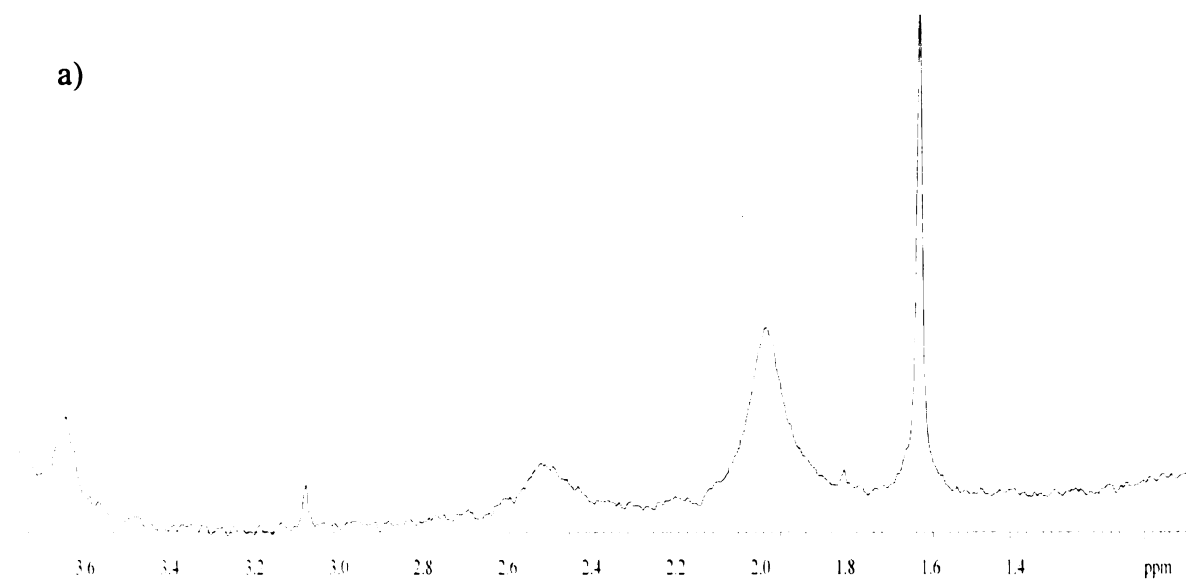
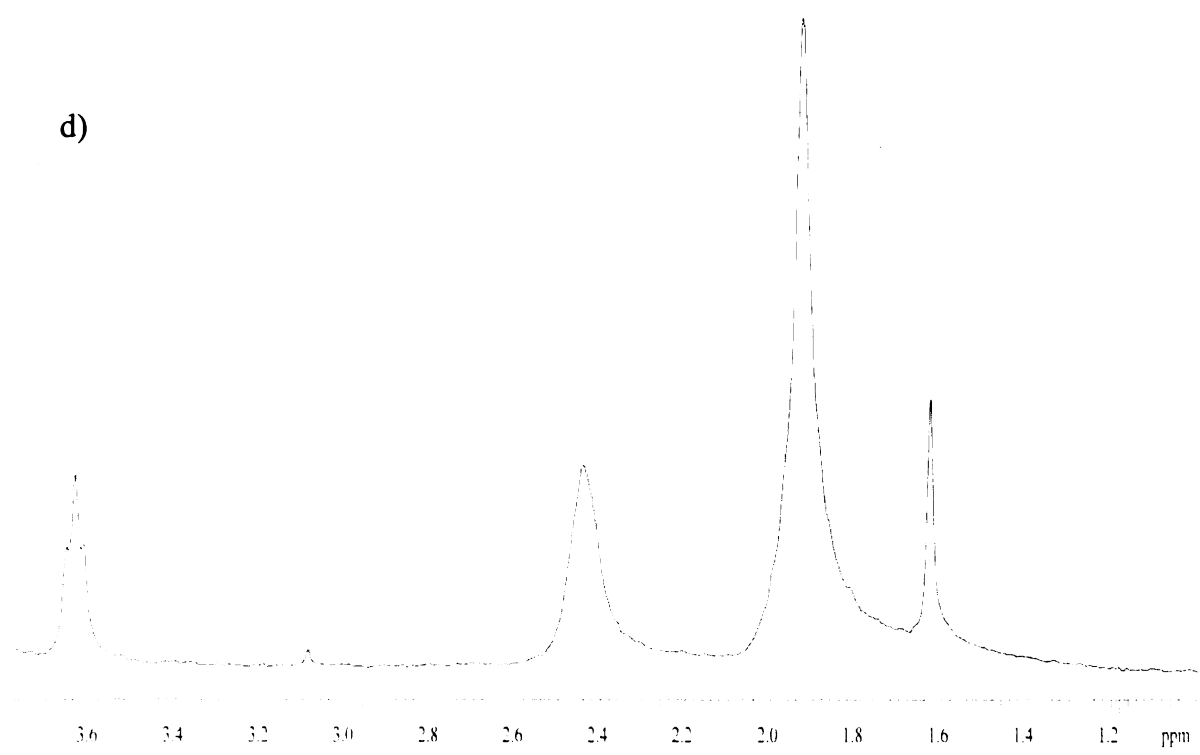
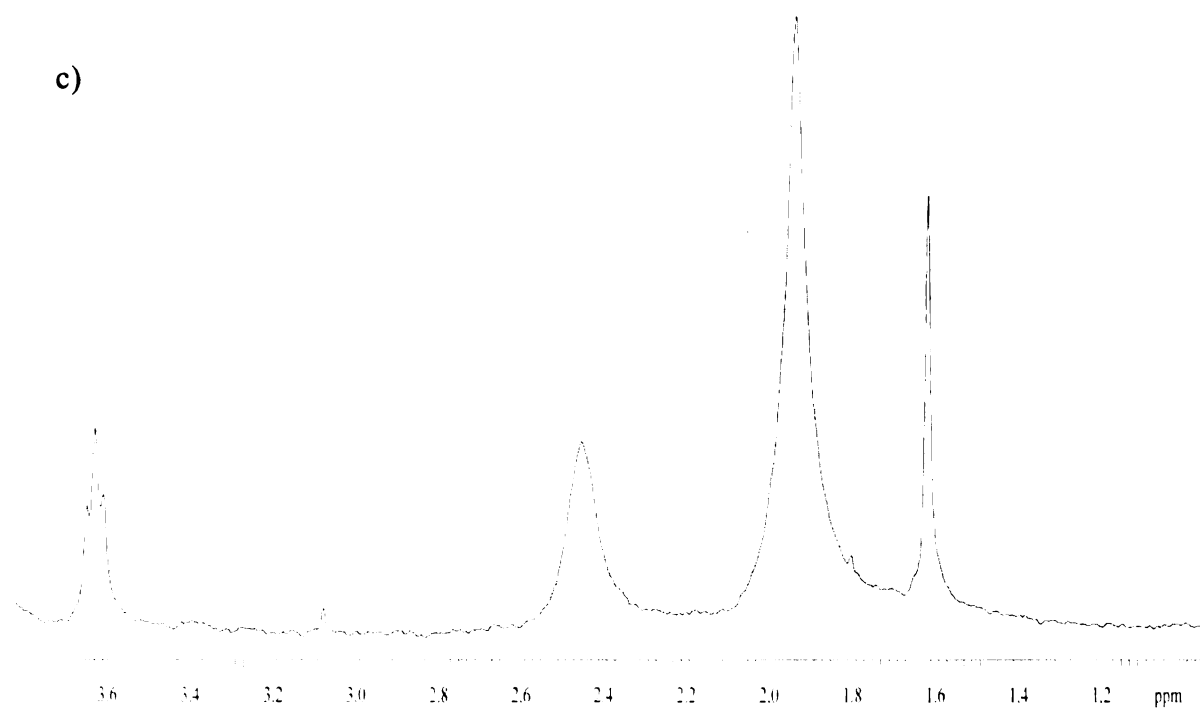


Figure A6. ^1H NMR reaction of $\text{Rh}_2(\text{O}_2\text{CCH}_3)_4$ with methionine. a) 1:1 ratio, b) 1:2 ratio, c) 1:3 ratio, and d) 1:4 ratio.



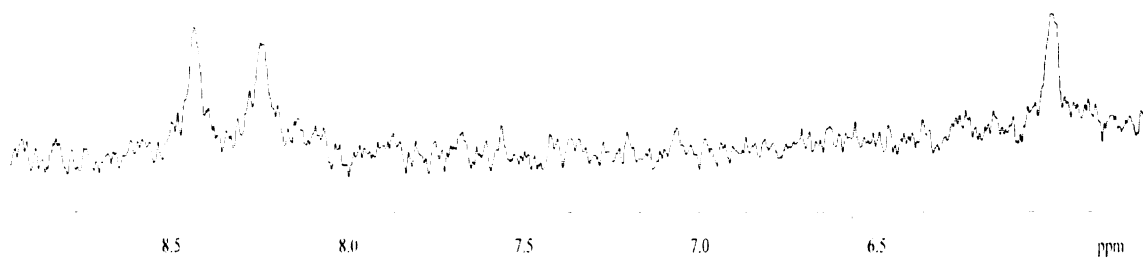
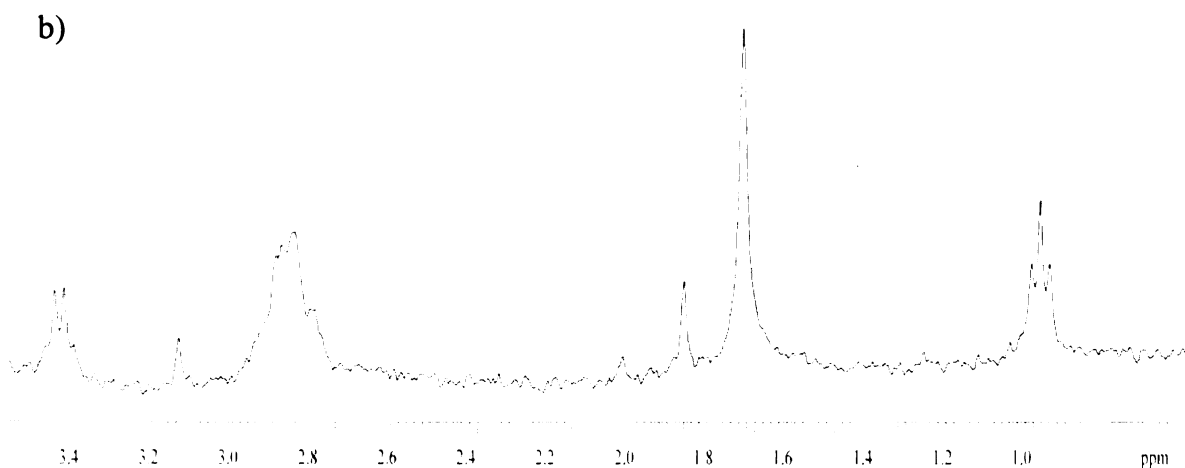
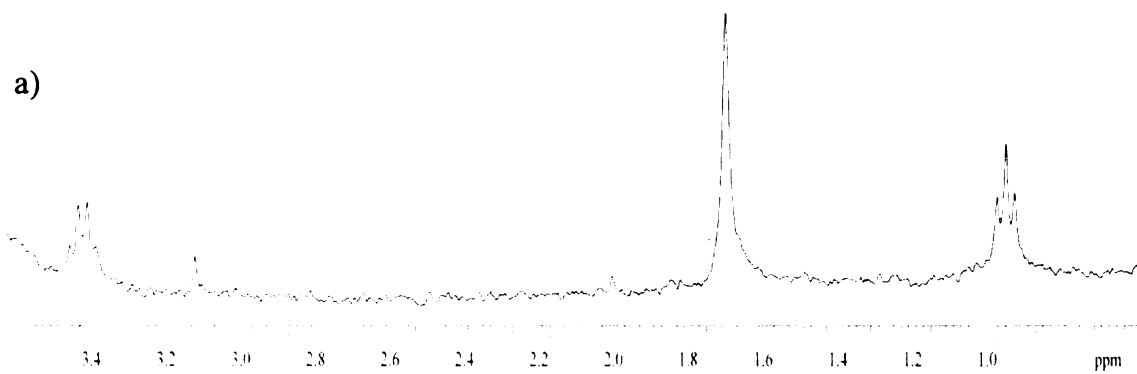
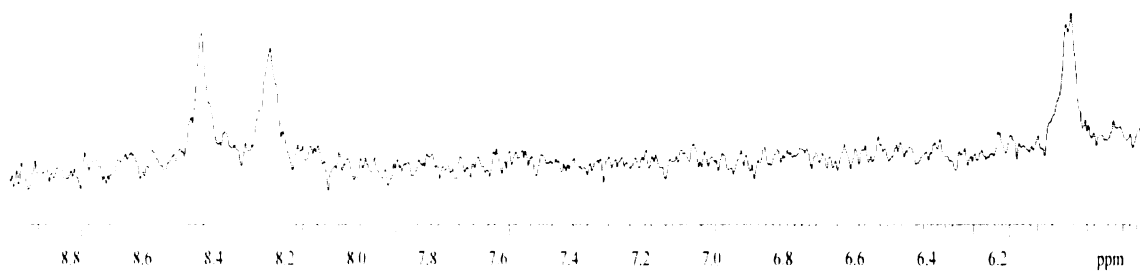
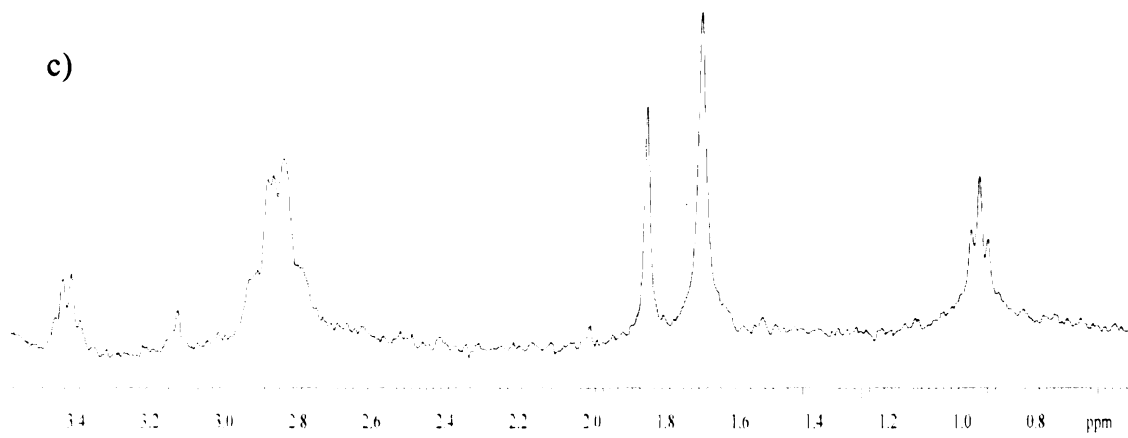
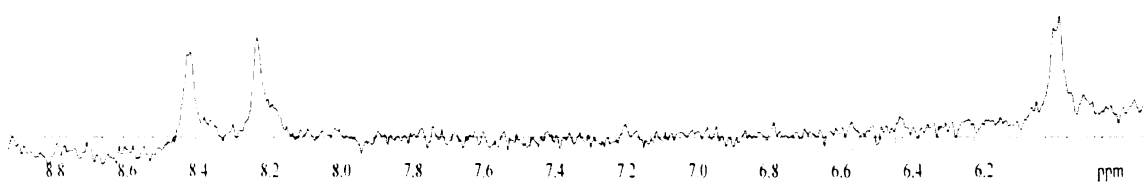
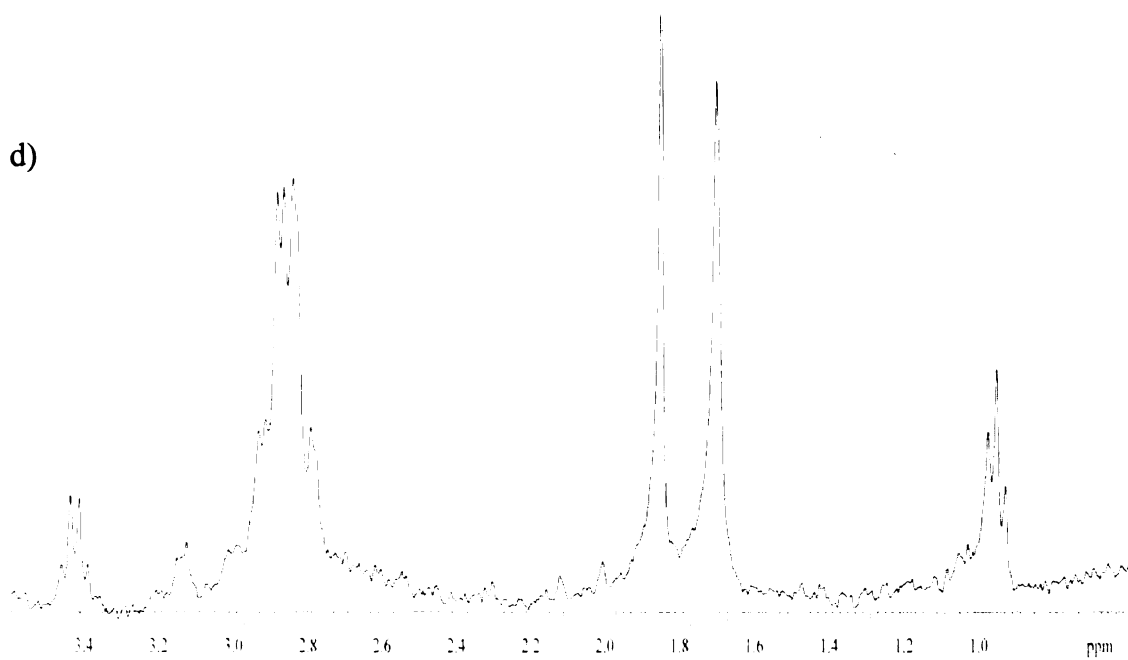


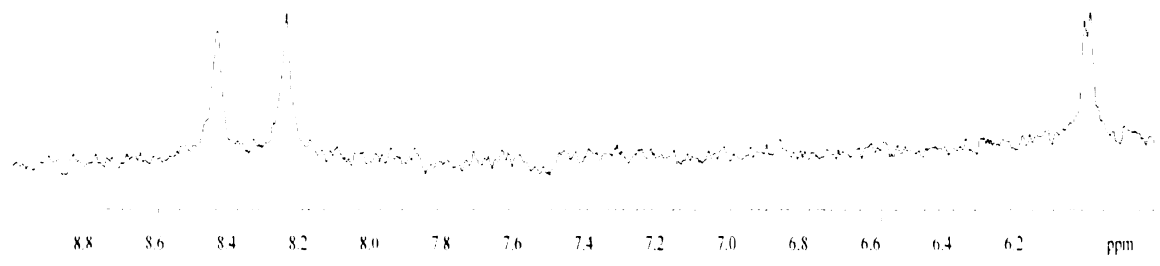
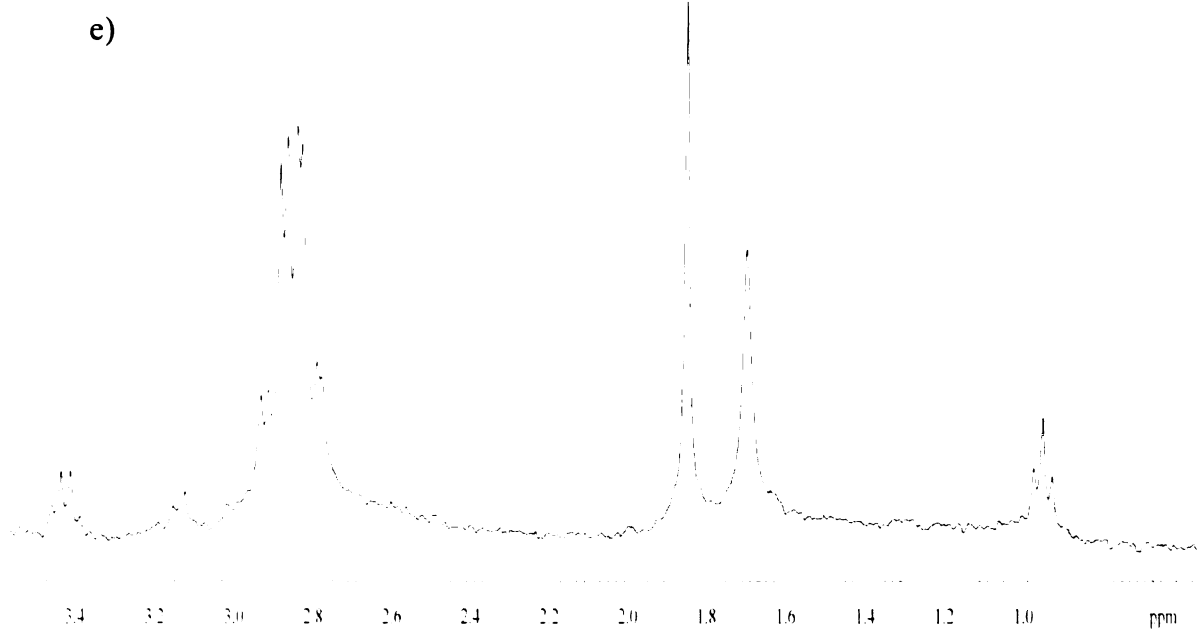
Figure A7. ^1H NMR reaction of $\text{Rh}_2(\text{O}_2\text{CCH}_3)_4(\text{ATP})_2$ with cysteine. a) $\text{Rh}_2(\text{O}_2\text{CCH}_3)_4(\text{ATP})_2$ standard, b) 1:1 ratio, c) 1:2 ratio, d) 1:3 ratio, and e) 1:4 ratio.

c)



d)





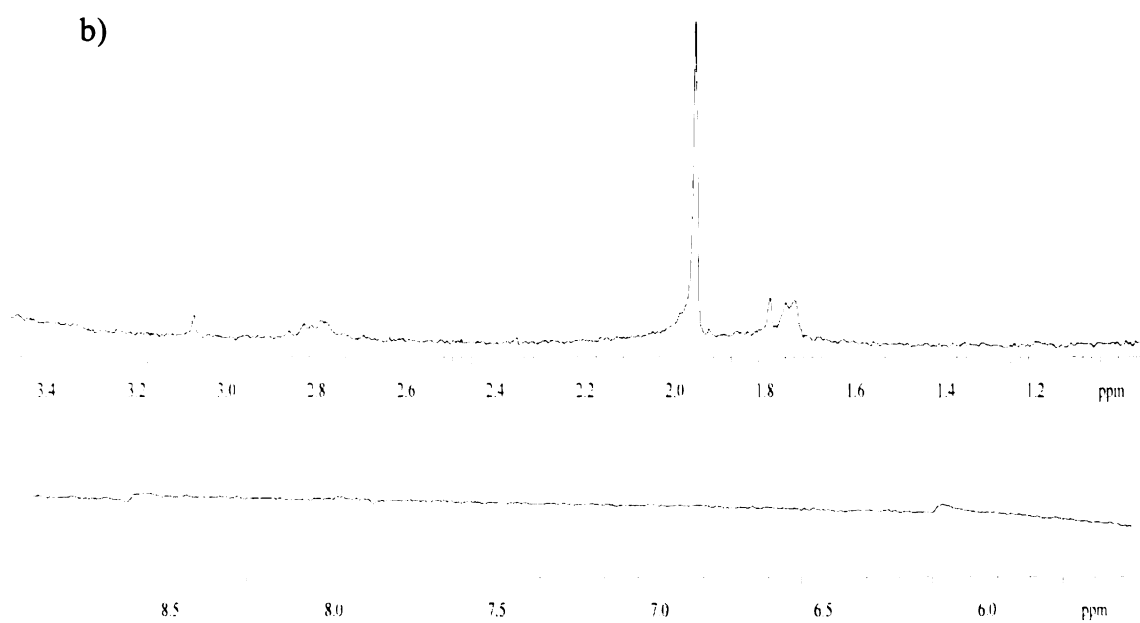
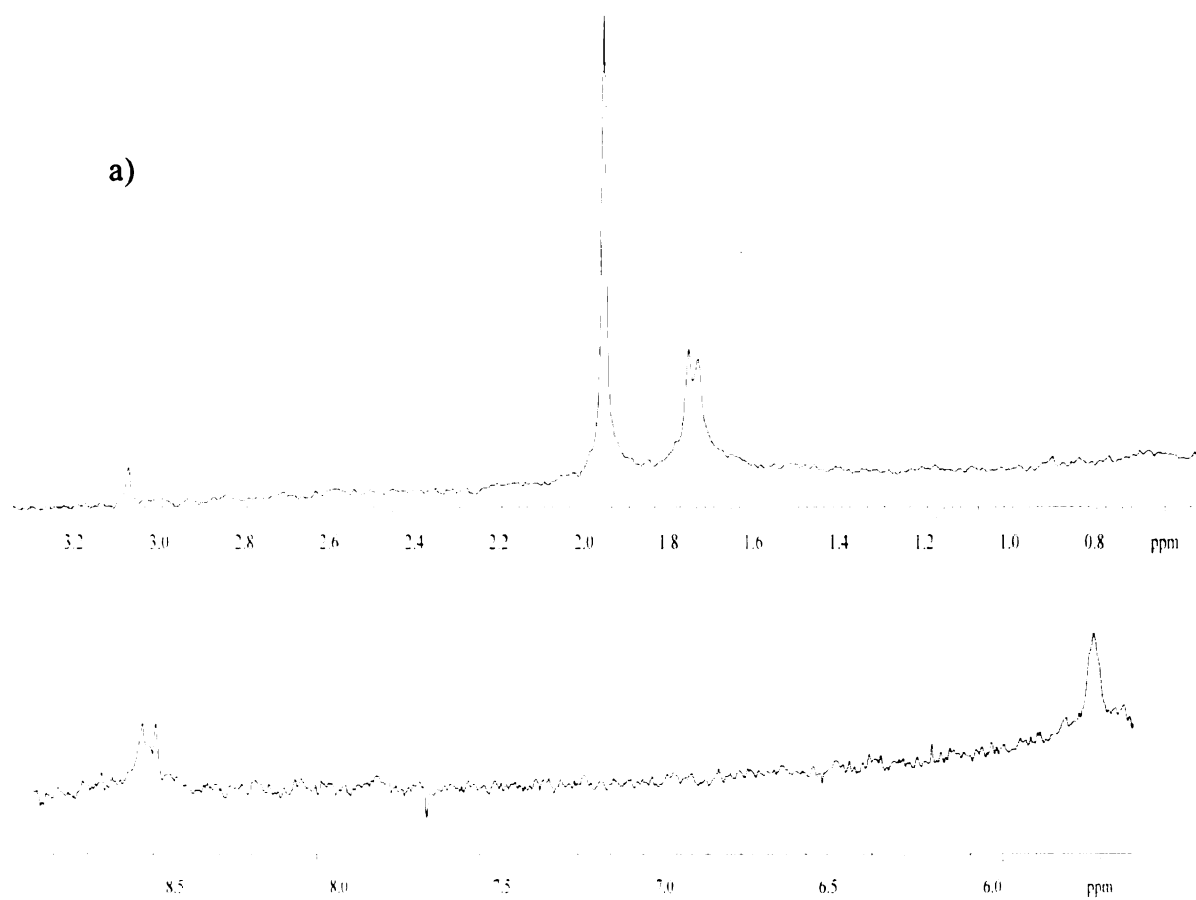
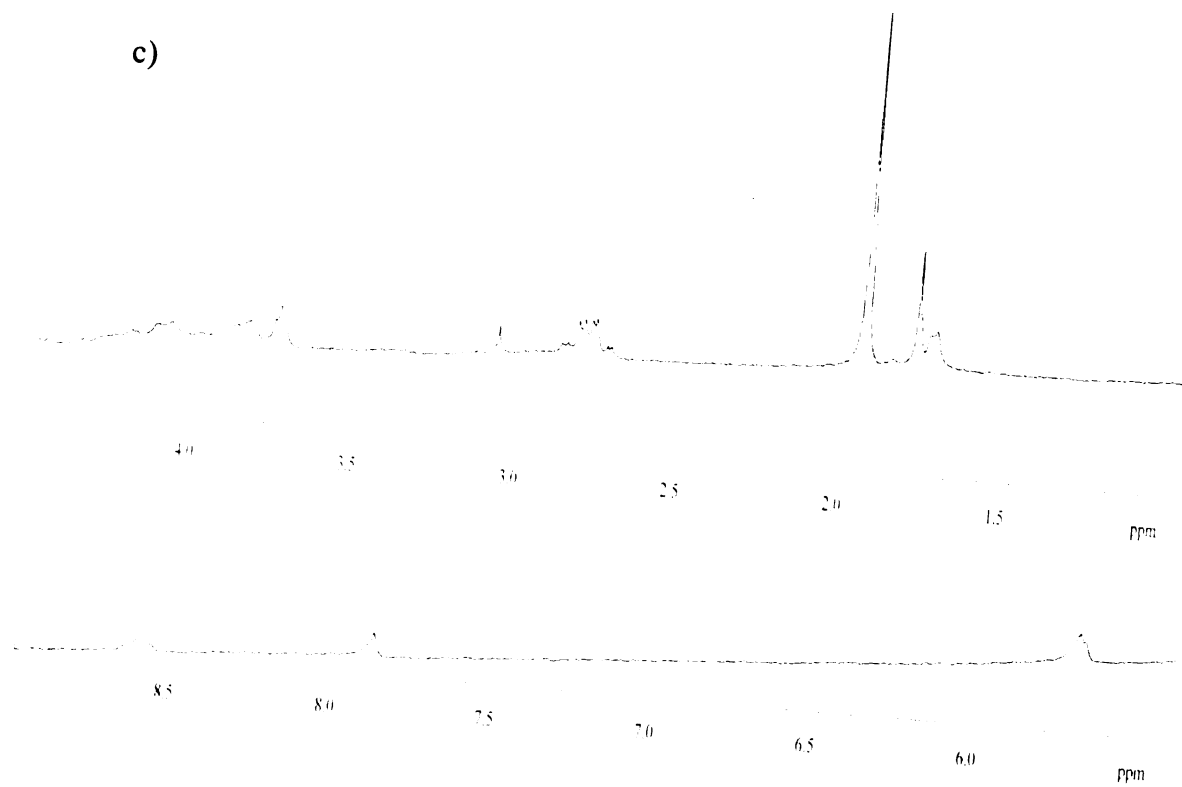
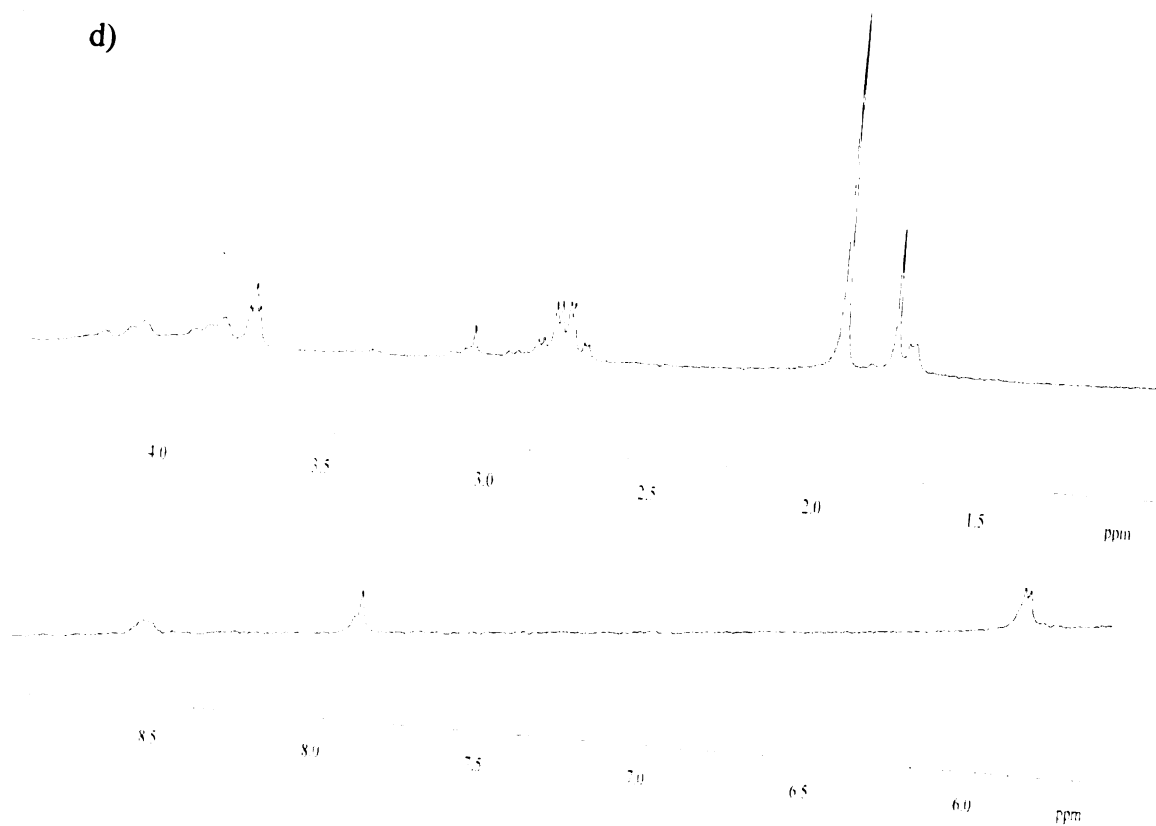


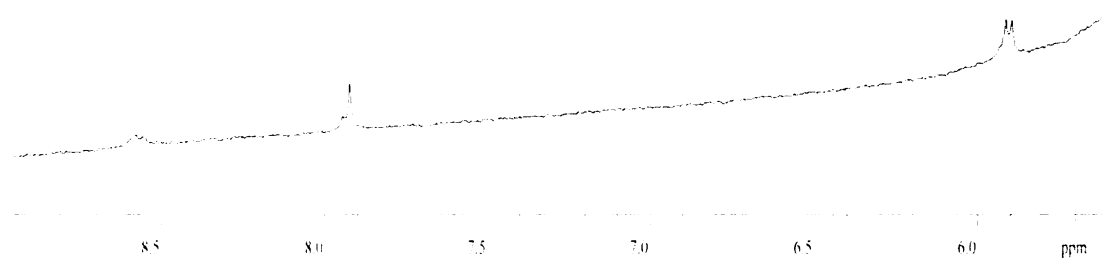
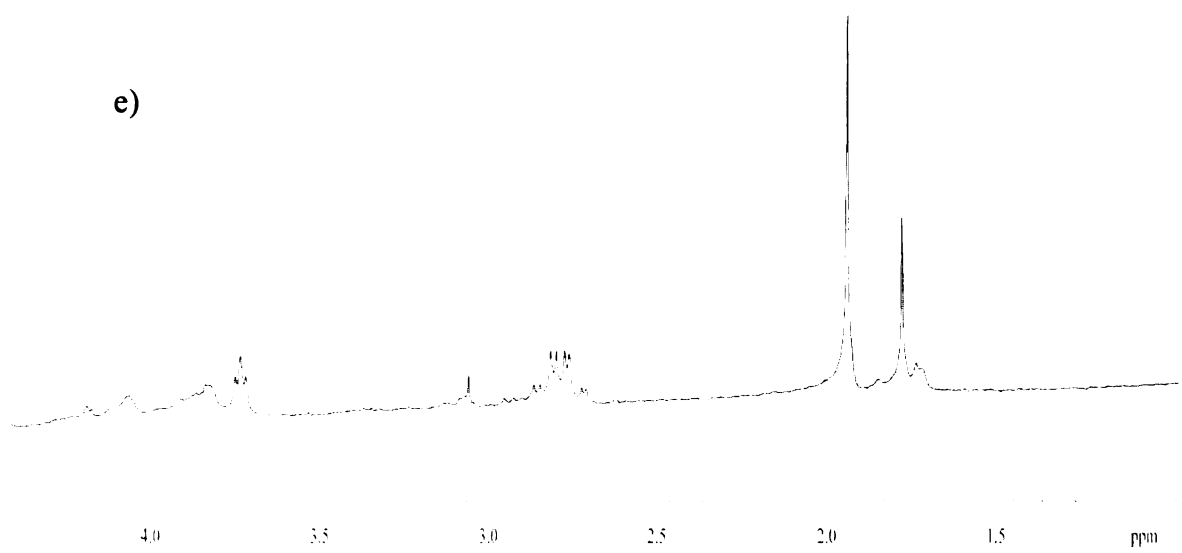
Figure A8. ^1H NMR reaction of $\text{Rh}_2(\text{O}_2\text{CCH}_3)_2(\text{GTP})_2 + \text{cysteine}$.
 a) $\text{Rh}_2(\text{O}_2\text{CCH}_3)_2(\text{GTP})_2$ standard, b) 1:1 ratio, c) 1:2 ratio, d) 1:3 ratio, and
 e) 1:4 ratio

c)



d)





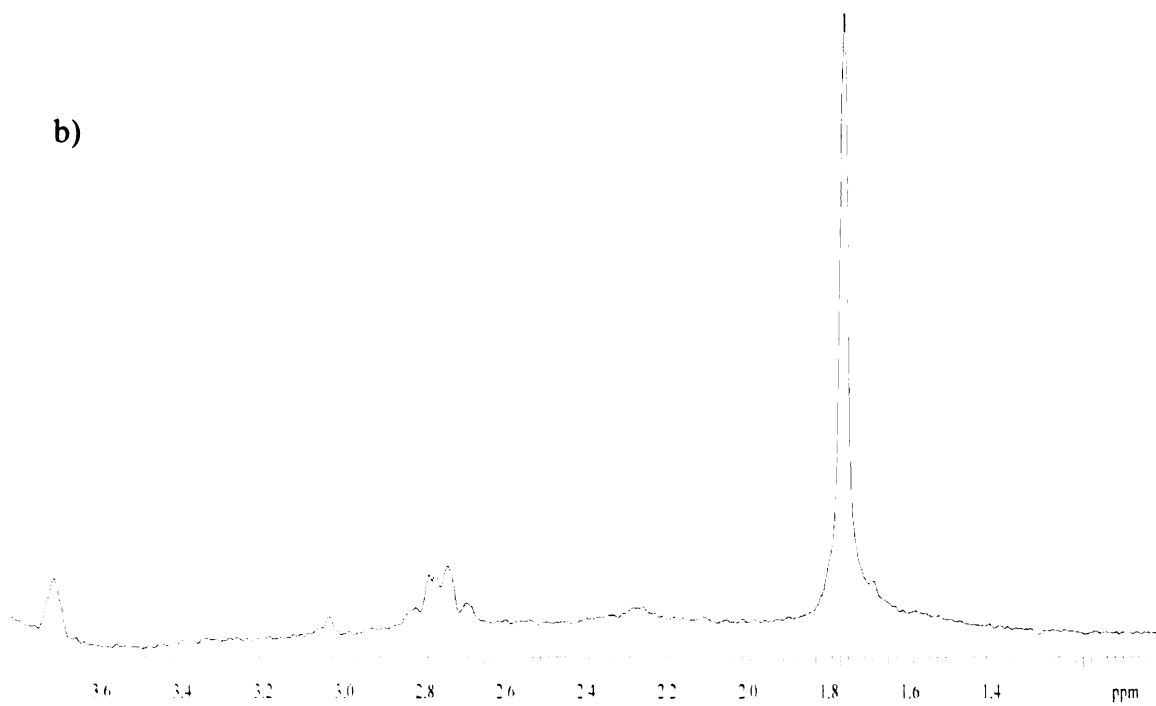
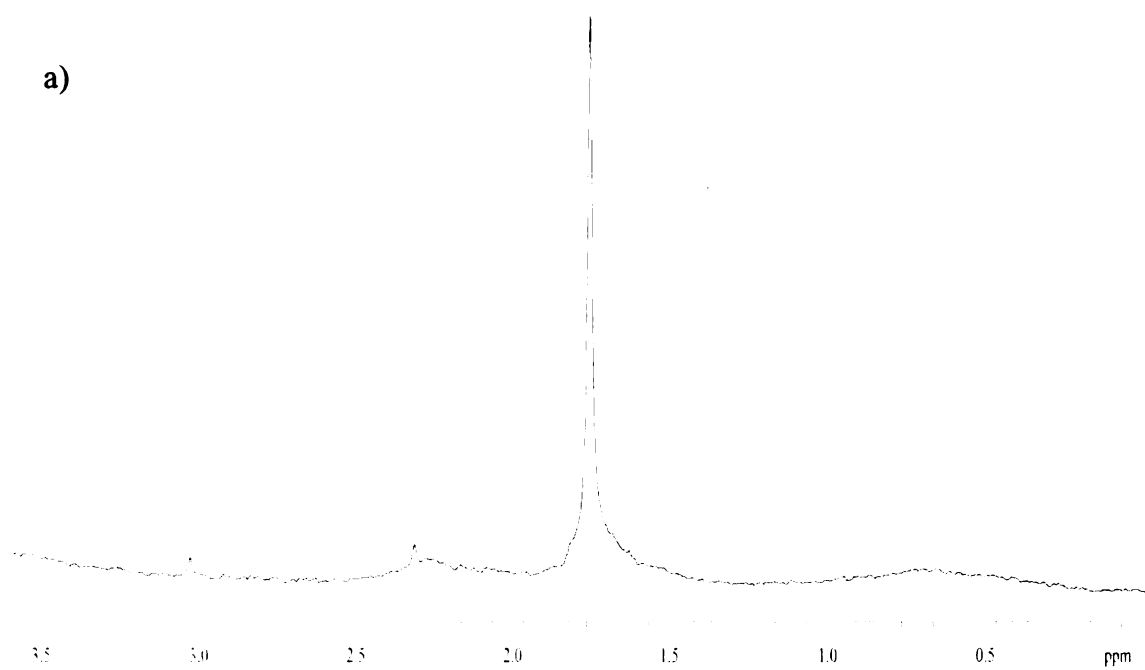
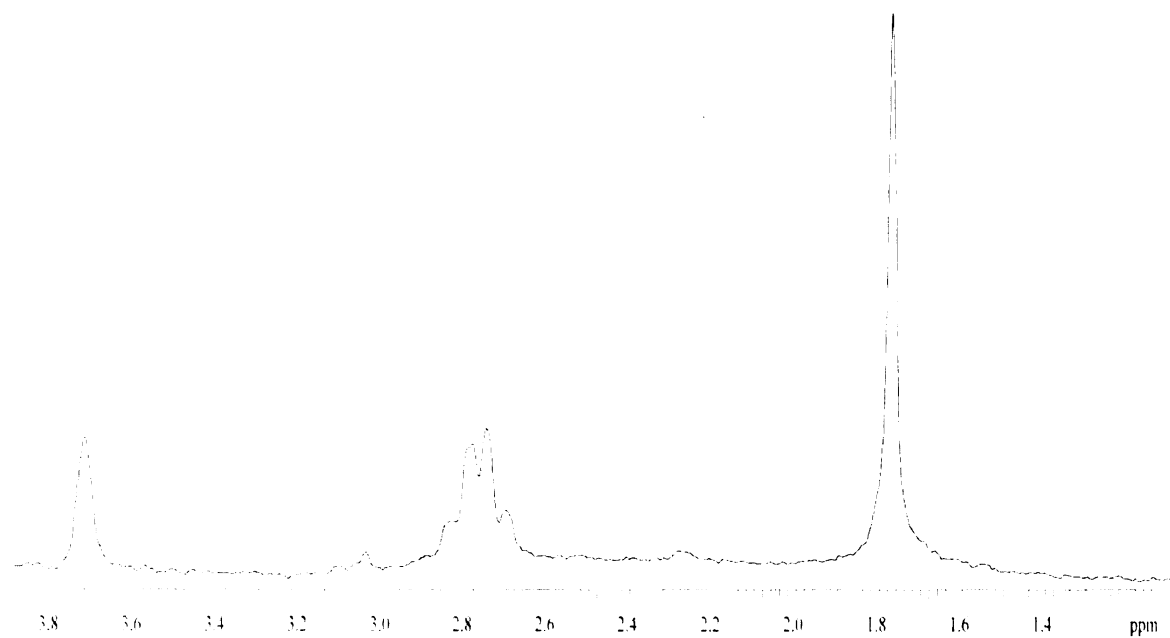
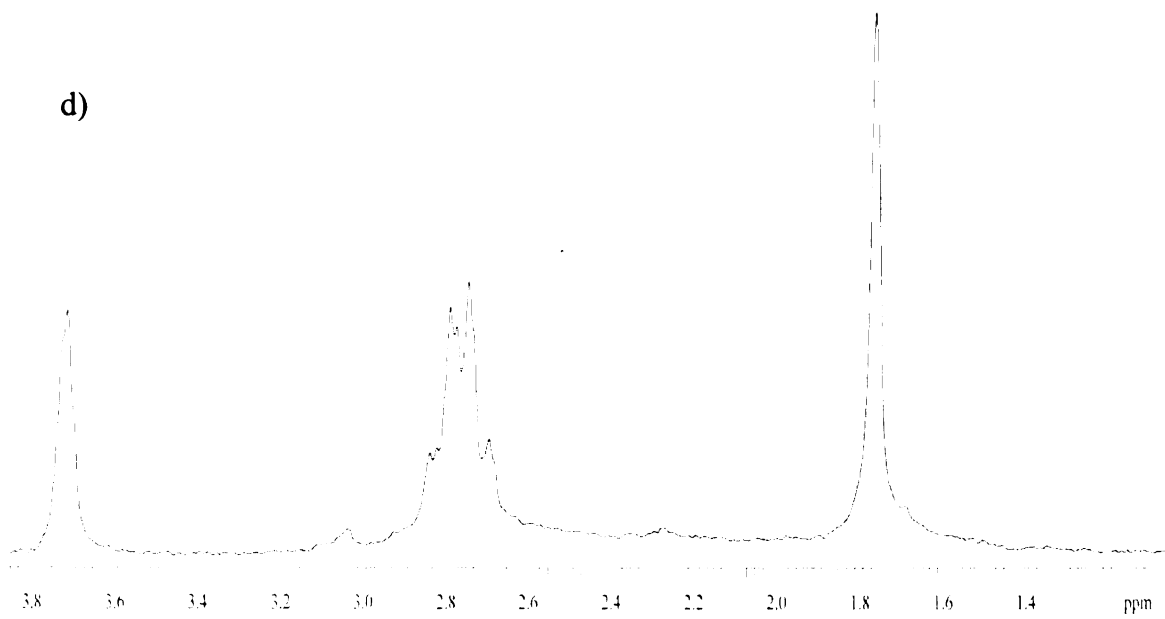


Figure A9. ^1H NMR reaction of $[\text{Rh}_2(\text{O}_2\text{CCH}_3)_2(\text{MeCN})_6][\text{BF}_4]_2$ with cysteine. A) 1:1 ratio, b) 1:2 ratio, c) 1:3 ratio, d) 1:4 ratio.

c)



d)



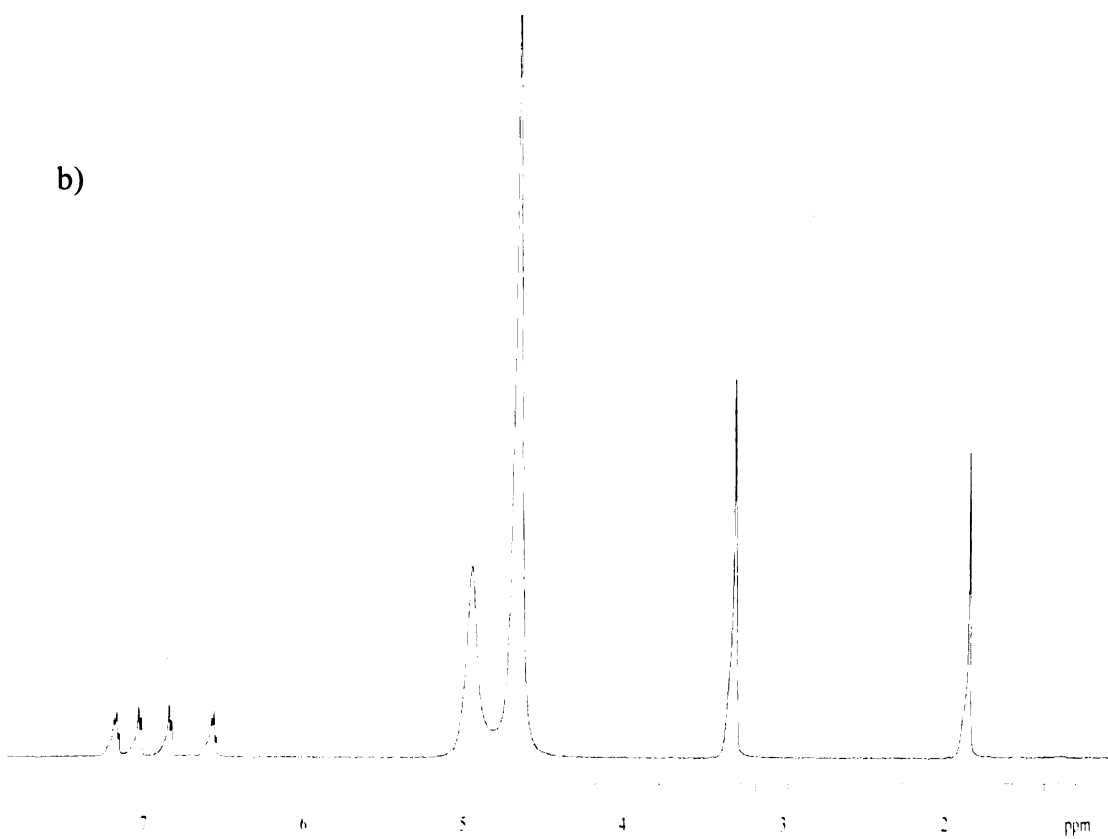
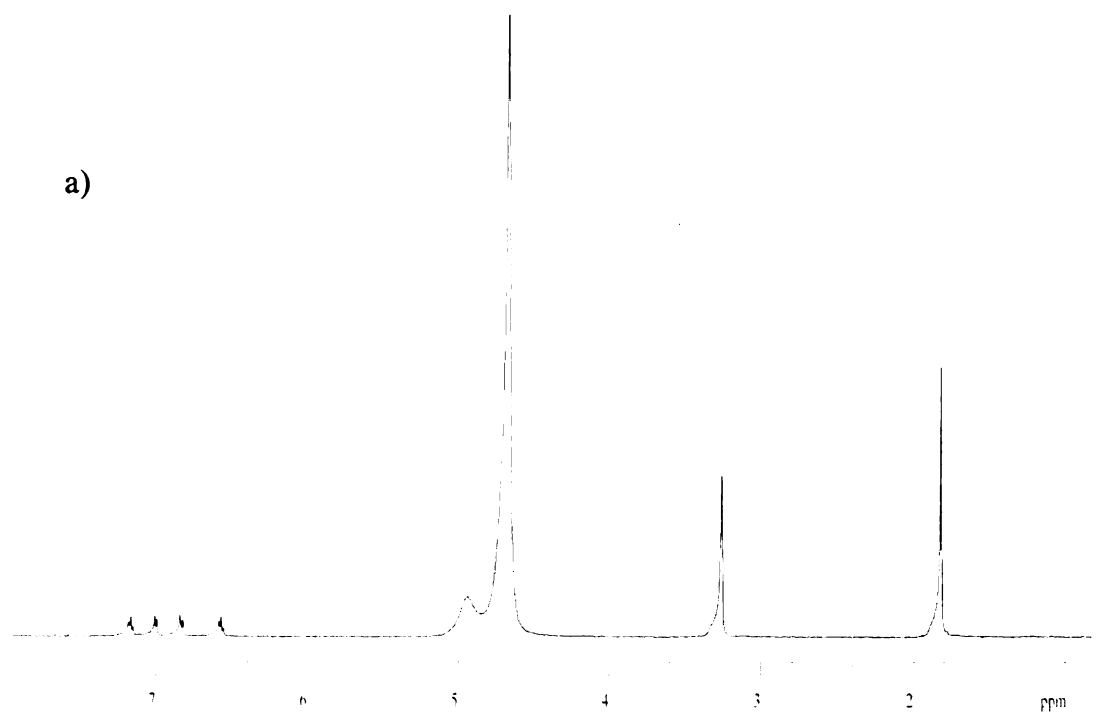
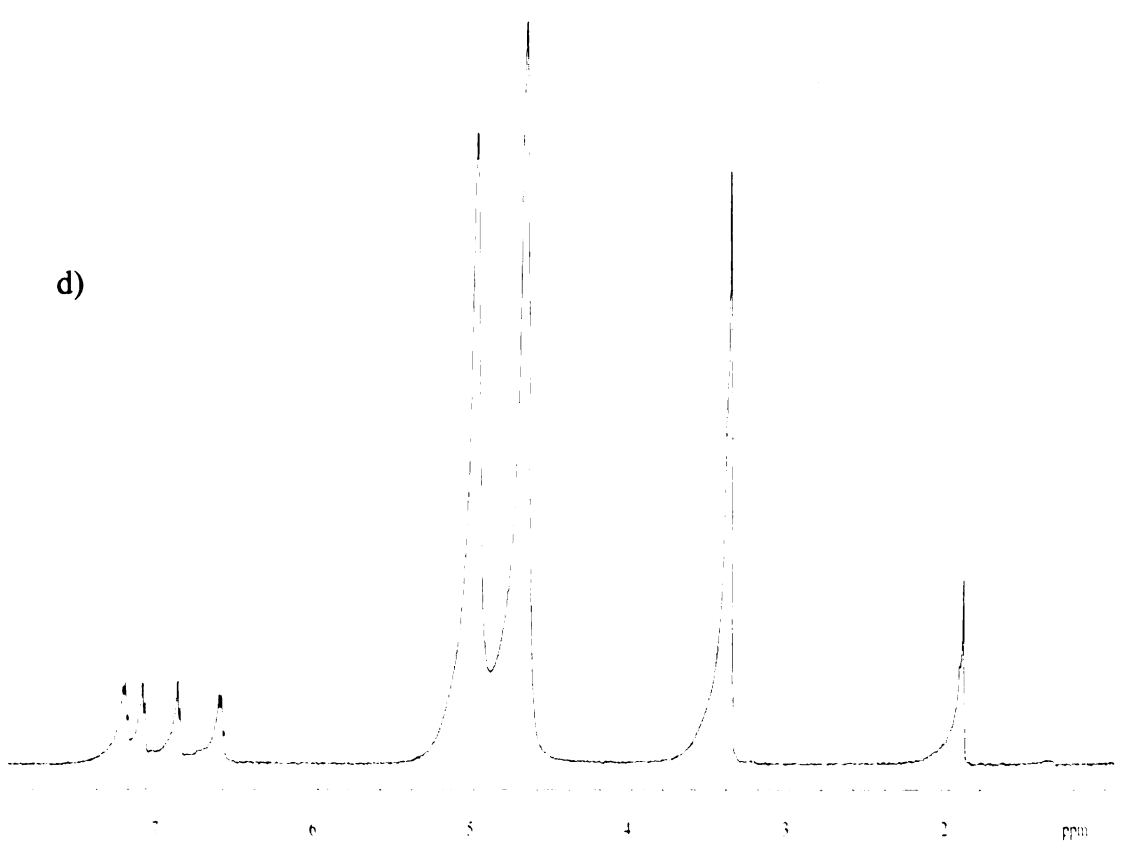
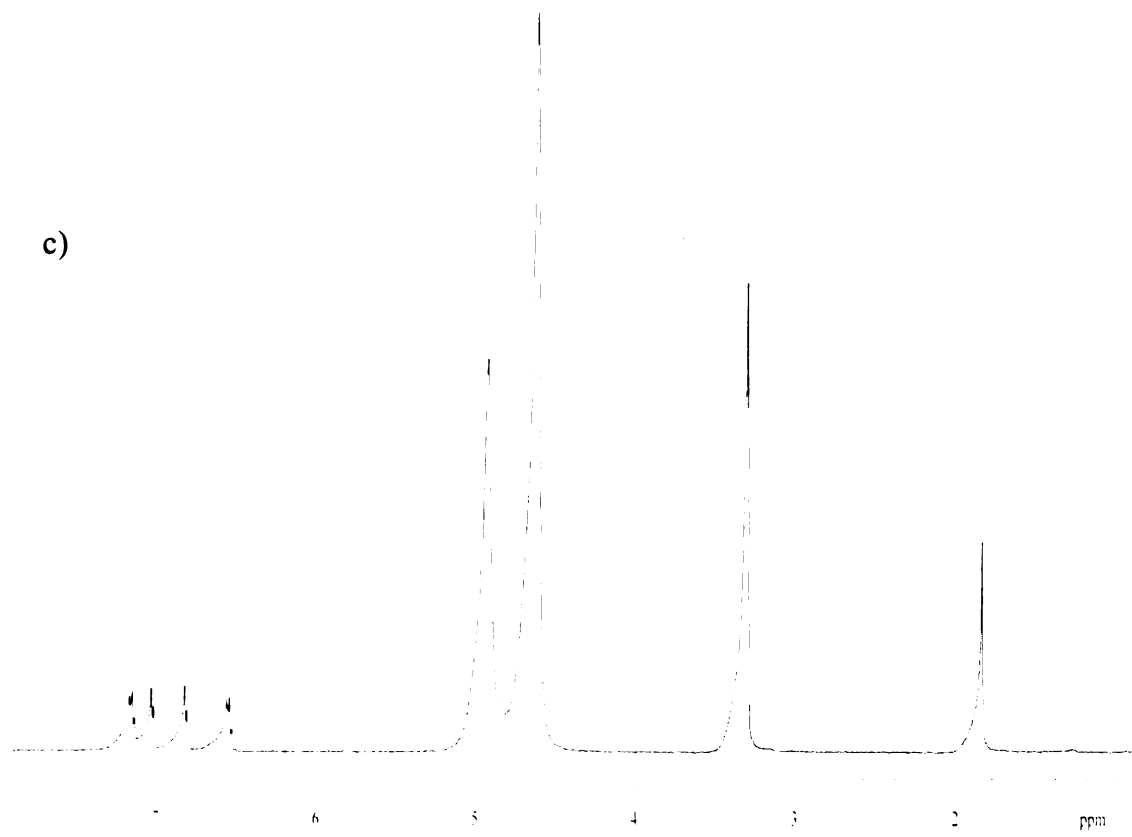


Figure A10. ^1H NMR reaction of $\text{Rh}_2(\text{O}_2\text{CCH}_3)_4$ + 2-Aminothiophenol. a) 1:1 ratio, b) 1:2 ratio, c) 1:3 ratio, and d) 1:4 ratio.



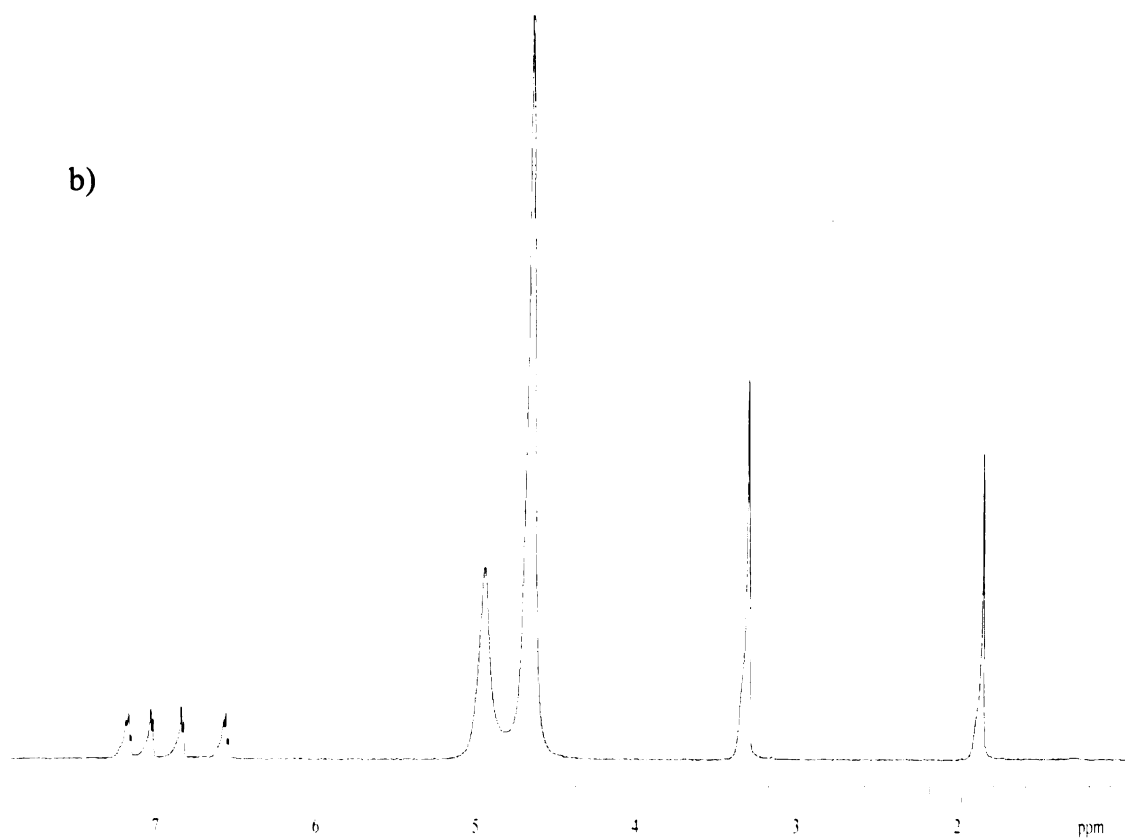
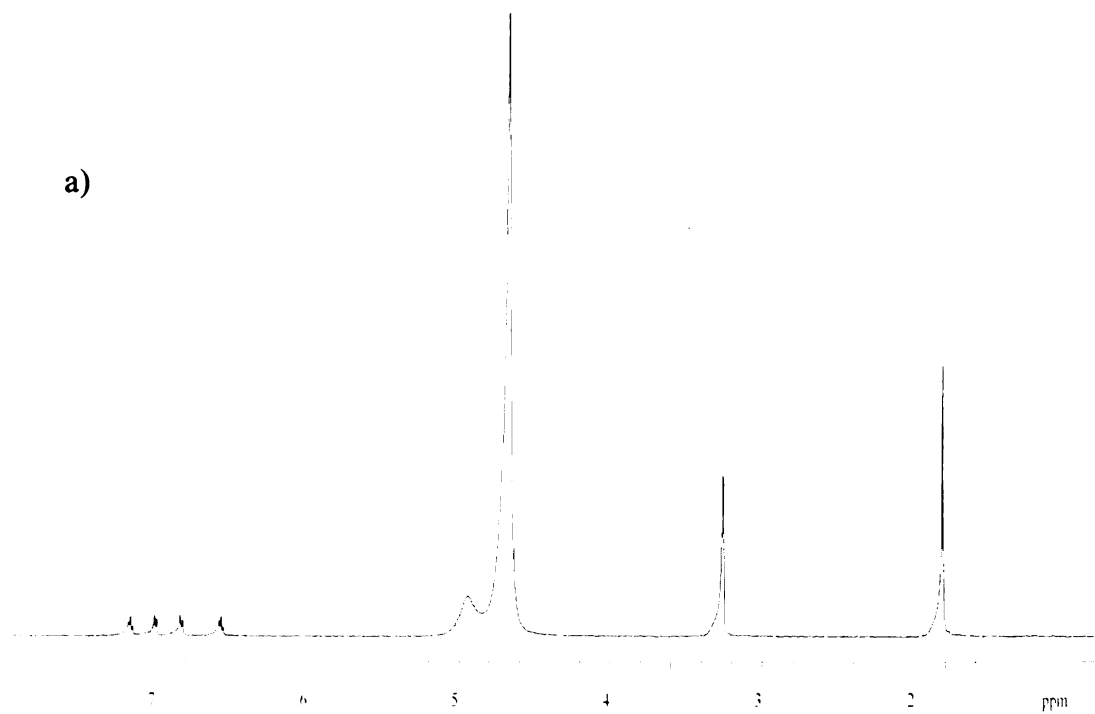
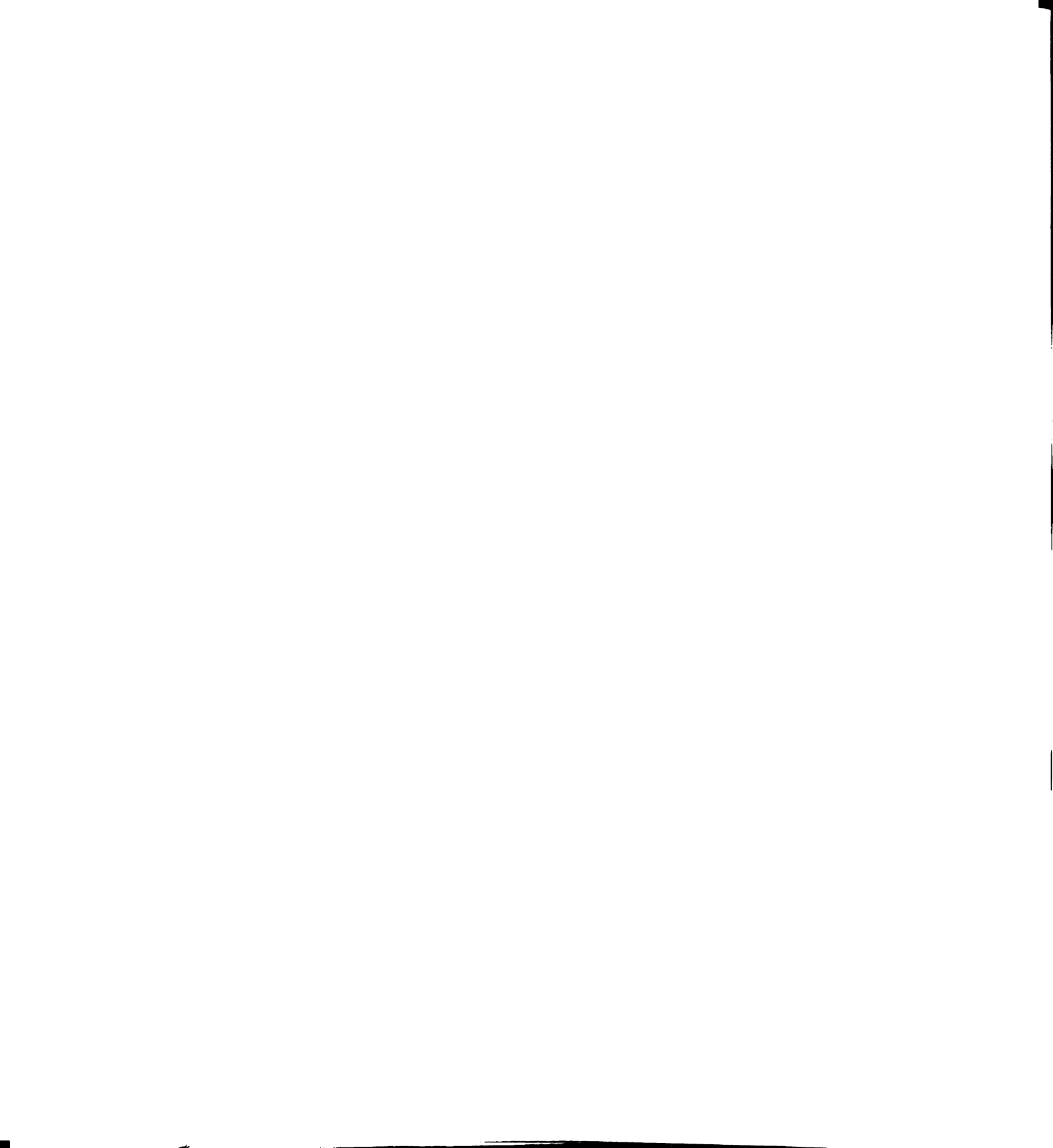


Figure A11. ^1H NMR reaction of $\text{Rh}_2(\text{O}_2\text{CCH}_3)_4$ + 2-Aminothiophenol. a) 1:1 ratio, b) 1:2 ratio, c) 1:3 ratio, and d) 1:4 ratio.



REFERENCES

References

- 1 ..Rosenberg, B.; VanCamp, L. *Nature* **1969**, *222*, 385.
2. Hambley, T. W. *Coordination Chemistry Reviews* **1997**, *166*, 181-223.
3. Sherman, S. E.; Lippard, S. J. *Chem. Rev.* **1987**, *87*, 1153-1181.
4. Lehninger, A. L.; Nelson, D. L.; Cox, M. M *Principles of Biochemistry* **1993**, Worth Pub. 111-130, 334-341.
5. Neidle, S. *Biopoly.* **1997**, *44*, 105-221.
6. Ohndorf, U.-M.; Witehead, J. P.; Raju, N. L.; Lippard, S. J. *Biochemistry* **1997**, *36*, 14807-14815.
7. Yaneva, J.; Leuba, S. H.; van Holde, K.; Zlatanova, J. *Proc. Natl. Acad. Sci. USA* **1997**, *94*, 13448-13451.
8. Vichi, P.; Coin, F.; Renaud, J.-P.; Vermeulen, W.; Hoeijmakers, J. H. J.; Moras, D.; Egly, J. -M. *The EMBO Journal* **1997**, *16*, **24**, 7444-7456.
9. Farrell, N.; Kelland, L. R.; Roberts, J. D.; Vanbeusichem, M. *Canc. Res.* **1992**, *52*, 5065.
10. Farrell, N.; Qu, Y.; Feng, L.; Vanhouten, B. *Biochemistry*, **1990**, *29*, 9522.
11. Bear, J. L.; Howard, R. A.; Dennis, A. M. *Curr. Chemother.* **1978**, 1321-1323.
12. Howard, R. A.; Spring, T. G.; Bear, J. L. *Cancer Research* **1976**, *36*, 4402-4405.
13. Kitchens, J.; Bear, J. L. *Inorg. Nucl. Chem.* **1969**, *31*, 2415-2421.
14. Fimiani, V.; Ainis, T.; Cavallaro, A.; Piraino, P. *Journal of Chemotherapy* **1990**, *2*, **5**, 319-326.
15. Piraino, P.; Tresoldi, G.; Lo Schiavo, S. *Inorg. Chim. Acta* **1993**, *203*, 101-105
16. (a) Eastland, G. W. Jr.; Yang, G.; Thompson, T. *Meth. and Find. Exptl. Clin. Pharmacol.* **1983**, *5*, **7**, 435-438. (b) Dimitrov, N. V.; Eastland, G. *Curr.*

- Chemother. Proc. Int. Congress. Chemother. 10th Meeting 1977*, 2, 1319-1321. (c) Cotton, F. A.; DeCanio, E. C.; Kibala, P. A.; Vidyasagar, K. *Inorg. Chim. Acta.* **1991**, 184, 221-228. (d) Chatterjee, M.; Achari, B.; Banerjee, R.; Chakrabarti, C.; Dattagupta, J. K.; Banerjee, S. *Inorganic Chemistry* **1998**, 37, 21, 5424-5430.
17. Van Boom, S. S. G. E.; Reedijk, J. *J. Chem. Soc. Chem. Commun.* **1993**, 1397-1398.
 18. Davidson, Y. Y.; Chang, S.-C.; Norman, R. E. *J. Chem. Soc. Dalton Trans.* **1995**, 77-81.
 19. Guo, Z.; Casellato, U.; Faraglia, G.; Graziani, R.; Sitran, S. *J. Chem. Soc. Dalton Trans.* **1994**, 3231-3235.
 20. Bednarski, P. J. *Journal of Inorganic Biochemistry* **1995**, 80, 1-19.
 20. Sheldrick, W. S.; Gleichmann, A. *Journal of Organometallic Chemistry* **1994**, 470, 183-187.
 22. Berners-Price, S. J.; Kuchel, P. W. *Journal of Inorganic Biochemistry* **1990**, 38, 305-326.
 23. Djuran, M. I.; Lempers, E. L. M.; Reedijk, J. *Inorg. Chem.* **1991**, 30, 2648-2652.
 24. Odenheimer, B.; Wolf, W. *Inorganica Chimica Acta* **1982**, 66, L41-L43.
 25. Perez-Benito, J. F.; Arias, C.; Amat, E. *New Journal of Chemistry* **1995**, 19, 1089-1094.
 26. Bose, R. N.; Ghosh, S. K.; Moghaddas, S. *Journal of Inorganic Biochemistry* **1997**, 199-205.
 27. Wyatt, K. S.; Harrison, K. N.; Jensen, C. M. *Inorg. Chem.* **1992**, 31, 3867-3868.
 28. Bose, R. N.; Li, D.; Kennedy, M.; Basu, S. *J. Chem. Soc. Chem. Commun.* **1995**, 1731-1732.
 29. Pneumatakakis, G.; Psaroulis, P. *Inorganica Chimica Acta* **1980**, 46, 97-100.
 30. Levason, W.; McAuliffe, C. A. *Inorg. Chem. Nucl. Lett.* **1977**, 13, 123-127.
 31. Bukanova, A. E., et. al. *J. Inorg. Chem (Russ)* **1990**, 35, 2003-2006.

32. Erck, A.; Sherwood, E.; Bear, J. L.; Kimball, A. P. *Cancer Research* **1976**, *36*, 2204-2209.
33. Felthouse, T, R. *Prog. Inorg. Chem.* **1982**, *29*, 72-97.
34. Nakamoto, K. *Infrared and Raman Spectra of Inorganic and Coordination Compounds* **1978**, Wiley and Sons, 305-307.
35. Boyar, E. B.; Robinson, S. D. *Coord. Chem. Rev.* **1983**, *50*, 109-208.
36. Catalan, K.; Hess, J.; Maloney, M.; Mindiola, D.; Ward, D.; and Dunbar, K. submitted to *Inorg. Chem.*
36. Pasini, A.; Zunino, F. *Angew. Chem. Int. Ed. Engl.* **1987**, *26*, 615-624.
37. Barnham, K. J.; Berners-Price, S. J.; Frenkiel, T. A.; Frey, U.; Sadler, P. J. *Angew. Chem. Int. Ed. Engl.* **1995**, *34*, **17**, 1874-1877.
38. Erck, A.; Rainen, L.; Whileyman, J.; Chang, I.-M.; Kimball, A. P.; Bear, J. *Proceedings of the Society for Experimental Biology and Medicine* **1974**, *145*, 1278-1283.
39. Bear, J. L.; Gray, Jr., H. B.; Rainen, L.; Chang, I. M.; Howard, R.; Serio, G.; Kimball, A. P. *Cancer Chemotherapy Reports* **1975**, *59*, **3**, 611-620.
40. Dunbar, K. R.; Matonic, J. H.; Saharan, V. P.; Crawford, C. A.; Cristou, G. J. *Am. Chem. Soc.* **1994**, *116*, 2201-2202.
41. Dennis, A. M.; Howard, R. A.; Bear, J. L. *Inorganica Chimica Acta* **1982**, *66*, L31-L34.
42. Waysbort, D.; Eichhorn, G. L. *Inorg. Chem.* **1993**, *32*, 4774, 4779.
43. Aoki, K.; Yamazaki, H. *J. C. S. Chem. Comm.* **1980**, 186-188.
44. Aoki, K.; Yamazaki, H. *J. Am. Chem. Soc.* **1984**, *106*, 3691-3692.
45. Farrell, N. *J. C. S. Chem. Comm.* **1980**, 1014-1016.
46. Rainen, L.; Howard, R. A.; Kimball, A. P.; Bear, J. L. *Inorganic Chemistry* **1975**, *14*, **11**, 2752-2754.
47. Oriskovich, T. A.; White, P. S.; Thorp, H. H. *Inorganic Chemistry* **1995**, *34*, **7**, 1629-1631.
48. Day, E. F.; Crawford, C. A.; Folting, K.; Dunbar, K. R.; Cristou, G. *J. Am.*

- Chem. Soc.* **1994**, *116*, 9339-9340.
49. Crawford, C. A.; Day, E. F.; Saharan, V. P.; Folting, K.; Huffman, J. C.; Dunbar, K. R.; Cristou, G. *Chem. Commun.* **1996**, 1113-1114.
50. Catalan, K. V.; mindiola, D. J.; Ward, D. L.; Dunbar, K. R. *Inorg. Chem.* **1997**, *36*, 2458-2460.
51. Farrell, N. *Journal of Inorganic Biochemistry* **1981**, *14*, 261-265.
52. Chifotides, H. T.; Dunbar, K. R.; Matonic, J. H. *Inorg. Chem.* **1992**, *31*, 4628-4634.
53. Pneumatakakis, G.; Hajilidis, N. *J. C. S. Dalton* **1979**, 596-599.
54. Gibson, D.; Arvanitis, G. M.; Berman, H. M. *Inorg. Chim. Acta* **1994**, *218*, 11-19.
55. Davidson, Y. Y.; Chang, S.-C.; Norman, R. E. *J. Chem. Soc. Dalton Trans.* **1995**, 77-81
56. Djuran, M. I.; Lempers, E. L. M.; Reedijk, J. *Inorg. Chem.* **1991**, *30*, 2648-2652.
57. Barnham, K. J.; Djuran, M. I.; del Socorro Murdoch, P.; Sadler, P. J. *J. Chem. Soc. Chem. Commun.* **1994**, 721-722.
58. Bose, R. N.; Moghaddas, S.; Weaver, E. L.; Cox, E. H. *Inorg. Chem.* **1995**, *34*, 5878-5883.
59. Appleton, T. G.; Connor, J. W.; Hall, J. R.; Prenzler, P. D. *Inorg. Chem.* **1989**, *28*, 2030-2037.
60. Nunn, C. M.; Garman, E.; Neidle, S. *Biochemistry* **1997**, *36*, 4792-4799.
61. Kopka, M. L.; Goodsell, D. S.; Baikalov, I.; Grzeskowiak, K.; Casico, D.; Dickerson, R. E. *Biochemistry* **1994**, *33*, 13593-13610.
62. (a) Werner, M. H.; Huth, J. R.; Gronenborn, A. M.; Clore, G. M. *Cell* **1995**, *81*, 705-714. (b) Love, J. J.; Li, X.; Case, D. A.; Geise, K.; Grosschedl, R.; Wright, P. E. *Nature* **1995**, *376*, 791-795.
63. Takahara, P. M.; Rosenzweig, A. C.; Frederick, C. A.; Lippard, S. J. *Nature* **1995**, *377*, 649-652.
64. Wing, R. M.; Pjura, P.; Drew, H. R.; Dickerson, R. E. *The EMBO Journal*

1984, 3, 5, 1201-1206.

65. (a) Sherman, S. E.; Gibson, D.; Wang, A. H.-J.; Lippard, S. J. *J. Am. Chem. Soc.* **1988**, *110*, 7368-7381. (b) Sherman, S. E.; Gibson, D.; Wang, A. H.-J.; Lippard, S. J. *Science* **1985**, *230*, 412-417.

66. (a) Girault, J.-P.; Chottard, G.; Lallemand, J.-Y.; Chottard, J.-C. *Biochemistry* **1982**, *21*, 1352-1356. (b) Yang, D.; van Boom, S. S. G. E.; Reedijk, J.; van Boom, J. H.; Wang, A. H.-J. *Biochemistry* **1995**, *34*, 12912-12920.

67. Admiraal, G.; van der Veer, J. L.; de Graff, R. A. G.; den Hartog, J. H. J.; Reedijk, J. *J. Am. Chem. Soc.* **1987**, *109*, 2, 592-594.

MICHIGAN STATE UNIV. LIBRARIES



31293017893136